Optical Pulse Generation and Signal Processing for the Development of High-Speed OTDM Networks

A Thesis Submitted in Partial Fulfillment of the
Requirements for the Degree of
Doctor of Philosophy
(Electronic Engineering)

By

Paul Maguire

B Eng , MIEEE, MIEI

School of Electronic Engineering
Faculty of Engineering and Computing
Dublin City University

Research Supervisor
Dr Liam P Barry

January 2006

Approval

Name   Paul Maguire

Degree   Doctor of Philosophy (Electronic Engineering)

Title of Thesis   Optical Pulse Generation and Signal
Processing for the Development of
High-Speed OTDM Networks

Chairperson   Dr Noel Murphy

Internal Examiner   Prof Patrick J McNally

External Examiner   Prof Ravinder K Jain

Declaration

I hereby certify that this material, which I now submit for assessment on the programme of study leading to the award of Doctor of Philosophy is entirely my own work and has not been taken from the work of others save and to the extent that such work has been cited and acknowledged within the text of my work

Signed _Paul Maguire_

ID Number _97092720_

Date _5/May/2006_

Acknowledgments

"We are so often caught up in our destination that we forget to appreciate
the journey, especially the goodness of the people we meet on the way"

I would like to take this opportunity to thank the following people First and foremost my supervisor, Dr Liam Barry, for all his support and advice over the duration of this thesis Without his guidance and encouragement, this work would have no doubt been a lot more difficult

Appreciation is also due to Prof Charles McCorkell and Mr Jim Dowling for their support in relation to all aspects of my work in Dublin City University Also, I am very grateful to all the technical support staff in the Department of Electronic Engineering, Billy Roarty, Ger Considine, Conor Maguire, Robert Clare, Liam Meany, Paul Wogan and John Whelan, for all their assistance in various aspects of my work and on a number of important GAA issues

I would like to show appreciation to Torsten Krug, John O'Dowd and Prof John Donegan and the other staff members from the Semiconductor Photonics Group, Department of Physics Department, Trinity College Dublin for all their assistance will all aspects of the operation and functionality of the TPA microcavity

I wish to acknowledge the following members of the Radio and Optical Communications Lab in DCU who have made the last number of years so enjoyable The newbies Rob and Krzysztof, the middlies Aisling, Celine, Marc and Eoin, returnee Frank, and the oldies Brendan, Prince and Ola Thanks is also due to the folllowing past members Antonia, Ling and Ciara, and to the labs honourary members Damien O'Rourke and Eoin Kennedy

Finally, special mention has to go to all my friends and family, in particular, Declan, Sam, Conor, and Niamh, Deborah and Alan, and Rich In particular I would like to single out my parents, Frank and Mary, for special recognition Thanks for giving me the opportunity to be all that I am capable of being

Paul Maguire, January 2006

Contents

List of Figures

List of Tables

List of Acronyms

ACF Autocorrelation Function

APD Avalanche Photodiode

ASE Accumulated Spontaneous Emission

AWG Arranged Waveguide Grating

BER Bit-Error Rate

CClkW Counterclockwise

ClkW Clockwise

CDMA Code Division Multiple Access

CW Continuous Wave

CWDM Coarse Wavelength Division Multiplexing

DBR Distributed Bragg Reflector

DCF Dispersion Compensating Fibre

DFB Distributed Feedback Laser

DFF Dispersion Flattened Fibre

DGD Differential Group Delay

DS Digital Signal

DSF Dispersion Shifted Fibre

DSO Digital Sampling Oscilloscope

DWDM Dense Wavelength Division Multiplexing

EAM Electro-absorption Modulators

EBER Electrical Bit-Error Rate

ECL External Cavity Laser

EDFA Erbium Doped Fibre Amplifier

EM Electro-magnetic

ETDM Electrical Time Division Multiplexing

F Finesse

FBG Fibre Bragg Grating

FDM Frequency Division Multiplexing

FP Fabry-Perot

FPL Femtosecond Pulse Laser

FROG Frequency Resolved Optical Gating

FSR Free Spectral Range

FWHM Full-Width Half-Maximum

FWM Four-Wave Mixing

GRIN Graded Index

GVD Group Velocity Dispersion

IP Internet Protocol

ISI InterSymbol Interference

ITU International Telecommunication Union

ITU-T Telecommunications Standardization Sector of ITU

KdV Korteweg-deVries

LED Light Emitting Diode

MAN Metropolitan Area Network

MBE Molecular Beam Epitaxy

MZI Mach-Zehnder Interferometer

NALM Nonlinear Amplifying Loop Mirror

NLE Nonlinear Element

NLSE Nonlinear *Schrodinger* Equation

NOLM Nonlinear Optical Loop Mirror

NRZ Non-Return-to-Zero

OBER Optical Bit-Error Rate

OC-1 Optical Carrier-1

OCDM Optical Code Division Multiplexing

OCDMA Optical Code-Division Multiple Access

ODL Optical Delay Line

OOK On-Off Keying

OSA Optical Spectrum Analyser

OSO Optical Sampling Oscilloscope

OSNR Optical Signal-to-Noise Ratio

OTDM Optical Time Division Multiplexing

PC Polarisation Controller

PCM Pulse Code Modulation

PDH Plesiochronous Digital Hierarchy

PLL Phase-Locked Loop

PMD Polarisation Mode Dispersion

PMT Photomultiplier Tube

PPG Programmable Pattern Generator

PPLN Periodically Poled Lithium Niobate

PRBS Pseudo-Random Bit Sequence

PSP Principal States of Polarisation

RCE Resonant Cavity Enhanced

rms root-mean square

RZ Return-to-Zero

RZ-DPSK Return-to-Zero Differential Phase Shift-Keying

RZ-DQPSK Return-to-Zero Differential-Quadrature Phase Shift-Keying

SBS Stimulated Brilluoin Scattering

SDH Synchronous Digital Hierarchy

SHG Second Harmonic Generation

SHG-FROG Second Harmonic Generation - Frequency Resolved Optical Gating

SMF Single-Mode Fibre

SMSR Side-Mode Suppression Ratio

SNR Signal-to-Noise Ratio

SOA Semiconductor Optical Amplifier

SONET Synchronous Optical Network

SPA Single-Photon Absorption

SPM Self-Phase Modulation

SRD Step-Recovery Diode

SRS Stimulated Raman Scattering

SSB Single-Sideband

SSFBG Superstructured Fibre Bragg Grating

SSGS Self-Seeded Gain-Switched

STM-1 Synchronous Transfer Module-1

STS-1 Synchronous Transport Signal-1

SWE Standing Wave Effect

TBG Tunable Bragg Grating

TDM Time Division Multiplexing

TOAD Terahertz Optical Asymmetric Demultiplexer

TOJ Turn-on Delay Time Jitter

TPA Two-Photon Absorption

VCO Voltage-Controlled Oscillator

WDM Wavelength Division Multiplexing

XPM Cross-Phase Modulation

Abstract

Optical Pulse Generation and Signal Processing
for the Development of High-Speed OTDM Networks

Paul Maguire

B Eng , MIEEE, MIEI

Due to the continued growth of the Internet and the introduction of new broadband services, it is anticipated that individual channel data rates may exceed 100Gbit/s in the next 5-10 years In order to operate at such high line rates new techniques for optical pulse generation and optical signal processing will have to be developed

As the overall data rate of an OTDM network is essentially determined by the temporal separation between data channels, an optical pulse source that is capable of producing ultra-short optical pulses at a high repetition rate and with wavelength tunability will be important, not only for OTDM, but for various applications in WDM and hybrid WDM/OTDM networks This work demonstrates that by using the gain-switching technique, commercially available laser diodes can be used in the development of nearly transform-limited optical pulses that are wavelength tunable over nearly 65nm with durations ranging from 12-30ps and a Side-Mode Suppression Ratio (SMSR) exceeding 60dB

New optical signal processing techniques will also have to be developed in order to operate at individual data rates in excess of 100Gbit/s Only nonlinear optical effects, present in fibres, semiconductors and optical crystals, can be employed as these occur on time scales in the order of a few-femtoseconds ($10^{-15}s$), with an example being Two-Photon Absorption (TPA) in semiconductors This thesis describes a specially designed microcavity that can enhance the Two-Photon Absorption (TPA) response by over three orders of magnitude at specific wavelengths A theoretical model demonstrating error-free demultiplexing of a 250Gbit/s OTDM signal via a TPA microcavity has been developed Experimental work is also presented demonstrating the use of a TPA microcavity for optical sampling of 100GHz signals with a temporal resolution of $1ps$, and system sensitivity of $0 009(mW)^2$ This value for the sensitivity is the lowest ever reported for a TPA-based sampling system

Introduction

Due to the continued growth of the Internet and the introduction of new broadband services, the ever-increasing demand for bandwidth is accelerating the use of optical fibre in optical communications networks. In order to continue to increase the data carrying capacity of the network, it is anticipated that individual channel data rates may exceed 100Gbit/s in the next 5-10 years. In addition, by taking advantage of optical multiplexing techniques such as Wavelength Division Multiplexing (WDM) and Optical Time Division Multiplexing (OTDM), total aggregate data rates in excess of 10Tbit/s might be feasible in the near future.

Three of the important issues relating to the successful implementation of bit-interleaved OTDM systems are the *Generation of Ultra-Short Optical Pulses, Optical Demultiplexing* and *Pulse Characterisation*. As the overall data rate of an OTDM network is essentially determined by the temporal separation between data channels, an optical pulse source that is capable of producing wavelength tunable, ultra-short optical pulses at a high repetition rate will be important, not only for OTDM, but for various applications in WDM and hybrid WDM/OTDM networks. New optical signal processing techniques will also have to be developed in order to handle the very high line rates being anticipated. The development of innovative devices that are capable of carrying out two of the most significant optical signal processing tasks, pulse characterisation for performance monitoring and the demultiplexing of a single channel from a multi-channel data signal, will be vital for future network design and operation. If, as expected, the individual channel data rate exceeds 100Gbit/s, only nonlinear optical effects that are present in optical fibres, semiconductors and optical crystals that occur on time scales on the order of a few femtoseconds $(10^{-15}s)$ can be employed. One such optical nonlinearity is TPA in semiconductors, and this is one of the main topics of this thesis.

The main contributions of this work are

- *Optical Pulse Generation* - We have demonstrated that by using the gain-switching technique, commercially available laser diodes can be used in the development of nearly transform-limited optical pulses that are wavelength tunable over nearly

1

65nm with a Side-Mode Suppression Ratio (SMSR) exceeding 60dB and optical pulse durations ranging from 12-30ps Such pulses may play a role in ensuring optimal performance of high-speed optical communications networks

- *Optical Demultiplexing* - A theoretical model demonstrating that error-free demultiplexing of a 250Gbit/s OTDM signal can be carried out via a TPA detector in a specially designed semiconductor microcavity has been developed

- *Optical Sampling* - Experimental work demonstrating the use of a TPA microcavity for optical sampling of 100GHz signals with a temporal resolution of $1ps$, and system sensitivity of $0\ 009(mW)^2$ has been performed This value for the sensitivity is, to the best of our knowledge, the lowest ever reported for a TPA-based sampling system

Report Structure

This thesis is divided up into 7 different chapters with the layout as follows

- *Chapter 1* A brief overview of the development and advantages of optical communications is given, along with a description of the three major components of basic fibre optic system It concludes with an overview of the main performance evaluation techniques employed

- *Chapter 2* This chapter focuses on the various optical multiplexing techniques that can be employed to increase the capacity of optical networks Particular emphasis is paid to OTDM, with the main components of a bit-interleaved OTDM system described The main limitations to high-speed optical transmission are also covered

- *Chapter 3* Various methods for optical pulse generation are discussed, along with a presentation of experimental work concerning the use of the gain-switching technique for optical pulse generation It is shown that by using self-seeding or external injection techniques, the temporal jitter and chirp associated with gain-switched pulses are reduced, and the pulse wavelength can be altered This allows the development of a compact and stable tunable optical pulse source for high-speed data transmission We have demonstrated the generation of optical pulses with durations of 12-30ps, over 65nm with a SMSR exceeding 60dB

- *Chapter 4* This section examines the use of optical nonlinearities in fibres, semiconductors, and crystals for high-speed optical signal processing in an OTDM network These optical signal processing tasks include optical clock recovery,

pulse characterisation and optical demultiplexing A number of different techniques are introduced, along with a brief discussion about the various disadvantages associated with them, resulting in the need to consider alternative optical nonlinearities

- *Chapter 5* One such alternative optical nonlinearity for high-speed optical signal processing is Two-Photon Absorption (TPA) in semiconductors, and this is the main topic of this chapter In order to overcome the efficiency problem associated with TPA, a specially design semiconductor microcavity is employed The design and characterisation of the microcavity is performed in this chapter, the results of which show that the microcavity enhances the TPA response by over 3 orders of magnitude, and allows an optical bandwidth of approximately 700GHz As the response is wavelength selective, a TPA-based detector may find various applications in a WDM, OTDM and hybrid WDM/OTDM systems

- *Chapter 6* This chapter examines the use of a TPA microcavity for high-speed optical demultiplexing and pulse characterisation (optical sampling) A theoretical model of an optical demultiplexer based on that TPA microcavity is presented It suggests that error-free demultiplexing of a 250Gbit/s OTDM data signal is possible Experimental work is then presented for the optical sampling of data signals in excess of 100GHz, with the sampling scheme having a temporal resolution of around $1ps$ and a sensitivity of $0\ 009(mW)^2$, which is the lowest ever reported for a TPA-based optical sampling scheme

- *Chapter 7* A brief summary and analysis of the main points of the work presented in this thesis will be given

CHAPTER 1

Basic Optical Transmission Systems

Introduction

Telecommunications can be described as the transfer of information over long-distances (*tele* being the Greek for *far off*) using a transmitter, one or more receivers and a means of communications, such as air, satellite or cable. Optical communications makes extensive use of semiconductor technology in both the transmitter and the receiver, and propagates signals over optical fibre. This chapter will start with a brief overview of the development of optical transmission, from its first recorded use in ancient Greece to the development of the first laser and optical fibre in the 1960's. Next the main components of an optical communications system, namely the transmitter, transmission medium (optical fibre), and receiver, will be discussed. Finally the standard measures of performance that are used to evaluate a system will be introduced.

1.1   Early Telecommunications Developments

The use of light to convey information from one point to another is one of the earliest known forms of communications, dating back to ancient Greece, where, in the 8th century B.C., fire signals were used to warn of oncoming dangers or the announcements of certain events [1]. Only one type of signal was used, and this required *a priori* knowledge between the sender and the intended receiver. The addition of early relay stations were introduced in the fourth century B.C., allowing information to be conveyed over longer distances. By around 150 B.C. optical signals were encoded in relation to the alphabet so that any message could be sent. However, these systems were limited by speed of their human operators, transmission distance as they required light of sight, and the weather, as fog and rain made the transmission path unreliable. As such the development of optical communications networks came to a halt until Samuel Morse in 1838 invented the telegraph, which heralded the era of electrical communications. By incorporating Morse coding, the bit rate of the system could be increased to 10bit/s, and by using intermediary relay stations, communications over 1000km could be possible for the first time. The first successful transatlantic telegraph cable in 1866 and the invention of the telephone in 1876 [2] allowed analog electrical techniques to dominate

the world of communications for the next century or so By replacing the twisted wire pairs of these early communications networks with co-axial cables, the capacity of the system was increased to allow 300 voice channels to be transmitted simultaneously As these co-axial cables were limited to maximum bandwidths of 10MHz, primitive microwave carrier systems were introduced to further increase capacity, but it was not until the invention of the laser in 1960 that the revival of optical communication began

1.2 Lightwave System Development

Fiber optic communications systems were first deployed worldwide in the 1980's and have revolutionised the telecommunications sector, enabling enormous amounts of information to be carried at very high speeds over long distances The first major development in the realisation of optical communications came in 1960, when Maiman et al [3] demonstrated the first ruby laser, which theoretically offered a 5 orders of magnitude increase in capacity when compared the best available microwave systems at the time [2] However, it took another 6 years until Kao and Hockham [4] suggested the use of optical fibres for long-distance transmission Over the following years problems relating to the high loss associated with optical fibres were solved and the development of the first GaAs semiconductor laser allowed operation in the 0 8μm wavelength region at room temperature This allowed the first generation of lightwave systems to be become commercially available in 1980 [2] These operated at 45Mbit/s and allowed repeater spacing to be increased to around 10km With the discovery of the zero-dispersion wavelength in fibre at 1310nm by Payne and Gambling in 1975 [5], attention quickly turned to the development of semiconductor-based optical sources and detectors at this wavelength By operating m the 1310nm transmission window, optical pulses were able to propagate over long distances without being affected by fibre-induced pulse broadening The development of InGaAsP semiconductor technology allowed the second generation of lightwave systems to be deployed, and combined with the use of single-mode fibres, 2Gbit/s transmission over 44km was experimentally demonstrated in 1981 [2]

The next major advance was that of increasing the spacing between repeaters By moving the operating wavelength of the system to 1550nm to coincide with the minimum loss window of standard fibre, and by using single mode lasers to reduce the effects of fibre dispersion, 2 5Gbit/s per channel data transmission became commercially available by 1990 These third generation lightwave systems allowed higher data rates over longer distances but were still restricted by the use of electronic repeaters every 60-70km This restriction was mitigated with the introduction of the optical amplifier (in the early 90's) and the use of WDM, which allowed the first fibre-optic link around the globe (known as FLAG Europe-Asia cable system [6]) to become operational in 1998 It comprises of a 27,000km optical link connecting many parts of Asia to Europe with

5

data rates up to 10Gbit/s These fourth generation systems have demonstrated the true potential of optical communications, with the ability to transmit large amounts of data over very long distances For example, scientists at the University of Paderborn, Germany have reported C-band transmission at a record aggregate data rate of 5 94Tbit/s over a distance of 324km [7]

1.2.1 Why Use Optical Fibre?

As can be seen from the brief overview given, lightwave optical communication using optical fibres has many advantages over other forms communications utilising electrical signals over copper cables These include

- *Low Transmission Loss and Wide Bandwidth* - With current loss < 0 2dB/km [8], optical fibre is ideal for long haul communications network as it allows for large repeater/amplifier spacing In addition, the potential bandwidth is around 50THz [9], which is 5 orders of magnitude greater than the maximum bandwidth of coaxial cables (500MHz)

- *Small Size and Weight* - As optical fibres are lightweight and flexible, installation is very easy and can occur in difficult places such as underground pipes or overhead ceiling-mounted trays

- *Immunity to Interference* - Optical fibres do not suffer electromagnetic interference found m electrical systems and it is easy to ensure that no interference is introduced when different fibres are bundled together in a cable

- *Electrical Isolation* - Since optical fibers are made from glass, which is an insulator, there are no ground loop effects, also as fibres do not create any arcing or sparking, they are attractive for use in the petrochemical industry and other hazardous environments

- *Signal Security* - As optical signals are confined within the waveguide, optical fibre communication is very secure, since any power fluctuation associated with cable splicing can be easily detected

- *Abundant and Inexpensive Raw Material* - The main component in the manufacture of optical fibre is silica which is found in ordinary sand, with the main expense associated with the removal of impurities

1.3 Basic Optical Communications System

A basic optical communications system is shown in Figure 1 1 and comprises of three main elements, a transmitter, an optical fibre link and a receiver

6
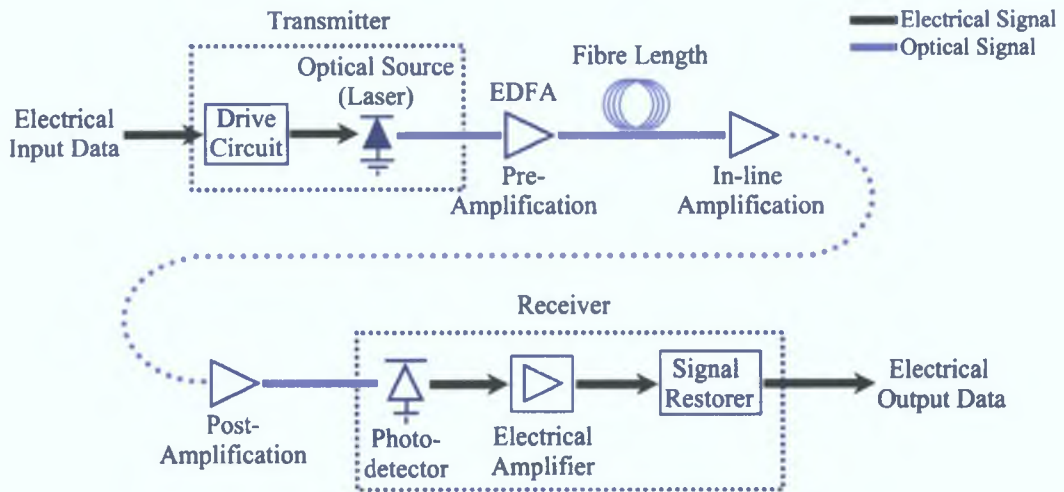
Figure 1.1: Schematic of a basic optical fibre network

1.3.1 Transmitter

The role of a transmitter in an optical communications network is to convert electrical data into an optical format that is suitable for transmission over optical fibres. The transmitter generally consists of an optical source and a modulator, though depending on the application and the source, the optical source can be modulated directly with electrical data. This scenario is shown in Figure 1.1 where the electrical data modulates the optical source via a drive circuit. For optical communications systems, semiconductor-based transmitters are preferred to solid-state, gas, and dye lasers since they allow direct modulation in the GHz frequency range by simply varying the drive current to the device, are smaller in size, have a higher efficiency, and are generally lower in cost [10].

Laser

The main operating principle of a laser diode is the radiative recombination of electron-hole pairings in the depletion region of a PN-junction, resulting in the formation of a photon. However, unlike a Light Emitting Diode (LED) where the phase of the emitted photons are random (spontaneous emission), emitted photons from a laser are at the same wavelength, phase, and polarisation, and travel in the same direction [11] as the incident photon (stimulated emission). These newly generated photons can then excite further bound electrons resulting in coherent optical gain. To ensure that stimulated emission dominates spontaneous emission, two conditions have to be met, namely the presence of optical feedback, and a high electron density in the excited state.

The optical feedback is provided by placing reflective facets at either end of the active region of the device forming a Fabry-Perot (FP) resonator cavity, which provides optical feedback in the longitudinal direction (see Figure 1.2). This increases the pho-

ton density inside the cavity providing a gain mechanism to overcome cavity losses due to poor waveguide confinement and material absorption. The rear facet is coated with a dielectric reflective layers, while the front facet is partially reflective. As mentioned,
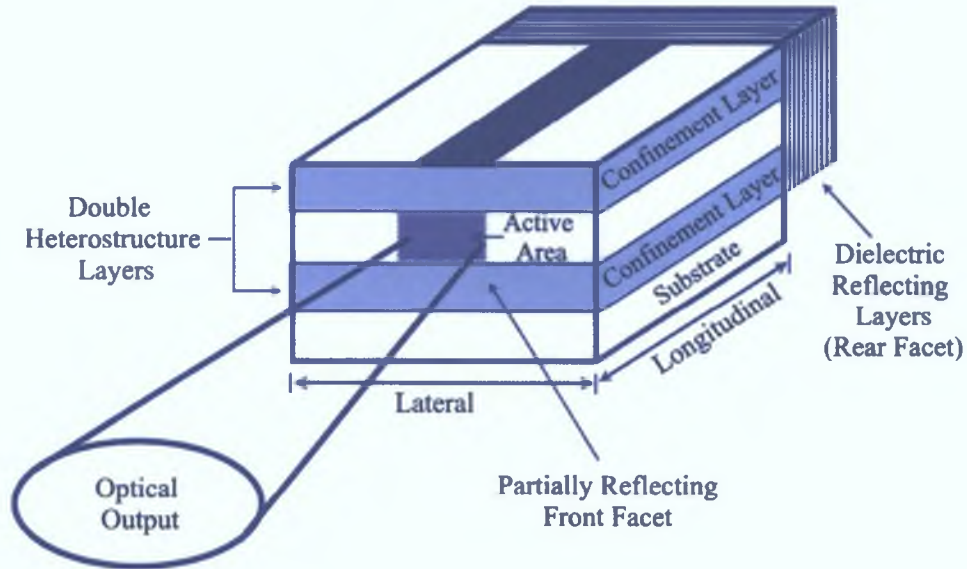
Figure 1.2: Schematic of a double heterostructure Fabry-Perot resonator cavity

a sufficiently high electron density in the excited state is also required for stimulated emission. This is achieved through external electrical pumping which results in population inversion, and allows stimulated emission to become the dominant radiative recombination process.

The optical radiation within the FP cavity comprises of longitudinal modes, which are related to the cavity length, and determine the structure of the frequency spectrum of the emitted optical radiation. The laser cavity is resonant at a number of different frequencies, determined by:

$$f_m = \frac{mc}{2nL} \tag{1.1}$$

with mode spacing:

$$\Delta f_c = \frac{c}{n2L} \tag{1.2}$$

were m is the number of modes present, n is the refractive index of the active layer of the device and $2L$ is the round trip time within the laser cavity. However, the output spectrum only contains those wavelengths where the gain exceeds the losses within the cavity (gain curve). The shape of the gain curve depends on a number of different mechanisms that are responsible for spectral broadening such as collision broadening, natural damping and Doppler broadening [12]. In Figure 1.3 (a) the passive cavity modes are shown as a comb of frequencies with only some of the axial modes fitting

8
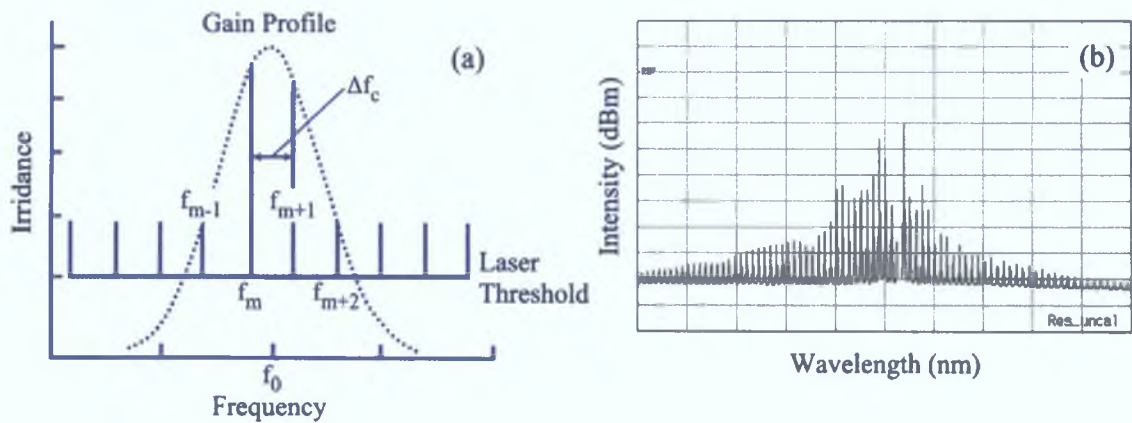
Figure 1.3: (a) Illustration of the gain curve of a Fabry-Perot laser diode; (b) Optical spectrum of 1.5μm Fabry-Perot laser diode under CW conditions

into the gain bandwidth of the laser diode [13]. As can be seen from Figure 1.3 (b), a standard FP laser diode spectrum contains a number of different wavelength modes. These propagate at different speeds when launched into the fibre as the refractive index of the fibre is a function of the wavelength. This can result in pulse broadening, and if left unchecked, can cause interference being introduced into adjacent data channels (Crosstalk), degrading overall system performance.

Even though the first lasers were demonstrated in 1960 [3], it was not until the mid-1970's that the first GaAs semiconductor laser diode operating at room temperature was demonstrated [14]. These devices operated mainly in the 850nm wavelength range. With the development of sophisticated lattice matching techniques new quaternary devices, such as InGaAsP, allowed emission wavelengths to cover both the 1310nm and 1550nm transmission windows [15]. Such a broad range of emission wavelengths, combined with improvements in fibre and amplifier technology, should allow the development of communications systems that will be able to operate continuously between 1200nm and 1700nm, allowing a possible transmission bandwidth of over 60THz per optical fibre [16].

Laser Characteristics

There are a number of important parameters that effect the usefulness of a laser diode in a high-speed optical communications system. These include:

- *Output Spectrum / Linewidth* - As already mentioned in the previous section, a standard FP device contains a number of different wavelength components, each traveling at a different velocity, which can result in pulse broadening during propagation in the fibre. There are a number of different ways to reduce the width of the output spectrum, including reducing the length of the laser cav-

ity so that the mode spacing is greater than the width of the gain curve of the device. Unfortunately this reduces the maximum power, and makes the device hard to handle [1]. An alternative is to apply a wavelength selective filter in the cavity, for instance, above the active region of the laser to suppress other longitudinal modes from reaching threshold. One such device is known as a Distributed Feedback Laser (DFB) laser diode, which employs a distributed feedback grating and enables the reduction of the spectral linewidth of the output to be less than 10MHz [17]. This reduced linewidth can significantly reduce the amount of pulse broadening incurred which makes DFB laser diodes highly attractive for use in high-speed optical communication systems.

- *Modulation Bandwidth* - The modulation bandwidth determines the maximum data rate that can be transmitted, and is an inherent property of the cavity materials and design, the drive current, as well as external parasitics associated with device contacts and supply leads to the device [18]. Modern commercially-available laser diodes have modulation bandwidths of the order of 10GHz or more, allowing the direct modulation of data rates in excess of 10Gbit/s.

- *Frequency Chirp* - Frequency chirp is defined as a variation of the emitted frequency as a function of time. During high speed direct modulation and pulse generation [10], the variation in the carrier density within the laser cavity results in a variation in the refractive index of the cavity [19], causing a variation in the emitted wavelength. The emitted wavelength can interact with chromatic dispersion (See Section 1.3.2) during fibre propagation resulting in pulse broadening and distortion, limiting the transmission distance.

Modulation

Modulation can be achieved either directly, where the drive current to the laser is varied by the electrical data to be transmitted, or externally, where the laser is operated at a constant power level and electrical data is encoded into optical form using a separate modulator. Direct modulation can be described by the dynamic relationship between the supply, annihilation, and creation of carriers and photons inside the laser cavity and is governed by the laser rate equations [20]:

$$\frac{dn}{dt} = \underbrace{\frac{J}{ed}}_{Injected\ Carriers} - \underbrace{\frac{n}{\tau_s}}_{Spontaneous\ Emission} - \underbrace{\frac{A(n - n_0)p}{1 + \epsilon p}}_{Stimulated\ Emission} \quad (1.3)$$

$$\frac{dp}{dt} = \underbrace{\frac{A(n - n_0)p}{1 + \epsilon p}}_{Stimulated\ Emission} - \underbrace{\frac{p}{\tau_p}}_{Carrier\ Recombination} + \underbrace{\beta n}_{Spontaneous\ Emission} \quad (1.4)$$

10

where n and p are the electron and photon densities, τ_s and τ_p are the carrier and photon lifetime, A is the gain constant, J is the injection current density, n_0 is the carrier density for transparency, β is the spontaneous emission factor, and ϵ is the gain compression factor. The gain compression factor must be included for analysis of the chirp and time dependent behaviour. By solving these equations, the chirp and output power waveforms can be obtained, and the necessary actions to minimise the amount of chirp on directly modulated optical pulses can be taken [16]. Direct modulation has a number of advantages including simplicity, cost, possibility of high output power, and low drive voltage, all of which are of important for systems operating with individual data channel rates of 2.5Gbit/s [21]. However, the major drawback with direct modulation, as already mentioned, is the chirp produced across the pulse [22]. This restricts the deployment of direct modulation in systems operating with individual channel data rates of 10Gbit/s and beyond. For such systems, external modulation should be employed.

External modulation involves operating the laser diode at a constant output power, and modulating the constant output externally with a modulator. As the laser is operated with a constant current, frequency chirp that is introduced in direct modulation is eliminated. The majority of modulators used for external modulation are based on a Mach-Zehnder Interferometer (MZI) devices, as very large modulation bandwidths in the order of 75GHz are possible [16]. The schematic of external modulation using a Mach-Zehnder interferometer is shown in Figure 1.4. The external modulator takes ad-
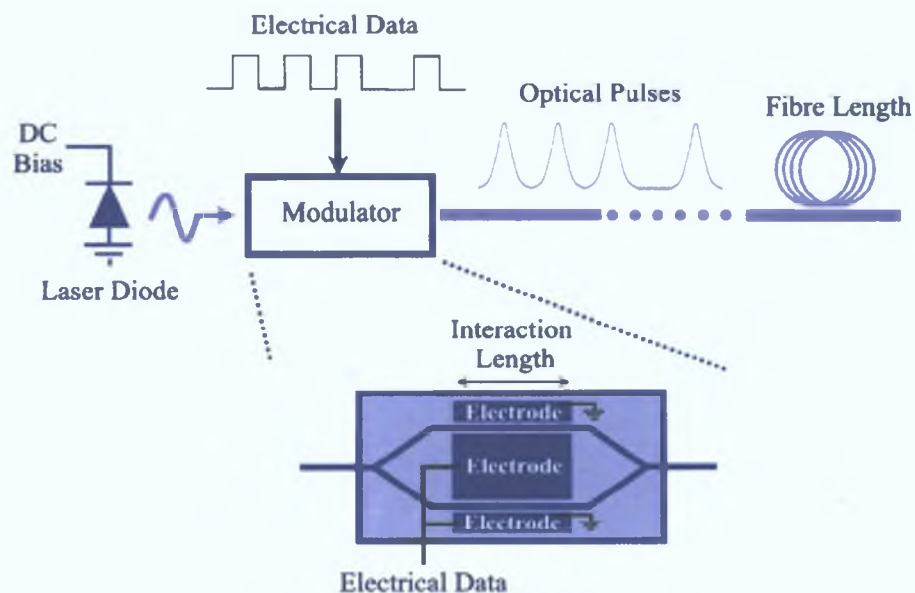
Figure 1.4: Schematic of external modulation using a Mach-Zehnder modulator

vantage of the electro-optic effect in lithium niobate to alter the optical path length and cause either constructive or destructive interference at the output node of the device. As lithium niobate has a high electro-optic coefficient [23], the application of a relatively

11

small voltage results in a change in the refractive index of the material. The structure of the device consists of a block of lithium niobate from which two waveguides are cut with electrodes placed on either side of the waveguides (along the interaction length). When light enters the device, it is split equally among the two branches and propagates over the same distance until recombining at the output node. An electric field, which is proportional to the electrical data being modulated, is applied, altering the path lengths between the two arms, resulting in either constructive of destructive interference at the output node. The data signal generated using external modulation is nearly chirp free, has low temporal jitter and allows bandwidths up to 40GHz [24]. The disadvantages of external modulation are increased cost and insertion loss associated with the use of a modulator.

1.3.2   Transmission

With the introduction of low loss fibres and optical amplification, one of the main limitations of optical fibre communications, namely high fibre attenuation limiting transmission distance, was significantly reduced. Attention quickly shifted to other factors that limit system performance, including dispersion and optical nonlinearities, which can limit data rates in single channel systems, and wavelength separation and repeater spacing in multi-wavelength systems.

Dispersion

There are two main categories of dispersion in optical communications systems; *Intermodal* dispersion and *Intramodal* dispersion. Both of these will result in the broadening of signals causing optical pulses to spread into adjacent bit slots, leading to errors at the receiver.

Intermodal dispersion, also known as Multi-mode Dispersion, occurs when the input waveform distorts during propagation as its energy is distributed among several fibre modes. As each propagating mode travels at a different velocity, different parts of the same wave arrive at the output at different times, spreading out the waveform. Multi-mode dispersion does not depend on the source linewidth ($\Delta\lambda$). Generally for long-haul, high bit rate optical transmission systems, Single-Mode Fibre (SMF) is employed. As such multi-mode dispersion is eliminated, but the signal still experiences signal broadening due to intramodal dispersion, with the two main forms of intramodal dispersion being *Material Dispersion* and *Waveguide Dispersion*. Material dispersion, also known as *chromatic dispersion*, arises when an electromagnetic wave interacts with the bound electrons of a dielectric medium, in this case the core/cladding boundary of the optical fibre. The response of the refractive index (n) of optical fibre is dependent on the frequency of the incident optical signal ($n(\omega)$). As all optical signals have a

12

finite spectral width, different spectral components will be affected by differing refractive indices and hence propagate at different velocities $(v = c/n(\omega))$. Depending on the operational wavelength, the dispersion parameter (D) of the fibre can be positive (normal dispersion regime), negative (anomalous dispersion regime), or zero, with D given by [25]:

$$D = \frac{-2\pi c}{\lambda^2}\beta_2 \qquad (1.5)$$

where β_2 is the Group Velocity Dispersion (GVD) term obtained from the Taylor's series expansion of the mode-propagation constant β. The zero dispersion point occurs at wavelength around 1310nm when $\beta_2 = 0$.

Waveguide dispersion arises from the fact that a small portion of the optical wave can successfully propagate in the cladding. However, due to the difference in refractive index between the core and cladding (necessary for total internal reflection), the signal propagating in the cladding will travel at a slower velocity compared to the signal propagating in the core, resulting in signal broadening. Main parameters associated with waveguide dispersion include the radius of the core and the difference in the core-cladding refractive indices. Recently fibre manufacturers have taken advantage of waveguide dispersion to shift the zero-dispersion wavelength in fibre to 1550nm (Dispersion Shifted Fibre (DSF)) to coincide with the minimum fibre attenuation window.

Nonlinear Effects

As the optical intensity of the incident signal increases, the nonlinear response of fibre becomes more prominent. This nonlinear response is becoming increasingly more important for the optimisation of optical network performance, especially as the transmission distances are being extended with an increase in launch power and the use of low loss fibres with small cross sectional core areas [2]. Generally, optical fibre nonlinearities can be grouped into two categories: those that arise due to the refractive index being a function of optical intensity (*nonlinear refraction*), and those that involve the transfer of optical power from one wavelength to another (*inelastic scattering*).

At low optical intensities, the response of the refractive index of the fibre is independent of the incident signal. However as the optical intensity increases, the response of the refractive index includes a nonlinear contribution (Kerr Effect). This is known as nonlinear refraction and can be described as:

$$n = n_0 + n_2 |E|^2$$

where n_0 is the refractive index at relatively low intensities, n_2 is the nonlinear index co-efficient, and $|E|^2$ is the optical intensity inside the fibre. This intensity dependence causes a number of nonlinear effects including *Self-Phase Modulation (SPM)* [26] and *Cross-Phase Modulation (XPM)* [27], both of which can contribute to spectral broad-

13

ening of the data signal, limiting the average optical power that can be transmitted and the length of fibre spans between amplifiers [28].

Nonlinear effects can result from the stimulated inelastic scattering in which the optical field transfers part of its energy to the nonlinear medium. Inelastic scattering results in the down-shift of the scattered light whereas elastic scattering, such as Rayleigh scattering, the scattered light remains at the same frequency. Two examples of inelastic scattering are *Stimulated Raman Scattering (SRS)* and *Stimulated Brilluoin Scattering (SBS)*. In general both will deplete certain optical waves and by means of frequency conversion, will generate interfering signals for other channels (crosstalk) [27]. In addition, SRS leads to increased power fluctuations and receiver noise, especially in long-haul fibre links where the signal is periodically amplified [2], whereas, SBS can cause feedback in the transmitter resulting in optical instabilities [26].

1.3.3 Photoreceiver

For normal telecommunications applications, single photon detectors, such as photodiodes, are the preferred detector choice due to their small size, high sensitivity and fast response times. The two main types of photodiodes are the PIN photodetector, and the Avalanche Photodiode.

PIN photodetectors are formed by sandwiching a very lightly doped n-type intrinsic (i) region between p-type and n-type materials. For normal operation, a reverse bias voltage is applied to ensure that the intrinsic region is fully depleted of carriers (depleted region). When photons of energy greater than the band gap energy ($E_{ph} > E_g$) of the device are incident on the intrinsic region, they are absorbed and their energy is used to excite an electron from the ground state (valence band) to the excited state (conduction band), thus generating photocarriers in the depleted region. The high reverse biased voltage applied to the intrinsic region results in the formation of a strong electric field which separates the electron-hole pairs, allowing current to flow in the external circuitry (photocurrent).

The absorption of light in the intrinsic region is highly dependent on the wavelength of the incident photon, as the energy of the photon must exceed the energy band gap for absorption. The upper wavelength limit is defined as:

$$\lambda_c = \frac{1.24}{E_g(eV)} \tag{1.6}$$

Longer wavelengths do not possess sufficient energy for single photon absorption, whereas shorter wavelengths are absorbed close to the surface of the photodetector and may recombine before they can contribute to the photocurrent [1].

Avalanche Photodiode's (APD)'s work on a similar principle to PIN photodetectors,

except that they have an inbuilt multiplication process, which amplifies the signal prior to the photocurrent reaching the external circuitry. When generated in the depletion region, the carriers cross a very high electric field region before reaching the metal contacts of the device. The electric field accelerates the photocarriers so that they gain sufficient energy to ionise bound electrons in the ground state upon colliding with them (*Impact Ionisation*). These newly generated photocarriers then gain enough energy to ionise further bound electrons from the electric field leading to an *Avalanche Effect*. Figure 1.5 shows the basic structure of an Avalanche Photodiode (APD) with the high electric field resulting in the avalanche effect between the n^+ and p regions.
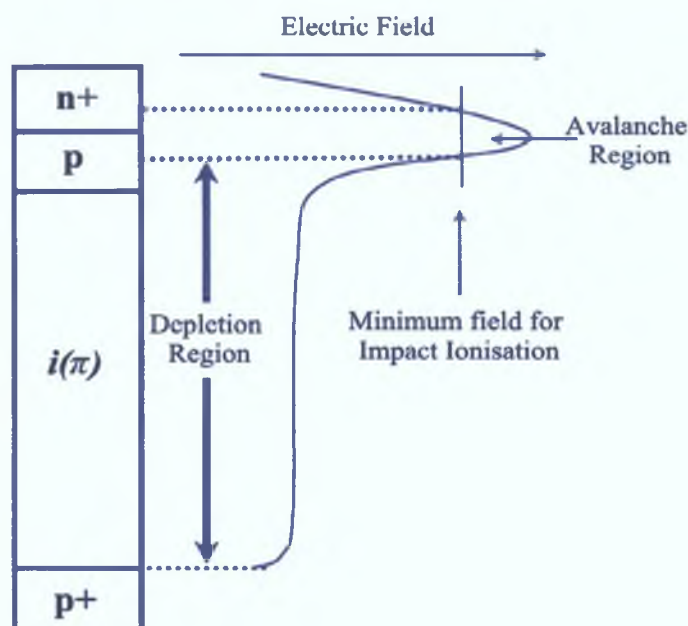
Figure 1.5: Illustration of an avalanche photodiode showing high electric field region

Photodetector Parameters

Some of the most important characteristics of a photodetector for use in high speed telecommunications include *quantum efficiency*, *response time*, *dynamic range* and *photodetector noise* of the device. The quantum efficiency, η, is defined as the number of electrons produced per incident photon of energy hf, and can be expressed as:

$$\eta = \frac{I_p}{q} \frac{P_0}{hf} \tag{1.7}$$

where P_0 is the incident optical power incident on the device, and I_P is the photocurrent produced. For practical devices, a quantum efficiency of 30 to 95% is expected [1], but for a high quantum efficiency a thick depletion layer is required to ensure high absorption of the incident photons. This results in a long delay time for carriers crossing

15

the depletion junction, slowing down the response speed of the device.

The response time depends on a number of different factors including the absorption co-efficient (α_s) of the depletion region, the width of the depletion region, and the resistance and capacitance associated with the PN junction and packaging of the device. The response time can be broken down into:

- *Transit Time* - The time taken to cross the depletion region depends on the carrier drift velocity and the width of the depletion region. The drift velocity is proportional to the magnitude of the applied electric field.

- *Diffusion Time* - This is the time taken for those photocarriers that are generated outside the depletion region to cross the depletion region and contribute to current flow. This is slow compared to the drift velocity associated with the transit time as they are generated outside the high electric field area.

- *RC Time Constant* - As practically all devices have some value of resistance and capacitance associated with their structure, the RC time constant will also contribute to the response time of a photodetector

Therefore in order to ensure that the response time of the device is as fast as possible, it is important to minimise the effects of carrier diffusion and maximise the fraction of carriers generated in the depletion region. Carrier diffusion can be minimised by ensuring that the majority of carriers are generated in the depletion region, while the transit time can be minimised by applying a high electric field and having a narrow depletion region. However, a narrow depletion region results in a lower quantum efficiency of the device. This again highlights the trade-off between having a high quantum efficiency and fast response time. Quantum efficiency and response time are a function of the band gap of the material used, the operating wavelength, the doping level and the thickness of the p, i and n regions of the detector.

As the photodetector is required to operate with very weak signals, the photodetector and other circuitry within the receiver are required to operate at a given Signal-to-Noise Ratio (SNR), which is defined as:

$$SNR = \frac{Signal\ from\ Photocurrent}{Photodetector\ Noise\ Power + Amplifier\ Noise\ Power} \tag{1.8}$$

In order to achieve a high SNR, it is necessary that the photodetector has a high quantum efficiency to generate as large a signal as possible, and that the noise within the receiver is kept as low as possible. As the quantum efficiency of most modern photodetectors is close to its maximum value, it is the noise that determines the minimum detectable optical power (sensitivity). For a standard PIN photodetector (no internal gain), noise arises from quantum (shot) noise, dark current and surface/leakage currents [1]

16

1.4 Performance Measurement

Two of the major measures of system performance are the maximum transmission data rate and the integrity of the data arriving at the detector. The primary measure of data integrity is the Bit-Error Rate (BER), with performance also measured using Eye-Diagrams, the SNR and the Q-Factor.

1.4.1 Bit-Error Rate (BER)

The BER is the ratio of the number of bits received in error at the detector to the total number of bits transmitted. The conventional method for BER testing utilises a pattern generator and an error detector [29]. The pattern generator produces either a user defined pattern, or a pattern intended to mimic random data (Pseudo-Random Bit Sequence (PRBS)). PRBS are classified according to length of the pattern, so $2^7 - 1$ corresponds to a repeating pattern length of 127 bits. The error detector either independently generates the same pattern or receives it from the pattern generator. The error detector is also synchronised to the clock signal from the pattern generator, and performs a bit-by-bit comparison between the data received from the pattern generator and that received from the system/device under test. Any discrepancies between the two are recorded as bit errors. Depending on the design of the system, a typical BER figure can vary between 10^{-12} and 10^{-15}. However, with the ever increasing data rates that are being transmitted, measuring the BER is becoming a more difficult and expensive task [30]. Therefore, alternatives such as the Q-factor are becoming more popular for the assessment of system performance.

1.4.2 Eye-Diagram

Whereas the BER gives a quantitative measure of system performance, the eye diagram indicates a qualitative measure of system performance. An eye diagram is the synchronised superposition of all possible bit sequences overlaid on top of one another, which can be achieved using the PRBS generator described above. Factors such as rise time and overshoot, dispersion, noise, jitter and InterSymbol Interference (ISI) [31] can be deduced from the size of the interior region of the eye pattern known as the eye opening. Figure 1.6 shows an example of an eye-diagram of a Non-Return-to-Zero (NRZ) data signal from a single channel back-to-back transmission system operating at 622Mbit/s. The width (Δt_e) of the eye opening indicates the amount of ISI that the system can tolerate, while the height (Δv_e) of the eye opening defines the noise margin of the system under test [32]. However, as with the BER measurement, the eye generation relies upon the synchronisation/clock extraction from the incoming data, which, again as per the BER, is becoming a difficult and expensive process as the data rates continue to
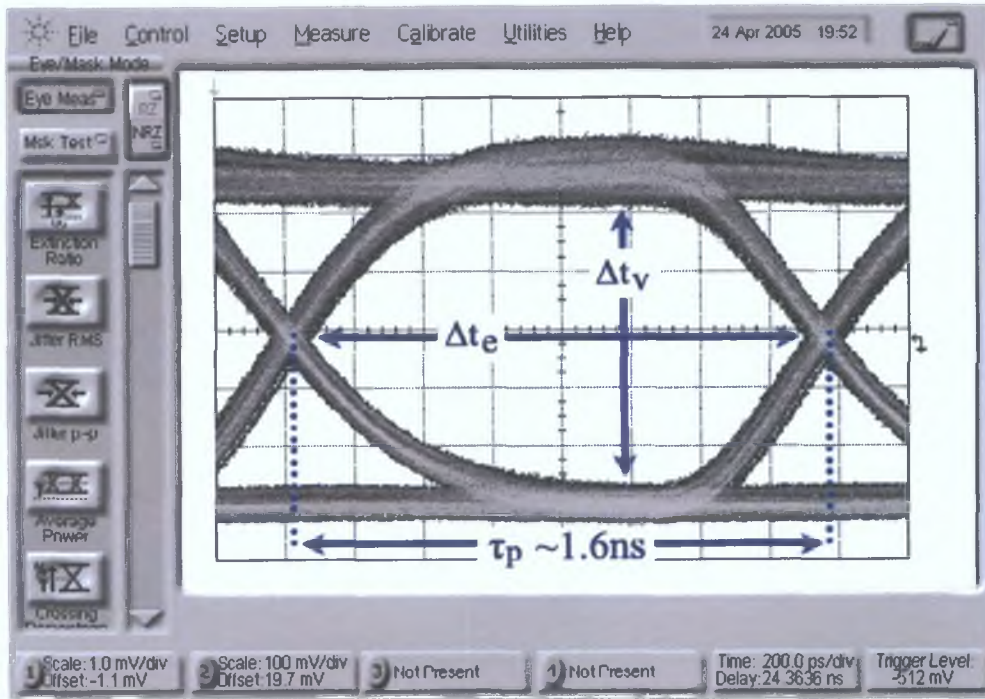
Figure 1.6: Eye diagram of a 622Mbit/s NRZ optical signal from a single channel back-to-back transmission system

increase.

1.4.3 Signal-to-Noise Ratio (SNR)

SNR is a measure of the signal strength relative to the background noise in the system measured in decibels (dB). Depending on the application, the SNR can be given in terms of electrical signal and noise, the Electrical SNR (SNR_E), or in terms of the optical signal and noise, the Optical SNR (SNR_O). The SNR is important as it is directly related to the BER in an optical communications network, with the BER, as mentioned, being a major indicator of system performance [29]. The (SNR_E) is defined as [33]:

$$SNR_E = \frac{S_E}{N_E} = \frac{v^2}{\sigma_v^2} \tag{1.9}$$

where v^2 is the power in an electrical waveform and σ_v^2 is the mean square average of the electrical noise power. Similarly the optical SNR can be expressed as [33]:

$$SNR_O = \frac{S_O}{N_O} = \frac{\left|\vec{E}\right|^2}{\sigma_o^2} \tag{1.10}$$

where $\left|\vec{E}\right|^2$ is the power in an optical signal and σ_o^2 is the mean square average of the optical noise power. The relationship between the SNR_E and the SNR_O is given

18

by [33]:

$$\sqrt{SNR_E} = SNR_O \qquad (1.11)$$

since the electrical power is related to the square of the voltage of the waveform and the optical power is related to the square of the magnitude of the electrical field $\left(\left| \vec{E} \right|^2 \right)$. The relationship between SNR and BER can be obtained using Gaussian statistics with results obtained through numerical integration [29]. Figure 1.7 shows a plot of the SNR versus BER using the standard normal distribution function NORMSDIST in Microsoft
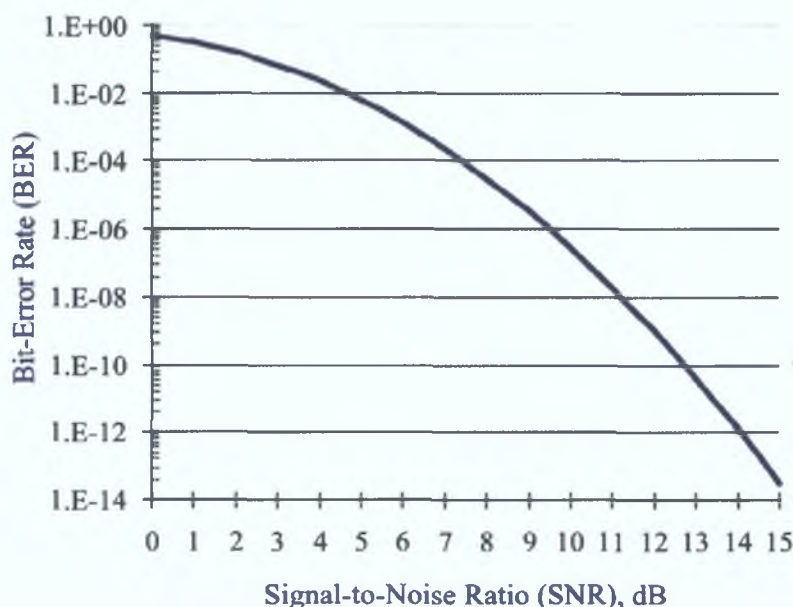
Figure 1.7: Plot of BER against SNR [29]

Excel. It can be seen from the plot that a SNR of 14dB corresponds to a BER of 10^{-12}.

1.4.4 Q-Factor

One other measure of system peformance is the Q-factor, which is the SNR at the decision circuit in terms of the voltage or current [34]. It takes into account the fact that the noise associated with the high and low signal levels in a binary optical digital communications system have a different values. The Q-factor combines these two SNR's into a single quantity providing a convenient measure of overall system performance. The Q-factor operates by setting an optimum threshold level where the probability of a bit error for the 1 and 0 level are equal [33]. Figure 1.8 shows the probability density functions for a binary system. It can be concluded that the probability of error is equal to the area (shaded area in Figure 1.8) under the density functions that extend beyond the threshold level. This area, and hence the BER, is determined by two factors, the voltage difference between V_L and V_H, and the standard deviations of the noise at each

19
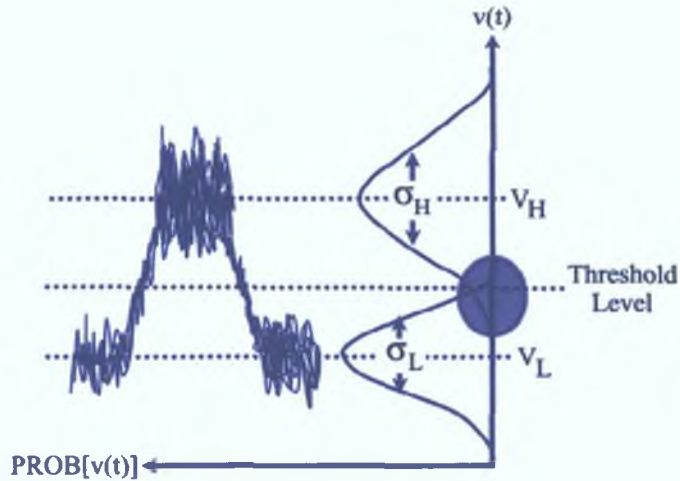
Figure 1.8: Probability of error for binary signaling [33]

level, σ_L and σ_H [2, 33]. Hence the Q-factor can be written as:

$$Q = \frac{v_H - v_L}{\sigma_L + \sigma_H} \tag{1.12}$$

A voltage histogram down the center of the eye can be measured with a digital sampling oscilloscope to estimate the Q value [34], allowing for a calculation of the SNR, and hence the BER from Figure 1.7.

Summary

This chapter began with a brief overview of optical communications, from early fire signals to the birth of modern optical communications in the 1960's with the demonstration of the first laser and optical fibre. The advantages of using optical fibre for transmission were then discussed, followed by a description of the three basic components of an optical communications network, namely a transmitter, fibre and receiver. With relation to each component, important operational characteristics that need to be considered if the devices are to used for high-speed operation were then outlined. Finally, the chapter concluded with a brief overview of some of the techniques used to determine and quantify the performance of an optical communications network.

The following chapter will examine the need to employ optical multiplexing techniques in an optical communications network, and will focus on one particular multiplexing scheme, namely Optical Time Division Multiplexing (OTDM). The main components of an OTDM network will be described, along with some of the main limitations to high-speed transmission.

Bibliography

[1] G. Keiser, *Optical Fiber Communications*. McGraw Hill, 3rd ed., 2000. ISBN 0-07-232101-6.

[2] G. P. Agrawal, *Fiber-Optic Communication Systems*. Academic Press, 1st ed., 1997. ISBN 0-471-17540-4.

[3] T.H.Maiman, "Stimulated Optical Radiation in Ruby," *Nature*, vol. 187, no. 4736, pp. 493–494, 1960.

[4] K.C.Kao and G.A.Hockham, "Dielectric-fibre surface waveguides for optical frequencies," *Proc. IEEE*, vol. 113, no. 7, pp. 1151–1158, 1966.

[5] D.N.Payne and W.A.Gambling, "Zero Material Dispersion in Optical Fibres," *Electronics Letters*, vol. 11, no. 8, pp. 176–178, 1975.

[6] FLAG Telecom, "About FLAG Telecoms History." HMTL Document, 2005. http://www.flagtelecom.com/About Flag/about history.htm.

[7] S.Bhandare, D.Sandel, B.Milivojevic, A.Hidayat, A.Fauzi, H.Zhang, S.K.Ibrahim, F.Wust, and E.Noe, "5.94Tbit/s, 1.49bit/s/Hz (40x2x2x40Gbit/s) RZ-DQPSK Polarisation Division Multiplex C-Band Transmission over 324 km," *IEEE Photonics Technology Letters*, vol. 17, no. 4, pp. 914–916, 2005.

[8] OFS, "Allwave Fiber - Product Description," 2006. http://www.ofsoptics.com/resources/1693849504410786fa5a28AllWave-117-web.pdf.

[9] D.K.Mynbaev and L.L.Scheiner, *Fiber-Optic Communications Technology*. Prentice-Hall, 1st ed., 2000. ISBN 0-13-962069-9.

[10] P. Vasil'ev, *Ultrafast Diode Lasers, Fundamentals and Applications*. Artech House Publications, 1st ed., 1995. ISBN 0-89006-736-8.

[11] A. Bar-Lev, *Semiconductors and Electronic Devices*. Prentice/Hall International, 1st ed., 1984. ISBN 0-13-806265-X.

[12] J.Wilson and J.F.B.Hawkes, *Lasers - Principle and Applications*. Prentice Hall, 1st ed., 1987. ISBN 0-13-523697-5.

[13] J.Hawkes and I.Latimer, *Lasers - Theory and Practice*. Prentice Hall, 1st ed., 1995. ISBN 0-13-521493-9.

[14] B. Labs, "About Bell Labs - Awards." HMTL Document, 2006. http://www.bell-labs.com/about/awards.html.

[15] B.R.Bennett, R.A.Soref, and J. Alamo, "Carrier-induced Change in Refractive Index of InP, GaAs, and InGaAsP," *IEEE Journal of Quantum Electronics*, vol. 26, no. 1, pp. 113–122, 1990.

[16] I. P. Kaminow and T. Li, *Optical Fiber Telecommunications IV A - Components*. Academic Press, 1st ed., 2002. ISBN 0-12-395172-0.

[17] ThorLabs, "PRO8000 DWDM Laser Modules." PDF Document, 2005. http://www.laser2000.se/datablad/thorlabs/8_channel_dwdm.pdf.

[18] K.A.Black, E.S.Bjorlin, J.Piprek, E.L.Hu, and J.E.Bowers, "Small-Signal Frequency Response of Long-Wavelength Vertical-Cavity Lasers," *IEEE Photonics Technology Letters*, vol. 13, no. 10, pp. 1049–1051, 2001.

[19] S.K.Shin, C.H.Kim, and Y.C.Chung, "Directly Modulated 2.5Gb/s x 16-channels WDM Transmission Over 640km of Single-Mode Fiber Using Dispersion Compensating Fiber," *IEEE Photonics Technology Letters*, vol. 11, no. 6, pp. 742–744, 1999.

[20] K.Y.Lau, "Gain switching of semiconductor injection lasers," *Applied Physics Letters*, vol. 52, no. 4, pp. 257–259, 1988.

[21] I. Tomkos, R. Hesse, N. Madamopoulos, C. Friedman, N. Antoniades, B. Hallock, R. Vodhanel, and A. Boskovic, "Transport Performance of an 80-Gb/s WDM Regional Area Transparent Ring Network Utilising Directly Modulated Lasers," *IEEE Journal of Lightwave Technology*, vol. 20, no. 4, pp. 562–573, 2002.

[22] R.A.Griffin, "Opto-Electronic Transmission and Receiver Hardware," in *Lasers and Electro-Optics Society Annual Meeting (LEOS2005)*, pp. 234–235, 2004.

[23] I. P. Kaminow, *Optical Fiber Telecommunications II*. Academic Press, 2nd ed., 1998. ISBN 0-12-497351-5.

[24] B. Guenther and D. Steel, *Encyclopedia of Modern Optics*. Elsevier, 1st ed., 2005. ISBN 0-12-227600-0.

[25] R.Ramaswami and K.N.Sivarajan, *Optical Networks - A Practical Perspective*. Morgan Kaufmann Publishers, 2nd ed., 2002. ISBN 1-55860-655-6.

[26] G. P. Agrawal, *Nonlinear Fiber Optics*. Academic Press, 2nd ed., 1995. ISBN 0-12-045142-5.

[27] A. R.Chraplyvy, "Limitations on lightwave communications imposed by optical-fiber nonlinearities," *IEEE Journal of Lightwave Technology*, vol. 8, no. 10, pp. 1548–1557, 1990.

[28] K. Taira and K. Kikuchi, "Subpicosecond Pulse Generation Using an Electroabsorption Modulator and a Double-Stage Pulse Compressor," *IEEE Photonics Technology Letters*, vol. 15, no. 9, pp. 1288–1290, 2003.

[29] Maxim Integrated Products, "Physical Layer Performance: Testing the Bit Error Ratio BER," pdf document, Maxim, http://pdfserv.maxim-ic.com/en/an/3419.pdf, 2004.

[30] M Westlund, H Sunnerud, M Karlsson, and P Andrekson, "Software-Synchronised All-Optical Sampling for Fiber Communications Systems," *IEEE Journal of Lightwave Technology*, vol 23, no 3, pp 1088–1099, 2005

[31] R L Jungerman, G Lee, O Buccafusca, Y Kaneko, N Itagaki, and R Shioda, "Optical Sampling Reveals Details of Very High Speed Fiber Systems," pdf document, Agilent Technologies, www agilent com, 2004

[32] S Haykin, *Communication Systems* Wiley, 3rd ed , 1994 ISBN 0-471-57178-8

[33] Maxim Integrated Products, "Optical Signal-to-Noise Ratio and the Q-Factor in Fiber-Optic Communication Systems," pdf document, Maxim, http //pdfserv maxim-ic com/en/an/4hfan902 pdf, 2002

[34] N S Bergano, F Kerfoot, and C R Davidson, "Margin Measurements in Optical Amplifier Systems," *IEEE Photonics Technology Letters*, vol 5, no 3, pp 304–306, 1993

CHAPTER 2

High-Speed Optical Transmission

Introduction

Due to the continued growth of the Internet and the introduction of new broadband services such as e-commerce, video-on-demand and mobile telephony, there is a need for network providers to better utilise their installed fibre networks. One way to achieve this is to employ multiplexing techniques, where multiple data channels are transmitted simultaneously over a single optical fibre. This chapter will discuss the origins of multiplexing, the different multiplexing standards that are used, and discuss the two main optical multiplexing schemes carried out in the temporal and wavelength domains. A brief overview of the main components of an Optical Time Division Multiplexing (OTDM) system will be given, followed by a discussion of the various dispersive and nonlinear limitations that time and wavelength multiplexing suffer from. Finally the chapter concludes with a description of a new multiplexing technique that combines the merits of time multiplexing and wavelength multiplexing, and an overview of the main modulation formats that are employed in high-speed long-haul optical transmission.

2.1 Need for Multiplexing

As mentioned in Chapter 1, one of the major advantages of using optical fibre is the enormous bandwidth that it offers. By taking advantage of new manufacturing techniques, the absorption peak around 1400nm can be removed, allowing the low loss transmission window to extend from 1260nm to 1675nm uninterrupted [1]. The optical spectrum is divided up into a number of different wavelength bands, with Table 2.1 showing the band name, description and wavelength range. Current high-speed optical transmission is confined to the C-band due to the availability of optical amplifiers and the low loss transmission window around 1550nm still present in the majority of installed optical fibres [1]. Even by restricting transmission within the C-band, there is over 4THz of available bandwidth.

However according to [2], the amount of Internet traffic is set to exceed 5000Petabit per day by 2007, or, 27 times the amount of traffic that was transmitted per day in 2002. This increase is been accounted for by the predicted growth of new services such

24

Band	Description	Range (nm)
O	Original	1260-1360
E	Extended	1360-1460
S	Short Wavelength	1460-1530
C	Conventional	1530-1565
L	Long Wavelength	1565-1625
U	Ultra-Long Wavelength	1625-1675

Table 2 1 Spectral-band classification scheme

as E-commerce, video-on-demand and mobile gaming With such phenomenal growth predicted over the coming years, determining the most efficient way to maximise fibre usage is a critical consideration for network operators There are a number of different ways to increase the amount of bandwidth within the network, including

- *Installing more fibre* - Laying additional fibre cables, which requires substantial planning and investment

- *Increasing individual channel bit rate* - By increasing the data rate at which each channel operates can greatly increase the amount of data transmitted per second However this might require advanced technology that might not yet be commercially available

- *Increasing the number of data channels* - per optical fibre, known as *multiplexing* is another alternative for increasing the system bandwidth This takes advantage of existing fibre and only requires changing the equipment at the transmitters and receivers

Due to the cost advantages associated with only altering components at the transmitter and receiver ends of the network, multiplexing has become the preferred choice for the majority of network providers to increase data capacity

2.1.1 Early Multiplexing Techniques and Standards

While working on the invention of the telephone in the 1870's, Alexander Graham Bell realised that is was possible to send several notes simultaneously along the same wire if the notes differed in pitch By varying the combinations of the notes, Bell realised that is was possible to successfully recreate the human voice He called his invention the harmonic telegraph [3], and it laid the foundations for the development of the first frequency multiplexing scheme [4] However owing to pressure from investors and other inventors, Bell was forced to halt any further work on the harmonic telegraph and instead concentrate all his efforts on the development of the telephone

25

Two ways to achieve multiplexing are Frequency Division Multiplexing (FDM) and Time Division Multiplexing (TDM). Both of these techniques can be implemented in the electrical and optical domains; optical FDM is usually referred to as Wavelength Division Multiplexing (WDM), while TDM in the optical domain is usually referred to as Optical Time Division Multiplexing (OTDM).

One of the first applications of FDM was for the transmission of multiple voice calls over a single electrical cable. FDM operates by first filtering the voice signal before modulation to restrict the bandwidth from 0.3kHz to 3.4kHz. The carrier signal is then amplitude modulated by the voice signal, with one of the sidebands removed to conserve bandwidth. The analogue trunk circuit is then divided amongst 12 (or a multiple of 12) separate signals, with 4kHz separation between each channel, occupying the frequency range from 60 to 108kHz [4, 5]. At the receiver, a locally generated carrier of the same frequency as the suppressed carrier is used to recover the original voice signal. FDM was used extensively during the early deployment of the telephone network, but since the signals were transmitted in analogue form, impairments accumulated as the transmission distance and number of users increased [6]. This eventually led to the analogue voice signals being converted to digital form (via Pulse Code Modulation [5]) prior to transmission, resulting in FDM being replaced in 1962 by a digital multiplexing technique, called Electrical Time Division Multiplexing (ETDM) [3, 7]. Digital transmission allowed for improved transmission quality, while at the same time, reducing costs.

In ETDM, a number of lower speed (baseband) sub-channels are multiplexed in the time domain using electronics [8]. This high speed electrical signal is then converted into optical form and transmitted via optical fibre to the receiver. The signal is then first converted back into electrical form before being separated (demultiplexed) back into the individual baseband channels. Figure 2.1 shows a basic ETDM optical communications system operating at an aggregate data rate of 10Gbit/s [9]. At the transmitter, sixteen
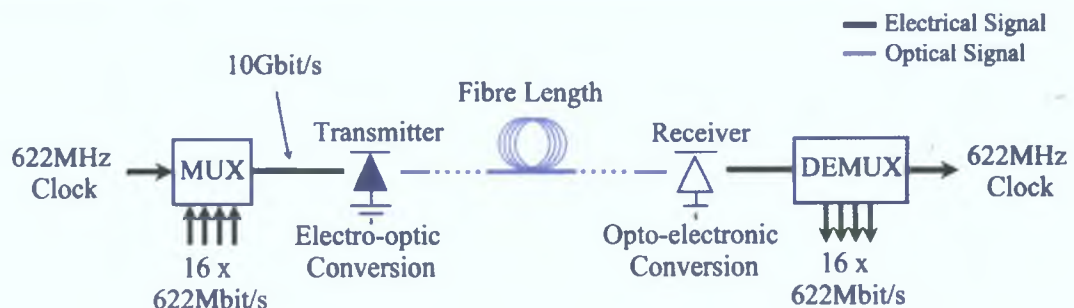
Figure 2.1: Schematic of a basic ETDM optical communications system operating at a SDH line rate of STM-4 (see Table 2.3) [9]

622Mbit/s data signals are electronically multiplexed together and then converted into

optical format using external modulation The resulting signal is then transmitted over fibre to the receiver were the optical signal is converted back into electronic form, before each channel is separated out in the demultiplexer One of the advantages of employing ETDM is that all the phase alignments are performed electrically, so no additional optical components are necessary and stable phase relationships are easily obtained [9]

With the advent of TDM, a number of different digital hierarchies were developed All are based upon first converting analogue voice signal to digital format using Pulse Code Modulation (PCM) By adhering to the Nyquist Theorem, the sampling of a voice signal occurs at 4kHz resulting in 8,000 samples per second Each sample is then encoded using 8 bits, resulting in a digital representation of an analogue signal at 64kbit/s Each 64kbit/s channel is then multiplexed together using TDM, and placed in timeslots within frames The frames also include provision for signalling and frame synchronisation There are two main schemes that define this process, European CEPT PCM-30 (E1) and North American PCM (T1), each making slightly different provisions for signalling and frame alignment

CEPT PCM-30 multiplexing hierarchy consists of combining 30 PCM channels forming a frame of 2 048Mbit/s (known as E1) The frame also includes two 64kbit/s timeslots used for frame alignment, administration and signalling Frames are delivered every $125\mu s$ in order to maintain real-time voice quality The next hierarchal level consists of combining 4 E1 frames, resulting in 120 PCM channels with overheads at a data rate of 8 448Mbit/s The various levels of the CEPT PCM-30 multiplexing hierarchy, along with data rate, and number of PCM channels, are shown in Table 2 2 [10]

Level	North America	Ch	Europe/CEPT	Ch
DS0	64kbit/s	1	64kbit/s	1
DS1	1 544Mbit/s(T1)	24	2 048Mbit/s(E1)	30
DS2	6 312Mbit/s(T2)	96	8 448Mbit/s(E2)	120
DS3	44 736Mbit/s(T3)	672	34 3368Mbit/s(E3)	480
DS4	247 176Mbit/s(T4)	4032	139 264Mbit/s(E4)	1920
DS5	-	-	564 992Mbit/s(E5)	7680

Table 2 2 Plesiochronous Digital Hierarchy for North America and Europe

The North American standard, PCM T1, differs from CEPT PCM-30 in that for the first level only 24 PCM channels are multiplexed together All of the 24 timeslots are used for PCM voice channels, with 1 extra bit used in frame alignment resulting in the base level T1 consisting of a 1 544Mbit/s signal $(24 \times 64kbit/s + 8kbit = 1\ 544Mbit/s)$ Again, as per CEPT PCM-30, each frame is delivered each $125\mu s$ to maintain the real-time voice signal As these early PCM networks had no major clock signal, each component within the system (buffers, multiplexers) had to generate their own clock signals, resulting in a number of different clock frequencies operating over the same network

As such, the PCM multiplexing hierarchy is also called Plesiochronous Digital Hierarchy (PDH) PDH based systems had no in-built monitoring or network control functions, and lacked any information relating to the quality of the traffic transmitted

The telephone companies soon realised that PDH was not very flexible and was costly to implement as it required separate multiplexers for each Digital Signal (DS) level Bellcore in the United States began work on an alternative hierarchy which resulted with the development of Synchronous Optical Network (SONET) [11] However SONET made no provision for the different multiplexing rates which operated in Europe so the ITU standardised an alternative scheme known as Synchronous Digital Hierarchy (SDH) SDH is based on a 155 52Mbit/s rate known as Synchronous Transfer Module-1 (STM-1) whereas SONET is based on 51 84Mbit/s, which is known as Optical Carrier-1 (OC-1) for optical communications systems, Synchronous Transport Signal-1 (STS-1) for electrical cable systems, and STM-0 in SDH The bit rates and corresponding number of voice channels for various SONET, optical transmission and SDH levels are shown in Table 2 3

SONET	Optical	SDH	Ch Data Rate (Mbit/s)	No Voice Channels
STS-1	OC-1	-	51 84	672
STS-3	OC-3	STM-1	155 52	2,016
STS-12	OC-12	STM-4	622 08	8,064
STS-48	OC-48	STM-16	2,488 32	32,256
STS-192	OC-192	STM-64	9,953 8	129,024
STS-768	OC-768	STM-256	39,813 12	516,096

Table 2 3 SONET, optical, SDH line rates and number of voice channels

The benefits of these new standards include the fact that a single multiplexer can perform the function of an entire PDH multiplexer mountain, equipment became standardised allowing for interoperability between items from different vendors, and that it helps setup the Operations, Administration, Maintenance and Provisioning (OAM&P) for high-speed transmission of information [12], including non-voice (data) transmission

As the demand for bandwidth continues to increase, it is expected that individual channel data rates will operate at 40Gbit/s (OC-768) by late 2006 to early 2007 [13] This will cause the formation of electronic bottlenecks in the multiplexer and demultiplexer, as well as the electro-optic and opto-electronic conversion points in the transmitter and receiver The bottlenecks are formed at these points as the electronics have to operate at the multiplexed data rate, with the speed of the electronics in the modulators and amplifiers [8] limited by the current electronic circuit design [14] One way to overcome these limitations is to use optical multiplexing techniques

2.2 Optical Multiplexing Techniques

Optical multiplexing can be carried out in the time domain, the wavelength domain, or by using a combination of the two resulting in a hybrid wavelength/time multiplexing schemes WDM is similar to FDM, except that each channel is assigned an individual wavelength, instead of frequency, with multiple wavelengths being transmitted simultaneously OTDM, on the other hand transmits multiple signals on a single wavelength by allocating each channel to a specific bit slot in the overall multiplexed data channel This section will describe in more detail the operation of WDM and OTDM

2.2.1 Wavelength Division Multiplexing (WDM)

The first experiments dealing with the possibility of sending multiple beams of light over long distances in optical fibre were undertaken by DeLange et al based in Bell-Labs in the late 1960's [15] The possibility of dividing up the optical spectrum into a number of non-overlapping wavelength bands was examined, with each wavelength band representing a single data channel Tomlinson in 1977 [16] reported a 3 channel wavelength multiplexer using a reflection grating and GRIN optics which could be used in conjunction with multi-mode fibres A nine channel single-mode grating wavelength-division multiplexing scheme, employing 2nm wavelength spacing was demonstrated in 1984 [17], and a 2-channel WDM experiment, operating at 3Gbit/s [18] carried out in the same year Since then, the number of transmitted channels and individual data rates per wavelength channel has grown considerably This has been accompanied with a reduction in the channel separation to improve the spectral efficiency (see below), allowing commercial WDM systems to transmit aggregate data rates in excess of 1Tbit/s

WDM technology can be divided into two different categories depending on the spacing between adjacent wavelength channels in the multiplexed signal Dense Wavelength Division Multiplexing (DWDM) operates in the C- and L-bands (see Table 2 1), and historically started by dividing up the standardised 100GHz International Telecommunication Union (ITU) grid of earlier WDM multiplexing standards [19] into smaller wavelength bands The current wavelength grid recommended by the Telecommunications Standardization Sector of ITU (ITU-T) [19] for DWDM has frequency separations of 12 5GHz, 25GHz, 50GHz, and 100GHz, translating to wavelength spacing of ~ 0 1, 0 2, 0 4, 0 8nm Thus for operation over the entire C- and L-bands, with 12 5GHz channels spacing, over 950 different wavelength channels could be transmitted If each operated at a channel data rate of 10Gbit/s, over 9Tbit of information could be transmitted per second However, most telecommunications providers limit transmission to the C-band in order to take advantage of current optical amplification techniques, and the low loss transmission window around 1550nm of currently installed optical fibre

The amount of information that can be transmitted is also a function of the spectral efficiency of the modulation format that is employed The spectra of various modulation formats differ in their bandwidths and shapes The number of bits per second that can be transmitted per Hz of bandwidth defines the encoding's spectral efficiency [20] Thus the maximum transmission capacity of optical fibre will be determined by the modulation format employed, the optical transmitter, and the optical filters employed within the network [11,21]

Coarse Wavelength Division Multiplexing (CWDM) employs channels with wavelength spacings greater than 20nm, extending from the O-band to the middle of the L-band (1271-1611nm) [22] By operating with such wide channel spacings, uncooled laser and wide passband filters can be employed for a number of cost-effective applications, such as in a Metropolitan Area Network (MAN), where the total transmission distance is relatively short and bit rates are low This allows reduced transmission power, and wider channel spacings, minimising the dispersive and nonlinear effects encountered during propagation [23] However, CWDM may not be suitable for long haul communications as the increased transmission power, higher bit rates, and longer amplifier spans may result in unacceptable levels of dispersion and degradation

A typical WDM network is shown in Figure 2 2 Each electrical channel is represented by a transmitter-receiver pairing operating at a different wavelength (λ_1, λ_2, , λ_N) The electrical data, which has already been electrically multiplexed together (STM-n), is modulated onto the optical carrier, with the optical signal from each laser combined using a passive fibre coupler The WDM signal is then post-amplified using an Erbium Doped Fibre Amplifier (EDFA), before being periodically amplified using in-line optical amplifiers Dispersion compensation may also take place at the in-line amplifiers to counteract the effect of dispersion encountered by the propagating signal in the fibre

At the receiver end of the network, the WDM signal is split separated out into individual wavelengths using an Arranged Waveguide Grating (AWG) The circuit structure of a typical AWG is shown in Figure 2 3 A multi-wavelength input signal enters the AWG and is split by diffraction into N-copies, where N corresponds to the number of wavelengths being transmitted simultaneously Each copy then propagates through an arrayed waveguide, the structure of which is designed so that adjacent waveguides have a specific length difference (ΔL) This introduces a corresponding phase shift between adjacent signals Upon exiting the arrayed waveguides, the signals are again spread by diffraction at a specified wavelength Accordingly, the signals of differing wavelengths are focused at different positions on the output side of the output slab waveguide, thereby extracting signals λ_1 through λ_n as shown in Figure 2 3 [24,25] The advantages of using an AWG are lower loss compared to a coupler filter combination, flatter passband, and easier to realise on an integrated-optic substrate [20] The indi-
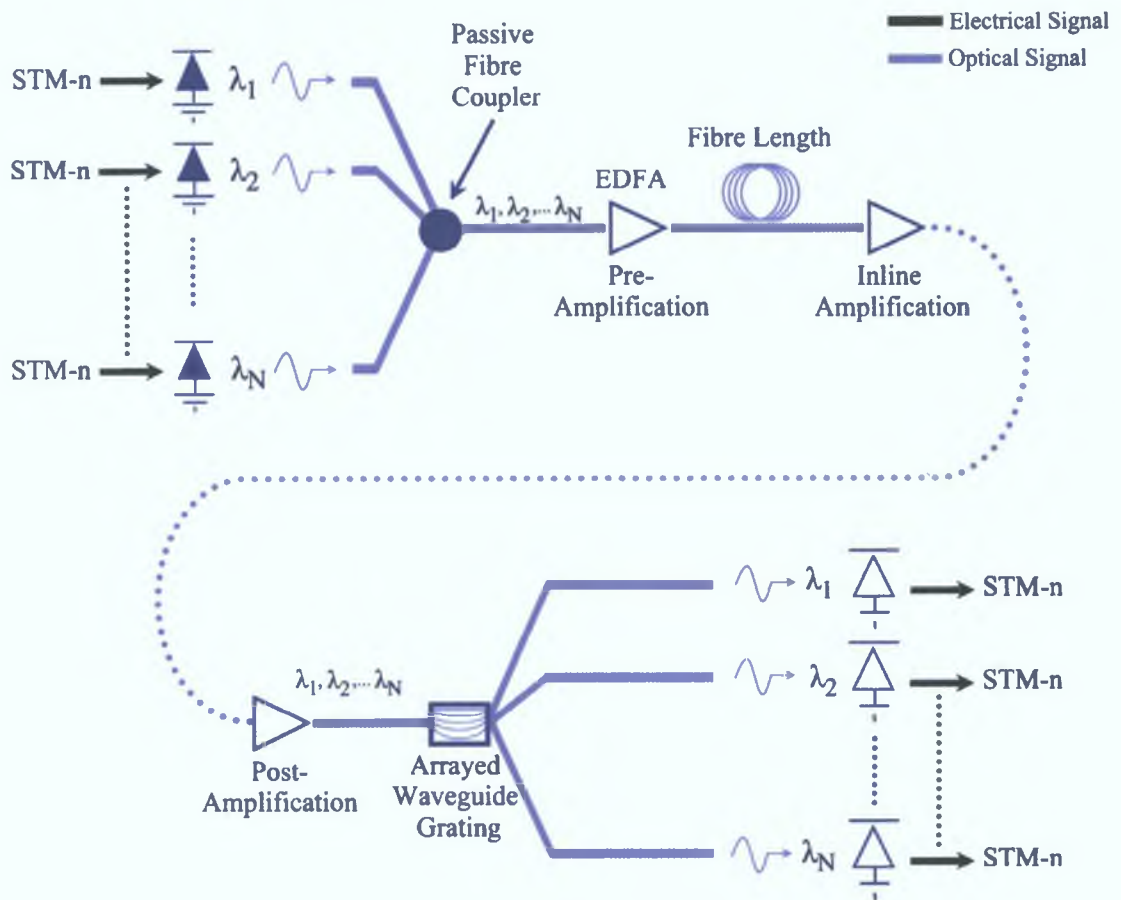
Figure 2.2: Schematic of a basic WDM optical communications system

vidual wavelengths are then incident on photodetectors, generating the electrical data signal for that wavelength channel.

Current long-haul telecommunications networks utilise DWDM for transmission, with current systems employing between 40-80 different wavelength channels over a single optical fibre, with individual channel rates of between 2.5Gbit/s to 10Gbit/s. Recent experimental work has demonstrated transmission of 5.94Tbit/s over 324km entirely within the C-band [26] by employing Return-to-Zero Differential-Quadrature Phase Shift-Keying (RZ-DQPSK) with polarisation-division multiplexing, and operating each of the 40 lasers at 160Gbit/s. This achieved a spectral efficiency of 1.49 bit/s/Hz and clearly shows how the spectral efficiency is a function of the modulation scheme employed.

2.2.2 Optical Time Division Multiplexing

Two of the most straightforward ways to increase the overall capacity of WDM systems are to increase the bit rate of the individual channels and to increase the number of channels transmitted by employing narrower channel spacing. The former is confined by the

31
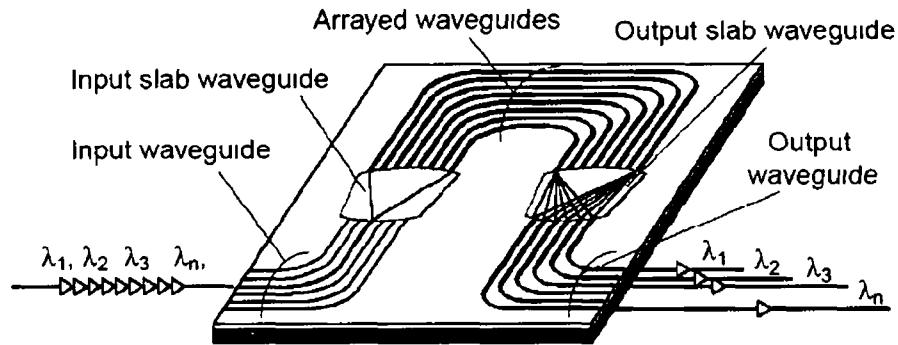
Figure 2 3 Optical waveguide circuit structure of an arrayed waveguide grating [25]

maximum speed at which the driver amplifiers and modulators can work at, whereas the latter can suffer from severe performance degradation due to the effects of optical nonlinearities, and the additional stringent requirements imposed on the transmitter and filters that are employed in the network

An alternative is to multiplex in the time domain Optical Time Division Multiplexing (OTDM) was first reported by Tucker et al in 1988 as a way to overcome the speed limitation of electronic devices in ETDM systems [14] OTDM allows Tbit/s aggregate data signals to be transmitted over a single wavelength by using ultrashort optical pulses to represent data and multiplexing these optical data pulses in the time domain, instead of the wavelength domain as in WDM There are a number of different techniques available to implement OTDM, including bit-interleaving and slotted TDM [27]

2.3 Bit-Interleaved OTDM

Bit-interleaving OTDM [28] multiplexes in the time domain by allocating each channel specific bit slots in the overall multiplexed signal The basic configuration for a bit-interleaved OTDM transmitter is shown in Figure 2 4

The main component of such a scheme is an ultrashort Return-to-Zero (RZ) optical pulse source often used in telecommunication systems [28] The optical pulse train generated is at a repetition rate R and is split into N copies of itself by a passive optical fibre coupler, where N corresponds to the number of optical channels to be multiplexed together Each copy of the pulse tram is then individually modulated with electrical data, also at a repetition rate R As the modulators are operating at the individual channel data rate, they are readily accessible using current electronic components [29] This overcomes the electronic bottlenecks that exist in ETDM (at the electro-optic conversion points in the transmitter) The resulting output from the modulator is an optical data channel where the electrical data is imposed on the short optical pulses For clar-

32
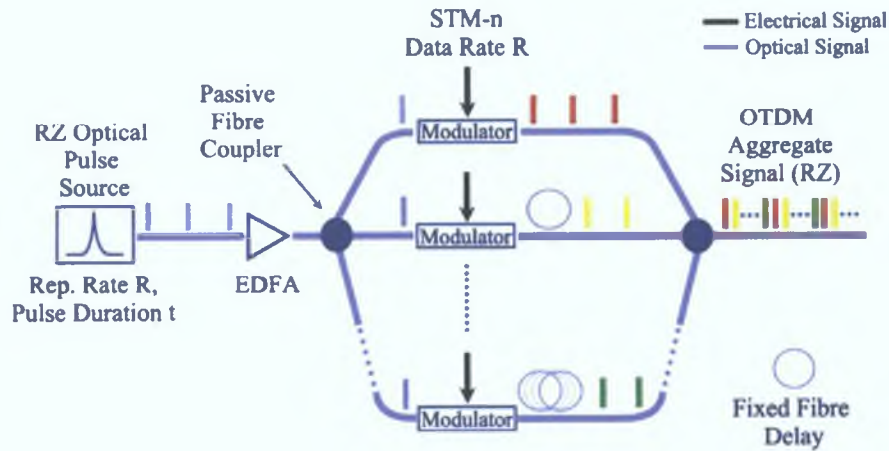
Figure 2.4: Schematic of a bit-interleaved OTDM system [28]

ity, each modulated data channel is symbolised in Figure 2.4 with a different colour (Red, Green and Yellow), remembering that OTDM operates on a single wavelength. The modulated optical signal then passes through a fixed fibre delay length which delays each channel by $\frac{1}{RN}$ relative to adjacent channels in the system [28]. This ensures that the optical data channels arrive at the output at a time corresponding to its allocated bit slot in the overall OTDM signal. The N optical data channels are then recombined using a second passive fibre coupler resulting in the OTDM data signal.

In order to demonstrate the differing requirements for WDM and OTDM systems, a simple example for a given capacity and channel number is now given. In data capacity terms, a 40Gbit/s OTDM transmission system is equivalent to 16 WDM channels, each operating at a base rate of 2.5Gbit/s. The bit period of a 40Gbit/s OTDM system is 25ps, resulting in approximately 8ps optical pulses being used for data representation[1]. For transform-limited Gaussian pulses, the corresponding spectral width of a 8ps pulse is 55GHz which, which in the wavelength domain corresponds to:

$$\lambda = \frac{c}{f}$$
$$\Rightarrow \frac{d\lambda}{df} = c\frac{d}{df}\frac{1}{f}$$
$$= -\frac{c}{f^2}$$
$$\Rightarrow d\lambda = -\frac{c}{f^2}df$$
$$\Rightarrow d\lambda = -\frac{\lambda^2}{c}df$$

(2.1)

Using this relationship, the 55GHz spacing at 1550nm corresponds to 0.44nm. Reference [30] describes a WDM system consisting of 16 channels, each operating at

---

[1]To avoid intersymbol interference, pulse duration should be kept to 1/3 of the bit slot

2 5Gbit/s It describes how the 16 different laser sources were operated at the ITU-standardized wavelengths with channel spacing of 100GHz Thus the spacing between two adjacent channels in this WDM system is greater than the bandwidth required for the entire OTDM system (100GHz versus 55GHz) Channel spacing of 12 5GHz (0 1nm) has been demonstrated in [31], but even with this channel spacing, a 16 channel system would still occupy 1 6nm, nearly 4 times that for the 40Gbit/s OTDM system described above Unlike WDM, OTDM does not require accurate control of filters or transmitter wavelengths and requires only a single laser source However there are a number of problems associated with OTDM, including synchronisation and demultiplexing These will be brief discussed later in this chapter, and returned to in more detail in Chapter 4

2.4 Main Components of a Bit-Interleaved System

Two of the most important issues relating to the implementation of a bit-interleaved OTDM system are the choice of a suitable optical pulse source and the demultiplexing of the high-speed OTDM data signal

2.4.1 Optical Pulse Source

An optical pulse source is one of the most important elements in a high-speed OTDM network since the overall data rate of the system is essentially determined by the temporal separation between data channels There are a number of important criteria that have to be met, including

- *Pulse Duration* - The duration of the optical pulse determines the upper limit of the bit rate that can be transmitted [32] and must be short enough to support the desired overall transmission rate [28] For Tbit/s OTDM systems sub-picosecond optical pulses are required, but as pulse durations are reduced to accommodate higher data rates, their optical spectra increase, which may increase the amount of dispersion [14]

- *Spectral Width* - In order to minimise the effects of fibre dispersion, and maximise transmission distance, optical pulses should be as spectrally pure as possible [32] A standard figure of merit which is employed is the time-bandwidth product, $\delta v \delta t$, with δt being the temporal width of the optical pulse and δv the spectral width in the frequency domain Ideally the pulse source is required to be transform limited, that is, the spectral width of the generated optical pulses are as small as possible for the associated pulse width [28] The transform-limited value is a function of the shape of the optical pulse, with 0 44 for a *Gaussian* and 0 315 for

34

a $sech^2$ [33], with the majority of pulse shapes having a transform limited value between 0 32-0 45 [29]

- *Timing Jitter* - Timing jitter is the random fluctuation in the pulse repetition period and can be responsible for degradation of the temporal resolution, thereby limiting the number of channels in an OTDM network [34] In order to ensure a BER of 10^{-12}, the rms value of the temporal jitter must be less than 7% the width of the temporal bit slot [35]

- *Stability* - As can be seen from Figure 2 4, bit-interleaving relies upon the use of different lengths of fibre to delay each multiplexed channels so that the optical pulse arrives at the output coupler at a time corresponding to its allocated bit slot It is necessary to consider the effects of temperature fluctuations will have on the optical path lengths, as a 10^oC change in temperature in a 10m long length of fibre results in a timing change of about 5ps [36] This can result in significant crosstalk between adjacent pulses One way to overcome this is to use planar lightwave circuits to integrate and control the delay lengths of the optical path [29]

- *Side-Mode Suppression Ratio (SMSR)* - The SMSR of the laser is defined as the difference in amplitude between the main spectral mode of a single-mode laser and the most dominant side mode, with a SMSR >30dB required for optical communications [37] If the SMSR of an optical pulse is degraded, the mode partition effect can interact with fibre dispersion resulting in amplitude noise that can degrade system performance [38]

- *Other Important Parameters* - The wavelength of the generated optical pulse should be tunable to allow for optimised propagating through the fibre [39] A variable repetition rate is also required to allow the pulse source to synchronise to other signals and multiplexing rate such as SDH and SONET [39]

The generation of optical pulses is not entirely confined to the telecommunications sector, but finds other applications in electro-optic sampling, time-resolved spectroscopy, and optical testing of materials and devices [40] Details regarding different pulse generation techniques will be given in Chapter 3

2.4.2 Optical Signal Processing Techniques

Given a suitable pulse source and the use of bit-interleaving, it is possible to generate a single channel operating at a data rate in excess of 100Gbit/s In order to operate at such high-speeds, it will be necessary to develop new signal processing techniques that will enable performance monitoring and high-speed demultiplexing operations Due to

their response occurring on time scales in the order of a few-femtoseconds (10^{-15}), optical nonlinearities that are present in optical fibres, semiconductor devices and optical crystals are being investigated for use in optical signal processing elements for future high-speed optical networks

To operate at data rates in excess of 100Gbit/s per channel, networks will require a sensitive and ultrafast technique for precise optical *signal monitoring* [32] The standard method of characterising and monitoring optical communications systems involves using a fast photodetector in conjunction with a high-speed sampling oscilloscope The opto-electronic conversion process in the photodetector places a limit on the overall bandwidth ($\approx 80GHz$ [41]) due to the speed limitations of current integrated electronic circuit design [42] This limits the maximum data rate of a single channel that can be accurately analysed to around 40Gbit/s Therefore, electrical sampling schemes are unable to accurately characterise high-speed data pulses used to represent data Critical information such as pulse duration, pulse separation and pulse rise-time, which are crucial for the optimisation of the networks performance, are distorted As a result interest has shifted to the use of nonlinear optical effects in the construction of Optical Sampling Oscilloscope (OSO) for performance monitoring of high-speed signals Such an instrument would become essential to both network designers and network operators for system development, testing and performance monitoring

The majority of optical switches that are installed today have an electrical switching core [43] Such devices, commonly known as O-E-O switches, rely upon the conversion of the optical signals to the electrical domain to perform the switching operation before converting the signal back into the optical format to continue on its journey [44] This results in the device being expensive to upgrade and maintain, as 90% of the cost associated with O-E-O switching resides in the electronics [45], especially the transponders, which have to be replaced every time the data rate is increased These transponders also consume vast amounts of power and heat, and occupy a large footprint [44] By employing *all-optical switching*, where the entire switching operation is carried out in the optical domain, cost and complexity can be vastly reduced as no high-speed electronics would be required, leading to considerable savings and improved reliability to the network operator Also the switching process would become data rate and data protocol independent [44], resulting in optical switching becoming the only core technology capable of supporting dynamic bandwidth allocation and cost-efficient transportation of high-speed optical data [43] Various methods to carry out all-optical switching and optical signal monitoring will be discussed in more detail in Chapter 4

2.4.3 Slotted TDM/Packet Interleaving

Unlike bit-interleaved OTDM in which each user is allocated a particular bit slot in each frame, slotted TDM [46] transmits a block of bits from a single data stream, and then accepts another block of bits from the same or a different user. This allows users to burst at very high-speeds (>100Gbit/s) onto the network whenever an empty slot comes available, providing improvements in terms of user access time, delay and throughput through statistical multiplexing of multiple user traffic [47]. A schematic of the filling of bit slots in slotted TDM scheme is shown in Figure 2.5.
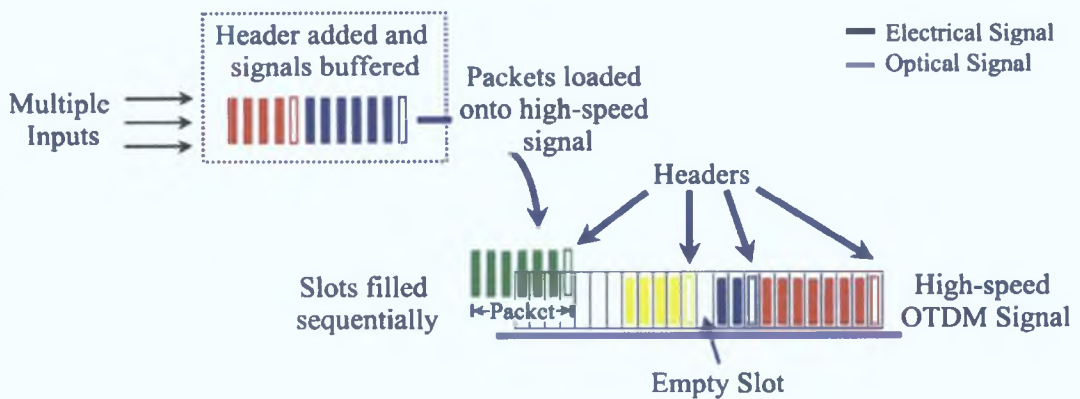
Figure 2.5: Schematic of a slotted TDM system [46]

As opposed to bit-interleaving, where data bits are identified by their position in the overall multiplexed signal, slotted TDM requires the use of packet headers for each transmitted block of data. Incoming bits are packaged with a header and are then transmitted at the higher output speed, with the receiver requiring the ability to process bits as they arrive at the raw data rate of the high speed line [46].

However there are a number of obstacles to successfully implementing slotted TDM. One problem is the need for optical buffering to queue packets until a particular user has finished and free data slots arrive [48]. This might result in long propagation errors and inefficient bandwidth sharing between users [49].

2.4.4 Optical Code Division Multiple Access

The provisioning of a dedicated wavelength channel per user can make WDM have an extremely poor spectral efficiency and thus a higher operational cost [50]. This is especially true for packet based services such as Internet usage, where the average data rate per user are frequently two orders of magnitude lower than the required peak data rate. Thus, interest has focused on alternative, more flexible multiplexing techniques, with Optical Code-Division Multiple Access (OCDMA) being one such multiplexing scheme.

In Code Division Multiple Access (CDMA), each individual user is allocated a specific address (code) that can be used to label bits that are either to be transmitted to the user or transmitted by the user. The encoding can be performed in the time or frequency domain. For time domain encoding, each data bit to be transmitted is defined by a code composed of a sequence of individual pulses, referred to as chips. Coded bits are then broadcast onto the network and will only be received by users having the receiver designed to recover data bits encoded with that specific address. For frequency domain coding, the carrier-frequency of the chips is altered for each user.

A number of different ways have been demonstrated and proposed to generate and decode the appropriate code sequence. Figure 2.6 uses a Superstructured Fibre Bragg Grating (SSFBG) for the encoding and decoding processes [51]. The grating imposes
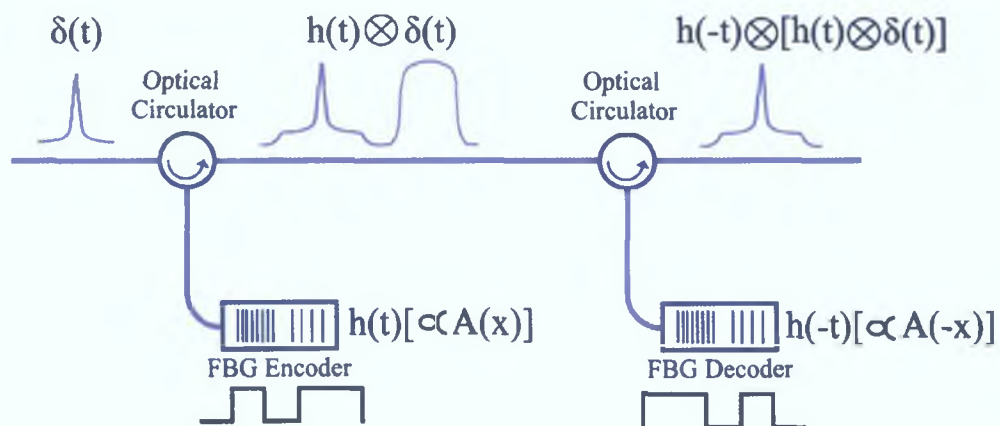
Figure 2.6: Schematic of pulse encoding and decoding using SSFBG for a OCDMA system [51]

its shape onto the impulse response with code recognition accomplished by matching the transmitted code with a decoder grating which has the exact time reversed impulse response to the encoding grating. When the encoder and decoder match, the filtering process results in the generation of the pulse which has the same shape as the codes autocorrelation function. Those pulses that do not match the decoding grating generate the cross-correlation function. Both the auto- and cross-correlation can then be displayed as oscilloscope traces.

2.5 Limitations to High Speed Optical Transmission

Even with the development and deployment of low loss optical fibres, the main limitations to network performance come from attenuation, dispersion and nonlinear effects (See Table 2.4). This section describes how attenuation, dispersion and optical nonlinearities limit WDM and OTDM performance and briefly discusses some of the mea-

sures that can be put in place to minimise their effects, and therefore maximise system performance

Limitation	WDM	OTDM
Attenuation	√	√
Dispersion		
GVD	√	√
Dispersion Slope	√	√
PMD	√	√
Optical Nonlinearities		
SPM	√	√
XPM	√	-
SBS	√	-
SRS	√	-

Table 2 4   Comparison of impairments in WDM and OTDM systems

2.5.1   Fibre Attenuation and Optical Amplification

Even with the introduction of low loss fibres, optical signals still need to be amplified periodically in order to overcome fibre attenuation due to Raleigh scattering and infra-red absorption Prior to the deployment of optical amplifiers in the 1990's, optical signals were electrically amplified, which involved conversion between optical and electrically formats, which was expensive and inefficient With the introduction of the first Erbium Doped Fibre Amplifier's (EDFA's) in the mid 1990's, optical gain in excess of 20dB over the entire C-band was possible, allowing longer fibre spans and transmission distances

With the deployment of optical amplifiers, the speed limitations associated with the opto-electronic conversion of electrical amplifiers was removed, allowing higher data rates to be transmitted However, EDFA's did impose a number of restrictions These include

- *Limited Gain* - The gain of an EDFA is limited to the C-band only which restricts the usually bandwidth to about 35nm More wavelength channels can be accommodated by decreasing the channel separation, but this can increase the possibility of optical nonlinearities degrading system performance

- *Flat Gain* - In order to amplify all wavelength channels by the same amount, the gain of the amplifiers needs to be flat over the entire C-band Generally this is not the case, resulting in different Optical Signal-to-Noise Ratio (OSNR) for different channels, degrading overall system performance [11]

39

- *Noise* - Accumulated Spontaneous Emission (ASE) introduced by the EDFA will contribute to the overall noise figure for the system This is especially a problem in long-haul communications systems, where the signal will be amplified many times during transmission This ASE limits the maximum reach and capacity of the system

There are a number of ways in which the restrictions imposed by the use of EDFA's on system performance can be minimised These include the use of either tellurite-based EDFA's or Raman amplifier's [11] These devices have bandwidths of 80nm and 92nm respectively [8], and should allow the number of channels to be increased in a WDM system However, this would involve the replacing of all amplifiers within the network

Transient gain control at each amplifier can help to maintain constant power per channel [23], while gain equalising filters after the EDFA can equalise the optical power in each channel as they are designed to approximate the inverse characteristic of the EDFA and the fibre span [52] Finally the amount of noise introduced can be reduced by shortening the fibre spans between repeaters, but this adds to cost An alternative is to increase launch power from the transmitters, but this can give rise to optical nonlinearities

2.5.2 Dispersion

As seen, the deployment of EDFA's allowed the upgrade and simplification of existing fibre systems by allowing higher data rates be transmitted over long distances by increasing the number of fibre spans possible without the need for electronic repeaters These helped to reduce the importance of attenuation in the design of optical communications system, resulting in pulse dispersion now being one of the major limiting factors for system designers

As mentioned in the previous chapter, chromatic dispersion arises from the refractive index of fibre being a function of wavelength resulting in different spectral components traveling at different speeds, causing the optical pulse to broaden Fortunately, due to its deterministic nature [53], there are a number of ways to counteract the effects of chromatic dispersion One method is to replace the installed fibre, which is generally a non-dispersion shifted variant with low dispersion in the 1310nm transmission window [54], with Dispersion Shifted Fibre (DSF) or Dispersion Flattened Fibre (DFF)

Dispersion shifted fibre shifts the zero dispersion wavelength to the 1550nm wavelength region by compensating the material dispersion encountered with increased waveguide dispersion This can be achieved by reducing the diameter of the core accompanied by an increase in the fractional index difference of the core and cladding [55] Dispersion flattened fibres have a low dispersion value over the entire low loss wave-

length region extending from the O-band right through to the L/U bands, by having a multi-layer index profile [55] The major drawback associated with replacing the installed fibre network would be the cost

An alternative to totally replacing all installed optical fibres is to employ *Dispersion Management* which varies the amount of positive and negative dispersion of the fibre throughout the fibre span by employing different types of fibres [28], such as Dispersion Compensating Fibre (DCF) This involves including in the transmission path a length of fibre which is chosen to obtain a negative dispersion that is equal in magnitude to the accumulated positive dispersion encountered by the pulse in standard single mode fibre [54] The length of compensating fibre can be placed at the transmitter, receiver or at any point along the transmission path, with an additional loss encountered being compensated by the EDFA's that are already present within the system Initial designs of DCF only permitted total dispersion compensation for one particular wavelength, which made it unsuitable for multi-wavelength systems [56] Today, DCF can be designed not only to compensate for bulk dispersion but also for the fibres dispersion variation with wavelength (dispersion slope) and slope mismatches between DCF and transmission fibre (dispersion curvature) [57]

Polarisation Mode Dispersion (PMD) is another limiting factor in optical communications network, especially when the optical data rate per channel exceeds 10Gbit/s [58,59] It results from the fact that single-mode fibres actually support two degenerate modes in orthogonal directions These modes are known as the two Principal States of Polarisation (PSP) of the fibre In a perfectly circular fibre, these two orthogonal modes travel at the same velocity However due to imperfections in the fibre fabrication process, incorrect installation and changes in ambient conditions, installed fibres are locally [58] causing each mode to propagate at different velocities resulting in pulse spread [60] This allows first-order PMD to be represented by a Differential Group Delay (DGD) between two PSP, which can be compensated for by delaying one state of polarisation with respect to the other [61] Unfortunately unlike chromatic dispersion, PMD is a random process which varies along a fibre link due to temperature changes or mechanical stresses [61] making even first order compensation difficult Also as the DGD and PSP are frequency-dependent, first-order compensators can only compensate for a specific channel at any given time To compensate for PMD in WDM systems, the data channels have to be first demultiplexed, with each channel compensated for individually, which increases cost and complexity [61] Considerable research is currently been undertaken to develop techniques that can simultaneously compensate PMD in a number of WDM channels without the need to demultiplexing [61,62]

41

2.5.3 Nonlinear Effects

With the introduction of optical amplification and dispersion compensation methods, the effects of optical nonlinearities on system performance could no longer be ignored In a typical high capacity, long-haul transmission systems, it is desirable to launch the highest signal power possible in order to maximise performance However, as the launched power of the individual channels is increased, combined with an increase in the number of channels transmitted per fibre, the impairments resulting from optical nonlinearities will limit the overall system performance [11] As a result, these non-linear effects impose limits on the amount of optical power per channel, the number of channels and spacings between them, the maximum transmission distance, the effects of chromatic dispersion and the modulation format employed

Optical nonlinearities in fibre can be classified into two categories those arising from the *nonlinear index of refraction* (Kerr Effect) and those resulting from *stimulated scattering* (Raman and Brillouin)

Nonlinear Refraction

Nonlinear refraction in optical fibres results from the Kerr effect where the response of the optical fibre is a function of the optical intensity, which results in an intensity dependent phase shift across the pulse The propagation of short optical pulses in single mode fibres can be described using the Nonlinear *Schrodinger* Equation (NLSE)

$$\frac{\delta u}{\delta z} + \frac{i}{2}\beta_2\frac{\delta^2 u}{\delta t^2} + \frac{\alpha}{2}u = i\gamma|u|^2 u \tag{2 2}$$

where u is the normalised pulse amplitude, z is the propagated distance in the fibre, β_2 is the Group Velocity Dispersion (GVD) value of single mode fibre, α is the fibre loss and $|u|^2$ is the pulse power γ is the fibre nonlinear co-efficient, and is defined as

$$\gamma = \frac{n_2\omega_0}{cA_{eff}} \tag{2 3}$$

where ω_0 is the optical carrier frequency of the pulse and A_{eff} is the effective core area of the optical fibre This dependency on the nonlinear refractive index (n_2) gives rise to 3 nonlinear phenomena, namely *Self-Phase Modulation (SPM)*, *Cross-Phase Modulation (XPM)* and *Four-Wave Mixing (FWM)*, which affect overall system performance

SPM, which is present in both single and multi-wavelength systems, refers to the self-induced intensity dependent phase shift that occurs across an optical pulse during propagation As the optical intensity in a pulse varies from the leading edge to the trailing edge, each part of the pulse will experience a different optical phase shift (due to the nonlinear refraction) As frequency is defined as being the rate of change of phase

42

with respect to time, SPM-induced phase shift is known as *frequency chirp*. The amount of phase shift encountered ($\Delta\phi$) after the pulse has propagated a distance L is given by:

$$\Delta\phi = 2\frac{\pi}{\lambda}Ln_2I \tag{2.4}$$

where n_2 is the nonlinear index co-efficient of the fibre and I is the optical intensity. This equation clearly shows that the amount of phase shift induced is proportional to the optical intensity. As the SPM-induced chirp increases with distance, new frequency components are being continuously generated resulting in spectral broadening of the optical pulse [63]. The extent of spectral broadening depends on the initial pulse shape and any initial chirp arising from the pulse generation process.

When combined with the effects of fibre dispersion (GVD), this self-induced phase modulation is converted to intensity modulation [11]. In the normal dispersion regime ($\beta_2 > 0, D < 0$), the SPM blue-shifted (higher frequency) components at the leading edge of the pulse are accelerated, while the red-shifted (lower frequency) components at the trailing edge are slowed down. This is shown in Figure 2.7. This results in
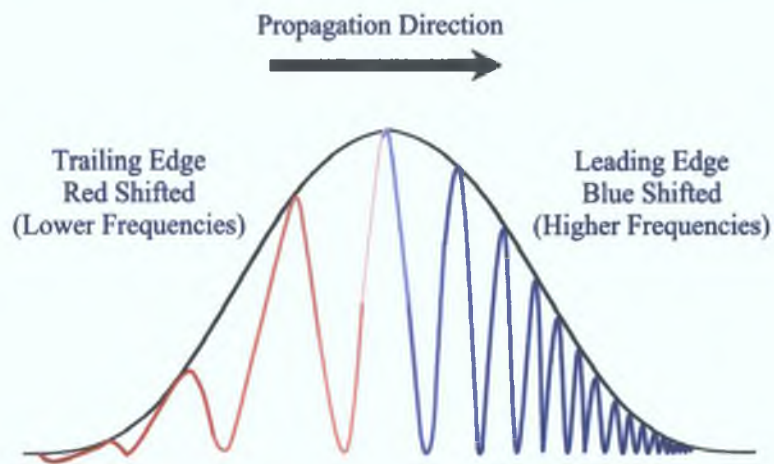
Figure 2.7: SPM-induced frequency chirp in a pulse propagating in the normal dispersion regime (D<0)

pulse broadening, which can increase both the ISI, and BER. Also for system employing modulation formats such as phase shift keying, SPM can severely affects system performance. However, in the anomalous dispersion regime ($\beta_2 < 0, D > 0$), pulse compression may take place, which can be advantageous for communications systems operating in this wavelength range.

XPM occurs when the phase of a signal in one channel is modulated by the intensity fluctuations of other channels propagating in the same fibre. It arises from the nonlinear refraction of the fibre depending not only on the intensity of that wave, but also on the intensity of other co-propagating waves [63]. Due to its reliance on other wavelengths

propagating in the same fibre, XPM is not present in a single wavelength OTDM transmission system In order to take into account this phase variation introduced by other channels, Equation 2 2 can be written as [11]

$$\frac{\delta u_s}{\delta z} + \frac{i}{2}\beta_2 \frac{\delta^2 u_s}{\delta t^2} + \frac{\alpha}{2}u_s = i\gamma \left(|u_s|^2 + 2\,|u_p|^2\right)u_s \tag{2 5}$$

where u_s is the amplitude of the signal of interest and u_p is the amplitude of a interfering signal, assuming the channels are linearly polarised Therefore the XPM phase shift induced on channel s due to channel p over a propagation distance Δz is

$$\Delta\phi_{XPM} = 2\gamma P_P \Delta z \tag{2 6}$$

with P_P being the power of the interfering channel p By comparing Equations 2 2 and 2 5 XPM introduces twice as much distortion as SPM It originates from the counting of terms in the expansion of the nonlinear polarization [63] The overall affect of XPM, as per SPM, strongly depends upon whether the amplitude or the phase is modulated when the information is transmitted When the information is transmitted through amplitude modulation and demodulated using direct-detection, the nonlinear phase shift introduced by XPM is of little consequence However for phase modulation system, where coherent demodulation is used, such phase changes can severely limit the system performance [63] Overall, the contribution of XPM can become large as the number of different wavelength channels increases

The third nonlinear effect that arises due to the nonlinear refraction is Four-Wave Mixing (FWM) Four-Wave Mixing (FWM) is the nonlinear process in which three waves of frequency f_i, f_j, f_k interact through the third order electric susceptibility of the optical fibre to generate a new frequency component f_{ijk} [11], where

$$f_{ijk} = f_i + f_j - f_k \tag{2 7}$$

For a WDM system, this happens for every possible choice of three frequency waves, resulting in the generation of hundreds of new frequency components by FWM in a DWDM system [64] For a system employing equally spacing between channels, FWM gives rise to crosstalk, degrading system performance [65] One way to overcome this is to employ unequal channel spacing However, this still does not resolve the signal depletion due to energy coupling between different channels [66]

Stimulated Scattering

At low power densities, optical fibre loss will be determined by factors including spontaneous Raman, Brillouin and Rayleigh scattering, absorption in the bulk material and

scattering at the core-cladding interface [67] Once the optical intensity has passed a certain threshold value (determined by factors including effective core area and α), Raman and Brillouin scattering become stimulated, introducing an intensity dependent gain or loss [67] to the system Stimulated Raman Scattering (SRS) arises due to the interaction between the incident signal and the silica molecules of the optical fibre [68] and can result in power fluctuations and receiver noise, degrading system performance Stimulated Brilluoin Scattering (SBS) arises due to the interaction between the signal and the acoustic vibrations within the fibre which causes some of the energy to the transferred to a backwards propagating signal [67] This causes power fluctuations even at relatively low intensities, resulting in fluctuations in the BER and SNR of the system [63]

Minimising Optical Nonlinearities

There are a number of ways to minimise nonlinear effects These include

- *Low Output Power* - By operating each channel at the lowest amount of power possible, the effects of fibre nonlinearities can be minimised However, even by doing this, as the number of transmitted WDM channels increase, then the total amount of power within the fibre also increases Also there is a minimum amount of power that must be transmitted in order to ensure that an adequate BER is achieved for the system

- *Change Fibre* - Replacing the standard single mode fibre with a variant with a larger effective core area would reduce the peak optical intensities within the fibre, but this would involve replacing the installed fibre network

- *Raman Amplification* - As already mentioned, Raman amplifiers have a much larger gain bandwidth when compared to standard EDFA's This would allow the spacing between adjacent wavelength channels to be increased Unfortunately the gain offered by Raman amplifiers is lower than that provided by EDFA's, requiring more amplifiers to be installed Also new dispersion compensation techniques over the broader bandwidth would have to implemented

- *Orthogonal Polarisation* - Employing orthogonal polarisation for adjacent WDM channels reduces the nonlinear contribution from XPM and FWM, but increases the effects of PMD

2.6   Hybrid WDM-OTDM System

There are a number of technological advances that will be required if WDM or OTDM are able to operate at future ultra-high data rates For WDM, electronic speed restric-

45

tions with current modulator and amplifier design limits the maximum individual channel data rate Therefore, the number of wavelength channels has to be increased to meet future demand for bandwidth Eventually the separation between adjacent channels will have to reduced to allow further expansion, increasing the possibilities of nonlinear effects reducing system performance For data rates above 1Tbit/s, OTDM requires the generation of sub-picosecond pulses which is not a straight-forward task Assuming transform-limited optical pulses are required to minimise dispersive effects, the spectral width of a sub-picosecond optical pulse would be of the order of 12nm, requiring low dispersion fibre or changes to the dispersion compensation techniques already installed in the network Also such a system would require strict timing accuracy $<100\text{fs}$ to avoid timing jitter

It is clear that operating either multiplexing scheme in the ultra-high-speed regime will require a number of technical problems to be resolved One solution is to employ a system that ensures that neither WDM nor OTDM is pushed to its limits This can be achieved using a combination of time and wavelength multiplexing, and was first proposed by Ali and Fussgaenger in 1986 [69] This hybrid approach works by utilising OTDM to enhance the bandwidth of a number of different wavelength channels in a WDM network by putting OTDM coding on top of the channels provided by WDM This would result in a smaller number of channels operating at a much higher data rate (>40Gbit/s) [70] Recently a consortium comprising of Alcatel, France Telecom and Deutsche Telekom (TOPRATE European Research Project) demonstrated 1 28Tbit/s transmission over 430km of single mode fibre using a hybrid system consisting of 8 wavelength channels, each operating at 170Gbit/s [71]

Figure 2 8 shows one possible layout for a hybrid multiplexing scheme It consists of 4 bit-interleaved OTDM systems each operating at a different wavelength ($\lambda 1, \lambda 2, \lambda 3, \lambda 4$) Each OTDM system consists of four different channels, each operating at 40Gbit/s resulting in a 160Gbit/s aggregate signal from each bit-interleaved system This results in an overall aggregate hybrid WDM/OTDM transmission rate of 640Gbit/s

To demultiplex out a single data channel, the hybrid signal would first be wavelength filtered and then time demultiplexed to select out the single data channel of interest [72] This approach would exploit the parallelism of WDM architecture and the speed of OTDM [72] with the resulting hybrid producing a highly flexible and spectrally efficient multi-terabit/s optical network

However as with increasing the capacity of WDM or OTDM networks, this hybrid approach does have a few problems of its own For the hybrid system described above, a 160Gbit/s data stream would have time slots approximately 6ps wide, requiring maximum optical pulse durations of 2ps to avoid interference from adjacent channels If this pulse was transform limited, then it would occupy 220GHz (assuming a Gaussian pulse shape) in the spectral domain requiring channel separation in the order of 400-600GHz

46
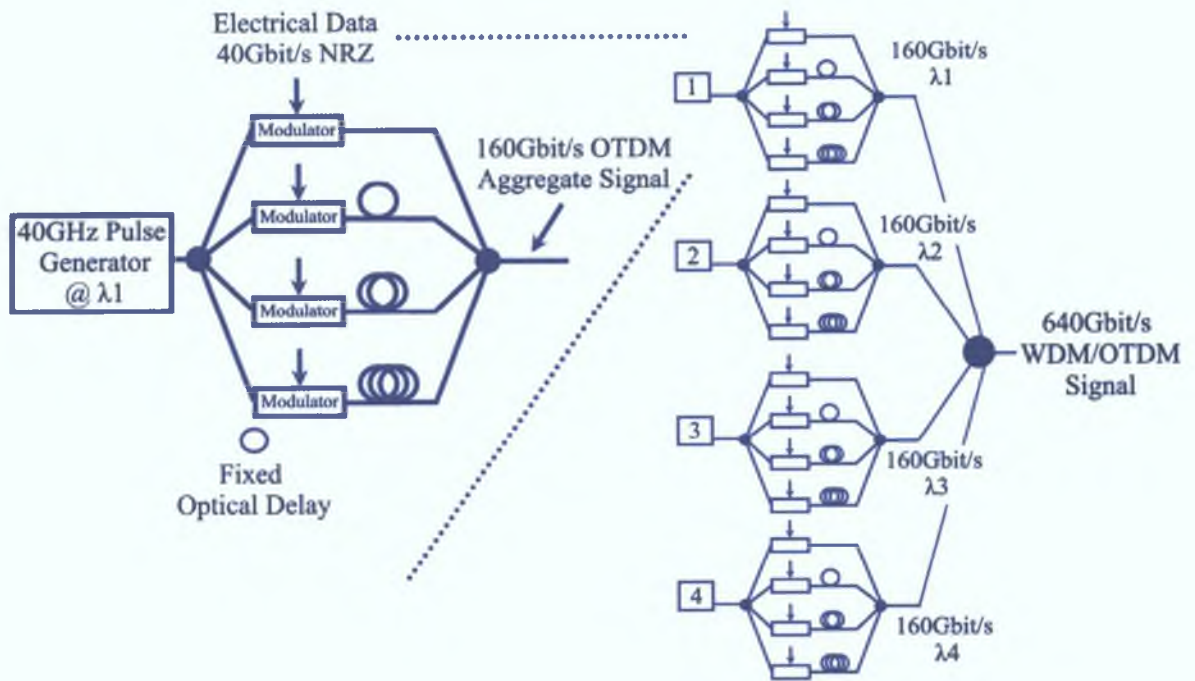
Figure 2.8: Schematic of a hybrid WDM/OTDM system

This value is of course dependent on the modulation format that is being employed, with reductions possible with the use of more complicated formats. This example still highlights the fact that for optimal performance there would exist a trade-off between temporal and spectral efficiency if a hybrid WDM/OTDM scheme is to be employed.

2.7 Modulation Formats

Until recently, optical communications primarily employed binary amplitude modulation On-Off Keying (OOK), Non-Return-to-Zero (NRZ) or Return-to-Zero (RZ) formats [73]. However, nowadays, a number of advanced signal modulation techniques are available that can help to reduce the effects of chromatic dispersion and nonlinearities. These include phase modulation, duobinary, chirped RZ and carrier-suppressed RZ [73]. Information may also be encoded using multi-level amplitude or phase modulation schemes, and/or optical filtering can be employed to create Single-Sideband (SSB) signals to improve the spectral efficiency even further. In order to reduce nonlinear effects, polarisation multiplexing or modulation can also be used [74].

There are a number of different system parameters that will determine the choice of modulation format. These include cost, transmission distance, bit rate, robustness to dispersive and nonlinear effects, and the OSNR requirements of the system [74, 75]. For long haul optical communications operating with individual channel data rates of 40Gbit/s, RZ is more stable than NRZ as it is more resilient to dispersion and nonlin-

47

earities, and offers a higher receiver sensitivity [76] In order to improve performance even further, carrier-suppressed-RZ [76] can be used to reduce the spectral bandwidth of standard RZ, whereas Return-to-Zero Differential Phase Shift-Keying (RZ-DPSK) can increase the transmission distance by using balanced detection which yields a required OSNR advantage of approximately 3dB [73,77]

Summary

With the continued growth in network usage, network providers need to better utilise their installed fibre network This chapter examined the use of optical multiplexing techniques, both in the wavelength and temporal domain, as a means of increasing the overall aggregate transmission data rate for optical communications systems The history and standards used for multiplexing were introduced, along with a detailed description of OTDM One of the major components of an OTDM, an optical pulse, was then described, followed by a discussion of some of the limiting factors to high-speed optical transmission Finally a hybrid multiplexing technique, that takes combines both WDM and OTDM technology, was discussed The merits of such an approach is that ultra-high data rates can be provide without pushing either multiplexing to its limits

The following chapter describes a number of pulse generation techniques that could be used as the optical pulse source used in an OTDM network Particular emphasis will be paid to one particular technique, namely the gain-switching of a commercially available semiconductor laser

Bibliography

[1] B Labs, "AllWave Fiber From Bell Labs Squeezes Out Water for More Spectrum " HMTL Document, 1998 http //www bell-labs com/news/1998/june/4/4 html

[2] R Boncek, P Dickinson, and S Das, "Meeting metro capacity with cost reducing fibre infrastructure," *Lightwave Europe*, vol 2, no 9, pp 20–22, 2003

[3] Web ProForum Tutorials, "Fundamentals of Telecommunications," pdf document, The Internationl Engineering Consortium, http //www iec org, 2001

[4] S Winder, *Telecommunications Pocket Book* Newnes, 3rd ed, 2001 ISBN 0-7506-52985

[5] S Haykin, *Communication Systems* Wiley, 3rd ed, 1994 ISBN 0-471-57178-8

[6] F T Andrews, "The Telephone Network of the 1960's," *IEEE Communications Magazine*, vol 40, no 7, pp 49–53, 2002

[7] Privateline, "Telecommunications fundamentals and chapter 3 Analog and digital transmission" HMTL Document, 2003 http //www privateline com/manual/three html

[8] S Kawanishi, "High bit rate transmission over 1Tb/s," *IEICE Transactions in Communications*, vol E84-B, no 5, pp 1135–1141, 2001

[9] C Scheerer and C Glingener, "WDM and ETDM for Future Optical Transmission Systems," in *Global Telecommunications Conference (Globecom 98)*, vol 2, pp 1007–1011, 1998

[10] J Palais, *Fiber Optic Communications* Pearson - Prentice Hall, 5th ed, 2005 ISBN 0-13-129350-8

[11] I Kaminow and T Li, *Optical Fiber Communications IV B - Systems and Impairments* Academic Press, 1st ed, 2002 ISBN 0-12-395173-9

[12] Web ProForum Tutorials, "Dense Wavelength Division Multiplexing (DWDM)," pdf document, The Internationl Engineering Consortium, http //www iec org, 2001

[13] T Hausken, "The 40Gbit/s optical network why, how and when?," *Fibre Systems Europe*, pp 16–20, 2004

[14] R S Tucker, G Eisenstein, and S K Korotky, "Optical Time-Divison Multiplexing For Very High Bit-Rate Transmission," *IEEE Journal of Lightwave Technology*, vol 6, no 11, pp 1737–1749, 1988

[15] O E DeLange, "Some Optical Communications Experiments," *Applied Optics*, vol 9, no 5, pp 1167–1175, 1970

[16] W J Tomlinson, "Wavelength multiplexing in multimode optical fibres," *Applied Optics*, vol 16, no 8, pp 2180–2194, 1977

[17] J Hegarty, S D Poulsen, K A Jackson, and I P Kaminow, "Low-loss single mode wavelength-division multiplexing with etched fibre arrays," *Electronics Letters*, vol 20, no 17, pp 685–687, 1984

[18] N A Olsson, R Logan, and L F Johnson, "Transmission experiment at 3 Gbit/s with close-spaced wavelength-division-multiplexed single-frequency lasers at 1·5µm," *Electronics Letters*, vol 20, no 17, pp 673–674, 1984

[19] International Telecommunication Union, "ITU-T recommendation G 694 1 Spectral grids for WDM applications DWDM frequency grid," *Series G Transmission Systems and Media, Digital Systems and Networks*, vol Transmission media characteristics - Characteristics of optical components and subsystems, no G 694 1, 2002

[20] R Ramaswami and K N Sivarajan, *Optical Networks - A Practical Perspective* Morgan Kaufmann Publishers, 2nd ed , 2002 ISBN 1-55860-655-6

[21] P Mamyshev, C Rasmussen, and B Mikkelsen, "Technical and Commercial Perspective of 40Gbs Transmission," in *Lasers and Electro-Optics Society Annual Meeting-LEOS, Conference Proceedings, Puerto Rico*

[22] International Telecommunication Union, "ITU-T recommendation G 694 2 Spectral grids for WDM applications CWDM wavelength grid," *Series G Transmission Systems and Media, Digital Systems and Networks*, vol Transmission media characteristics - Characteristics of optical components and subsystems, no G 694 2, 2002

[23] I Tomkos, R Hesse, N Madamopoulos, C Friedman, N Antoniades, B Hallock, R Vodhanel, and A Boskovic, "Transport Performance of an 80-Gb/s WDM Regional Area Transparent Ring Network Utilising Directly Modulated Lasers," *IEEE Journal of Lightwave Technology*, vol 20, no 4, pp 562–573, 2002

[24] H Takahashi, s Suzuki, K Kato, and I Nishi, "Arrayed-waveguide grating for wavelength division multi/demultiplexer with nanometre resolution," *Electronics Letters*, vol 26, no 2, pp 87–88, 1990

[25] T Saito, T Ota, T Toratani, and Y Ono, "16-ch Arrayed Waveguide Grating Module with 100-GHz Spacing," 2005 http //www furukawa co jp/review/fr019/fr19_09 pdf

[26] S Bhandare, D Sandel, B Milivojevic, A Hidayat, A Fauzi, H Zhang, S K Ibrahim, F Wust, and E Noe, "5 94Tbit/s, 1 49bit/s/Hz (40x2x2x40Gbit/s) RZ-DQPSK Polarisation Division Multiplex C-Band Transmission over 324 km," *IEEE Photonics Technology Letters*, vol 17, no 4, pp 914–916, 2005

[27] Advanced Networks Group TDM, "Advanced networks group ultra-fast time-division multi-access networks" HMTL Document, 2002 http //www 11 mit edu/AdvancedNetworks/tdm html

[28] B Guenther and D Steel, *Encyclopedia of Modern Optics* Elsevier, 1st ed , 2005 ISBN 0-12-227600-0

[29] D M Spirit, A D Ellis, and P E Barnsley, "Optical time division multiplexing systems, networks," *IEEE Communications Magazine*, vol 32, no 12, pp 56–62, 1994

[30] S K Shin, C H Kim, and Y C Chung, "Directly Modulated 2 5Gb/s x 16-channels WDM Transmission Over 640km of Single-Mode Fiber Using Dispersion Compensating Fiber," *IEEE Photonics Technology Letters*, vol 11, no 6, pp 742–744, 1999

[31] H Suzuki, M Fujiwara, N Takachio, K Iwatsuki, T Kitoh, and T Shibata, "12 5-GHz Spaced 128-Tb/s (512-channel x 2 5Gb/s) Super-Dense WDM Transmission Over 320-km SMF Using Multiwavelength Generation Technique," *IEEE Photonics Technology Letters*, vol 14, no 3, pp 405–407, 2002

[32] S Kawanishi, "Ultrahigh-Speed Optical Time-Division-Multiplexed Transmission Technology Based on Optical Signal Processing," *IEEE Journal of Quantum Electronics*, vol 34, no 11, pp 2064–2079, 1998

[33] N Onodera, H Ito, and H Inaba, "Generation and control of bandwidth-limited and single-mode picosecond optical pulses by strong rf modulation of a distributed feedback ingaasp diode laser," *IEEE Journal of Quantum Electronics*, vol 21, no 6, pp 568–575, 1985

[34] P Vasil'ev, *Ultrafast Diode Lasers, Fundamentals and Applications* Artech House Publications, 1st ed , 1995 ISBN 0-89006-736-8

[35] M Jinno, "Effects of Crosstalk and Timing Jitter on All-Optical Time-Division Demultiplexing Using a Nonlinear Fiber Sagnac Interferometer Switch," *IEEE Journal of Quantum Electronics*, vol 30, no 12, pp 2842–2853, 1994

[36] H Takara, "High-speed optical time-division-multiplexed signal generation," *Optical and Quantum Electronics*, vol 32, pp 795–810, 2001

[37] P Anandarajah, P J Maguire, A Clarke, and L P Barry, "Self-Seeding of a Gain-Switched Integrated Dual-Laser Source for the Generation of Highly Wavelength-Tunable Picosecond Optical Pulses," *IEEE Photonics Technology Letters*, vol 16, no 2, pp 629–631, 2004

[38] L P Barry and P Anandarajah, "Effect of Side-mode Suppression Ratio on the Performance of Self-Seeded Gain-Switched Optical Pulses in Lightwave Communications Systems," *IEEE Photonics Technology Letters*, vol 11, no 11, pp 1360–1362, 1999

[39] M Saruwatari, "All-Optical Signal Processing for Terabit/Second Optical Transmission," *IEEE Journal of Selected Topics in Quantum Electronics*, vol 6, no 6, pp 1363–1374, 2000

[40] S Bouchoule, N Stelmakh, M Caveher, and J -M Lourtioz, "Highly Attenuating External Cavity of Picosecond-Tunable Pulse Generation from Gain/Q-Switched Laser Diodes," *IEEE Journal of Quantum Electronics*, vol 29, no 6, pp 1693–1700, 1993

[41] Physikalisch-Technische Bundesanstalt (PTB), "Ultra-fast optical sampling oscilloscopes " html document, 2004 http //www ptb de/en/suche/suche html

[42] R L Jungerman, G Lee, O Buccafusca, Y Kaneko, N Itagaki, and R Shioda, "Optical Sampling Reveals Details of Very High Speed Fiber Systems," pdf document, Agilent Technologies, www agilent com, 2004

[43] S V Kartalopoulos and C Qiao, "Editorial - Our First Anniversary Issue," *IEEE Optical Communications*, vol February, p S4, 2004

[44] P Dobbelaere, K Falta, L Fan, S Gloeckner, and S Patra, "Digital mems for optical switching," *IEEE Communications Magazine*, vol 40, no 3, pp 88–95, 2002

[45] G Ellinas, J A Walker, and L Lin, "Network Control and Management Challenges in Opaque Networks Utilising Transparent Optical Switches," *IEEE Communications Magazine*, vol 42, no 2, pp S16–S23, February 2004

[46] J Hecht, "OTDM promises higher communications speeds using optical processors," *Laser Focus World*, no 11, pp 121–4, 2003

[47] S A Hamilton, B S Robinson, T E Murphy, S J Savage, and E P Ippen, "100 Gb/s Optical Time-Division Multiplexed Networks," *IEEE Journal of Lightwave Technology*, vol 20, no 12, pp 2086–2100, 2002

[48] Y Liu, M T Hill, N Calabretta, H de Waardt, and G an H J S Dorren, "All-Optical Buffering in All-Optical Packet Switched Cross Connects," *IEEE Photonics Technology Letters*, vol 14, no 6, pp 849–851, 2002

[49] X Chen, "Optical time-division multiplexing " HMTL Document, 2001 The optical networks project - http //www ari vt edu/ece5516/opticalnetworks/otdm hmtl

[50] H Sotobayashi, W Chujo, and K Kitayama, "Highly Spectral-Efficient Optical Code-Division Multiplexing Transmission System," *IEEE Journal of Selected Topics in Quantum Electronics*, vol 10, no 2, pp 250–258, 2004

[51] D J Richardson, P C Teh, M A F Roelens, B C Thomsen, C Tian, Z Zhang, P Petropoulos, and M Ibsen, "Direct Sequence OCDMA Systems Based on Fibre Grating Technology," in *European Conference on Optical Communications (ECOC2005)*, vol 4, pp 867–870, 2005

[52] N S Bergano and C R Davidson, "Wavelength Division Multiplexing in Long-Haul Transmission Systems," *IEEE Journal of Lightwave Technology*, vol 14, no 6, pp 1299–1307, 1996

[53] R DeSalvo, A G Wilson, J Rollman, D F Schneider, L M Lunardi, S Lumish, N Agrawal, A H Steinbach, W Baun, T Wall, R Ben-Michael, M A Itzler, A Fejzuli, R A Chipman, G T Kiehne, and K M Kissa, "Advanced Components

and Sub-System Solutions for 40Gb/s Transmission," *IEEE Journal of Lightwave Technology*, vol. 20, no. 12, pp. 2154–2181, 2002.

[54] A.J.Antos and D.K.Smith, "Design and Characterisation of Dispersion Compensating Fiber Based on the LP_{01} Mode," *IEEE Journal of Lightwave Technology*, vol. 12, no. 10, pp. 1739–1745, 1994.

[55] I. P. Kaminow, *Optical Fiber Telecommunications II*. Academic Press, 2nd ed., 1998. ISBN 0-12-497351-5.

[56] C.M.Weinert, R.Ludwig, W.Pieper, H.G.Weber, D.Breuer, K.Petermann, and F.Kuppers, "40Gb/s, 4 x 40Gb/s TDM/WDM Standard Fiber Transmission," *IEEE Journal of Lightwave Technology*, vol. 17, no. 11, pp. 2276–2284, 1999.

[57] L.Gruner-Neilsen, C.C.Larsen, M.Nelson, and P.Emery, "Cost-effective dispersion management for emerging network upgrade paths." html document, January 2003. http://lw.pennnet.com.

[58] S.J.Savory and F.P.Payne, "Pulse Propagation in Fibers with Polarisation-Mode Dispersion," *IEEE Journal of Lightwave Technology*, vol. 19, no. 3, pp. 350–357, 2001.

[59] L. Chen, M. Yanez, C. huang, and X. Bao, "Pulsewidth Compression in Optuical Components with Polarisation Mode Dispersion Using Polarisation Controls," *IEEE Journal of Lightwave Technology*, vol. 19, no. 6, pp. 830–836, 2001.

[60] R. Hui, B. Zhu, R. Huang, C. T.Allen, K. R.Demarest, and D. Richards, "Subcarrier Multiplexing for High-Speed Optical Transmission," *IEEE Journal of Lightwave Technology*, vol. 20, no. 3, pp. 417–427, 2002.

[61] R.Khosravani, S.A.Havstad, Y.W.Song, P.Ebrahimi, and A.E.Willner, "Polarisation-Mode Dispersion Compensation in WDM Systems," *IEEE Photonics Technology Letters*, vol. 13, no. 12, pp. 1370–1372, 2001.

[62] C.Xie and X.Liu, "Multi-Channel Shared PMD Compensation in WDM systems," in *Conference on Optical Fiber Communication (OFC) 2003*, vol. 86, pp. 265–266, 2003.

[63] G. P. Agrawal, *Nonlinear Fiber Optics*. Academic Press, 2nd ed., 1995. ISBN 0-12-045142-5.

[64] F.Forghieiri, R.W.Tkach, and A.R.Chraplyvy, "WDM Systems with Unequally Spaced Channels," *IEEE Journal of Lightwave Technology*, vol. 13, no. 5, pp. 889–897, 1995.

[65] G. P. Agrawal, *Fiber-Optic Communication Systems*. Academic Press, 1st ed., 1997. ISBN 0-471-17540-4.

[66] W.Wu and P.Yeh, "Energy Coupling by Partially Degenerate Four-Wave Mixing in Multichannel Lightwave Systems," *IEEE Photonics Technology Letters*, vol. 7, no. 5, pp. 585–587, 1995.

[67] R G Smith, "Optical Power Handling Capacity of Low Loss Optical Fibers as Determined by Stimulated Raman and Brillouin Scattering," *Applied Optics*, vol 11, no 11, pp 2489–2494, 1972

[68] A R Chraplyvy, "Limitations on lightwave communications imposed by optical-fiber nonlinearities," *IEEE Journal of Lightwave Technology*, vol 8, no 10, pp 1548–1557, 1990

[69] A M Ali and K W Fussgaenger, "Services Integration and Multiplexing for Broad-Band Communication Systems," *IEEE Journal on Selected Areas in Communications*, vol SAC-4, no 4, pp 551–564, 1986

[70] M Attygalle, H F Liu, and A Nirmalathas, "An all-optical WDM to TDM conversion scheme with simultaneous all-optical synchronization for WDM/OTDM network nodes," *Optical and Quantum Electronics*, vol 33, pp 827–840, 2001

[71] fibers org, "European consortium enters terabit regime," html document December, fibers org - The Optical Communications Source, http //fibers org/articles/news/6/12/8/1, 2004

[72] B K Mathason, H Shi, I Nitta, G A Alphonse, J Abeles, J C Connolly, and P J Delfyett, "Multiwavelength All-Optical TDM switching using a semiconductor optical amplifier in a loop mirror," *IEEE Photonics Technology Letters*, vol 11, no 3, pp 331–333, 1999

[73] A H Gnauck and P J Winzer, "Optical Phase-Shifted-Keyed Transmission," *IEEE Journal of Lightwave Technology*, vol 23, no 1, pp 115–130, 2005

[74] A H Gnauck, "Advanced Amplitude- and Phase Coded Formats for 40Gb/s fiber transmission," in *Lasers and Electro-Optics Society Annual Meeting (LEOS2004), Conference Proceedings, Puerto Rico*, vol 2, pp 605–606, 2004

[75] S Schmid, "Lithium niobate to rule 40G modulation," *Lightwave Europe*, vol 2, pp 13–16, 2003

[76] J -X Cai, M Nissov, Carl R Davidson, A N Pilipetskii, G Mohs, H Li, Y Cai, E A Golovchenko, A J Lucero, D G Foursa, and N S Bergano, "Long-haul 40Gb/s DWDM Transmission With Aggregate Capacities Exceeding 1Tb/s," *IEEE Journal of Lightwave Technology*, vol 20, no 12, pp 2247–2258, 2002

[77] A H Gnauck, X Liu, X Wei, D M Gill, and E C Burrows, "Comparison of Modulation Formats for 42 7-Gb/s Single-Channel Transmission Through 1986km of SSMF," *PTL*, vol 16, no 3, pp 909–911, 2004

CHAPTER 3

OTDM Pulse Generation

Introduction

The generation of ultra short optical pulses will be vital in the development of WDM, OTDM and hybrid WDM/OTDM, and in optical signal processing techniques such as optical sampling and switching As mentioned in 2 4 1 there are a number of important criteria that have to be met if a particular optical pulse source is to be employed in an OTDM network These include pulse duration, spectral width, timing jitter, stability, SMSR and to be both wavelength and repetition rate tunable There are a number of different techniques that can be employed to generate short optical pulses for an OTDM network, with one of the simplest being gain-switching of a semiconductor laser diode This chapter will present experimental results showing that a wavelength-tunable optical pulses suitable for WDM and OTDM applications can be generated by the gain-switching of one or more semiconductor laser diodes

3.1   Optical Pulse Generation Techniques

3.1.1   External Modulation

External modulation is an optical pulse generation technique that involves the pulse shaping of Continuous Wave (CW) light using the nonlinear response of an external modulator [1] By biasing the modulator around the null point and applying an electrical sinusoidal signal, the CW light passing through the modulator becomes shaped into optical pulses, with the optical pulse train being at twice the repetition rate of the applied electrical signal [2] The operation of the modulator has already been discussed in 1 3 1 The pulses generated are normally transform limited, with low timing jitter The repetition rate is arbitrary, and is limited by the modulation bandwidth of the modulator The major disadvantages associated with external modulation are the insertion loss and extra cost associated with the modulators

3.1.2 Mode Locking

Mode locking is a technique that can be used to obtain a train of ultra short (sub-100fs) optical pulses It originates from that the fact that under normal operating conditions, the output of a laser consists of the sum of frequency components that corresponds to the oscillating modes of the device The number of modes is determined by the spectral bandwidth (gain curve) of the device In general the phase between modes is not fixed, resulting in the laser output randomly varying over time [3] If the modes were forced to maintain a fixed phase and amplitude relationship then the output would be a periodic, resulting in the generation of a train of optical pulses This form of operation is known as mode locking The repetition rate of the mode-locked signal corresponds to the cavity round-trip frequency, which is related to the cavity mode spacing [4]

Mode locking can be carried out either actively or passively Active mode locking of a laser normally involves modulating the amplitude of the optical field inside the laser cavity at a frequency which is equal to the mode spacing of the laser This can be carried out by applying an electrical sinusoidal signal at the correct frequency, resulting in the generation of optical pulses at a repetition rate of the applied signal This method has been used to generate sub-picosecond optical pulses at repetition rates of 40GHz and beyond [2] Passive mode locking [5] on the other hand does not require the application of an external RF signal to result in mode locking The majority of passive techniques employ an intensity-dependent saturable absorber in the cavity, which absorbs light at low intensities, while allowing high-intensity light to be transmitted Thus high-intensity light is allowed to oscillate within the cavity, eventually leading to mode locking and pulse generation

Even though mode locking can be used to produce optical pulses with excellent spectral and timing jitter characteristics, a major problem of mode locking is its inability to synchronise to a specific SDH data rate [2] Also the devices are more susceptible to vibrations and changes in the ambient temperature [6], and it is more difficult to control the pulse width, shape and position in a particular time slot [7]

3.1.3 Q-Switching

Q-switching is another method for picosecond optical pulse generation It uses an intra-cavity device to switch rapidly between the cavity gain and loss [5], controlling the amount of optical feedback by the resonator The Q-factor is a measure of how much light is fed back into the gain-medium of the laser cavity by the resonator, with a high Q value corresponding to low resonator losses per cavity round trip

Initially the device is continually pumped and operated with a low Q-factor (high losses) resulting in a population inversion until the carrier density reaches a maximum level (gam saturation) At this point, the Q-switch device is quickly changed from a

low Q to a high Q-factor, and the stored energy is rapidly emitted in an output optical pulse [3]

As for the case of mode locking, Q-switching can be carried out either actively or passively In active Q-switching, a mechanical device (shutter, chopper) or a modulator (acouto-optic, electro-optic) is inserted into the laser cavity [3] An external electrical signal is then used to switch the device from a high Q-factor to a low Q-factor and vice versa, allowing the repetition rate to be externally controlled Passive Q-switching uses a saturable absorber or a passive semiconductor device as the Q-switch device In the case of the saturable absorber [8], the loss is initially high, but low enough to enable energy build up in the gain-medium As the amount of stored energy increases, the absorber becomes saturated, rapidly reducing resonator losses, allowing faster energy build up Eventually the loss of the absorber is reduced to allow all of the stored energy to be released in the form of an optical pulse After the pulse has been emitted, the absorber returns to a high loss state as the stored energy starts increasing again

Q-switching has been used to generate optical pulses with durations less than 50ps at 10GHz [5] However as for the case of mode locking, Q-switching requires a specially fabricated device that increases cost and complexity

3.2 Gain Switching

Gain switching is one of the simplest techniques that can be used to generate picosecond optical pulses It has many advantages over alternative pulse generation techniques including that fact that the repetition rate is tunable [9], temporal compression can be easily achieved using a length of dispersion compensation fibre [10] and by using self- or external-injection seeding, wavelength tuning and a reduction in timing jitter can be achieved [11] Also gain switching does not require specially fabricated devices [5], making it attractive for use as a relatively simple, stable and compact optical pulse source [10]

Before explaining the gain-switching process, the temporal variation of the carrier and photon densities within the laser cavity for a constant current step input will be examined, and this is shown in Figure 3 1 When the current step is applied (dashed line), the injected carrier density (dotted line) rapidly increases, with a slow increase in the photon density (solid line) Eventually, the injected carrier density will increase beyond the threshold density value, resulting in stimulated emission and a rapid increase in the number of photons due to the very short roundtrip time for light propagating within the cavity [13] As photons are generated faster than the rate of carrier injection, the carrier density eventually falls, resulting in the formation of the first peak of the relaxation oscillation As the input current step continues to inject further carriers, subsequent strongly damped peaks are generated eventually leading to a steady state
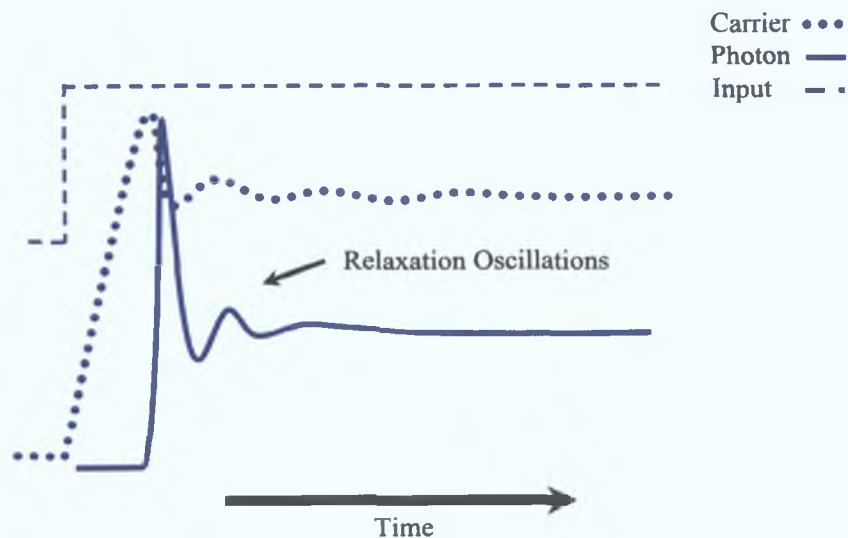
Figure 3.1: Temporal evolution of photon and carrier densities for a current step [12]

constant optical output power.

Ito et al. [14] discovered in 1979 that by applying a sub-gigahertz sinusoid signal to a laser diode biased below threshold, a train of optical pulses (with a pulse duration of a few-tens of picoseconds) were generated at the same repetition rate as the modulation signal. The optical pulse train generated corresponded to the continuous generation of the first peak of the relaxation oscillation, with the width of the applied electrical pulse chosen carefully so that the drive current terminates before the onset of subsequent peaks [3]. By doing so, Ito demonstrated that optical pulses with durations of around 30ps could be easily produced. To better explain the gain-switching process, let us return to the description given for the relaxation oscillation phenomenon and replace the constant current step input with an electrical pulse. This is represented in Figure 3.2, which shows the temporal relationship between the injected carrier density and photon densities within a laser cavity for a single gain-switched cycle [12].

When a current pulse is applied to a laser biased below threshold, the injected carrier density rises rapidly in the absence of stimulated emission. The injected carrier density continues to rise until it reaches a point when stimulated emission begins, which starts to significantly consume the number of injected carriers. This peak is known as the inversion point [12]. As the injected carriers are consumed faster than they are being supplied, the carrier and photon densities starts to drop and if the current pulse is terminated at the appropriate time after the initial peak of the relaxation oscillation, the second oscillation will not be obtained. This results in the generation of a single optical pulse, with a duration of between 10-30ps depending on the laser parameters and the drive conditions [15].

The duration and peak power of the generated optical pulses depends on a number of
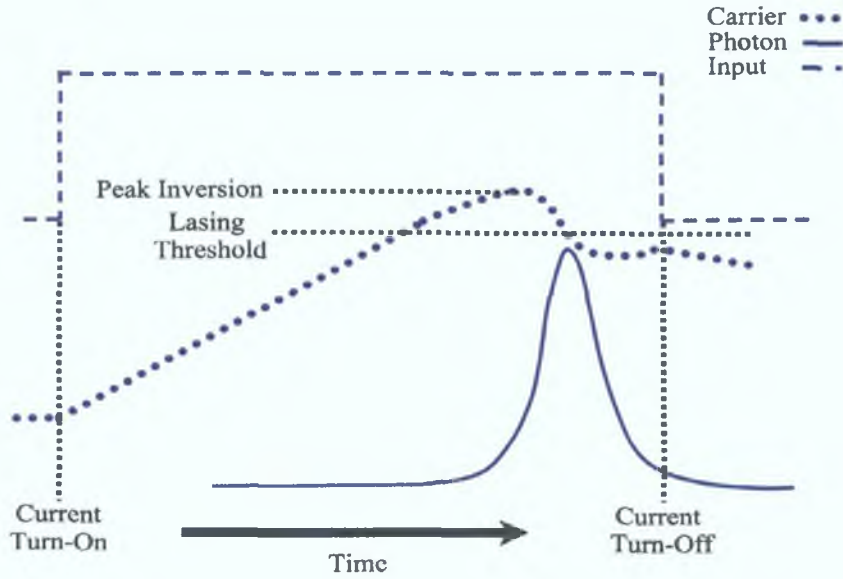
Figure 3.2: Temporal evolution of photon and carrier densities during a single gain-switch cycle [12]

different parameters, including device structure and bias current level, and this will be investigated next. The modulation signal for *gain switching* can either be a short electrical pulse (generated from a comb generator, picosecond photoconductive switches, or avalanche transistor generators), or a strong sine wave at sub-gigahertz or gigahertz frequency [3].

3.2.1 Gain-Switched Optical Pulse Shape and Duration

The energy, peak power and width of a gain-switched optical pulse can be derived using the rate equations which connects the photon density to the carrier density within the laser diode. The rate equations for a gain-switched optical pulse are [12]:

$$\frac{dn}{dt} = \frac{J}{ed} - \frac{n}{\tau_s} - \frac{A(n - n_o)p}{1 + \epsilon p} \tag{3.1}$$

$$\frac{dp}{dt} = \frac{A(n - n_o)p}{1 + \epsilon p} - \frac{p}{\tau_p} + \beta n \tag{3.2}$$

where n and p are the electron and photon densities, τ_s and τ_p are the carrier and photon lifetimes, A is the gain constant, J is the injection current density, n_o is the carrier density for transparency, β is the spontaneous emission factor, and ϵ is the gain compression factor.

Pulse Duration

The minimum pulse duration possible depends upon the strength and frequency of the relaxation oscillation [5], the modulating current and the bias current. The relaxation oscillation results from the interplay between the optical fields and the population inversion within the laser cavity [16]. The strength of the resonance depends upon a number of factors such as spontaneous emission and carrier diffusion. There are a number of ways to increase the frequency of the relaxation oscillation of the device. These include an increase in the optical gain coefficient, an increase in the photon density or a decrease in the photon lifetime [16].

The gain coefficient, which is directly related to the material properties, can be increased by cooling the laser diode [17] below room temperature, or using a quantum-well diode instead of a bulk semiconductor device. Both produce a higher population inversion level, resulting in a decrease in pulse width and increase in pulse peak power [3], but at the expense of increased cost and device complexity. The photon density in the active region can be increased by operating the laser at higher bias currents, which simultaneously increases the optical output power [16]. Possible damage to the laser mirrors at high photon densities is the main limitation of increasing photon density. Finally the photon lifetime can be decreased by reducing the length of the laser cavity.

However a short optical cavity will limit the maximum peak power that can be generated by limiting the number of carriers that can be injected in the device at any one time. Therefore, the laser has to be driven at a higher bias current level. This results in a trade-off between achieving a minimum pulse width (function of modulation signal) and maximum peak power (function of bias current). Regardless of which method is used to minimise the pulse duration, the shortest optical pulse that can be generated directly from a gain-switched laser diode is in the region of 10ps.

Apart from the relaxation oscillation, the bias current and modulation signal are also important parameters in the gain-switching process. There is an optimal DC bias level which allows a minimum pulse width with a maximum possible amplitude, and this is generally just below threshold [17]. Biasing further below threshold results in an increase in optical pulse duration and decrease in amplitude, accompanied with a longer delay in optical emission, compromising the speed of the device [17]. There would also be an increase in the amount of frequency chirp across the pulse, resulting in additional penalties especially in long-distance fibre-optic links. If biased above threshold, or if the electrical pulses applied to the laser are relatively long, multiple optical pulses can be generated within a single modulation period [3]. The advantage of operating the laser above threshold is that the amount of frequency chirp across the pulse is reduced, but there is a reduction in the on/off contrast ratio [17].

Pulse Shape

The shape of a gain-switched optical pulse depends on the material and structure of the laser diode and can be described as a combination of two exponential curves, with fall-time of the trailing edge being about twice the rise-time of the leading edge [17] The rise-time is inversely proportional to the net charge transfer by the electrical pulse to the active region during modulation, with the fall-time depending on how far down below threshold the carrier density is pulled during formation of the optical pulse [3] If the carrier density is not brought down far enough below threshold then a pedestal will form on the trailing edge of the optical pulse The optical pulse will also become more asymmetric as the amplitude of the drive signal is increased further [17] Figure 3 3
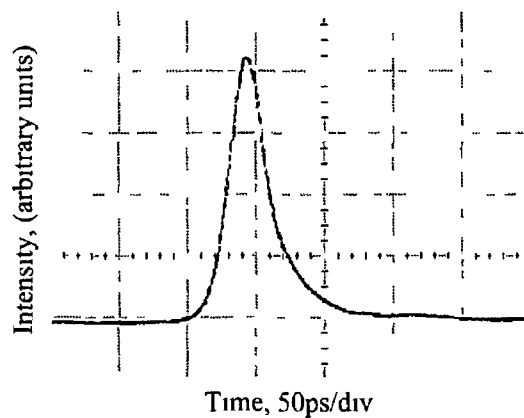
Figure 3 3 Gain-switched optical pulse

shows a typical gain-switched optical pulse It shows the classical gain-switched pulse shape, with the fall time of the trailing edge being twice the rise-time of the leading edge
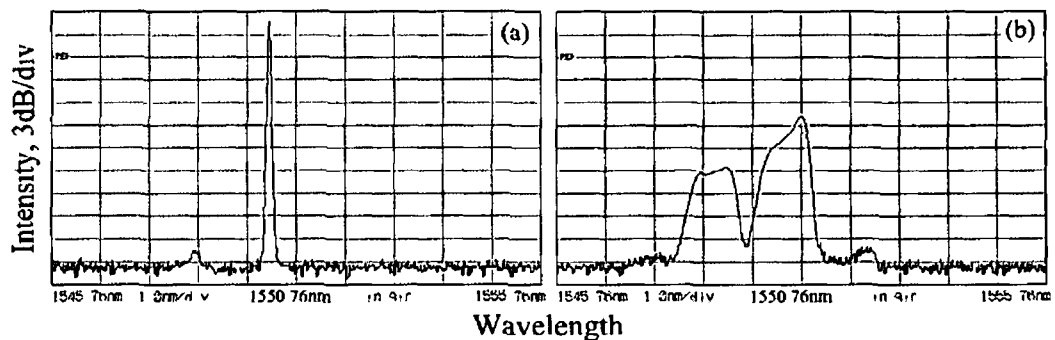
Figure 3 4 Optical Spectra under (a) CW and (b) gain-switched conditions

Figure 3 4 shows a comparison between the optical spectra for the DFB laser operating under CW (a) and gain-switched (b) conditions The optical spectrum under

gain-switched conditions has a spectral width (measured 3dB down from peak) of approximately 1nm, which is an increase in the original CW measured spectral width of approximately 0 1nm The spectral width of a typical DFB would be in the 10's of MHz range, but here the measurement is confined by the resolution bandwidth of the Optical Spectrum Analyser (OSA) employed Regardless of this, Figure 3 4 illustrates the fact that gain-switching results in a chirp-induced broadening of the spectral output of the laser It also shows that the SMSR is also degraded, from approximately 30dB under CW conditions to about 7dB when gain-switched

3.2.2 Gain-Switching Induced Frequency Chirp

Figure 3 2 showed that the gain-switching process is dependent on variations in the carrier and photon densities within the laser cavity during the emission of an optical pulse The refractive index of the laser cavity can be calculated if the absorption coefficient is known for all frequencies Therefore, if there is a change in the absorption coefficient, then there will be an accompanying change in the refractive index [18] There are a number of affects that can alter the absorption coefficient Some of them, such as plasma refraction and bandgap shrinkage [3], are related to the injection of carriers into the active region This leads to a dependence between the emitted wavelength and the injected carrier concentration This relationship can be described by [19]

$$\Delta\lambda = -\frac{\Gamma\rho\lambda}{\mu}\Delta n \qquad (3\ 3)$$

where $\Delta\lambda$ is the variation in emitted wavelength, Γ is the optical confinement factor, ρ is a constant of proportionality, λ is the emission wavelength, μ is the refractive index, and Δn is the variation of the carrier density within the cavity This shows that there is a frequency variation (chirp) across the pulse due to the variation in carrier density in the active region during the injection of the electrical modulation signal [20] The gain-switched frequency chirp results in the frequency components of the optical pulse being shifted in a negative or red direction during pulse generation [21,22]

The term negative shift can be explained by [19]

$$\frac{d\mu}{dn} = -\Gamma\rho \qquad (3\ 4)$$

where the rate of change of the refractive index with respect to carrier concentration is negative, indicating that the instantaneous frequency is shifted from higher frequencies at the leading edge (blue shift) to lower frequencies at the trailing edge (red shift) This is shown in Figure 3 5 The initial blue shift can be accounted for by the sudden increase in the injected carrier density prior to pulse formation resulting in a temporary decrease in the refractive index in the active region This in turn shortens the optical path length
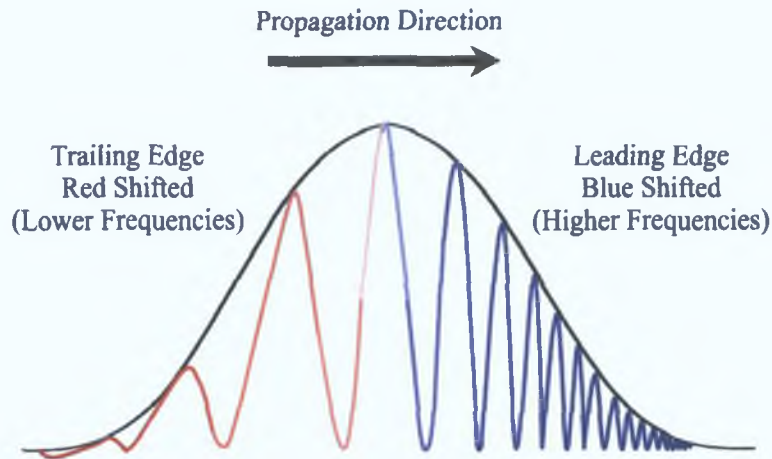
Figure 3.5: Gain switched pulse with negative chirp

of the laser cavity causing the emitted wavelength to initially shift to blue wavelengths [23]. During pulse formation, the injected carrier density rapidly decreases, causing the frequency to shift from blue to red wavelengths. This frequency chirp is observed experimentally as spectral broadening on the output spectrum [9], and was shown in Figure 3.4 (b).

3.2.3 Timing Jitter

Timing jitter is the random fluctuation in the temporal position of an optical pulse compared to a perfectly periodic pulse train. Timing jitter affects the SNR of the optical signal and limits the maximum amount of data that can be transmitted [24]. Timing jitter can be classified into two categories; correlated jitter and uncorrelated jitter. Correlated jitter, which for a gain-switched laser diode is usually $<$1ps [25], arises from the drive circuits and frequency synthesisers used to drive the gain-switched laser. This can be minimised by employing low phase noise electronics, especially in the frequency synthesiser.

Uncorrelated jitter originates from random fluctuations of the spontaneous emission in the laser cavity during the initial stages of optical pulse formation [3], and is generally accepted to be the overall fundamental limit of timing jitter. Typical values range from 1 to 10ps and depend on a number of issues, including device structure and bias currents. The jitter of a single-mode DFB is considerably higher than that of multi-moded laser diodes at the same injection current due to the lower photon density arising from fewer modes in the spectrum [26]. As individual optical channel data rates continue to increase up to 100Gbit/s, the control of timing jitter will be a more difficult task, requiring optical pulses with timing jitter $<$ 7% the width of the temporal bit slot [27].

Figure 3.6 shows a typical gain-switched pulse as displayed on a high-speed Dig-

ital Sampling Oscilloscope (DSO), with the oscilloscope average turned off. A packaged DFB lasers operating with $\lambda_{central}$=1551nm and a bias current of 15mA was gain-switched using an electrically amplified sine at 2.5GHz. The generated optical pulses had a duration of 12ps and a root-mean square (rms) temporal jitter of about 1ps (as measured using the DSO).
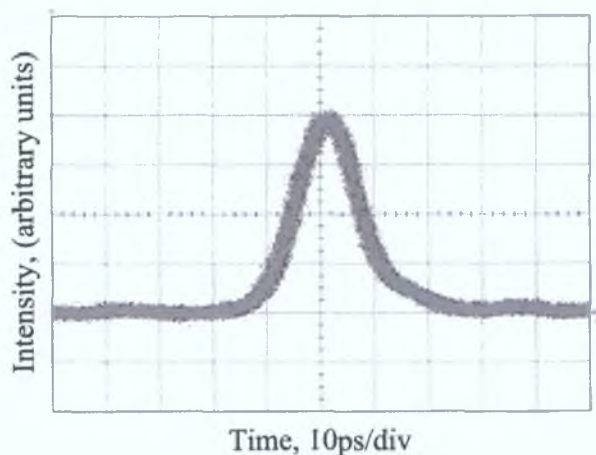
Figure 3.6: Gain-switched pulse with oscilloscope averaging turned off

3.2.4   Gain Switching Experimental Setup

One of the major advantages with gain switching is that it can be accomplished using a standard telecommunications Fabry-Perot (FP) or Distributed Feedback Laser (DFB) laser diode. For convenience, earlier experimental work used a single-moded DFB laser for gain-switching, with the DFB replaced with a FP device in later work concerned with the reduction of jitter and the generation of a tunable optical source. The setup for a basic gain switching experiment is shown in Figure 3.7.
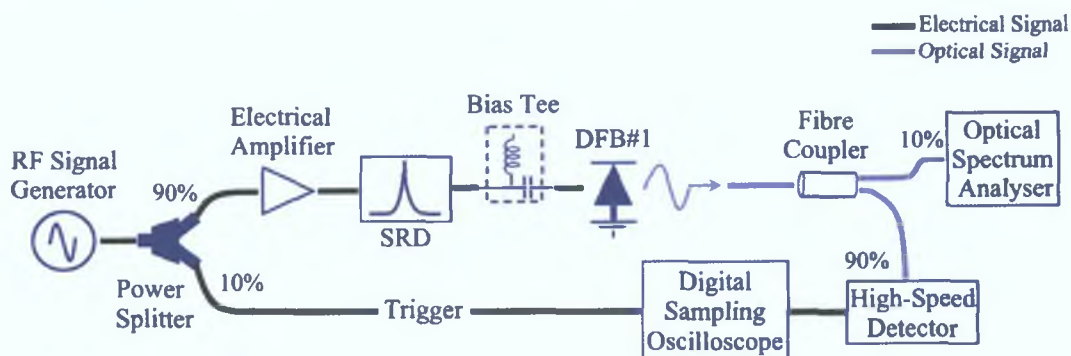
Figure 3.7: Schematic of a basic gain switching experimental setup

The modulation signal was created using a signal generator, electrical amplifier, Step-Recovery Diode (SRD) and bias-tee. The SRD converts the sine wave from the

signal generator to a stream of high-power short electrical pulses, which are used to modulate the laser. The SRD operates as follows. When diodes are switched from forward to reverse bias, the diode still conducts for a very short period of time since there is still some charge present in the device. Normal diodes remove this excess charge very slowly, but the SRD is optimised so that the charge is removed rapidly, causing the reverse conduction to halt very abruptly. This abrupt change can be used to create very fast switching pulses, or to generate harmonics of the switching signal. The ideal characteristics of a SRD are shown in Figure 3.8.
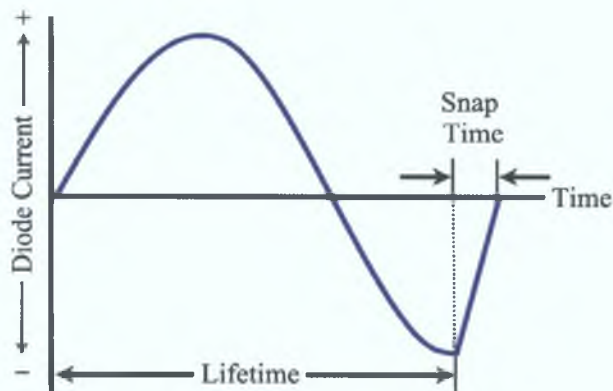
Figure 3.8: Illustration of the ideal operation of a SRD [28]

During the positive half cycle of the applied sinusoid signal, electrical charge is stored, which is extracted during the negative going half cycle. The current pulse produced has a rise-time equivalent to the recovery time of the diode, which is the time taken for the SRD to dissipate all stored charge and return to a high-impedance, non-conducting state [28]. This recovery time of the device used was in the order of 100ps. The short electrical pulse produced is at a repetition rate of the applied sinusoidal signal.
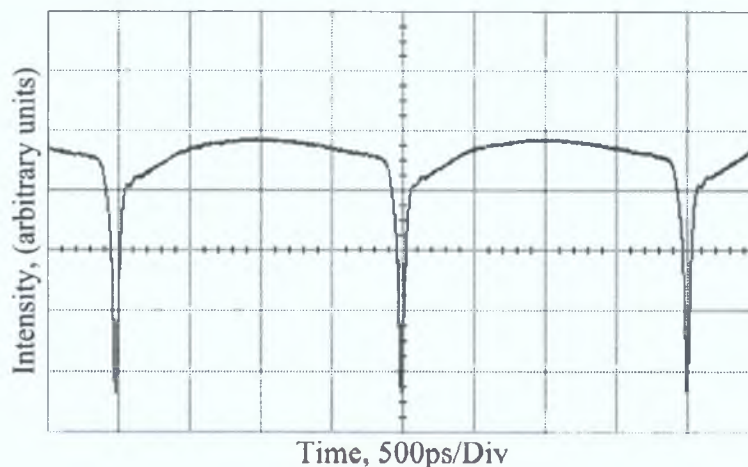
Figure 3.9: Electrical pulse train from 500MHz SRD

Figure 3 9 shows a train of electrical pulses generated from the 500MHz SRD, with an electrical pulse duration of approximately 60ps

Returning to the experimental setup shown in Figure 3 7, a Hewlett Packard E4437B signal generator [29], produced a 500MHz sine wave at 0dBm This signal passed through a 10-90 electrical power splitter, with 10% of the modulating signal used to trigger a sampling oscilloscope with the remaining 90% being electrically amplified before being fed into the SRD The SRD (Herotek GC 500 RC [30]) produced a high-power electrical pulse train, with a pulse width around 60ps, at a repetition rate of the applied electrical sine wave, which in this case was 500MHz The resulting electrical pulse train is then combined with a DC bias via a bias-tee and applied to the DFB laser diode The DFB laser diode was a NTT InGaAsP device, with a threshold current of 19 9mA, centre wavelength of 1537nm, and maximum output power of 5mW at 60mA and 25°C The specification for the DFB laser is given in Appendix A, with the CW spectrum shown in Figure 3 10
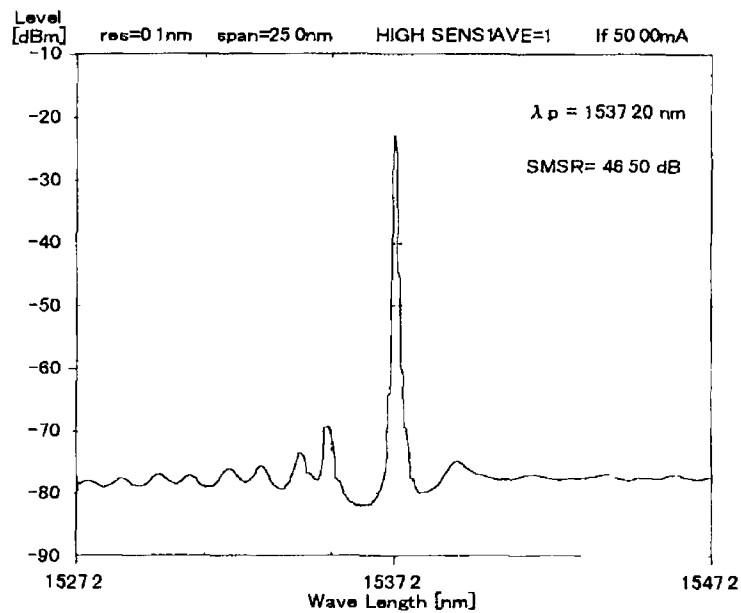
Figure 3 10 Optical spectrum of DFB1 under CW conditions

After optimisation, the DC bias current was set to 9 5mA, with the resulting optical signal coupled into a 90 10 optical fibre coupler using an anti-reflecting (AR) coated Graded Index (GRIN) lens (similar to [31]), with 90% passing to a high-speed photodetector and sampling oscilloscope, with the remaining 10% going to a optical spectrum analyser The photodetector used was a u^2t Photonics 50GHz photodetector [32] with a rise-time of 9ps The oscilloscope was an Agilent infinium DCA Wide-Bandwidth Oscilloscope [33] with a 50GHz bandwidth (Module Number 83484A) The optical spectrum analyser was an Anritsu MS9717A Optical Spectrum Analyser [34] with a wavelength resolution < 0 07nm in the C-band These measurement instruments were

used to throughout the rest of the experiments for pulse characterisation The result-
ing optical pulse train and individual optical pulse are shown in Figure 3 11 and Figure
3 12 respectively The separation between pulses in Figure 3 11 is about 2ns indicating
a 500MHz repetition rate
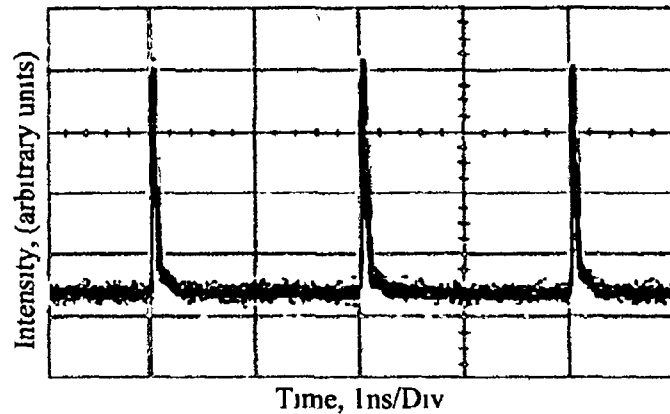
Figure 3 11 500MHz gain-switched optical pulse train from DFB1
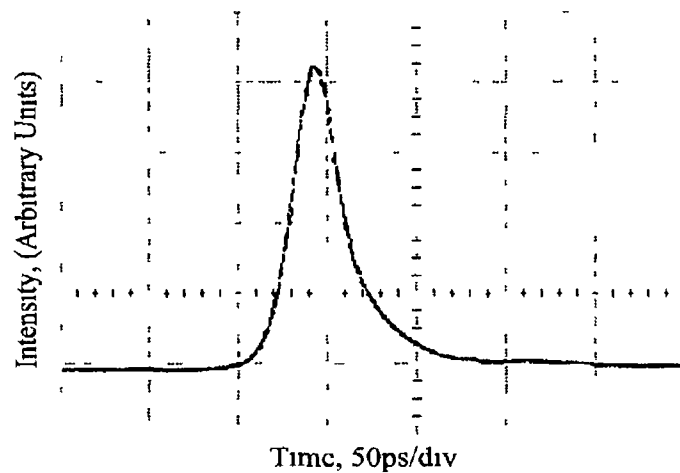
Figure 3 12 Single gain-switched optical pulse from DFB1

The measured optical pulse width (Full-Width Half-Maximum (FWHM)) on the os-
cilloscope was 33ps To calculate the actual pulse width the rise times of the oscillo-
scope and the photodetector has to be taken into account This convolved rise-time,
denoted τ_{system} is given by

$$\tau_{system} = \sqrt{\tau_{DSO}^2 + \tau_{photo}^2}$$
$$= \sqrt{7ps^2 + 9ps^2} \tag{3 5}$$
$$= 11\ 4ps$$

where the rise-time of the oscilloscope (τ_{DSO}) is 7ps and the rise-time of the photodetec-

tor (τ_{photo}) is 9ps . Therefore the measured pulse width as recorded on the oscilloscope is given by :

$$\tau_{measured} = \sqrt{(\tau_{system})^2 + (\tau_{actual})^2} \tag{3.6}$$

where $\tau_{system} = 11.4ps$ and $\tau_{measured}$ is the FWHM as measured on the oscilloscope. Thus for the 33ps FWHM value for the optical pulse shown in Figure 3.12, the deconvolved duration of the optical pulse:

$$\begin{aligned} \tau_{actual} &= \sqrt{(\tau_{measured})^2 - (\tau_{system})^2} \\ &= \sqrt{33ps^2 - 11.4ps^2} \\ &= 30.9ps \end{aligned} \tag{3.7}$$

All of the measured optical pulse widths given in the rest of this chapter will be the deconvolved pulse width calculated using Equation 3.7.

The gain-switched pulse spectrum is shown in Figure 3.13. The spectral width of
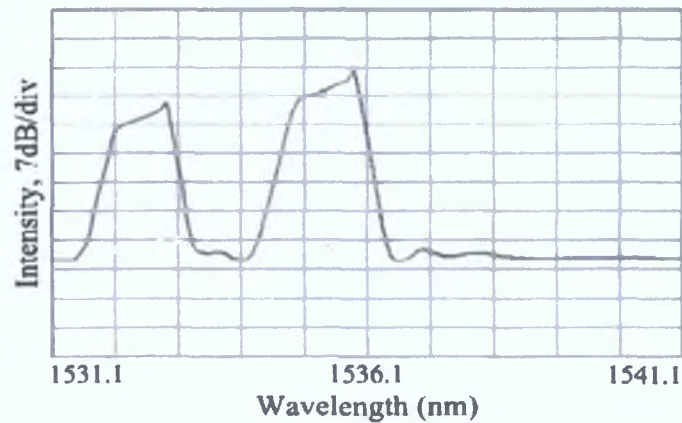
Figure 3.13: Optical spectrum of DFB1 under gain-switched conditions

the gain-switched pulse increased to 0.5nm, resulting in a time-bandwidth product of 1.854, which is far from the transform limit of 0.44 for a Gaussian pulse. Along with an increase in the spectral width, the SMSR has been degraded due to the gain switching process. The measured SMSR for the gain-switched pulse was 7dB, which is significantly reduced from the 40dB obtained when the device was operating under CW conditions (see Figure 3.10).

The degradation in the SMSR during the gain switching process arises due to the very large fluctuations in the photon density caused by the laser being pulled below threshold. This results in the side-modes of the laser being strongly excited [35], and an increase in the noise of the pulse due to the mode partition effect [36]. If the SMSR is not sufficient (<25dB), then the interaction of mode partition noise effect with either fibre dispersion, or spectral filtering, will result in an large amount of amplitude noise

on the transmitted signal, rendering such pulses unsuitable for data transmission in an optical communications network [37].

3.3 Reduction of Chirp and Timing Jitter

As shown in the previous section, there are a number of problems associated with the gain-switching process including an increase in the spectral width, degradation of the SMSR (see Figure 3.13) and an increase in the amount of temporal jitter present in the pulse (see Figure 3.6). Therefore if gain-switched optical pulses are to be used in optical communications, the amount of chirp and temporal jitter will have to be reduced, accompanied with a significant improvement in the SMSR.

There are a number of different techniques available that can reduce the jitter, improve the SMSR, and result in transform limited optical pulses. Two of the most popular techniques are *self seeding* and *external injection*. Both of these techniques involve the injection of an optical signal into the laser cavity during the initial stages of pulse build-up resulting in control over the optical output from the laser. If carried out on a gain-switched FP laser diode, both techniques also allow the generation of wavelength tunable optical pulses.

3.3.1 Self Seeding

Self seeding involves the re-injection of a small portion (limited to between 0.2%-6% to prevent any damage to the laser diode [38]) of the laser's output signal back into the laser cavity during the build-up of the next pulse. If operating conditions are correct, self seeding results in decreased jitter and chirp. The term self seeding refers to the weak injection which only serves to establish the required initial conditions ('seed' the output), from which the laser oscillation builds up as the electrical injection signal is applied. Therefore the basis of self seeding is to govern the laser's output at the initial pulse build up stage using the injected seeding signal rather than relying upon spontaneous emission.

Figure 3.14 shows a basic Self-Seeded Gain-Switched (SSGS) optical pulse source. The gain-switched section comprises of a high-power electrical pulse source modulating a DC-biased laser diode. The self-seeding components comprise of an external cavity consisting of a wavelength-selective element, Polarisation Controller (PC), Optical Delay Line (ODL) and fibre coupler. Figure 3.14 shows the simplest configuration with a reflective wavelength-selective element and PC.

The first gain-switched pulses from the laser will still exhibit the same gain-switched spectrum as before since it has not been seeded yet (Figure 3.15 [a]). The first pulse is then filtered by the wavelength selective element and fed back into the laser diode
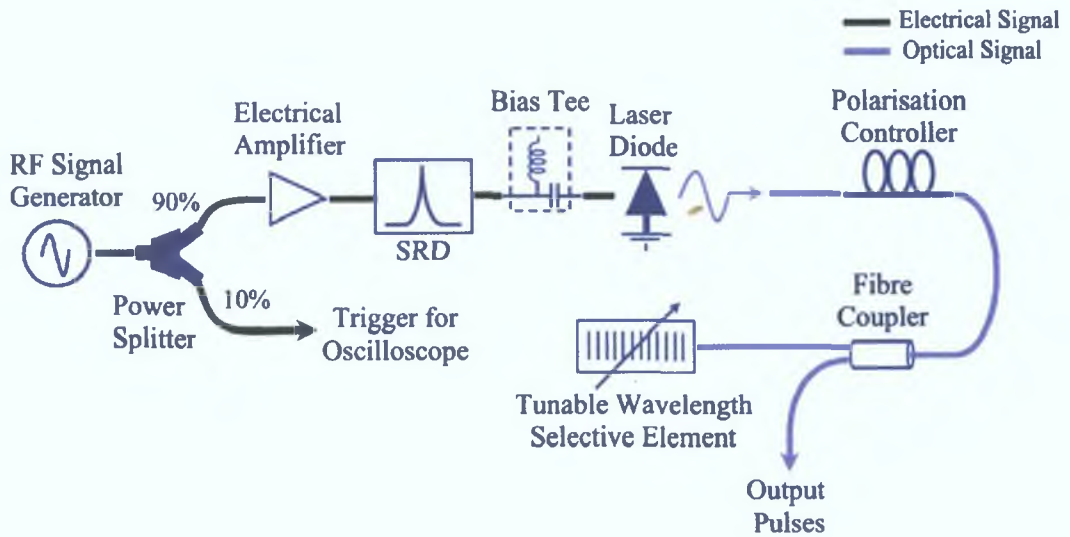
Figure 3.14: Schematic of basic self-seeding experimental setup

(Figure 3.15 [b]). The spectral output power of the longitudinal mode that coincides with the filtered injected signal increases with the injected gain, while all of the other modes are suppressed. In terms of the temporal formation of the pulse, the feedback signal advances the laser emission, with the oscillations within the laser building up from the injected signal rather than spontaneous emission. This drives the laser more quickly into saturation, causing a reduction in the peak carrier inversion level. This results in the laser switching faster producing optical pulses with longer duration and lower gain [39]. However, the pulses do exhibit a reduction of timing jitter, improved SMSR (Figure 3.15 [c]) and reduced chirp.
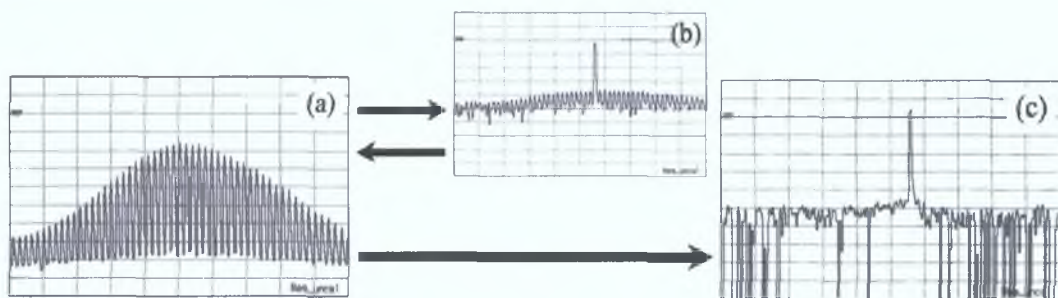
Figure 3.15: Optical spectrum of FP: (a) Under gain-switched conditions; (b) After optical filtering; (c) Self-seeded single-moded output

The improvement in the SMSR results from the feedback signal causing an initial excitation well above the spontaneous emission noise level for the dominant mode, causing the laser's emission to be strongly single-moded with a high SMSR [40]. In addition to a drastic improvement in the SMSR, the feedback signal also decreases the amount of timing jitter of the pulse. As already mentioned, uncorrelated timing jitter

originates from random fluctuations of the spontaneous emission during pulse build-up within the cavity. As the influence of spontaneous emission is decreased by the optical feedback signal, the amount of timing jitter is also reduced [41]. Finally, the injection signal also reduces the amount of chirp across the pulse, which reduces the width of the central laser mode [40]. This arises from the fact that the injected optical feedback signal lowers the variation of the carriers within the cavity during pulse build-up.

There is a short temporal window within which the re-injection signal must arrive back in the laser diode in order to prevent pulse build-up from spontaneous emission. The start of the temporal window begins when the applied electrical signal starts to inject carriers into the laser cavity and finishes just before the carrier density reaches laser threshold. As stated, during this time the optical field building up in the cavity is dominated by spontaneous emission, meaning that a small amount of optical input can dramatically influence the output signal. Before the seeding window, any additional input will be quickly damped by internal absorption of facet losses, while after the seeding window, the number of photons is growing exponentially due to stimulated emission, requiring a much stronger optical input signal to alter the signal [42, 43].

In order to ensure that the seeding signal arrives at the correct time, fine adjustments to the gain-switched frequency can be carried out to ensure that repetition rate is tuned to an exact integer multiple of the round-trip frequency of the feedback loop. An alternative is to alter the external cavity length, via the use of a variable Optical Delay Line (ODL). Optimal performance (maximise the SMSR) may also require adjusting the polarisation of the reflected signal using a PC [21] after the laser diode.

3.3.2   Self-Seeding Experimental Setup

Figure 3.16 shows the experimental setup used for self-seeding. As before, the gain-switched optical pulses are generated by applying a high-power electrical pulse to a DC-biased laser diode. The DFB used in the initial experiments was replaced with a FP (FP2) device to provide a wide tuning range. The FP device was a commercially available NTT $1.5\mu m$ InGaAsP laser diode with a threshold current of 19mA, central wavelength of 1528nm, and maximum output power of 4mW at 60mA. The specification for this device is given in Appendix A. The FP device was biased below threshold at 8mA with the RF signal generator at 500MHz with 0dBm of output power. The CW and gain-switched spectra for FP2 are shown in Figure 3.17 (a) and (b) respectively, showing a spectral width of over 50nm extending from 1497nm to 1547nm. Figure 3.17 (c) and (d) shows a zoom in on the modes of FP2 under CW conditions and gain-switched conditions respectively. These show that as a result of the gain-switching process, the spectral width of the modes broadens (d) compared when under CW conditions (c). The asymmetry at the peaks of the gain-switched modes results from the frequency
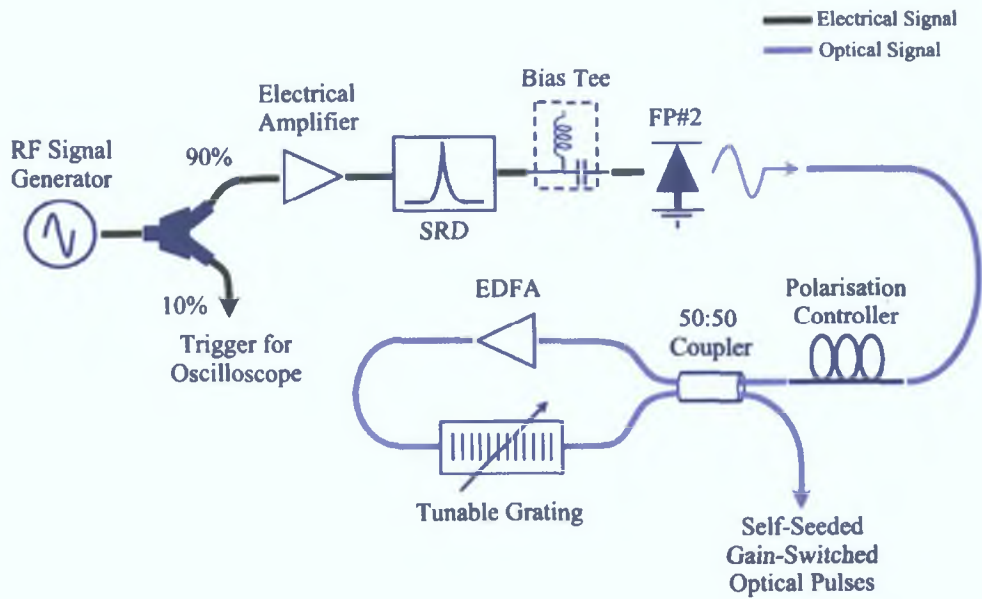
Figure 3.16: Schematic of self-seeding experimental setup
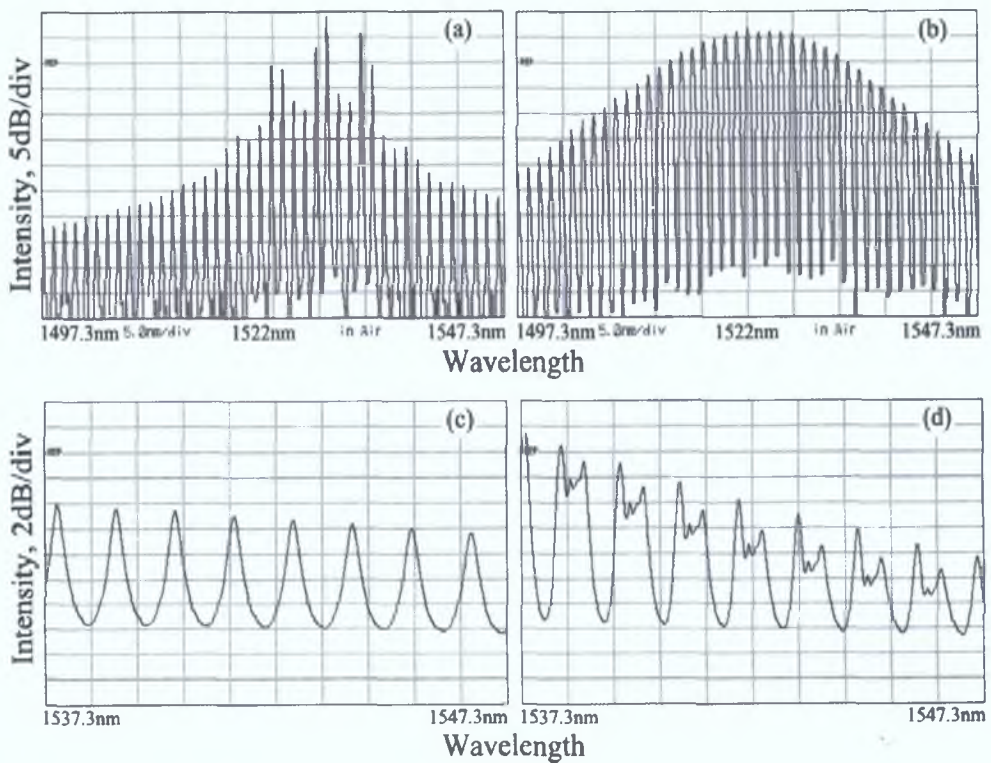
Figure 3.17: Optical spectra of FP2 under: (a) CW conditions; (b) Gain-switched conditions; (c) Zoom of CW spectra; (d) Zoom of gain-switched spectra

chirp imposed during pulse build-up within the cavity.

The external cavity consists of a PC, and a filter loop, containing of 3dB optical coupler, an EDFA and tunable optical filter. The EDFA is required to overcome the insertion loss of the filter, and to ensure that there is sufficient light reinjected back

into the cavity. An isolator on the EDFA ensure that light only propagates in one direction around the feedback loop, and the tunable filter eliminates unwanted amplified spontaneous noise from the EDFA, in addition to selecting the laser mode to be seeded.

The tunable filter that was used in the experiment was a JDS Uniphase TB9 transmissive grating-based optical filter. It has a tuning range of over 100nm, from 1460nm to 1575nm, with a bandwidth of 0.22nm. As the bandwidth of the filter is less than the mode spacing of the gain-switched spectrum, it was possible to isolate a single mode. To achieve optimum pulse generation, the filter was tuned to one of the longitudinal modes of the gain-switched laser. The frequency of the modulation signal was then varied to ensure that the re-injected light entered the laser cavity during the build-up of the next pulse. An operating frequency of 497.59MHz was found to be most suitable. The threshold of the laser was also reduced to 5mA. The EDFA pump power was set to 21.3mW, with the polarization controller adjusted to maximise the SMSR.

The output pulses in the time and spectral domains, as seen from the second input of the coupler, are shown in Figures 3.18 and 3.19 respectively. As expected with the
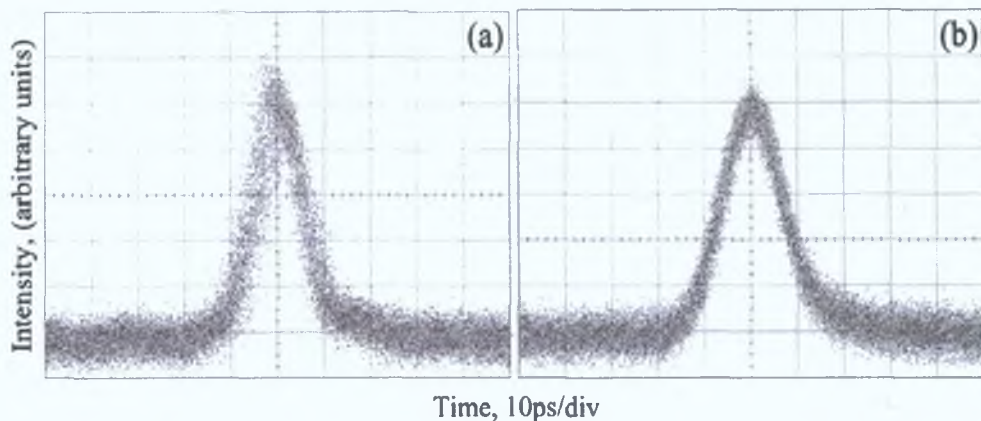
Figure 3.18: Gain-switched pulses: (a) Before self-seeding; (b) After self-seeding

seeding process, the optical pulse duration has increased from 10ps to 12.3ps, with rms jitter reduced from 2.1ps to 1ps. Figure 3.19 (a) shows the filtered spectrum after the filter prior to re-injection, with (b) shows the filtered self-seeded spectrum measured at the second port of the output coupler. The peak wavelength was 1525nm, with SMSR of the signal exceeding $35dB$.

Figure 3.20 shows a comparison in the spectral width of individual modes of FP2 under CW, gain-switched and self-seeded conditions. The spectral width as measured on the OSA for the CW was 0.05nm (limited by the minimum resolution of the OSA), 0.78nm for the gain-switched spectrum, and 0.54nm for the self-seeded gain-switched pulse. This results in a time-bandwidth product of 0.936 for the gain-switched pulse, and 0.797 for the self-seeded gain-switched pulse. The reduction in the spectral width of the mode under self-seeding conditions when compared to gain-switched operation
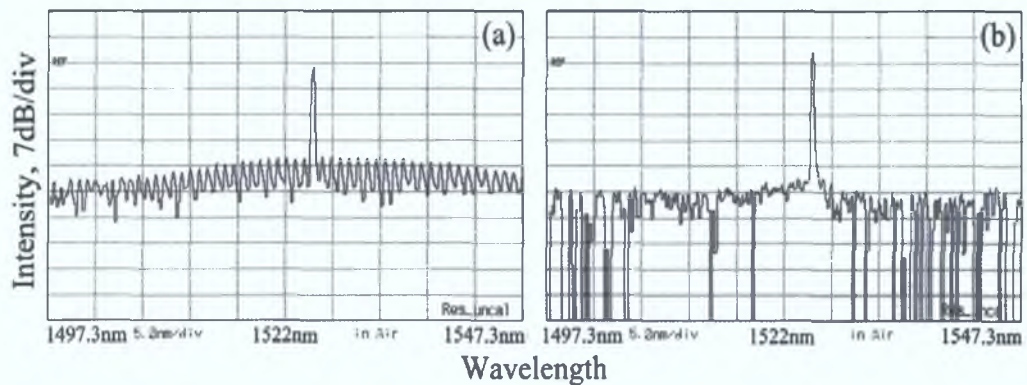
Figure 3.19: Optical spectrum of FP: (a) After optical filtering; (B) Self-seeded single-moded output

results from the reduction in the frequency chirp. As already mentioned, chirp reduction arises from the fact that the injected optical feedback signal lowers the variation of the carrier density within the laser cavity during pulse build-up.
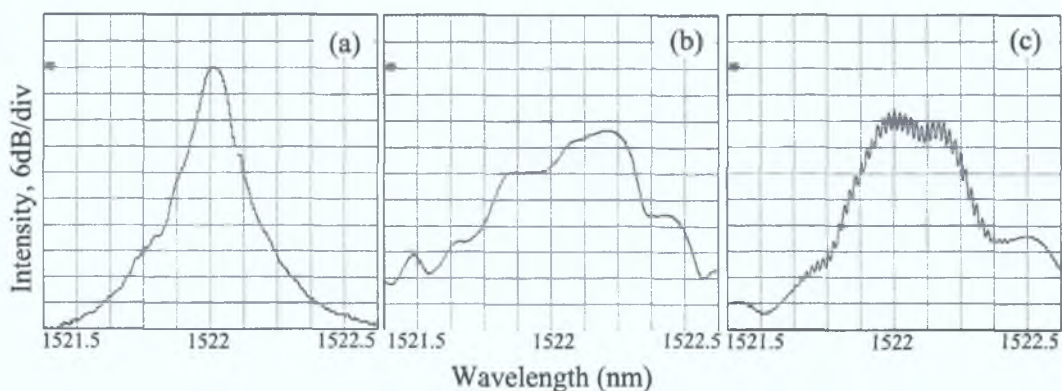
Figure 3.20: Optical spectrum of FP: (a) Under CW conditions; (b) Gain-switched conditions; (c) Self-seeded conditions

3.3.3 External Injection

As shown in the previous section, one of the most reliable methods to generate tunable optical pulses is by employing self seeding of a FP laser diode. By doing so, high-quality, wavelength tunable, single-mode optical pulses, with low timing jitter and good spectral purity can be achieved. However, one of the main disadvantages of self-seeding is that the length of the external cavity has to be continuously tuned to the pulse repetition frequency, to ensure that the seeding signal arrives back into the laser cavity at a time corresponding to the initial stages of the generation of the next optical pulse.

An alternative technique, which requires no adjustment of the repetition rate or external cavity length is external injection of light from a CW source into a gain-switched

74

laser [44]. This can provide more stable operation as the required wavelength can be selected and easily tuned without the need to alter the length of the external cavity [45]. It has been demonstrated in [46] that the CW tunable laser source can be replaced by a DC-biased FP laser diode and a Fibre Bragg Grating (FBG) as the external injection light source. However, additional components such as an optical delay line are required to ensure that the optical signal arrives into the cavity at the correct time.

As per the self-seeding process already described, the external injected signal provides an excitation above the spontaneous emission level within the laser cavity, reducing the relative fluctuations in the photon density, resulting in a reduction of the timing jitter of the optical pulses produced [47]. However, as per self-seeding, an increase in injected power levels correspond to an increase in the pulse duration as the maximum carrier inversion level is reduced.

3.3.4 External Injection Experimental Setup

The external injection setup is shown in Figure 3.21. As with the self seeding, the
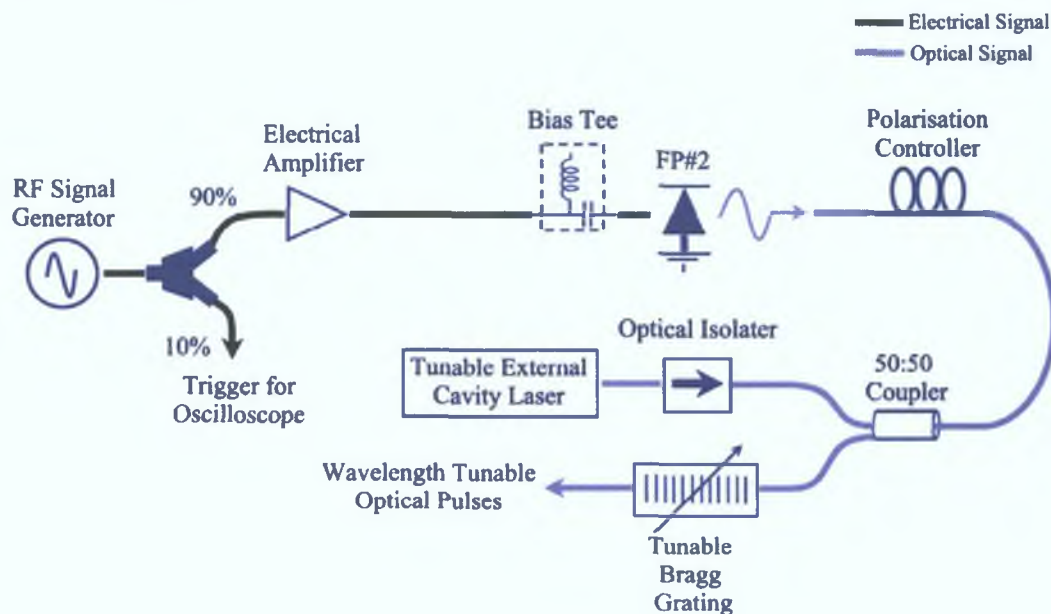
Figure 3.21: Schematic of external injection experimental setup using FP2

laser diode was a commercially available Fabry-Perot $1.5\mu m$ InGaAsP device, with a threshold current of 19mA. Gain-switching was carried out at 2.5GHz, with the bias current was set to 15mA. The CW injection signal was provided by a tunable External Cavity Laser (ECL) (Hewlett Packard 8168F Tunable Laser Source, Wavelength Range 1450-1590nm, Output Power -7 to 7dBm) which injects light into one of the modes of the gain-switched device via an isolator, 3dB fibre coupler and a PC. The isolator prevents any back reflection from damaging the ECL. The PC was varied to optimise

75

the coupling of the injected signal from the ECL into the laser cavity, thus maximising the output SMSR The output of the ECL was set to -3dBm, which taking into account various losses, corresponds to an injection level of about -13dBm The resulting single-mode output obtained after the external injection is then passed through the same tunable filter used in the self-seeding setup to enhance the SMSR of the generated pulses The output pulses were then characterised using the same equipment as used in the previous work

Figure 3 22(a) shows the gain-switched spectrum of FP2 while Figure 3 22(b-d) shows three selected modes at 1510nm, 1520nm and 1530nm respectively before passing through the tunable filter The three selected modes each exhibit a SMSR in excess
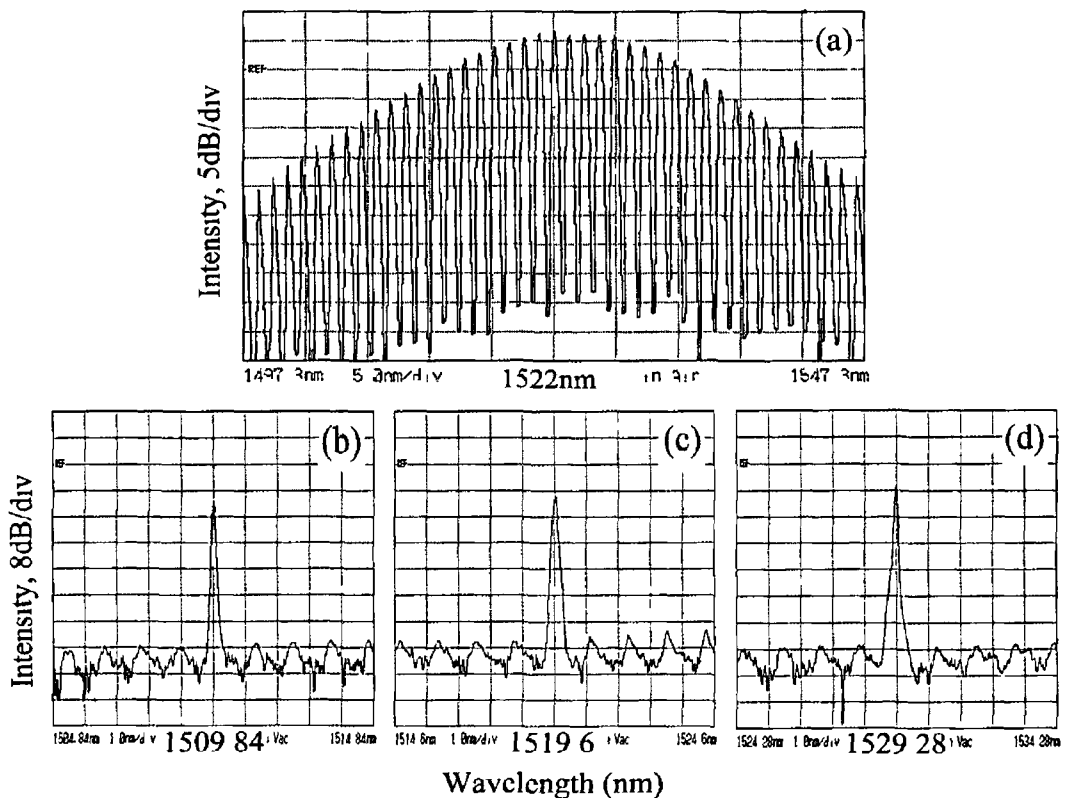
Figure 3 22 Optical spectra of FP2 (a) FP2 Under gain-switched conditions, Optical filtering (b)1510nm, (c) 1520nm, (d) 1530nm

of $35dB$ With the addition of the optical filter, the SMSR of the output pulses were improved such that is becomes almost impossible to detect the side-modes above the noise floor of the OSA (see Figure 3 23) The resulting SMSR is around 60dB over the entire wavelength tuning range

Figure 3 24 shows an optical pulse after filtering The duration of the filtered optical pulse was calculated to be 16ps with the spectral width determined by the bandwidth of the optical filter (0 23nm) This results in a time-bandwidth product of 0 45, which is close is to the transform-limited value for a Gaussian pulse

76
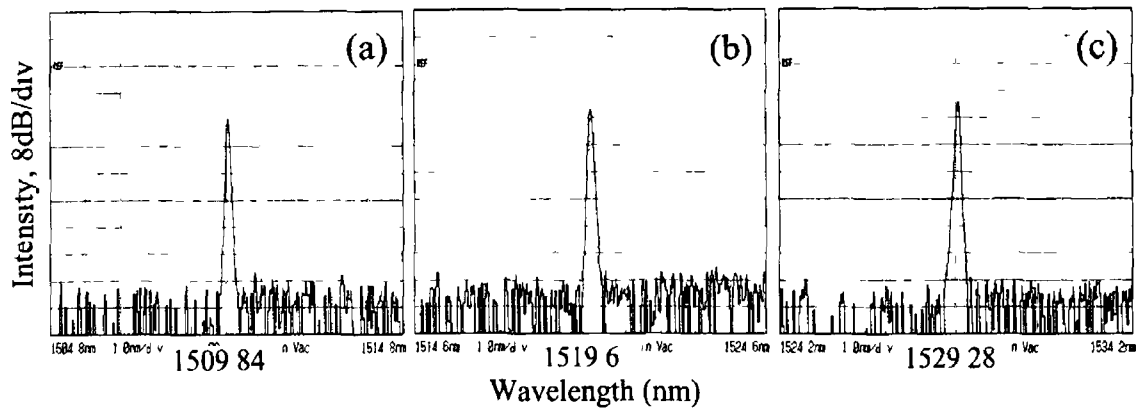
Figure 3 23 Optical spectra of FP2 under externally injection at (a) 1510nm, (b) 1520nm, (c) 1530nm
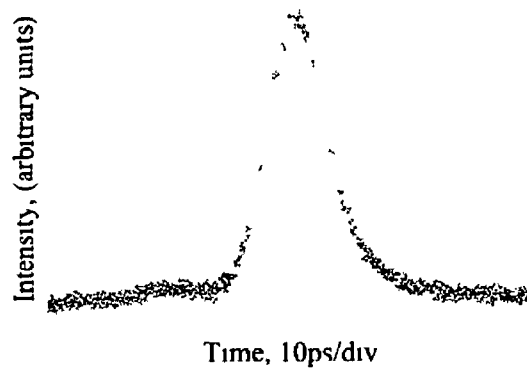
Figure 3 24 Optical pulse at 1530nm under external injection conditions

3.4 Pulse Compression

The previous experiments have demonstrated the generation of wavelength tunable gain-switched optical pulses, with the narrowest pulse width generated around 15ps This would allow data rates of approximately 20Gbit/s, considering that the bit slots in an OTDM system are generally 3 times the width of the optical pulses used to represent the data being transmitted This helps to minimise the effect of ISI For future OTDM systems operating at data rates in excess of 100Gbit/s, optical pulses with durations around 3ps will be required Therefore if gain-switched pulses are to be used in such systems, their duration will have to be reduced There are a number of different techniques available for pulse compression including the use of a fibre grating, dispersion compensating fibre and solitonic compression

Optical pulse compression was first described in 1968 in [48] by linearly sweeping the instantaneous optical frequency of each pulse in a way that the optical cycle at the beginning of the pulse is at a higher frequency than those at the end of the pulse Then by propagating the pulse through a dispersive medium, the trailing edge of the pulse

was able to catch up with the leading edge, in a fashion analogous to the compression of frequency-swept wave trains in chirp radar [48]

3.4.1 Fibre Pulse Compression

If an unchirped optical pulse propagates in standard optical fibre, the width of the pulses increases due to dispersion However, if the pulse is initially chirped, the pulse will either be broadened or compressed depending on the sign of the fibre dispersion parameter and the sign of the initial chirp The optimal fibre compression for a Gaussian pulse with linear chirp is given by [15],

$$-DL = \frac{\Delta t}{\Delta \lambda} \tag{3 8}$$

where D is the dispersion parameter of the fibre in ps/(km nm), L is the fibre length in km, Δt is the optical pulse duration in ps and $\Delta \lambda$ is the spectral width in nm As the latter two terms are functions of the gain switching process, optimal performance can be achieved with fine adjustment of the bias current Generally the time-bandwidth product of a fibre compressed pulse will deviate from the transform limited value for that particular pulse shape This arises as both linear and nonlinear chirp are present across a gain-switched pulse, with fibre compression only compensating for the linear chirp across the central part of the pulse [49]

3.4.2 Grating-Fibre Compression

An alternative to fibre compression is to employ a grating fibre compression scheme [3] This employs a length of fibre with normal GVD to impose a positive chirp followed by an external fibre grating to compress the optical pulse, and was first demonstrated in [50] As the optical pulse is incident on the grating, different frequency components are diffracted at slightly different angles, resulting in different spectral components experiencing different time delays as the pulse hits the grating The grating provides the anomalous GVD that can be used to compress the positive chirp imposed on the pulse by the length of fibre [49] Recent gain switched experimental work at 1 06μm has shown that optical pulse durations can be reduced from 57ps to 15 6ps using a grating-fibre compressor [51]

3.4.3 Solitons

With current commercially available DCF, linear compression is able to produce pulses with durations of around 5ps However, in order to produce even narrower gain-switched

pulses, alternative pulse compression schemes are required One such method is non-linear pulse compression using higher-order solitons

As an optical pulse propagates in optical fibre, the effects of fibre dispersion and nonlinearities usually results in the temporal and spectral shape of the pulse changing The effect of SPM is to increase the frequency in the trailing edge of the pulse while at the same time decrease the frequency at the leading, while dispersion causes different spectral components to travel at different speeds In the anomalous region, dispersion will cause higher frequency components to propagate at a higher group velocity then lower frequencies If the higher frequency components are at the trailing edge, then this portion of the pulse will propagate faster than the leading edge, causing the pulse to narrow Under certain conditions (no fibre loss) these two effects (SPM and GVD) can exactly cancel one another resulting in the temporal and spectral shape of the pulse remaining unaltered, even over long propagation distances For this to happen, the pulse must have a particular shape, duration and energy Such a pulse is known as a soliton, and finds applications in ultra long haul high-speed optical transmission [52] and optical pulse compression [53]

The word soliton was first coined by Zubusky and Krushal in 1965 [54] who published a paper citing a numerical solution of the Korteweg-deVries (KdV) equation using a periodic boundary conditions The KdV equation was derived in the 19th century to model a wave propagating on the surface of water The paper described how a train of solitary waves were formed that could pass through one another without deformation due to the collision As a result, these solitary waves was called solitons

Two years after the Zubusky and Krushal work, Gardner et al used the inverse scattering method [28] to show a mathematical interpretation of these solitary wave solutions proving that the KdV equation can be solved exactly for a localised initial condition In contrast to the KdV soliton which describes the motion of a wave, optical solitons in fibre belong to a separate category known as envelope solitons, as an optical pulse in fibre can be described as an envelope of light The equation that describes such an envelopes propagation in optical fibre is the Nonlinear *Schrodinger* Equation (NLSE) Therefore if the NLSE was solved in terms of dispersion and nonlinearity only, remembering that the soliton arises from the interplay between GVD and SPM, the solutions would be a solitary wave, once the pulse envelope satisfied the necessary conditions This would allow the initial conditions (pulse shape, width, power) necessary for soliton propagation to be identified

To derive an expression for the NLSE, Maxwell's equations can be used to obtain the basic propagation equation [3]

$$\frac{\delta A}{\delta z} + \beta_1 \frac{\delta A}{\delta t} + \frac{i}{2}\beta_2 \frac{\delta^2 A}{\delta t^2} + \frac{\alpha}{2}A = i\gamma |A|^2 A \qquad (3\ 9)$$

where A is the amplitude of the pulse envelope, z is the transmission distance, β_1 is the mode propagation constant, β_2 is the group velocity dispersion term, α is the fibre loss and γ is the nonlinear coefficient of the fibre, which can be expressed as

$$\gamma = \frac{n_2 \omega_0}{c A_{eff}}$$

(3 10)

where A_{eff} is the effective core area

In order to describe the relationship between GVD and SPM that leads to soliton formation, a frame of reference moving with the pulse at a group velocity v_g is employed, which results in Equation 3 9 becoming

$$i\frac{\delta A}{\delta z} = \frac{1}{2}\beta_2 \frac{\delta^2 A}{\delta \eta^2} - \frac{i\alpha}{2} A - \gamma |A|^2 A$$

(3 11)

where $\eta = t - \dfrac{z}{v_g}$ In the absence of any fibre loss ($\alpha = 0$), Equation 3 11 is known as the NLSE [55] It is useful to employ a normalised time and amplitude scale into Equation 3 11 This results in an equation for the normalised pulse envelope that is a function of both distance and time

$$i\frac{\delta U}{\delta z} = \frac{sgn(\beta_2)}{2L_D} \frac{\delta^2 U}{\delta \tau^2} - \frac{e^{-\alpha z}}{L_{NL}} |U|^2 U$$

(3 12)

where $sgn(\beta_2) = \overset{+}{-} 1$ (depending on the sign of β_2), L_D is the fibre length over which dispersive effects become important and L_{NL} being the fibre lengths over which non-linear effects become important L_D is defined as

$$L_D = \frac{T^2}{|\beta_2|}$$

(3 13)

with L_{NL} being

$$L_{NL} = \frac{1}{\gamma P_0}$$

(3 14)

Now by neglecting fibre loss, and assuming that the optical communications systems is operating in the anomalous fibre dispersion region ($\lambda > 1310nm$), Equation 3 12 can be re-written as

$$i\frac{\delta U}{\delta \zeta} = -\frac{1}{2}\frac{\delta^2 U}{\delta \tau^2} - N^2 |U|^2 U$$

(3 15)

with $\zeta \equiv \dfrac{z}{L_D}$ Using the variable $u = NU$, N can be eliminated and Equation 3 15 can be written in the standard NLSE for a pulse propagating in the anomalous region of a fibre which has no fibre loss

$$i\frac{\delta u}{\delta \zeta} + \frac{1}{2}\frac{\delta^2 u}{\delta \tau^2} + |u|^2 u = 0$$

(3 16)

In 1972, Zakharov and Shabat [54] showed that Equation 3.16 can be solved using the inverse scattering method [28], similar to the way in which the KdV equation was solved. According to the inverse scattering method, the solution of Equation 3.16 can be described as a soliton. This was confirmed a year later by Hasegawa and Tappert [52,56] who theoretically showed that an optical pulse propagating in a fibre forms a solitary wave once the pulse envelope satisfies the NLSE (Equation 3.16).

The solution of the NLSE, sometimes referred to as the envelope soliton can be described by the complex eigenvalues of Dirac-type equations, with the fundamental soliton corresponds to the case of a single eigenvalue η_1. Its general form is given by:

$$u(\zeta, \tau) = 2\eta_1 sech(2\eta_1\tau)exp(2i\eta_1^2\zeta) \tag{3.17}$$

The eigenvalue value η_1 determines the soliton amplitude, with the fundamental soliton obtained by choosing u(0,0)=1 so that $2\eta_1=1$. The general form of the fundamental soliton can therefore be written as:

$$u(\zeta, \tau) = sech(\tau)exp(\frac{i\zeta}{2}) \tag{3.18}$$

The soliton order is given by N, where:

$$N^2 = \frac{L_D}{L_{NL}} \tag{3.19}$$

N = 1 corresponds to a fundamental soliton, and N > 1 corresponds to higher-order solitons. By substituting Equations 3.13 and 3.14 into 3.19, N^2 becomes:

$$N^2 = \frac{T^2\gamma P_0}{|\beta_2|} \tag{3.20}$$

Therefore, if a hyberbolic secant pulse with a particular pulse width (T) and peak power P_0 such that N = 1, is launched into a lossless fibre with specific values of β_2 and γ such that Equations 3.13, 3.14 and 3.20 are satisfied, Equation 3.18 states that this pulse can propagate over a long distance totally undistorted. From Equation 3.20, the peak power (P_0) required for a fundamental soliton can be given by:

$$P_0 = \frac{|\beta_2|}{\gamma T^2} \tag{3.21}$$

where the width T is related to the Full Width at Half Maximum (FWHM) by T_{FWHM} = 1.76T. Therefore the peak power to excite a fundamental soliton can be expressed as:

$$P_0 = \frac{3.11|\beta_2|}{\gamma T_{FWHM}^2} \tag{3.22}$$

81

In order to see this effect, wave distortion due to fibre loss had to sufficiently lower than the effects of fibre dispersion and fibre nonlinearities This required an optical fibre with fibre loss <1dB which was not available at the time Seven years after the publication of Hasegawa and Tappert work, Mollenauer et al [53] were finally able to experimentally demonstrate the theoretical findings of Hasegawa and Tappert, thus proving soliton propagation Optical transmission of 1 28Tbit/s over 4,000km has been experimentally demonstrated in 2003 [57], thus generating the true potential of soliton transmission

3.4.4 Higher-Order Solitons

As already mentioned, with specific values for L_D and L_{NL}, Equation 3 19 can result in N values greater than 1, and these are referred to as higher-order solitons An interesting property of higher-order solitons is that their periodic behaviour in the anomalous dispersion regime is different to that of the fundamental soliton Whereas the fundamental soliton is able to propagate totally undistorted, higher-order solitons have an initial stage where the pulse shortens to a fraction of its initial width, followed by a splitting of the pulse into two or more distinct pulses, before merging back to recover the original shape This distance over which this happens is known as the soliton period, and is denoted as z_0 This initial narrowing stage of higher-order soliton propagation can be exploited for optical pulse compression

The power required to form a N-order soliton is given by [55]

$$P_N = 3\ 11N^2 \frac{D\lambda^2}{2\pi c\gamma T_{FWHM}^2}$$ (3 23)

A very important feature of higher-order solitons is that the solution $|u(\zeta, \tau)|$ is a periodic function of time with the soliton period z_0 given by

$$z_0 = \frac{\pi}{2}L_D$$ (3 24)

Therefore with an appropriate choice of fibre length, the initial pulses can be compressed by a factor that depends on the soliton order N and the parameters of the fibre [3] The compression factor F_C and the optimum length of the soliton-effect compressor z_{opt} can be approximated by

$$F_C \cong 4\ 1N$$ (3 25)

$$z_{opt} \cong z_o \left(\frac{0\ 32}{N} + \frac{1\ 1}{N^2} \right)$$ (3 26)

Figure 3 25 shows a simulation of 4th order soliton propagation Note the pulse

82

shape evolution, with maximum pulse compression after propagation in 100m of SMF, before the pulse starts to split.
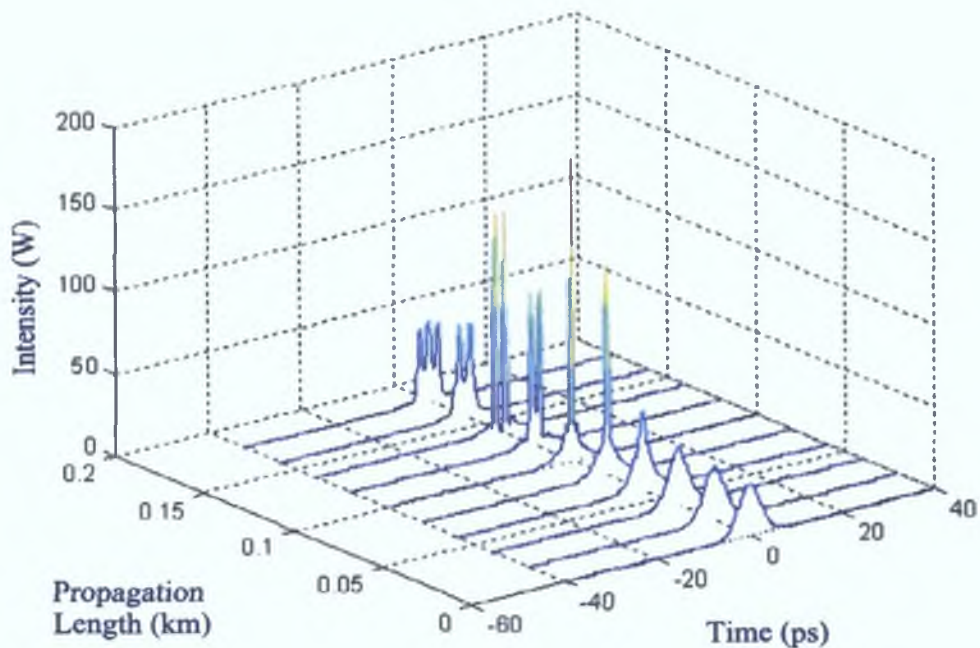
Figure 3.25: Plot of the 4th-order soliton propagation as a function of pulse duration, pulse power and propagation distance

Properties of Higher-Order Solitons

As already mentioned, for soliton formation the pulse must have a specific shape, duration and peak power, all of which are functions of the different fibre parameters. A second important property necessary for soliton propagation is that the pulse must be transform-limited and chirp free. If there is initial chirp present, then this will superimpose on the SPM induced chirp and effect the balance between GVD and SPM necessary for soliton propagation. Therefore in order for the gain-switched pulses to propagate as solitons, it is necessary to first compensate for the gain-switched induced chirp across the pulse. There are a number of ways to carry this out, with the simplest being to propagate the gain-switched pulse in an appropriate length of DCF.

One of the more interesting properties of soliton formation is that if the initial pulses are not a hyberpolic secant shape or if the peak power and pulse duration do not satisfy Equation 3.20 for N = integer, the pulse can still evolve into solitons provided that the minimum energy threshold conditions for soliton formation has been achieved [58]. For example, if the conditions for an N=1 soliton are satisfied but the pulse shape is not exactly hyperbolic secant shape, then the pulse shape will change and adjust itself

to evolve into a fundamental soliton If the pulse does have the necessary hyberpolic secant shape, but N is not an integer, then the pulse will adjust its width in order to become a soliton The disadvantage of this is that the part of the pulse energy that is not required will be spun off as a spurious pulse, which may lead to undesired distortion The analysis carried out so far has worked on the assumption that the soliton is propagating in fibre with no loss Therefore for an accurate analysis, the inclusion of fibre loss has to included For fundamental sohtons, the effect of fibre loss is to reduce the peak power of the pulse, so to remain a soliton the width of the pulse will increase Eventually the pulse power will become so small that the nonlinear effect will be negligible compared to the dispersion encountered, resulting in the pulse starting to broaden For higher-order solitons, fibre loss will result in an increase in the soliton period For a $N = 2$ soliton, the pulse will undergo some compression before developing a double peak and then return to its original shape at the end of the soliton period When fibre loss is included, the next double peak will take longer to occur Thus fibre loss weakens the structure of the soliton until the pulse starts to broaden

3.4.5 Generation of Sub-Picosecond Optical Pulses

The experimental setup used for optical pulse compression is shown in Figure 3 26 It consists of a gain-switched DFB laser diode producing a train of optical pulses at 500MHz The optical pulses are then linearly compressed by propagating the optical pulses through 200m of DCF, before being optically amplified in an EDFA and transmitted through 100m of SMF The EDFA and the 100m of SMF comprise the higher-order soliton compression stage The resulting pulses then pass through a 10 90 fibre coupler, with 10% of the optical power entering an OSA, with the remaining power entering an autocorrelator The resulting autocorrelation trace was displayed on a standard low-bandwidth electrical oscilloscope [59]

Figure 3 27 shows the autocorrelation trace of the gain-switched optical pulse as displayed on the electrical oscilloscope As the autocorrelation process results in a symmetric pulse shape, the rise-time of the leading edge of the pulse is the same as the fall-time of the trailing edge The measured FWHM was 2 8ms, which gives an autocorrelation pulse width of 12 8ps This was calculated using

$$\tau_{actual} = \tau_{autocorrelation} \times \text{conversion ratio} \times \text{pulse shape factor}$$

$$\tau_{actual} = 2\ 8ms \times 6\ 5ps \times 0\ 707 \tag{3 27}$$

$$\tau_{actual} = 12\ 8ps$$

The conversion ratio is defined here as time scale relating the displayed time base on the oscilloscope to the real pulse width, and was calculated to be 1ms=6 5ps The pulse

84
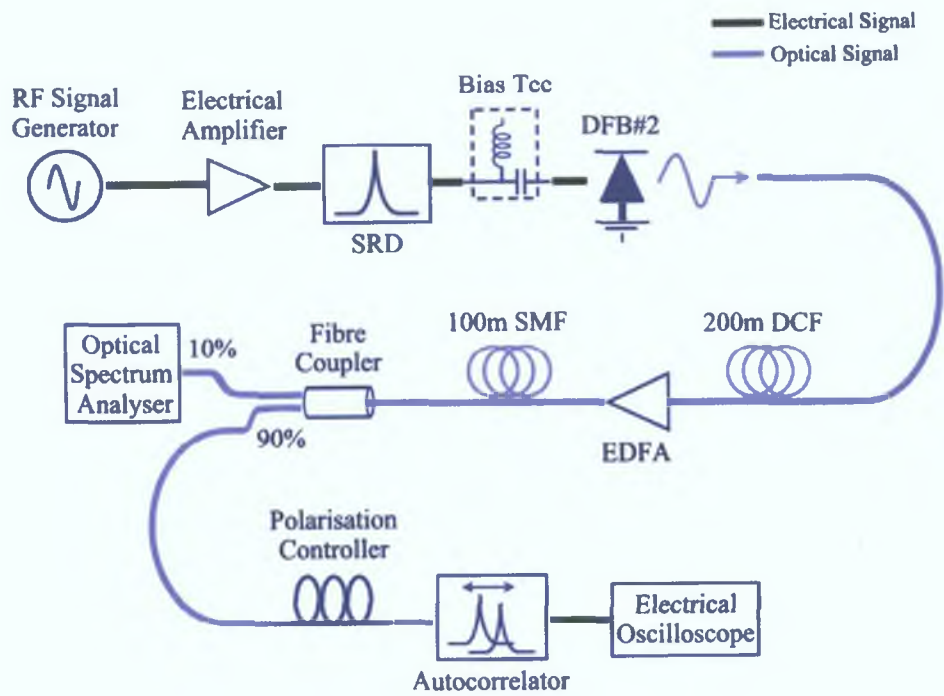
Figure 3.26: Schematic of soliton compression experimental setup
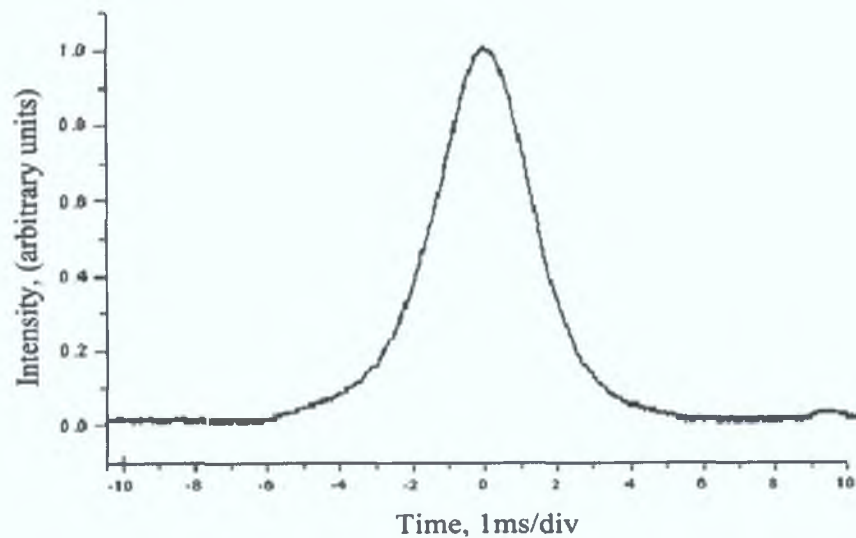
Figure 3.27: Autocorrelation trace of an optical pulse from DFB2 under gain-switched conditions

shape was approximately Gaussian, which results in an Autocorrelation Function (ACF) multiplication factor of 0.707. This is explained in more detail in Section 4.4.1 of Chapter 4.

The corresponding gain-switched optical spectrum is shown in Figure 3.28, with the spectral width measured to be 0.6nm. This results in a time-bandwidth product of
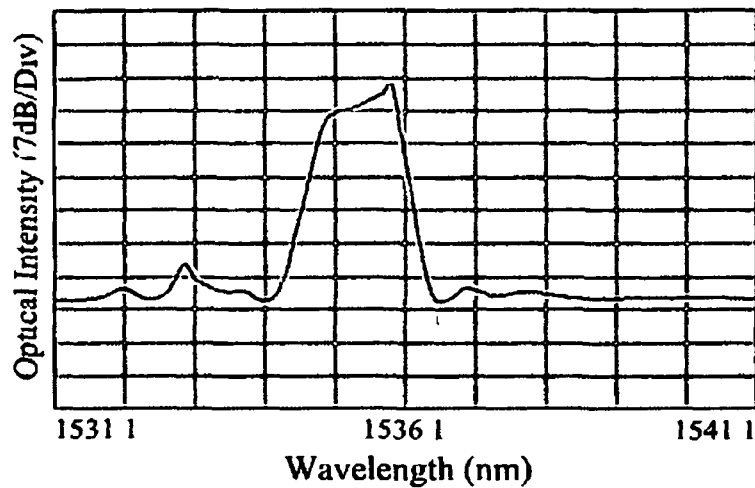
Figure 3 28 Optical spectrum of DFB2 under gain-switched conditions

approximately 1, which is far from the transform-limit value of 0 441 for a Gaussian pulse This deviation can be accounted for by the presence of frequency chirp across the pulse which results from variation of carrier density within the laser cavity during pulse build up

As mentioned, soliton formation arises due to the interaction between GVD and SPM In order for the two processes to counteract one another, the optical pulses must be close to transform limited This was accomplished by propagating the gain-switched optical pulses through dispersion compensating fibre To determine the optimum length, Equation 3 8 was used The dispersion parameter D of the DCF used was -99 $3ps/km$ nm at 1550nm, with a dispersion slope of -0 $21ps/km$ nm^2 Therefore the value of D at 1535nm was calculated to be -96 $15ps/km$ nm, with $\delta t=12$ 8ps and $\delta\lambda=0$ 6nm resulting in a length of approximately 200m The optical pulse duration was measured on the autocorrelator, with the bias current varied to achieve the narrowest pulse width possible This autocorrelation trace for the linearly compressed gain-switched optical
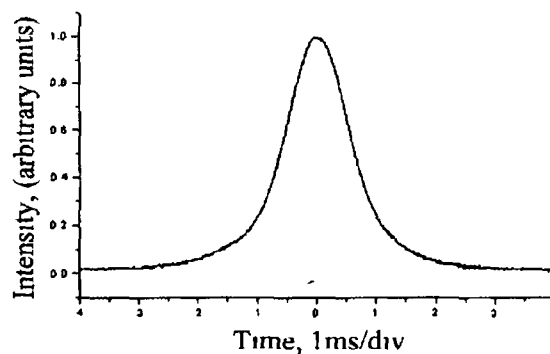
Figure 3 29 Autocorrelation trace of DFB2 under gain-switched and linear compression conditions

86

pulse is shown in Figure 3 29, with the optical spectrum shown in Figure 3 30

After the propagation through the 200m of DCF, the optical pulse duration has been reduced from 12 8ps to 6 8ps This value for the pulse duration, combined with a spectral width of 0 6nm at 1536nm, results in a time-bandwidth product reduced to 0 51 The deviation between this and the transform-limited value is due to the fact that there is both linear and nonlinear chirp present across gain-switched optical pulses, and the propagation through the DCF only compensates for the linear chirp present in the central part of the pulse The uncompensated nonlinear chirp results in the formation of a pulse pedestal which should be removed if the minimum pulse width is to be achieved As the optical compression relies totally on GVD, the spectrum obtained after propagation through the 200m of DCF is the same as the gain-switched spectrum in Figure 3 28
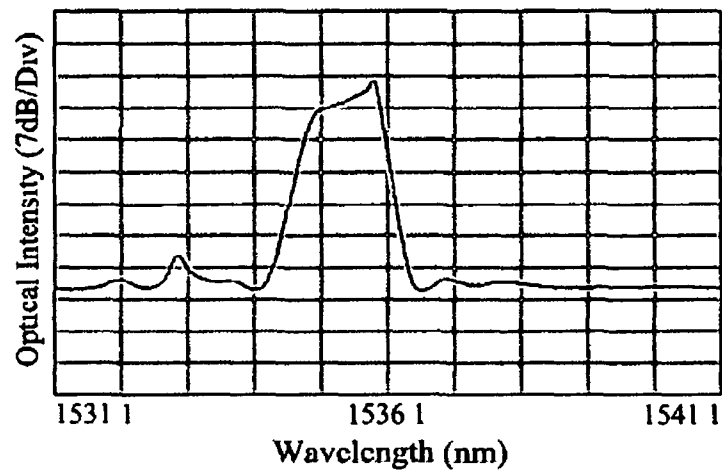
Figure 3 30   Optical spectrum of DFB2 under gain-switched and linear compression conditions

The higher-order soliton compression stage comprises of a high-power EDFA and a length of optical fibre In order to determine the length of fibre, and the soliton order required for the minimum pulse width, a Matlab computer simulation was carried out By using the formulae given in Sections 3 4 3 and 3 4 4, together with the parameters of the linear compressed pulse and SMF, it was possible to carry out various simulations to determine the optimum length of fibre of SMF and peak power required from the soliton compressor stage Some of the parameters used were

- $T_o = 5\ 6ps$

- $P_o = 31W$

- $\lambda = 1535nm$

- $D = 15\ 8ps/km\ nm$ at $1535nm$

- $\alpha = 0\ 184dB/km$

87

- $n_2 = 2.35e^{-16}cm^2/W$

The pulse shape was assumed to be Gaussian. It was also assumed that there was no chirp present, even though there would be some nonlinear chirp present on either side on the central part of the pulse. It was felt that the pulse width could be optimised by varying the bias current to the laser, and the output power of the EDFA. A computer simulation of the temporal evolution of a 4th-order soliton in SMF is shown in Figure 3.31. It shows higher-order soliton propagation, with the initial narrowing stage, followed by pulse splitting, and then returning to the original shape at the end of the soliton. As we are only concerned with the pulse compression aspect of higher-order soliton propagation, the optimum fibre length giving a projected pulse width of 350fs was 95m, with optimum performance achieved by varying the DC bias and the EDFA pump power.
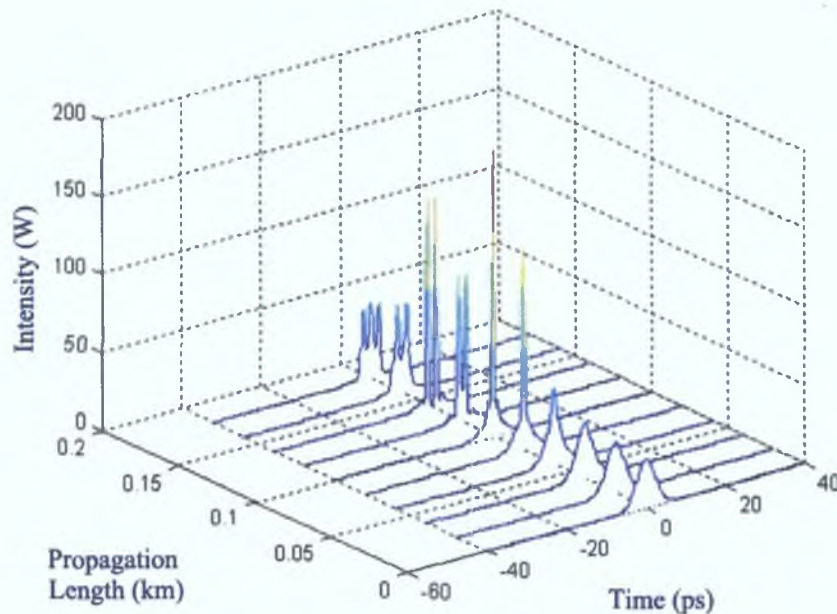
Figure 3.31: Plot of temporal evolution of a 4th-order soliton in single-mode fibre

Figure 3.32 displays the autocorrelation trace of the optical pulse after propagation through 100m of SMF. It shows the compressed pulses consisting of a sharp narrow spike centered on a broad low intensity pedestal that carries a large proportion of the pulse energy. For use in an optical communications network employing OTDM technology, this broad pedestal will overlap with adjacent pulses, resulting in a high level of crosstalk, limiting the overall data rate that is achievable.

The pulse width was calculated to be 420fs, assuming a Gaussian shape. In the previous section regarding soliton propagation, it stated that solitons are hyperbolic secant pulses, and even if the initial pulse shape differs from this, it will evolve to such
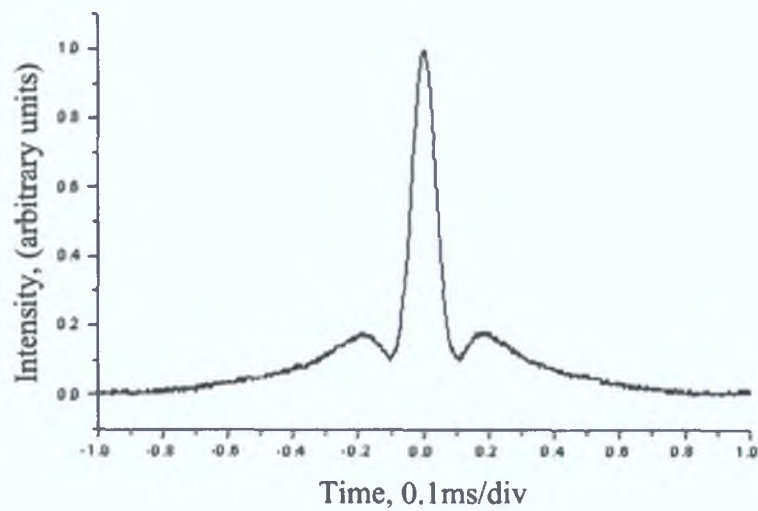
Figure 3.32: Autocorrelation trace of an optical pulse after 4th-order soliton compression

a shape during propagation. However as the soliton compression employed here occurs after only 100m of fibre, it is assumed that the pulse shape is still Gaussian.
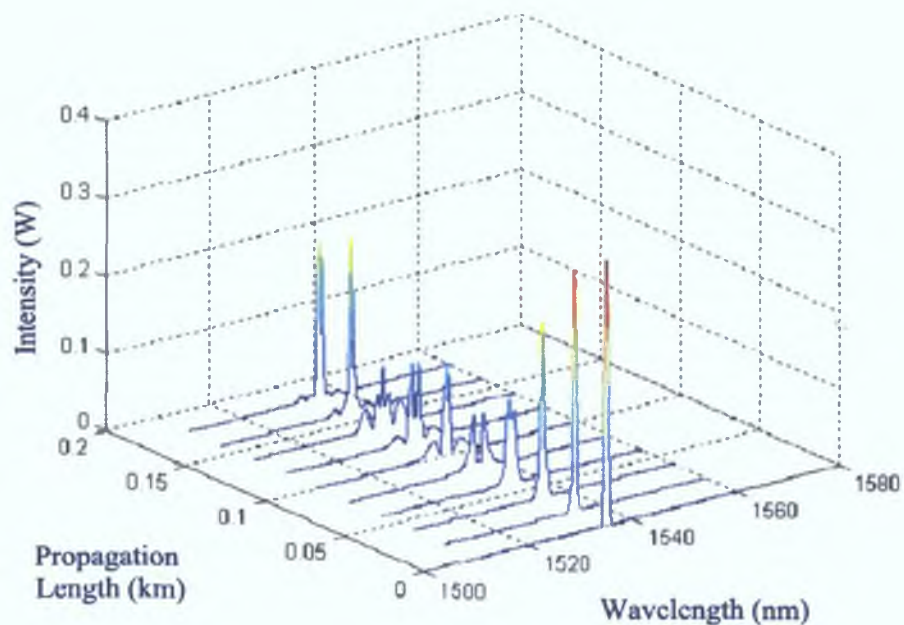
Figure 3.33: Plot of the frequency evolution of a 4th-order soliton in single-mode fibre

Figure 3.33 shows the simulated spectral evolution of the soliton. After the 100m when the pulse has the shortest duration, the spectral profile of the pulse comprises of

two lower intensity lobes, each on either side of a main central lobe of much reduced intensity compared to the input optical intensity. This spectral shape is confirmed by Figure 3.34, which shows the optical spectrum of the solitonic compressed pulse. The spectral broadening shown in Figure 3.34 is due to SPM, with the large background spectrum due to ASE noise from the EDFA.
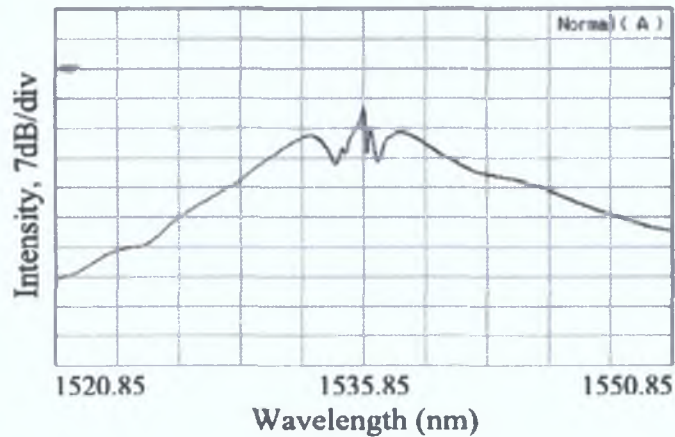
Figure 3.34: Optical spectrum of DFB2 under gain-switched conditions after 4th-order soliton compression

Figure 3.35 shows the temporal profile of the gain-switched, linearly compressed and soliton compressed optical pulses on the same plot. As can be seen, the compression factor using this method is about 30, going from a pulse duration of 12.8ps to 420fs. However, as already mentioned, the large pulse wings can limit the usefulness of these pulses in an actual data communications system. As such, an important issue associated with soliton effect compressors is the removal of the pedestal. There are a number of possible techniques, including the use of a bandpass filter [60] or a Nonlinear Optical Loop Mirror (NOLM) to perform simultaneous pulse compression and reshaping [61].

3.5   Tunable Optical Pulses

It has already been shown that self-seeding and external injection of a FP laser diode can result in the generation of wavelength tunable optical pulses. One way in which to extend the tuning range is to employ multiple FP lasers. Recent work [6] demonstrated the generation of wavelength tunable self-seeded gain-switched pulses, with durations ranging from 90-130ps, with SMSR of 32dB over a tuning range of between 19-26nm. The major restriction in their work was the bandwidth of their optical filter. Here a self-seeding experiment involving two FP laser diodes is presented which can generate wavelength tunable optical pulses with durations $< 20ps$ over nearly 50nm. This will be further extended using external injection, allowing a tunable wavelength range

90
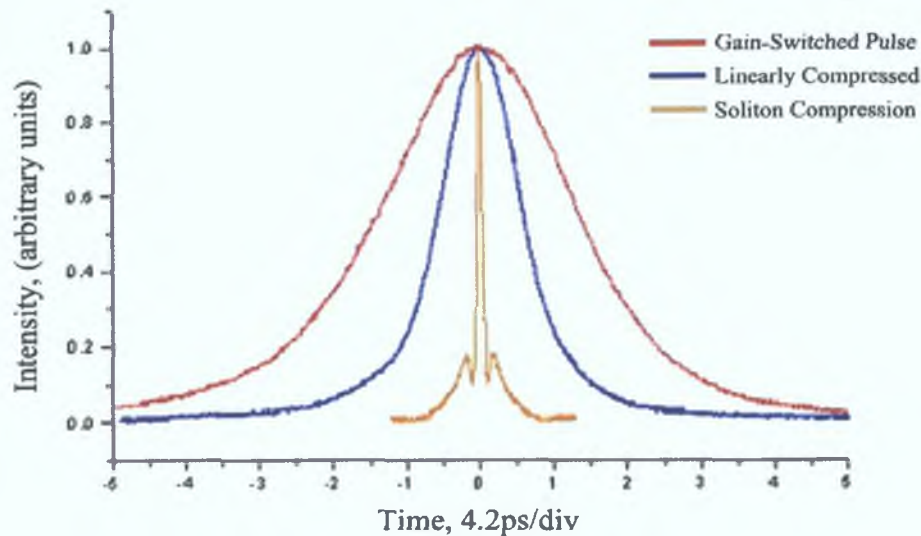
Figure 3.35: Comparison of the autocorrelation trace for DFB2 under gain-switched conditions, after linear compression and after 4th-order soliton compression

exceeding 60nm.

3.5.1 Very Wide Tunability Experimental Setup

Self-Seeding

Figure 3.36 illustrates the experimental setup used. It consists of two gain-switched FP laser diodes that are self-seeded using a single external cavity. The two FP lasers were chosen such that there was only a very small overlap between their gain profiles, with finer placement of the gain profile of the two lasers achievable with temperature controlling. The peak of FP1 is at 1524nm, while the peak of FP2 is at 1561nm.

Both lasers were commercially available $1.5\mu m$ InGaAsP devices with the same bias point of 26mA and longitudinal spacing of about 1.12nm. The two FP's were biased below threshold at 17mA and gain-switched at 2.5GHz. Self-seeding was then carried out using an external cavity consisting of a PC, a 3dB coupler, a Tunable Bragg Grating (TBG) (bandwidth of 0.23nm, over a tuning range 1460-1575nm, with rejection ratio of 40dB and insertion loss of 5dB) and an EDFA. An optical isolator in the EDFA ensures that light only propagates in one direction around the feedback loop, and the tunable filter eliminates unwanted amplified spontaneous emission from the EDFA in addition to selecting the laser mode to be seeded. The external cavity for FP2 also had a tunable optical delay inserted to ensure that both lasers were self-seeded at the same time. The EDFA in the external cavity is required to overcome the high losses obtained in the TBG and ensure that there is sufficient light re-injected into either laser to obtain sufficient
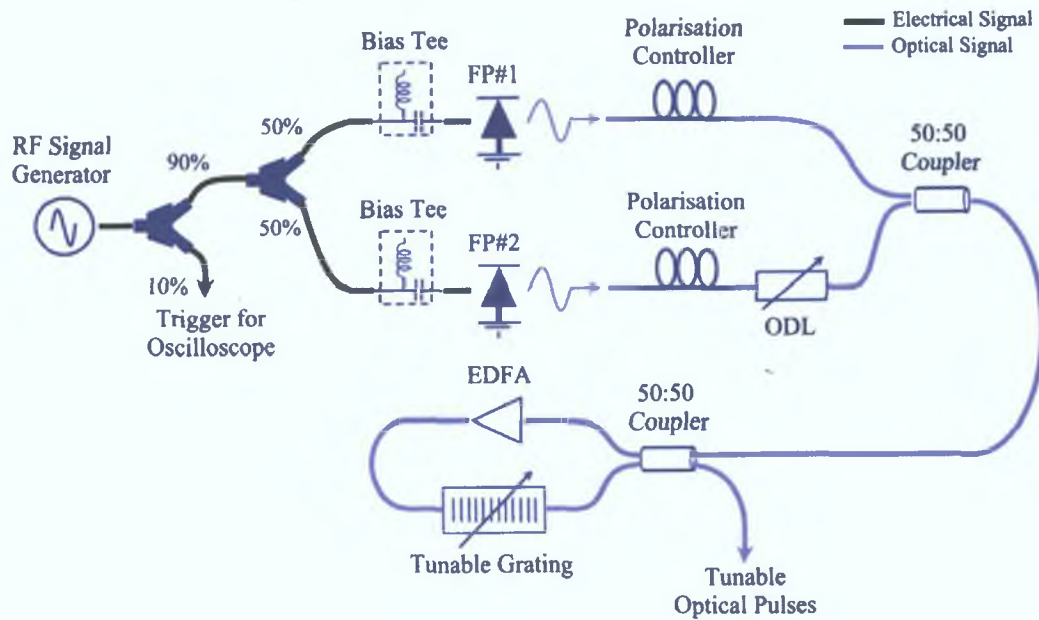
Figure 3.36: Schematic of the widely tunable self-seeded gain-switched experimental setup

SMSR on the output pulses.

In order to achieve optimal pulse generation, the grating was tuned to one of the longitudinal modes of the two gain-switched devices. The frequency of the modulation signal was then varied to ensure that the signal re-injected back into the laser cavity arrives during the build up of an optical pulse. A frequency of 2.498GHz was found to be most suitable. The bias of the two lasers were also adjusted (to 12mA) in order to minimise the pulse width of the optical pulses generated. The two polarization controllers were used to optimise the output SMSR of the tuned optical pulses. The grating was then tuned to one of the longitudinal modes of FP2 with the optical delay slightly adjusted to ensure that the re-injected light enters the laser at the precise time coinciding with the generation of the next optical pulse in FP2. This also helps to maximise the SMSR. The output from the return arm of the second 50:50 coupler was used to characterise the output.

The optical spectrum of the dual wavelength signal from the gain-switched lasers without self-seeding is shown in Figure 3.37 (a). It can be clearly seen that by combining the output of the gain switched lasers in the wavelength domain, the composite span of the gain profile that could be used for seeding has been greatly increased. The gain spectra of the two lasers overlap at approximately 16dB down from the peak of their gain curves. This overlap corresponds to the maximum wavelength of FP1 and the minimum wavelength of FP2 for which a suitable SMSR can be achieved. Different longitudinal modes of each FP laser were selectively excited when the seeding wavelength was tuned near the centre of the desired mode. Figure 3.37 (b,c,d) shows the short-
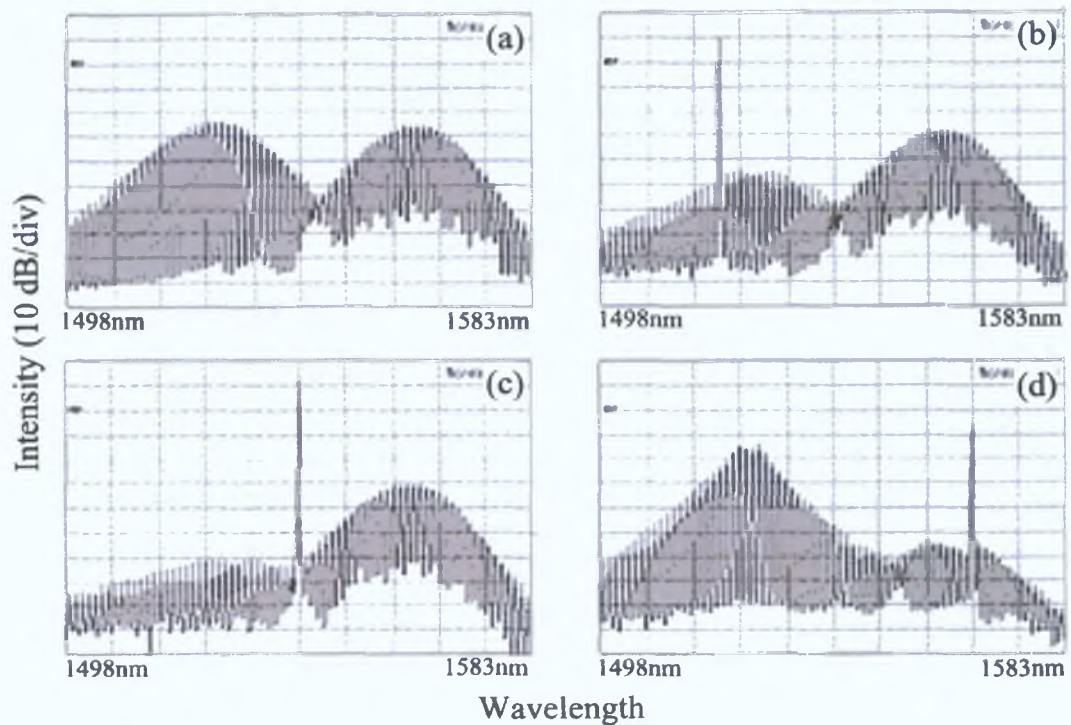
Figure 3.37: Optical spectra showing: (a) Composite of FP1 and FP2 under gain-switched conditions; (b) Shortest tunable wavelength; (c) Central tunable wavelength; (d) Longest tunable wavelength

est (1517nm), the central (1540nm) and the longest wavelength (1566nm) that could be seeded. The seeded spectra shown are the composite output of the two self-seeded gain-switched lasers before passing through the amplifier and the optical filter.

By passing the signals shown in Figure 3.37 through the filter for a second time, the SMSR of the generated optical pulses was further increased. The filter eliminates the signal from the unseeded laser, and greatly improves the SMSR of the generated optical pulses from the seeded laser. The results of this second pass through the filter are shown in Figure 3.38. Two output pulses, one from FP1 at 1524nm and the second from FP2 at 1560nm are also shown in Figure 3.38 (a,c). The pulse from FP1 had a (deconvolved) pulse width of 16ps with a spectral width of 27GHz while that for the pulse from FP2 had a temporal width of 18.5ps and spectral width of 26GHz, while the SMSR of the generated pulses were 54 and 56dB respectively. The pulse width was maintained almost constant (16-20ps) over the entire tuning range, except at the two extremities. This resulted in the time-bandwidth product being in the range 0.43 to 0.49 which is close the transform limited Gaussian pulses of 0.44. As can be seen from Figure 3.38 when the spectra pass through the filter for the second time, the unseeded laser is totally eliminated which increases the SMSR even further then with just self-seeding. This second filtering allows a SMSR greater than 50dB to be obtained over the entire tuning range.

93
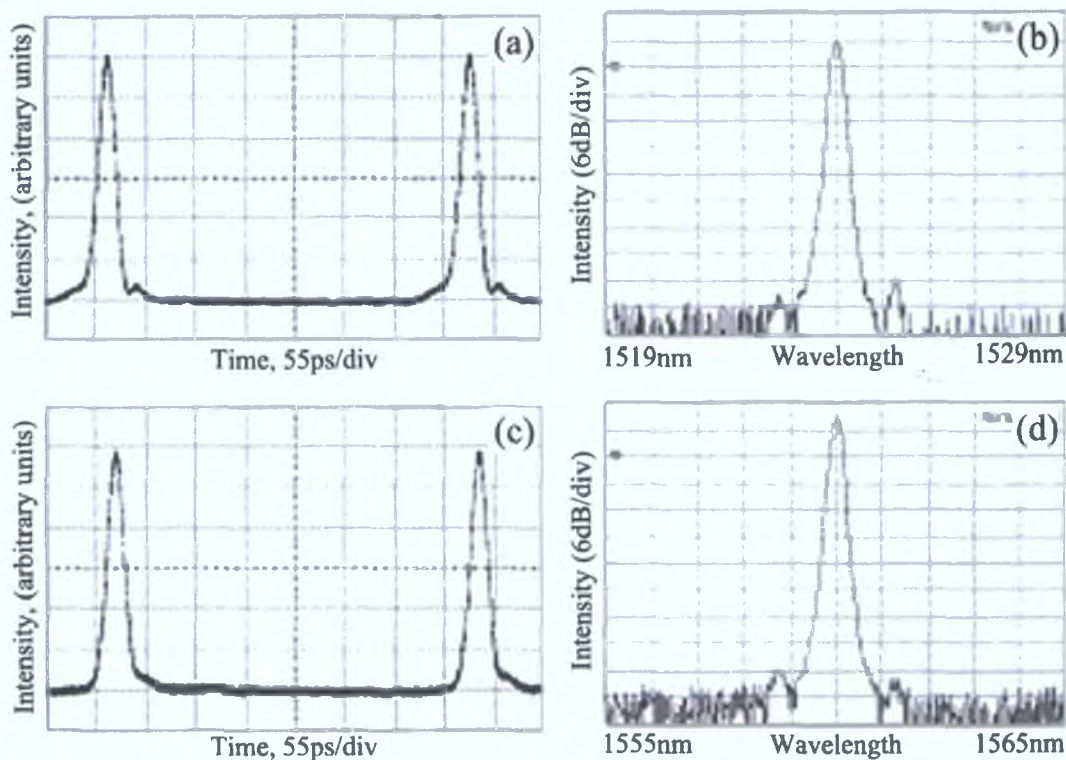
Figure 3.38: Self-seeding gain-switched output: (a) Optical Pulse at 1524nm; (b) Optical Spectrum at 1524nm; (c) Optical Pulse at 1560nm; (d) Optical Spectrum at 1560nm

The average output power of the optical pulses is approximately 1.8mW. The main limitation on the wavelength tuning of the generated pulses was imposed by the gain bandwidth of the EDFA used, with results taken at the optimum level of EDFA pump power (around 20mW) to ensure maximum SMSR is achieved without pulse deformation and instabilities. Reduction of the EDFA pump power leads to a degradation in pulse SMSR, but this relationship is heavily dependent on the operating wavelength, and its position relative to the gain curve of the EDFA and FP laser being self-seeded.

Figure 3.39 shows a plot of the SMSR and pulse width over the entire tuning range. It clearly shows that a SMSR greater than 50dB was obtained over a wavelength range of nearly 50nm. The figure also shows how the pulse width changes over the tuning range. The point where the pulse width jumps to 18ps from 16ps is the point were seeding changes from FP1 to FP2. At the extremities of the tuning range, the optical amplification of the seeding signal was increased, which enhanced the SMSR and widened the tuning range but caused pulse deformation and instabilities in the temporal domain due to excessive heating [62].

94
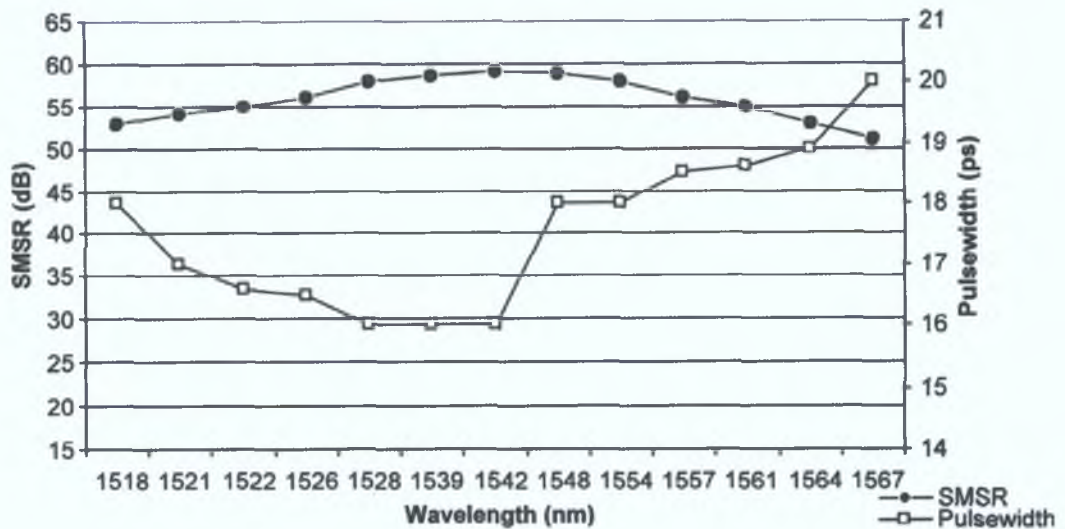
Figure 3.39: Plot of the SMSR (left axis) and the deconvolved pulse width (right axis) against tunable wavelength range for widely tunable self-seeded pulse source

External Injection

One way in which we can increase the tuning range is to replace the seeding loop of Figure 3.36 with an external injection setup as shown in Figure 3.40. The gain-
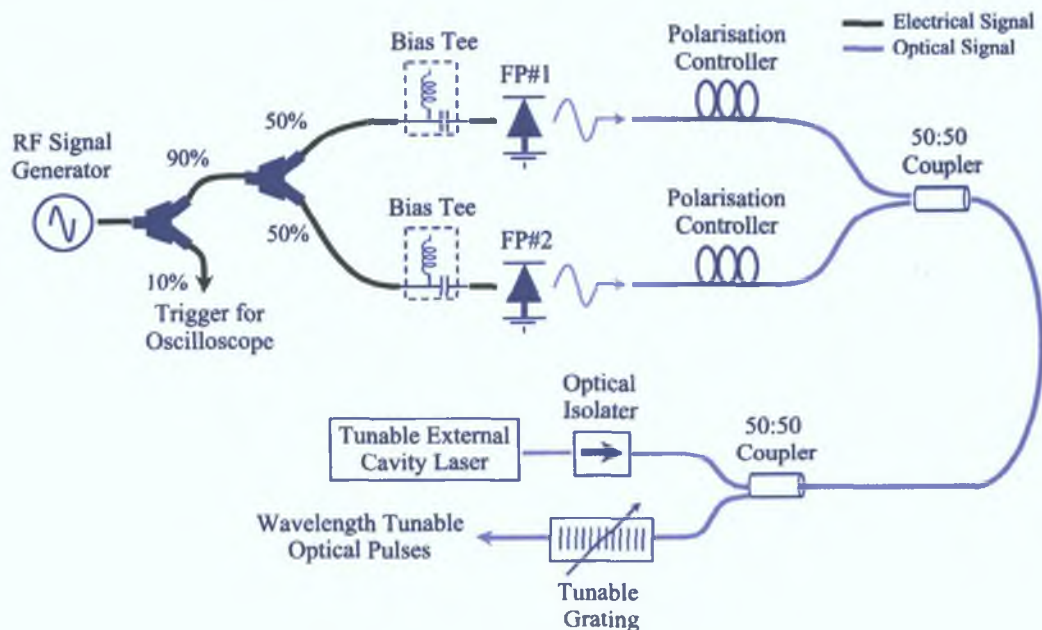
Figure 3.40: Schematic of experimental setup for a widely tunable external injection pulse source

switching section is similar to that employed for the self-seeding experiment except that the variable ODL from the arm of FP2 has been removed. As before, the external cavity

consists of a tunable ECL to provide the seeding signal, an optical isolator to prevent any backwards reflection of light that could damage the ECL, the repositioning of the tunable Bragg grating, and the removal of the EDFA. It was mentioned that one of the main limitations of the self-seeding setup was the bandwidth of the EDFA. Therefore, with the removal of the EDFA, the tuning range of nearly 70nm should be possible.

The output power of the CW source was set to -3dBm, and taking into account the various losses, this corresponds to an injection signal power level of -13dBm. When the ECL is tuned close to the desired mode of one of the gain-switched FP lasers, the resulting single-moded output obtained and the gain-switched signal from the other un-affected laser passes through the TBG. The Bragg filter is the same one as used in the self-seeding setup already described. The filter eliminates the output form the unaf-fected gain-switched signal, and enhances the SMSR of the external-injected pulses.
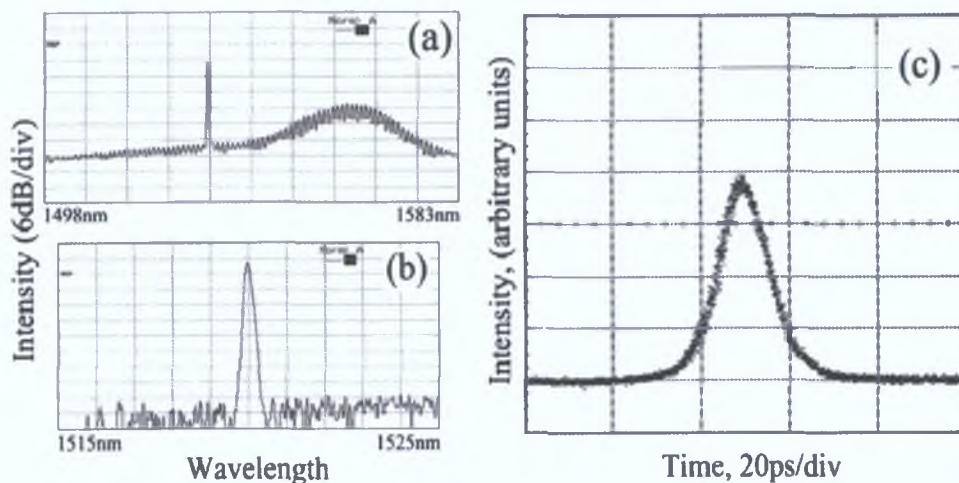
Figure 3.41: (a) Selected wavelength mode at 1519.9nm; (b) Filtered spectrum with mode at 1519.9nm; (c) Optical pulse at 1519.9nm

Figure 3.41 (a) displays the external injected spectrum at λ=1519.9nm prior to fil-tering. As can be seen, the left hand side of the spectrum corresponds to FP1, the seeded gain-switched laser, and displays a SMSR of about 30dB. The right hand side of the spectrum corresponds to the unaffected gain-switched spectrum of FP2. As the lasers were the same that were used for the self-seeding experiment, the composite gain-spectrum here is the same as Figure 3.37 (a). With the addition of the filter, the optical output from the unseeded FP lasers is eliminated, and the SMSR of the output spec-trum is improved. The resulting SMSR is around 60dB for the entire wavelength tuning range. This is shown in Figure 3.41 (b) while Figure 3.41 (c) shows an non-averaged optical pulse. The pulse duration was about 17ps, with a spectral linewidth of 30GHz, resulting in a time-bandwidth product of 0.51, which is slightly larger than the 0.44 for a Gaussian pulse.

Figure 3.42 shows the variation in pulse width and the SMSR over the tuning range. The deviation in pulse width around 1545nm is due to the external injection from the ECL changing from seeding FP1 to FP2. Differences in various physical parameters, for example gain, of the two lasers are responsible for the variation in output pulse width [44]. Also the spectral width of FP2 is limited by the bandwidth of the output filter.
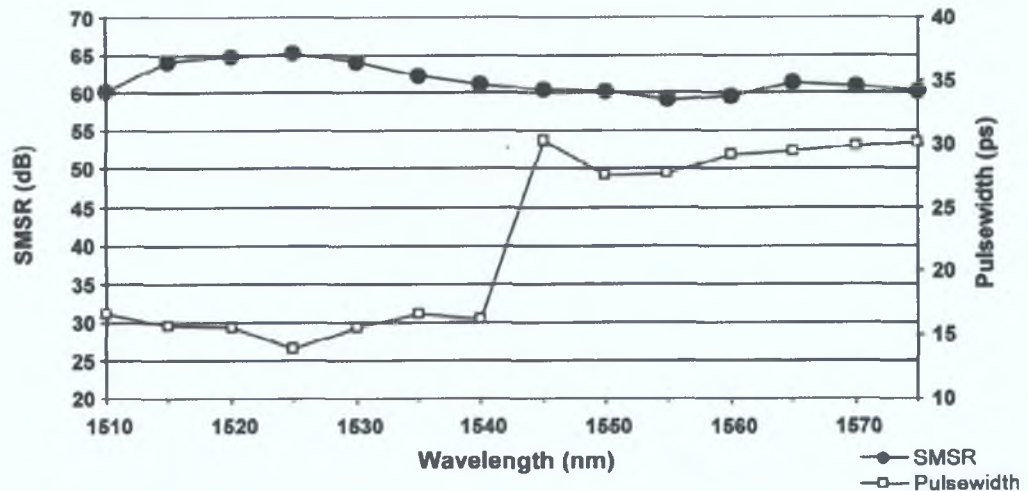
Figure 3.42: Plot of SMSR (left axis) and deconvolved pulse width (right axis) against tunable wavelength range for widely tunable external injection pulse source

Summary

This chapter has investigated the use of gain-switched optical pulses to represent data in a high-speed OTDM network. Experimental work demonstrated that the shortest pulse that could be generated from a gain-switched laser diode was in the region of 10ps. Unfortunately due to the gain-switching process, the pulses had high levels of temporal jitter and poor spectral purity, both of which limits the maximum possible data rate. Two methods which can be employed to reduce these effects are self-seeding and external injection. It was shown that by using either method, both the temporal jitter and spectral purity were improved, but at the expense of pulse width. One of the major advantages of employing self-seeding and external injection is that it also allows the emission wavelength of the device be tuned over the gain-switched spectrum. By using multiple FP laser diodes, it is possible to develop a simple and compact wavelength tunable optical pulse source. Finally, optical pulse compression was discussed, with experimental work demonstrating the reduction of gain-switched pulse duration to 420fs using linear and nonlinear compression techniques (via higher-order solitons). By employing both techniques, sub-picosecond optical pulses can be generated from a

gain-switched laser, permitting OTDM data rates in excess of 100Gbit/s

The next chapter will discuss optical signal processing tasks that are required for high-speed OTDM network, including the demultiplexing of a single channel from a multi-channel OTDM data signal, and characterisation of the optical data pulses used in OTDM

Bibliography

[1] S Kawanishi, "Ultrahigh-Speed Optical Time-Division-Multiplexed Transmission Technology Based on Optical Signal Processing," *IEEE Journal of Quantum Electronics*, vol 34, no 11, pp 2064–2079, 1998

[2] B Guenther and D Steel, *Encyclopedia of Modern Optics* Elsevier, 1st ed , 2005 ISBN 0-12-227600-0

[3] P Vasil'ev, *Ultrafast Diode Lasers, Fundamentals and Applications* Artech House Publications, 1st ed , 1995 ISBN 0-89006-736-8

[4] R Hui, B Zhu, K Demarest, C Allen, and J Hong, "Generation of Ultrahigh-Speed Tunable-Rate Optical Pulses Using Strongly Gain-Coupled Dual-Wavelength DFB Laser Diodes," *IEEE Photonics Technology Letters*, vol 11, no 5, pp 518–520, 1999

[5] K Y Lau, "Short-pulse and high-frequency signal generation in semiconductor lasers," *IEEE Journal of Lightwave Technology*, vol 7, no 2, pp 400–419, 1989

[6] M Suzuki, H Tanaka, N Edagawa, K Utaka, and Y Matsushima, "Transform-Limited Optical Pulse Generatiuon up to 20GHz Repetition Rate by Sinusoidally Driven InGaAsP Electroabsorption Modulator," *IEEE Journal of Lightwave Technology*, vol 11, no 3, pp 468–473, 1993

[7] H Murata, A Morimoto, T Kobayashi, and S Yamamoto, "Optical Pulse Generation by Electrooptic-Modulation Method and Its Application to Integrated Ultrashort Pulse Generators," *IEEE Journal of Selected Topics in Quantum Electronics*, vol 6, no 6, pp 1325–1331, 2000

[8] A E Siegman, *Lasers* University Science Books, 1st ed , 1986 ISBN 0-935702-11-3

[9] K Oh, U C Paek, and D Y Kim, "Picosecond pulse generation by gain switched," in *Conference on Lasers and Electro-Optics (CLEO 2001)*, (Baltimore Maryland USA), pp 196–197, 2001

[10] P Gunning, R Kashyap, A S Siddiqui, and K Smith, "Picosecond pulse generation of <5ps from gain-switched DFB semiconductor laser diode using linearly step-chirped fibre grating," *Electronics Letters*, vol 31, no 13, pp 1066–1067, 1995

[11] Y Matsui, S Kutsuzawa, S Arahira, and Y Ogawa, "Generation of Wavelength Tunable Gain-Switched Pulses From FP MQW Lasers with External Injection Seeding," *IEEE Photonics Technology Letters*, vol 9, no 8, pp 1087–1089, 1997

99

[12] K.Y.Lau, "Gain switching of semiconductor injection lasers," *Applied Physics Letters*, vol. 52, no. 4, pp. 257–259, 1988.

[13] P.Liu, C.Lin, I.P.Kaminow, and J.J.Hsieh, "Picosecond pulse generation from In-GaAsP lasers at 1.25 and 1.3μm by electrical pulse pumping," *IEEE Journal of Quantum Electronics*, vol. 17, no. 5, pp. 671–673, 1981.

[14] H.Ito, H.Yokoyama, S.Murata, and H.Inaba, "Picosecond optical pulse generation from an R.F modulated AlGaAs D.H. diode laser," *Electronics Letters*, vol. 15, no. 23, pp. 738–740, 1979.

[15] K.A.Ahmed, H.F.Liu, N.Onodera, P.Lee, R.S.Tucker, and Y.Ogawa, "Nearly Transform-Limited Pulse (3.6ps) Generation from Gain-Switched 1.55μm Distributed Feedback Laser using Fibre Compression technique," *Electronics Letters*, vol. 29, no. 1, pp. 54–56, 1993.

[16] K.Y.Lau and A.Yariv, "Ultra-High Speed Semiconductor Lasers," *IEEE Journal of Quantum Electronics*, vol. QE-21, no. 2, pp. 121–138, 1985.

[17] P. M.Downey, J. E.Bowers, R. S., and E. Agyekum, "Picosecond dynamics of a gain switched ingaasp laser," *IEEE Journal of Quantum Electronics*, vol. 23, no. 6, pp. 1039–1047, 1987.

[18] B.R.Bennett, R.A.Soref, and J. Alamo, "Carrier-induced Change in Refractive Index of InP, GaAs, and InGaAsP," *IEEE Journal of Quantum Electronics*, vol. 26, no. 1, pp. 113–122, 1990.

[19] J.O'Gorman and A.F.J.Levi, "Calculated Chirp in Intracavity Loss Modulated DFB Lasers," *Electronics Letters*, vol. 26, no. 21, pp. 1784–1787, 1990.

[20] J.M.Dudley, L.P.Barry, J.D.Harvey, M.D.Thomson, B.C.Thomson, P.G.Bollond, and R.Leonhardt, "Complete Characterization of Ultrashort Pulse Sources at 1550nm," *IEEE Journal of Quantum Electronics*, vol. 35, no. 4, pp. 441–450, 1999.

[21] L.P.Barry, J.M.Dudley, B.C.Thomsen, and J.D.Harvey, "Frequency-resolved optical gating measurement of 1.4Thz beat frequencies from dual wavelength self-seeded gain-switched laser diode," *Electronics Letters*, vol. 34, no. 10, pp. 988–990, 1998.

[22] K.Ahmed, H.H.Y.Cheng, and H.F.Liu, "Generation of 185fs pedestal-free pulses using a 1.55μm distributed feedback semicondutor laser," *Electronics Letters*, vol. 31, no. 3, pp. 195–196, 1995.

[23] R.A.Linke, "Transient chirping in single-frequency lasers: lightwave systems consequences," *Electronics Letters*, vol. 20, no. 11, pp. 472–474, 1984.

[24] M.R.H.Daza and C.A.Saloma, "Jitter Dynamics of a Gainswitched Semiconductor Laser Under Self-Feedback and External Optical Injection," *IEEE Journal of Quantum Electronics*, vol. 37, no. 2, pp. 254–264, 2001.

[25] M.Jinno, "Correlated and Uncorrelated Timing Jitter in Gain-Switched Laser Diodes," *IEEE Photonics Technology Letters*, vol. 5, no. 10, pp. 1140–1143, 1993.

[26] A G Weber, W Ronghan, E H Bottcher, M Schell, and D Bimberg, "Measurement and Simulation of the turn-on delay time jitter in gain-switched semiconductor lasers," *IEEE Journal of Quantum Electronics*, vol 28, no 2, pp 441–446, 1992

[27] M Jinno, "Effects of Crosstalk and Timing Jitter on All-Optical Time-Division Demultiplexing Using a Nonlinear Fiber Sagnac Interferometer Switch," *IEEE Journal of Quantum Electronics*, vol 30, no 12, pp 2842–2853, 1994

[28] M J Ablowitz and P A Clarkson, *Solitons, Nonlinear Evolution Equations & Inverse Scattering* Cambridge University Press, 1st ed, 1991 ISBN 0-521-38730-2

[29] Agilent, "E4437b ESG-DP Series Digital RF Signal Generator" PDF Document, 2005 http //cp literature agilent com/litweb/pdf/5965-3096E pdf

[30] Herotek, "Step Recovery Diode Comb (Harmonic) Generators" HMTL Document, 2005 http //www herotek com/datasheets/herote15 html

[31] ThorLabs, "GRIN Optics" http //www thorlabs com

[32] u2t Photonics, "50GHz Photodetector" PDF Document, 2005 http //www u2t de/pdf/Datasheet_XPDV2020R&2020_V42 pdf

[33] Agilent, "infinium DCA Agilent 86100B Wide-Bandwidth Oscilloscope" PDF Document, 2005 http //cp literature agilent com/litweb/pdf/5988-5311EN pdf

[34] Anritsu, "Optical Spectrum Analysers" http //www eu anritsu com

[35] D Marcuse and T-P Lee, "On Approximate Analytical Solutions of Rate Equation for Studying Transient Spectra of Injection Lasers," *IEEE Journal of Quantum Electronics*, vol QE-19, no 9, pp 1397–1406, 1983

[36] D Cutrer, P Pepeljugoski, and K Lau, "Noise properties of electrically gain-switched 1 5μm DFB lasers after spectral filtering," *Electronics Letters*, vol 30, no 17, pp 1418–1419, 1994

[37] L P Barry and P Anandarajah, "Effect of Side-mode Suppression Ratio on the Performance of Self-Seeded Gain-Switched Optical Pulses in Lightwave Communications Systems," *IEEE Photonics Technology Letters*, vol 11, no 11, pp 1360–1362, 1999

[38] D Huhse, M Schell, W Utz, J Kaessner, and D Bimberg, "Dynamics of Single Mode Formation in Self-Seeded Fabry-Perot Laser Diodes," *IEEE Photonics Technology Letters*, vol 7, no 4, pp 351–353, 1995

[39] S Bouchoule, N Stelmakh, M Cavelier, and J -M Lourtioz, "Highly Attenuating External Cavity of Picosecond-Tunable Pulse Generation from Gain/Q-Switched Laser Diodes," *IEEE Journal of Quantum Electronics*, vol 29, no 6, pp 1693–1700, 1993

[40] L P Barry, J Debeau, and R Boittin, "Simple technique to improve the spectral quality of gain-switched pulse from a DFB laser," *Electronics Letters*, vol 30, no 25, pp 2143–2145, 1994

[41] M Schell, W Utz, D Huhse, J Kassner, and D Bimberg, "Low jitter single-mode pulse generation by a self-seeded, gain-switched fabry-perot semiconductor laser," *Applied Physics Letters*, vol 65, no 24, pp 3045–3047, 1994

[42] M Schell, D Huhse, A G Weber, G Fischbeck, D Bimberg, D S Tarasov, A V Gorbachov, and D Z Garbuzov, "20nmn Wavelength Tunable Singlemode Picosecond Pulse Generation at 1 3μm by Self-Seeded Gain-Switched Semiconductor Laser," *Electronics Letters*, vol 28, no 23, pp 2154–2155, 1992

[43] M Schell, W Utz, D Huhse, J Kassner, and D Bimberg, "Low jitter single-mode pulse generation by a self-seeded, gain-switched fabry-perot semiconductor laser," *Applied Physics Letters*, vol 65, no 24, pp 30454–3047, 1994

[44] A M Clarke, P M Anandarajah, and L P Barry, "Generation of Widely Tunable Picosecond Pulses With Large SMSR by Externally Injecting a Gain-Switched Dual Laser Source," *IEEE Photonics Technology Letters*, vol 16, no 10, pp 2344–2346, 2004

[45] M Zhang, D N Wang, H Liu, W Jin, and M S Demokan, "Tunable Dual-Wavelength Picosecond Pulse Generation by the Use of Two Fabry-Perot Laser Diodes in an External Injection Seeding Scheme," *IEEE Photonics Technology Letters*, vol 14, no 1, pp 92–94, 2002

[46] X Fang and D N Wang, "Mutual Pulse Injection Seeding by the Use of Two Fabry-Perot Laser Diodes to Produce Wavelength-Tunable optical Short Pulses," *IEEE Photonics Technology Letters*, vol 15, no 6, pp 855–857, 2003

[47] D -S Seo, D Y Kim, and H -F Liu, "Timing jitter reduction of gain-switched dfb laser by external injection-seeding," *Electronics Letters*, vol 32, no 1, pp 44–45, 1996

[48] J A Giordmaine, M A Duguay, and J W Hansen, "Compression of Optical Pulses," *IEEE Journal of Quantum Electronics*, vol QE-4, no 5, pp 252–255, 1968

[49] G P Agrawal, *Applications of Nonlinear Fiber Optics* Academic Press, 1st ed, 2001 ISBN 0-12-045144-1

[50] E B Tracey, "Compression of picosecond light pulses," *Physics Letters*, vol 28A, no 1, pp 34–35, 1968

[51] A Piper, P Dupriez, M Ibsen, A Malinowski, J H V Price, B C Thomsen, D J Richardson, L M B Hickey, and M N Zervas, "A compact 1 GHz, 16ps pulse source operating at 1060nm incorporating a high-power gain-switched semiconductor laer and fiber grating pulse compressor," in *Conference on Lasers and Electro-Optics Europe (CLEO 2005)*, (Munich, Germany), p 358, 2005

[52] A Hasegawa and F Tappert, "Transmission of stationary nonlinear optical pulses in dispersive dielectric fibers I Normal dispersion," *Applied Physics Letters*, vol 23, no 3, pp 171–172, 1973

[53] L F Mollenauer, R H Stolen, and J P Gordon, "Experimental Observation of Picosecond Pulse Narrowing and Solitons in Optical Fibers," *Physical Review Letters*, vol 45, no 13, pp 1095–1098, 1980

[54] A Hasegawa, *Optical Solitons in Fibers* Springer-Verlag, 2nd ed , 1990 ISBN 0-387-51747

[55] G P Agrawal, *Nonlinear Fiber Optics* Academic Press, 2nd ed , 1995 ISBN 0-12-045142-5

[56] A Hasegawa and F Tappert, "Transmission of stationary nonlinear optical pulses m dispersive dielectric fibers I Anomalous dispersion," *Applied Physics Letters*, vol 23, no 3, pp 142–144, 1973

[57] Y Kao, A Leven, Y Baeyens, Y Chen, D Grosz, F Bannon, W Fang, A Kung, D Maymar, T Lakoba, A Agrawal, S Banerjee, and T Wood, "10Gb/s Soliton Generation for ULH Transmission Using A Wideband GaAs pHemt Amplifier," in *Optical Fiber Communications Conference (OFC2003)*, vol 2, pp 674–675, 2003

[58] Hariharan, *Optical Interferometry* Academic Press, 1st ed , 1985 ISBN 0-12-325220-5

[59] Tektronix, "Digital storage oscilloscopes" HTML Document, 2005 http //www tek com

[60] M Nakazawa, K Suzuki, and E Yamada, "Femtosecond optical pulse generation using a distributed-feedback laser diode," *Electronics Letters*, vol 26, no 24, pp 2038–2040, 1990

[61] M D Pelusi, Y Matsui, and A Suzuki, "Pedestal suppression from compressed femtosecond pulses using a nonlinear fiber loop mirror," *IEEE Journal of Quantum Electronics*, vol 35, no 6, pp 867–874, 1999

[62] Z Hu, H-F Chou, J E Bowers, and D J Blumenthal, "40-GHz Optical Pulse Generation Using Strong External Light Injection of a Gain-Switched High-Speed DBR Laser Diode," *IEEE Photonics Technology Letters*, vol 15, no 12, pp 1767–1769, 2003

103

CHAPTER 4

Optical Nonlinearities for Signal Processing

Introduction

Currently, the majority of signal processing such as data switching and performance monitoring are carried out using electronics Electronic processing is limited by the speed of current integrated electronic circuit design, resulting in electronic bottlenecks forming at the processing nodes These slow down the operation of the network and increases the cost of transmission As it is anticipated that individual channel data rates will exceed 100Gbit/s in the next 5-10 years [1], new highly-efficient, ultra-fast optical signal processing techniques will have to be developed

This chapter will examine three important optical signal processing tasks that will be required for the development of future high-speed optically multiplexed data networks These are optical clock recovery, optical demultiplexing of individual channels from a high-speed OTDM data signal, and signal characterisation of optical pulses used to represent data in OTDM networks

4.1 Optical Clock Recovery

In order to carry out vital signal processing tasks such as demultiplexing and performance monitoring, a clock signal needs to be recovered from the random data stream [2] The recovered clock signal is then used to drive the processing element, which opens up a short processing window repeated at the clock rate of the individual channel [3] Extraction of the clock component can be carried out using a number of different methods including a Phase-Locked Loop [electro-optical], self-pulsating laser diode [2] or using electro-optical multiplication of an optical signal in a Mach-Zehnder modulator [4]

4.1.1 Phase-Lock Loop

A Phase-Locked Loop (PLL) is a closed-loop feedback control system for maintaining the frequency and phase relationship between a locally generated signal and an input

reference signal [5]. It finds many different applications from a frequency synthesiser in a radio, clock multipliers in microprocessors and recovery of clock timing information from data streams [6].
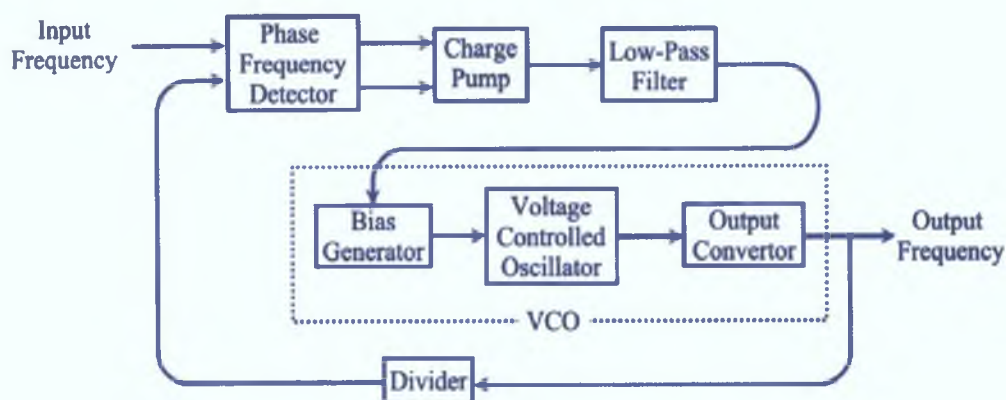
Figure 4.1: Schematic of the basic components of a phase-locked loop [6]

A basic PLL configuration is shown in Figure 4.1. It operates by raising or lowering the frequency of a controlled oscillator until it matches the frequency of the input reference frequency. PLL's generally consist of a phase frequency detector, a charge pump, low-pass filter and Voltage-Controlled Oscillator (VCO) [5]. There is usually a divider in the feedback path (as shown) or in the reference path in order to make the PLL's output clock a rational multiple of the input reference signal. The oscillator generates a periodic signal that is fed back and compared to the reference signal using the phase detector. If the frequency of the oscillator falls behind the reference signal, the phase detector alters the charge pump which in turn changes the control voltage to the oscillator (error signal). This speeds up the frequency of the oscillator. The low-pass filter smooths out the error signal from the charge pump, so that the system reaches a state where the phase detector makes very few corrections.

A PLL configuration has many advantages compared to alternative methods for clock recovery including the fact that there is no phase-error present and complete retiming can be achieved [7]. However, the maximum speed of a conventional PLL is still limited by the speed at which the electronics can operate, especially the response of the phase comparator. A number of research groups are developing optical PLL clock recovery methods, with recent demonstrations employing Electro-absorption Modulators (EAM) [8] and PhaseCOMB-lasers [9] for the phase comparison. Both methods have successfully demonstrated the recovery of a 10GHz [8] and 42.7GHz [9] clock signal, allowing the demultiplexing of individual data channels from a 160Gbit/s aggregate data signal.

4.2 Optical Demultiplexing

In modern long-haul telecommunications systems, data propagates along fibre in optical format but data switching still occurs in the electrical domain. This electronic switching involves first the conversion of the optical data into electrical format, switching the electrical data to the correct path and then converting it back into optical form to continue on its journey. Unfortunately due to the speed limitations of current integrated circuits, the maximum data rate that electrical switches can handle is, at most, 40Gbit/s, with today's technology. With line rates expected to exceed 100Gbit/s in the next 5-10 years [1], new optical techniques will have to be developed in order to successfully carry out successful demultiplexing of individual data channels. This section will focus on the use of optical fibre nonlinearities to carry out high-speed optical demultiplexing of individual channels from an OTDM data network.

4.3 Switching using Optical Fibre Nonlinearities

As optical nonlinearities, which are present in optical fibres, crystals and semiconductors, occur on timescales in the order of a few femtoseconds ($10^{-15}s$), they are ideal for operation in the Terabit/s data regime [10]. Some of the basic *performance requirements* for an optical switch include [11, 12]

- *Low Insertion Loss* - The insertion loss of a switch takes into account the coupling loss, waveguide propagation loss and excess loss. The amount of insertion loss is important, especially in a large network were the cascade effect of many switches can affect the overall power budget of the network

- *Switching Speed* - The switching speed is defined as the time period from the moment the command is given to the switch to change state to the moment when the insertion loss of the switched path achieves more than 90% of its final value. The required switching speed depends on the application that switch is intended for, with millisecond switching speed required for protection application, nanosecond for packet switching, picosecond for OTDM applications

- *Crosstalk* - Crosstalk is a measure of the signal interference between channels, with a low level of crosstalk and high extinction ratio representing high signal quality. Typical value for crosstalk is around 40 to 50dB

- *Polarisation* - As data rates continue to increase, the impact of polarisation on system performance increases. As new techniques are developed to counteract the effects of polarisation, a switch that is polarisation insensitive will be vital

106

- *Wavelength Response* - A wavelength-dependent response would enable the switch to carry out wavelength selection and detection in a WDM or hybrid WDM/OTDM network without the need for external filtering. This would reduce the overall losses of the switching node and reduce cost.

- *Bit Rate and Protocol Transparency* - As network providers are continually striving to increase the usable bandwidth of an optical fibre network, a switch that does not have to be upgraded or replaced every time the bit rate is changed is essential.

- *Sufficient Bandwidth* - Future switches should have to ability to operate at future data rates in order to eliminate the same transmission bottlenecks that are currently found using electronic-based data switching

System requirements would include [11]:

- *Stability and Reliability* - Given the amount of data that is transmitted per second across the network, the reliability of the switch is extremely important.

- *Repeatability* - Port-to-port repeatability refers to all paths across the switching fabric being of identical length.

- *Footprint* - The actual size of the switch will depend on the switching application and the location of the switch, with backbone networks requiring a switch capable of operating at a number of different wavelengths.

- *Power Consumption / Drive Voltage* - A high drive voltage and power consumption increases the overall cost and the associated hear dissipation increases the system's ambient temperature which may affect the stability and reliability of the switch.

- *Operational Temperature* - In order to meet stringent environmental requirements, switches must meet specified requirements for temperature variations and humidity.

- *Cost* - As network providers continue to lower prices to attract more customers, cost savings across the network are now a major factor in order to maximise profit margins.

4.3.1   Loop Mirror Reflectors

The majority of fibre-based switching relies upon the operating principle of a fibre loop reflector as shown in Figure 4.2. It consists of a loop of optical fibre formed between

the output ports of a directional coupler [13]. As light enters enters port 1 of the 50:50 coupler, half of the light is coupled to port 3 with the remaining light experiencing a $\pi/2$ phase shift as it is coupled to port 4. Taking into account this phase shift, the optical
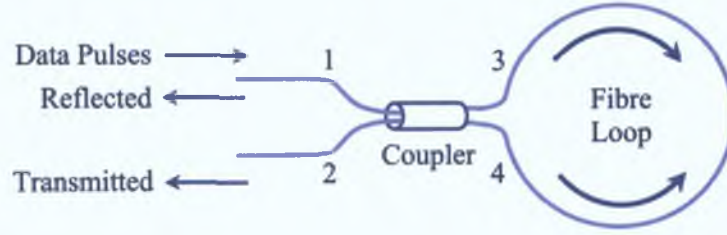
Figure 4.2: Schematic of the operation of a fibre loop reflector [14]

signal at ports 3 and 4 can be written as [14]:

$$A_{Port3} = \sqrt{\alpha}A_0, \qquad A_{Port4} = i\sqrt{1-\alpha}A_0 \qquad (4.1)$$

where A_0 is the amplitude of the input signal at port 1, i takes into account the phase shift introduced by the optical coupler, and α is the power splitting ratio of the coupler ($\alpha = 0.5$ in this case). After one round trip, both fields acquire a linear phase shift $\phi_0 = \beta L$ (β is the mode propagation constant, L is the length of fibre in the loop) and a nonlinear phase shift due to SPM and XPM [14]. The transmittivity of the loop can therefore be written as [15]:

$$T = \frac{P_t}{P_i} = 1 - 2\alpha(1 - \alpha)[1 + cos(1 - 2\alpha)\phi_{NL}] \qquad (4.2)$$

where P_t is the transmitted power and P_i is the initial power of the signal entering port 1 of the coupler. ϕ_{NL} is the nonlinear phase shift encountered by the propagating signal given by [15]:

$$\phi_{NL} = \left[\frac{2\pi}{\lambda}\right] n_2 l \left[\frac{P_i}{A_{eff}}\right] \qquad (4.3)$$

Note as the optical path length is the exactly same for both propagating signals, the linear phase shift encountered by both signals exactly cancel each other. For $\alpha = 0.5$, the transmitted signal equals 0, with all the signal being reflected back to port 1 [13], assuming that fibre loss and fibre birefringence is neglected.

It has been shown that by using an unbalanced optical coupler and/or separate switching pulse introduced into the fibre loop at the same time as the data pulses, the phase shift encountered by the propagating signal can be altered, permitting the switching out of a certain data channel from an aggregate signal. Such a device is known as a Nonlinear Optical Loop Mirror (NOLM) and will be discussed next.

Nonlinear Optical Loop Mirror

The use of the loop mirror reflector for high-speed switching of an optical data signal was first proposed by Doran and Wood in 1988 [16]. Their device employed an optical fibre coupler where $\alpha \neq 0.5$ resulting in the phase shift encountered by the clockwise and counter-clockwise propagating signals being no longer identical, as the phase velocity is intensity dependent. If the relative phase shift between the two signals becomes π, self-switching occurs and the beam can be transmitted. Their device was known as a Nonlinear Optical Loop Mirror (NOLM).

There are a number of different ways in which the optical intensity can be altered between the two beams. These include the use of an unbalanced optical coupler as described above, the introduction of a lumped loss near one of the ends of the coupler [17], and the use of separate switching pulses [18]. The use of the lumped loss, such as a fixed fibre attenuator, slightly attenuates one of the pulses resulting in the same energy mismatch as provided by the unequal power splitting coupler. This, and the unbalanced fibre coupler, relies on the input signal having sufficient optical intensity for SPM and XPM to introduce the required nonlinear phase shift for switching. As mentioned, the
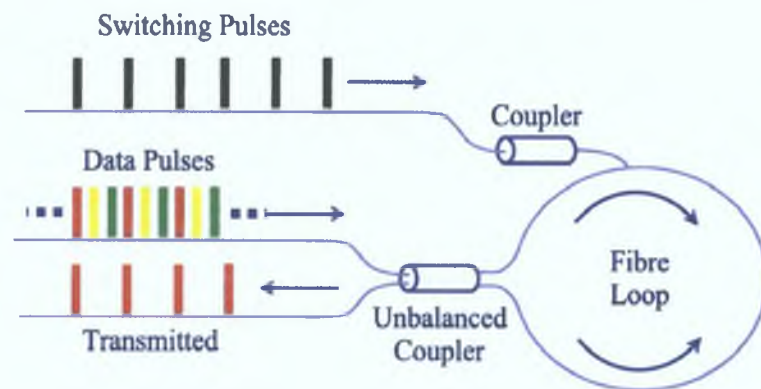
Figure 4.3: Schematic of all-optical demultiplexing using a NOLM and switching pulse [18]

third technique uses a switching pulse introduced via another coupler for switching, and this is shown in Figure 4.3. The switching pulse propagates around the loop in one direction only and through XPM alters the refractive index and consequently the phase of the low power signal propagating in the same direction. This change in phase means that for the period of switching pulse width, the loop becomes transmitting [19]. As this change only lasts for the period of the switching pulse width, exact timing is required for the introduction of the switching pulse so that the loop's nonlinear response only occurs during the time period corresponding to the channel to be transmitted. The switching pulses operate at a different wavelength than the data being switched out so that it can filtered out at the output of the device [18].

Terahertz Optical Asymmetric Demultiplexer

The Terahertz Optical Asymmetric Demultiplexer (TOAD) is similar in structure to the NOLM, except that the nonlinear response is introduced by the excitation of a Nonlinear Element (NLE), which is normally a Semiconductor Optical Amplifier (SOA), by a switching pulse [20] The NLE is offset from the loop's midpoint by a distance Δx, as shown in Figure 4 4 As with the NOLM, the input signal is split equally into a Clockwise (ClkW) propagating signal and a Counterclockwise (CClkW) propagating pulse The pulses of the ClkW and CClkW are always located on opposite sides of the loop and equidistant from the midpoint Each passes through the NLE once before returning to the input coupler The intensity of the ClkW and the CClkW signal are insufficient to alter the optical properties of the NLE

Switching pulses, which have sufficient energy to alter the NLE, are introduced into the loop via another fibre coupler When the control pulse reaches the NLE, it produces a rapid transition in the NLE's optical properties Those signal pulses that have already passed through the NLE prior to the arrival of the control pulse (green) experience no change, and are reflected at the input coupler [18]

A timing diagram showing the operation of a TOAD based switch is shown in Figure 4 4 As can be seen Channel A of the ClkW and CClkW signals pass through the NLE prior to the arrival of the control pulse and experience no relative phase change (black) The same occurs for Channel B of the ClkW signal (black) However by the time Channel B of the CClkW signal reaches the NLE, the control pulse has already arrived, and has altered the optical properties of the NLE As a result, Channel B of the CClkW experiences a phase change (red) with respect to Channel B of the ClkW Finally by the time that channel C of both the ClkW and CClkW signals reach the NLE, its optical properties still remain altered and both experience the same phase shift (red) Since B is the only channel with different phase shifts for the ClkW and the CClkW signals, it is the only channel that will be switched out when the signals recombine at the input coupler

In order for the correct channel to be switched out, the control pulses must be synchronised to allow the ClkW wave pass through the NLE unaltered, but alter the CClkW pulse The NLE requires a short response time to activate the device, but a longer relaxation time allowing the CClkW to pass through to permit switching [20]

Nonlinear Amplifying Loop Mirror

The Nonlinear Amplifying Loop Mirror (NALM) modifies the operation of the NOLM by using a balanced 3dB coupler and a gain medium within the fibre loop, usually an EDFA place close to one of the coupler ports [21] Since the gain medium is placed close to the coupler, one of the propagating signals is amplified at the entrance to the
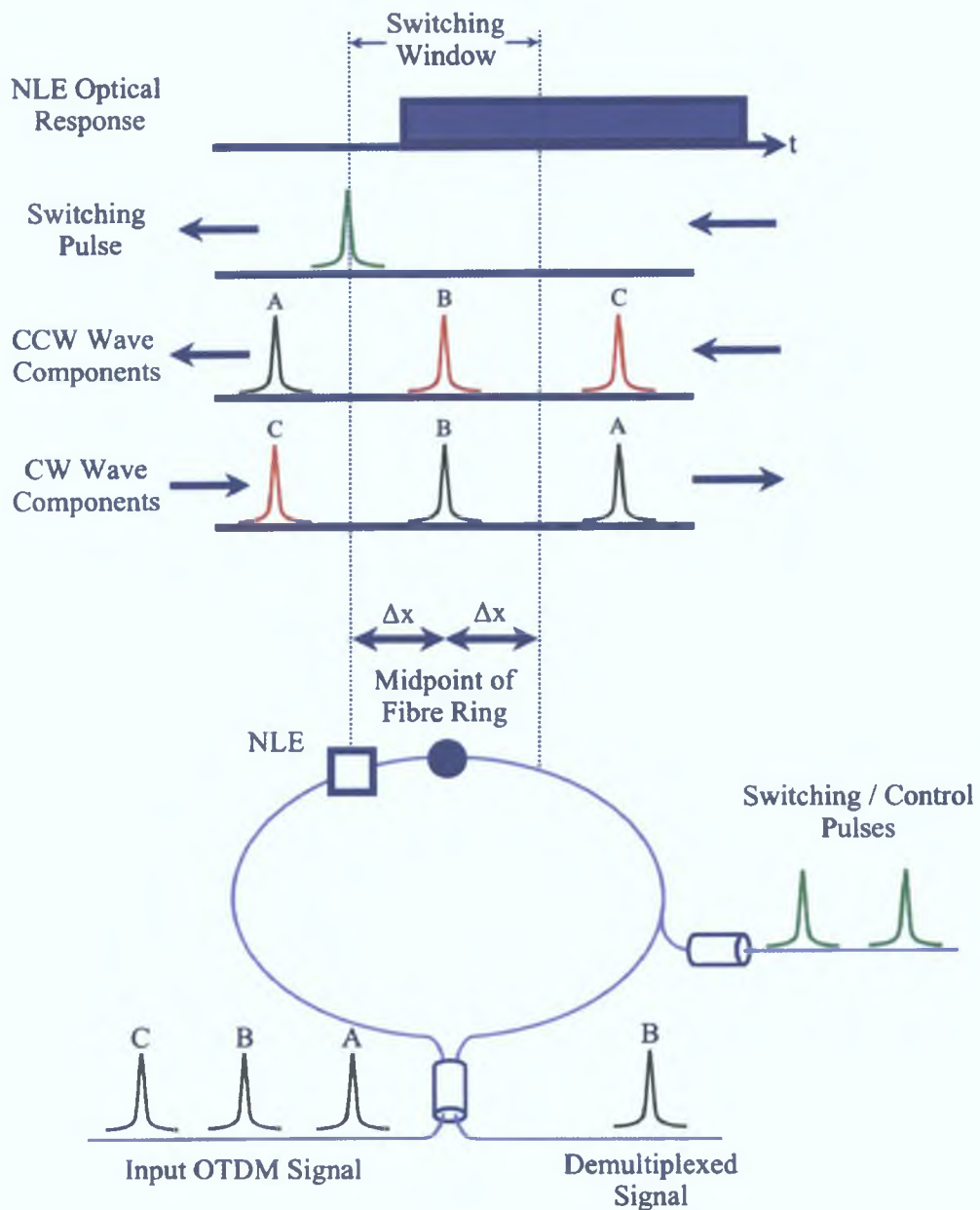
Figure 4.4: Illustration of the opeation of a TOAD [20]

loop while the other is amplified prior to exiting the loop. The waves experience differ-ent nonlinear shifts due to their different optical intensities while traveling within the loop. If the NALM is adjusted so that the relative phase difference between the two waves is π for the central part of the pulse, the NALM will act as a nonlinear ultrafast optical switch [22].

The phase difference introduced by the NALM is not constant but varies over the pulse profile. By using this, it is possible to separate a pulse from its pedestal (wings), since the pedestal gets reflected because it has a lower intensity and therefore lower phase shift. This would lead to pulse narrowing and has been used to improve the quality of soliton-compressed gain-switched optical pulses [14].

Although recent NOLM and TOAD-based demultiplexers have demonstrated all-optical demultiplexing in systems operating at up to 640Gbit/s [23, 24], there are a number of factors that limit the performance of these devices. For example, high-speed switching in the NOLM requires speciality fibre and precise control of the wavelength of the control and signal pulse around the zero fibre dispersion wavelength [25], while the maximum switching speed of the TOAD is confined by the width of the control pulse, which is limited by gain depletion in the SOA [26]. Due to these limitations, it is important to consider alternative optical nonlinearities for ultrafast optical demultiplexing. One possibility that takes advantage of an optical nonlinearity that is present in semiconductors will be described in more detail in the next chapter.

4.4 Performance Monitoring

To successfully operate at data rates in excess of 100Gbit/s per channel, networks will require a sensitive and ultrafast technique for precise optical signal monitoring [27]. The standard way of characterising high-speed optical signals utilises a fast photodetector in conjunction with a high-speed sampling oscilloscope. However current electronic monitoring techniques are limited to bandwidths of approximately 80GHz [28] due to difficulties associated with the design of high-speed electronic components [29]. These are just capable of accurately measuring data rates of 40Gbit/s. Therefore, electrical sampling schemes are unable to accurately characterise high-speed data pulses used to represent data. Critical information such as pulse duration, pulse separation and pulse rise-time, which are crucial for the optimisation of the networks performance, are distorted. As a result, it is necessary to consider alternative methods for high-speed performance monitoring. This section will examine three techniques, intensity autocorrelation, Frequency Resolved Optical Gating (FROG) and sequential optical sampling.

4.4.1 Autocorrelation and Crosscorrelation

Autocorrelation is a simple and easy to implement technique for the real time measurement of optical pulses with durations in the femtosecond to picosecond range. The basic layout of a conventional autocorrelator is shown in Figure 4.5. It uses a Michelson interferometer to generate two equal intensity replicas of the incoming pulse train. One of the replicas passes through a fixed optical delay comprising of two mirrors mounted on a translation stage. The other replica passing through a variable optical delay arm, which allows one of the replicas to be scanned across the other pulse. There are a number of different ways to accomplish this including the use of a stepper motor or a set of rotating mirrors [30]. Figure 4.5 shows the rotating mirrors variant, as this was the one used for the measurement of the compressed optical pulses in Chapter 3 Section

112
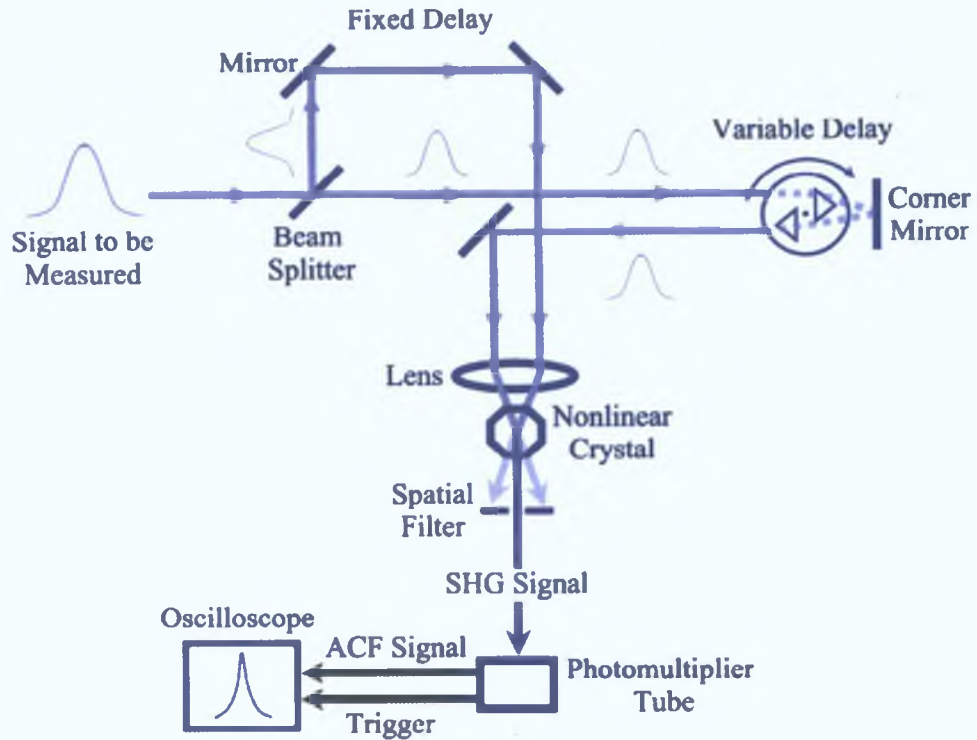
Figure 4.5: Schematic of a Michelson interferometer based SHG autocorrelator

3.4. The set of rotating mirrors provides the variable delay by reflecting the input beam against the first mirror of the rotating arm and then reflecting it onto the second mirror. The beam then hits a corner mirror before being reflected through the rotating mirrors again. As the mirrors have rotated since the first pass, the reflected beam hits the rotated pair at a slightly different angle than during the first pass, introducing a path difference, and thus a delay between the two replicas, which is denoted as τ [31].

The two signals are then focused by a lens so that they cross inside a nonlinear media, which in the case of Figure 4.5 is a nonlinear crystal. This results in Second Harmonic Generation (SHG), which is proportional to the product of the electric field of the two replica pulses [32]. The resulting optical autocorrelation signal ($G(\tau)$) can be expressed as:

$$G(\tau) = \langle I(t)I(t - \tau) \rangle \tag{4.4}$$

where the angle brackets are used to denote the time averaging. Due to the poor conversion efficiency of the SHG process, the resulting SHG signal is then measured by a photomultiplier tube (PMT), which integrates the measured signal over a long time period compared to the duration of the optical signal. This results in the photocurrent (i_{ph}) produced being a function of the relative delay (τ) between the replicas, and can be expressed as [32]:

$$i_{ph}(\tau) \propto \langle I^2(t) \rangle + 2G^{(2)}(\tau) \tag{4.5}$$

113

This is proportional to the second order Autocorrelation Function (ACF) of the pulse of Equation 4 4, and can then be easily displayed on a standard high-impedance oscilloscope The time scale as displayed on the oscilloscope can be related to the optical pulse duration by varying the path length of one of the arms of the autocorrelator and measuring the corresponding time displacement as shown on the display of the oscilloscope Then taking into account that the total optical delay is twice the path length, the time delay introduced by the autocorrelator (Δt) is

$$\frac{2x}{c} = \Delta t \qquad (4\ 6)$$

where x is the path length in the arm of the autocorrelator and C is the speed of light The value of Δt is compared to the time delay measured on the oscilloscope when the optical path delay of the correlator is altered A typical value for x and ΔT was 7mm and 7 4ms respectively This resulted in

$$7\ 4ms = \frac{(2)(7mm)}{c}$$

$$7\ 4ms = 47ps \qquad (4\ 7)$$

$$1ms = 6\ 38ps$$

As the autocorrelation process results in a symmetric pulse, an assumption has to be made in order to determine the actual pulse width [33] Once made, the actual pulse width is obtained by multiplying the measured pulse duration by the appropriate form factor Table 4 1 gives the form factors for a square, Gaussian and hyperbolic secant pulse shape This ambiguity can lead to errors in the pulse duration measurements, especially for gain-switched pulses which are asymmetric in nature, but appear symmetric on an autocorrelation trace

There are a number of other disadvantages associated with using an autocorrelator apart from ambiguity over pulse shape As the process relies upon the phase matching within the nonlinear crystal, it is necessary to tilt the crystal as the wavelength is varied Also the lack of phase or chirp information from an ACF is a serious disadvantage, especially for applications concerned with pulse compression and dispersion management One way to overcome some of the disadvantages of autocorrelation is to use the FROG technique

Pulse Shape	Multiplication Factor
Square	1
Gaussian	0 707
Hyperbolic Secant	0 645

Table 4 1 Autocorrelation form factors for square, gaussian and $sech^2$ pulse shapes

4.4.2 Frequency Resolved Optical Gating (FROG)

Frequency Resolved Optical Gating [34] allows for the complete characterisation of ultrashort optical pulses, providing information about the amplitude and phase of the electric field. It uses the same Michelson interferometer as in the autocorrelator except that the signal is spectrally resolved at each value of the temporal delay. This requires that the photomultiplier tube be replaced with a spectrometer, and that the temporal delay be provided by an electronically controlled translation stage.

As per the autocorrelator, for an input electric field $E(t)$, the second harmonic generated signal as a function of delay is $E_{sig}(t, \tau) = E(t)E(t - \tau)$. This is then spectrally resolved in a grating spectrometer at each value of optical delay, resulting in a FROG signal that is a function of both delay and frequency [35]:

$$I_{FROG}(\omega, \tau) = \left| \int_{-\infty}^{\infty} E_{SIG}(t, \tau) e^{j\omega t} dt \right|^2 \tag{4.8}$$

From this measured FROG signal, it is possible to completely recover both the amplitude and phase of the original field $E(t)$ using 2D phase retrieval techniques. The retrieval of the pulse phase $\phi(t)$ from the FROG data allows the frequency chirp $(\Delta f = -d\phi(t))$ to be calculated across the pulse. Therefore by using the FROG process, complete intensity and phase can be retrieved, yielding direct information about the pulse shape which is not possible with a conventional autocorrelation.

Figure 4.6 shows a print screen of the retrieval software interface for a Southern Photonics FROG. The top two displays are the spectrograms of the measured signal (linear and logarithmic), which in this case is an optical pulse from the u^2t tunable pulse source [36], which generates optical pulses with durations of about 1.8ps at a repetition rate of 10GHz. The bottom two pictures are the optical spectra of the second harmonic generated signal and the autocorrelation trace.

However there are a number of disadvantages associated with the FROG technique. The direction of the time axis cannot be determined unambiguously from the FROG data alone, requiring additional information to correctly distinguish the pulse leading and trailing edges [35]. Also as it is still based on a Michelson interferometer layout, phase matching of the crystal is still required, and the input signal must have a high optical intensity.

4.4.3 Sequential Sampling

For real-time sampling, the sampling rate must be at least twice the highest frequency content of the signal under test in order to obey Nyquist-Shannon sampling theorem and allow the accurate reconstruction of the original signal from the sampled version. However, a 10Gbit/s NRZ signal requires a sampling rate of about 30GSamples/s, which
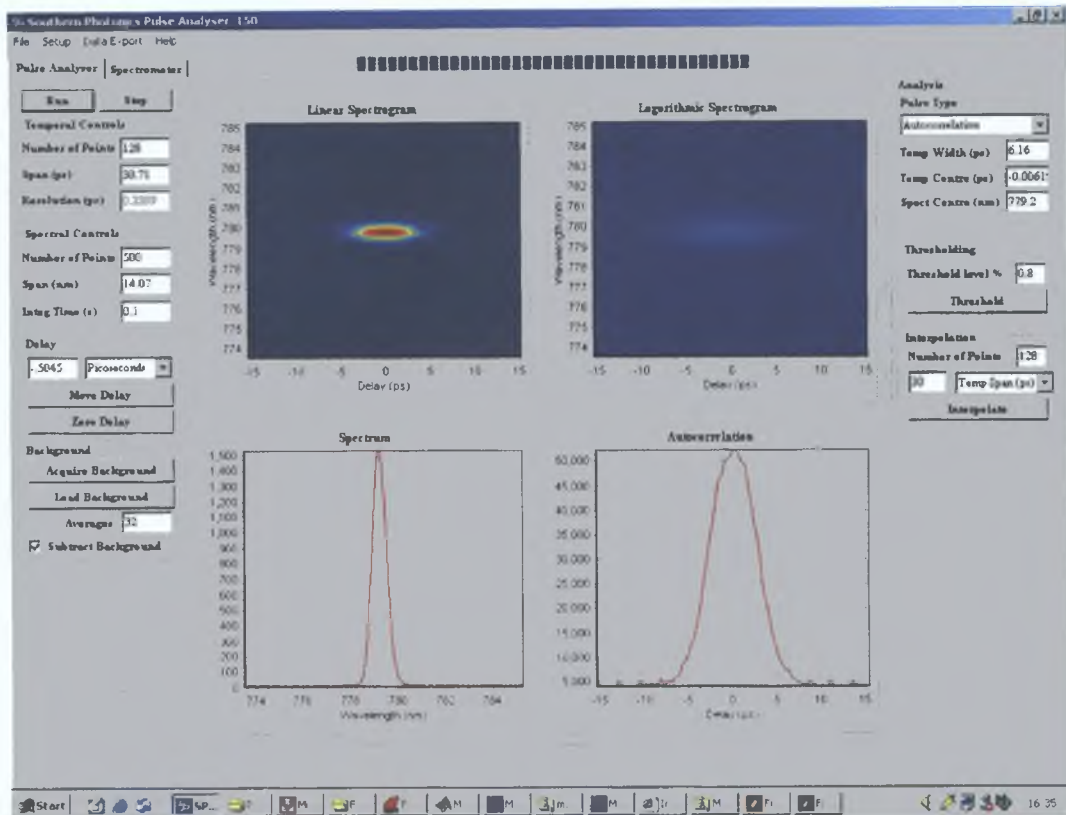
Figure 4.6: Screen shot of the retrieval software interface for a Southern Photonics FROG

is very challenging [37]. For test and measurement applications, such as performance monitoring in an optical communications network, the optical signal of interest is repetitive, rather than an unique singular event. This allows the use of sequential sampling, which uses the concept of equivalent time [38].

Sequential sampling uses narrow sampling pulses to measure the signal of interest. A sampling gate is opened by the narrow sampling pulse at a repetition rate of a subharmonic of the incoming signal. The repetition rate of the sampling pulse is also offset by a small frequency difference of the incoming signal such that the acquired samples are slowly scanned across the measured repetitive waveform [19]. This results in a crosscorrelation of the sampling pulse and the signal pulse, with the obtained signal being identical to the incoming signal, assuming the sampling pulse is short enough [37]. This is shown in Figure 4.7. The periodic waveform and the sampling pulses are combined, and then incident in some nonlinear media. The resulting detected signal is slower than the signal under test, and represents the original periodic signal except that the time scale has been stretched (as shown).

For practical implementations, the repetition frequency of the sampling pulse source is typically $\frac{f_{rep.data}}{(10^3 \rightarrow 10^6)}$, with the bandwidth given by the inverse of the sampling pulse duration [38]. Sequential sampling can be carried out using optical signals in a number

116
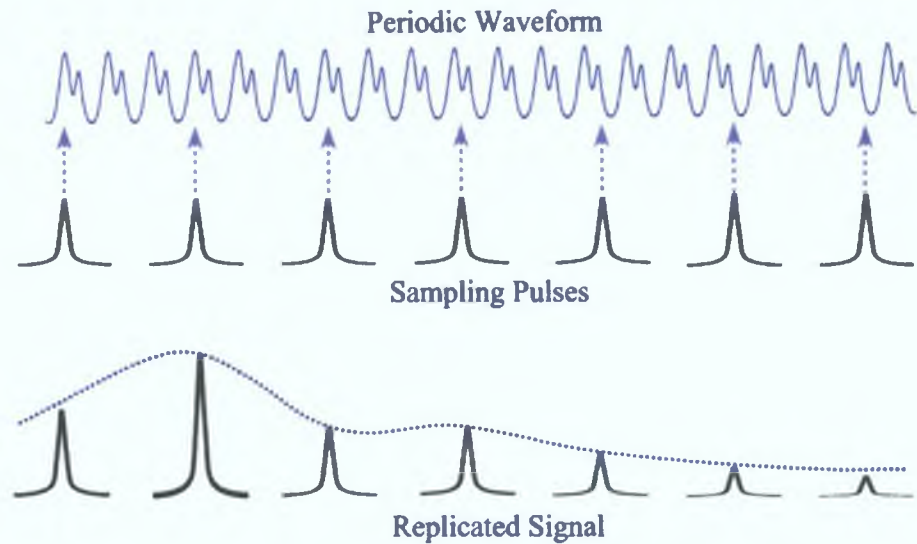
Figure 4.7: Principles of sequential sampling [38]

of different ways including electro-optic sampling and all-optical sampling [38].

Electro-optic Sampling

Electro-optic sampling uses the electro-optic effect (Pockels effect) for high resolution evaluation of electronic devices using optical pulses. It was first described in [39, 40], with the first demonstration by Kolner and Bloom [41] where they performed measurement using a GaAs (electro-optic material) integrated circuits.
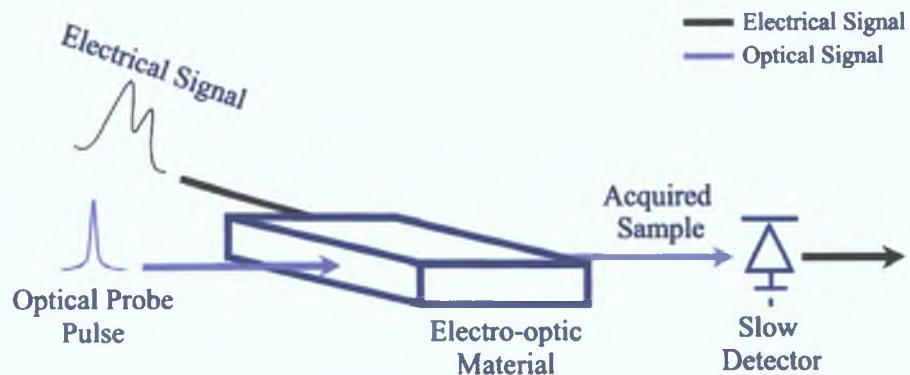
Figure 4.8: Schematic of electro-optic sampling operation [38]

Electro-optic sampling uses ultrashort optical pulses as a probe for the electrical signal under test (see Figure 4.8). When the electrical signal under test is incident on the electro-optic material, it alters the properties of the material, such as index of refraction or polarisation, which in turn alters the properties of the optical sampling pulse. As the optical pulse has a very short duration, there is only a small time in which

the electrical signal can influence the light. The intensity of the optical pulse, which if biased correctly, will be proportional to the voltage of the electrical signal under test, and is measured using a slow photodiode. By slowly varying the arrival time of the probe pulse, the full waveform of the periodic electrical signal can be obtained [41].

There are a number of factors that can influence the bandwidth of such a detection scheme including the response time of the electro-optic material, the width of the optical probe and the electrical contacts [38].

4.4.4 Optical Sampling

In order to evaluate the performance of the next generation of high-speed optical communications systems, future pulse characterisation techniques will require a subpicosecond resolution, allowing individual channel data rates in excess of 500Gbit/s to be monitored, and a low (sub-GHz) sampling rate, thus avoiding the need for high-speed electronics. This performance can be achieved using an optical sampling system [42].

Optical sampling builds upon the idea of sequential sampling already described, using ultrashort optical sampling pulses at a sub-harmonic of the repetitive signal under test, and second order susceptibility (χ^2) in nonlinear crystals or third-order susceptibility (χ^3) in optical fibres or semiconductors serving as the nonlinear gate [37]. The principle of optical sampling is shown in Figure 4.9. The sampling and signal pulses are optically combined using a passive fibre coupler, before being incident on a nonlinear optical material (acting as nonlinear sampling gate), with the resulting crosscorrelation signal detected and displayed on a low bandwidth oscilloscope. The detected signal is the same as the original periodic signal except that the time scale has been stretched.
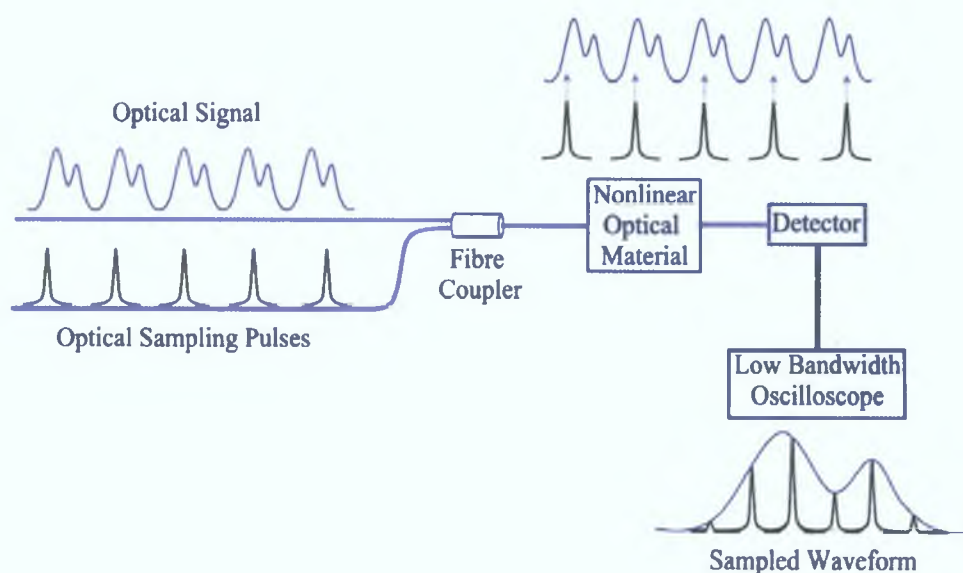
Figure 4.9: Schematic of optical sampling using a nonlinear detector [27]

118

In order for the sampling pulse to scan across the signal pulse, the sampling frequency (f_{sam}) is operated slightly detuned from a sub-harmonic of the signal frequency (f_{sig}) This results in a relationship between the signal and sampling frequencies of [19]

$$f_{sam} = \frac{f_{sig}}{(n + \delta)} \qquad (4\,9)$$

where n is an integer and $\delta << 1$ The small value of δ provides the slight frequency detuning, permitting the slow scan of the sampling pulse across the signal pulse This results in the sampling pulse scanning over the signal pulse at a rate [43]

$$f_{scan} = f_{sig}\frac{\delta}{(n + \delta)} \qquad (4\,10)$$

which can be easily displayed on a standard high-impedance oscilloscope

Some of the key performance requirements for a high-speed optical sampling technique include [38]

- *Temporal Resolution* - In order to operate at data rates in excess of 100Gbit/s, the temporal resolution needs to be high, requiring sampling pulses with durations less than 1ps

- *Timing Jitter* - As already mentioned in Chapter 2, in order to ensure a BER of 10^{-12}, temporal jitter must be less than 7% the width of the bit slot Thus for 160Gbit/s (bit slot about 6ps), the timing jitter must be less 0 4ps

- *Sampling Power* - A moderate sampling peak power, typically from 10 - 1000W is required However care must be taken to consider any nonlinear effects that may be encountered with the propagation of short, high power sampling pulse through optical fibre, even patch-cords

- *Polarisation* - For an analysis of PMD and polarisation-dependent losses in fibre links and circulating loop experiments, a sampling system with a small polarisation dependence is critical

- *Sensitivity* - The sensitivity of a sampling system determines the signal power required in order to achieve a specified sampled SNR [37] For optical powers typically found in an optical communications network, a low sensitivity will mean that the sampling pulse peak power is relatively low, reducing any nonlinear effects that may occur

- *Dynamic Range* - The dynamic range over which the sampling system operates at should be as large as possible The dynamic range will also affect the sensitivity of the system

- *Bandwidth* - An ideal sampling system would have the ability to operate continuously from the S- right through to the L-bands (see Table 2 1 in Chapter 2) without any loss of performance

As already mentioned, the nonlinear media employed utilising either χ^2 (nonlinear crystals) or χ^3 (nonlinear effects in fibres, semiconductors) interactions Those based on χ^2 are generally concerned with second-harmonic generation in $LiIO_3$ [44] and Periodically Poled Lithium Niobate (PPLN) [45] crystals Optical sampling has been carried out at data rates of 320Gbit/s with a temporal resolution of 700fs [46] However, there are a number of disadvantages associated with χ^2 techniques, including the requirements for a very high optical intensity for the sampling pulse due to the poor efficiency of the wavelength conversion process, stability problems associated with the use of free-space optics and the need for phase matching at different wavelengths

Optical sampling has also been demonstrated using χ^3 nonlinear effects in semiconductors (laser diodes [47], semiconductor waveguides [48], semiconductor optical amplifiers [49]) and optical fibre It has been shown that FWM in a SOA can be used to carry out optical sampling at 160Gb/s [49], with eye diagram measurement of a 500Gbit/s data signal using XPM in highly nonlinear fibre reported [50] However, as with SHG-based optical sampling, there are a number of disadvantages of using a fibre- and SOA-based sampling systems For fibre systems, high optical intensities or highly nonlinear fibre are required, the wavelength range can be limited [29, 51], and polarisation can be a problem For SOA-based systems, polarisation is still a problem, while gain-depletion limits the minimum sampling window [25]

Summary

This chapter has examined the use of optical nonlinearities for signal processing in a high-speed OTDM network, in particular focusing on optical clock recovery, optical demultiplexing and performance monitoring A number of different techniques were described for optical demultiplexing and sampling based on optical nonlinearities in fibre, semiconductors and crystals The disadvantages associated with these were then briefly discussed, highlighting the need to consider alternative optical nonlinearities for optical signal processing

The next chapter describes an alternative optical nonlinearity found in semiconductors and describes that with the aid of a specially designed device structure, a number of different applications, such as sampling, switching and thresholding in WDM, OTDM and OCDMA networks can be carried out

Bibliography

[1] R.Ludwig, "Ultrafast Transmission Technology," in *European Conference on Optical Communications (ECOC2005)*, vol. 5, pp. 159–168, 2005.

[2] P.Rees, P.McEvoy, A.Valle, J.O'Gorman, S.Lynch, P.Landais, L.Pesquera, and J.Hegarty, "A Theoretical Analysis of Optical Clock Extraction Using a Self-Pulsating Laser Diode," *IEEE Journal of Quantum Electronics*, vol. 35, no. 2, pp. 221–227, 1999.

[3] R.Penty, "Optical TDM makes faster networks possible," *Laser Focus World, January*, pp. 191–196, 2000.

[4] E.Shumakher, A.Hayat, A.Freimain, M.Nazarathy, and G.Eisenstein, "Timing Extraction of a 10-Gb/s NRZ Signal Using an Eelectrooptic Multiplication Scheme," *IEEE Photonics Technology Letters*, vol. 16, no. 10, pp. 2353–2355, 2004.

[5] K.Y.Lau, "Short-pulse and high-frequency signal generation in semiconductor lasers," *IEEE Journal of Lightwave Technology*, vol. 7, no. 2, pp. 400–419, 1989.

[6] Wikipedia, "Phase-locked loop." HMTL Document, 2005. http://en.wikipedia.org/wiki/Phase-Locked_loop.

[7] D.M.Spirit, A.D.Ellis, and P.E.Barnsley, "Optical time division multiplexing: systems, networks," *IEEE Communications Magazine*, vol. 32, no. 12, pp. 56–62, 1994.

[8] J.P.Turkiewicz, E.Tangdiongga, G.D.Khoe, and H.de Waardt, "Clock Recovery and Demultiplexing Performance of 160-Gb/s OTDM Field Experiment," *IEEE Photonics Technology Letters*, vol. 16, no. 6, pp. 1555–1557, 2004.

[9] J.Slovak, T.Tekin, C.Bornholt, B.Sartorius, E.Lach, M.Schmidt, S.Vorbeck, and R.Leppla, "Self-Pulsating Laser Based All-Optical Clock Recovery Applied in 421km Field Experiment for 170.6:42.7 Gbit/s OTDM Demultiplexing," in *European Conference on Optical Communications (ECOC2005)*, vol. 4, pp. 917–918, 2005.

[10] T.Miki, "The Potential of Photonic Networks," *IEEE Communications Magazine*, vol. 32, no. 12, pp. 23–27, 1994.

[11] X. Ma and G.-S. Kuo, "Optical Switching Technology comparison: Optical MEMS vs. Other Technologies," *IEEE Communications Magazine*, vol. 41, no. 11, pp. S16–S23, November 2003.

[12] H.S.Loka and P.W.E.Smith, "Ultrafast All-Optical Switching with an Asymmetric Fabry-Perot Device Using Low-Temperature-Grown GaAs: Material and Device Issues," *IEEE Journal of Quantum Electronics*, vol. 36, no. 1, pp. 100–111, 2000.

[13] D. B.Mortimore, "Fiber Loop Reflector," *IEEE Journal of Lightwave Technology*, vol. 6, no. 7, pp. 1217–1224, 1988.

[14] G. P. Agrawal, *Applications of Nonlinear Fiber Optics*. Academic Press, 1st ed., 2001. ISBN 0-12-045144-1.

[15] N.J.Doran, D.S.Forrester, and B.K.Nayar, "Experimental investigation of all-optical switching in fibre loop mirror device," *Electronics Letters*, vol. 25, no. 4, pp. 267–269, 1989.

[16] N.J.Doran and D.Wood, "Nonlinear optical loop mirror," *Optics Letters*, vol. 13, no. 1, pp. 56–58, 1988.

[17] M.D.Pelusi, Y.Matsui, and A.Suzuki, "Pedestal suppression from compressed femtosecond pulses using a nonlinear fiber loop mirror," *IEEE Journal of Quantum Electronics*, vol. 35, no. 6, pp. 867–874, 1999.

[18] M.M.Mosso, W.R.Ruziscka, F.S.Silva, and C. da Silva, "OTDM quasi-all-optical demultiplexing techniques comparative analysis," in *SBMO/IEEE MTT-S International Microwave, Optoelectronics Conference, Natal, Brazil*, pp. 692–697, 1997.

[19] B.P.Nelson and N.J.Doran, "Optical sampling oscilloscope using nonlinear fibre loop mirror," *Electronics Letters*, vol. 27, no. 3, pp. 204–205, 1991.

[20] J.P.Sokoloff, P.R.Prucnal, I.Glesk, and M.Kane, "A Terahertz Optical Asymmetric Demultiplexer (TOAD)," *IEEE Photonics Technology Letters*, vol. 5, no. 7, pp. 787–790, 1993.

[21] P. R.Prucnal, V. Baby, D. Rand, B. C.Wang, L. Xu, and I. Glesk, "All-Optical Processing in Switching Networks," *IEEE Lasers and Electro-Optics Society Newsletter*, vol. 16, no. 4, pp. 13–14, 2002.

[22] J.M.Dudley, L.P.Barry, J.D.Harvey, M.D.Thomson, B.C.Thomson, P.G.Bollond, and R.Leonhardt, "Complete Characterization of Ultrashort Pulse Sources at 1550nm," *IEEE Journal of Quantum Electronics*, vol. 35, no. 4, pp. 441–450, 1999.

[23] T.Yamamoto, E.Yoshida, and M.Nakazawa, "Ultrafast nonlinear optical loop mirror for demultiplexing 640Gbit/s TDM signals," *Electronics Letters*, vol. 34, no. 10, pp. 1013–1014, 1998.

[24] S.Diez, R.Ludwig, and H.G.Weber, "All-optical switch for TDM, WDM/TDM system demonstrated in a 640Gbit/s demultiplexing experiment," *Electronics Letters*, vol. 34, no. 8, pp. 803–805, 1998.

[25] B.C.Thomsen, J.D.Harvey, and L.P.Barry, "Error Free Demultiplexing in High-Speed OTDM Systems using a Two-Photon Absorption Based Switch," in *Optical Fibre Communication Conference (OFC2001)*, pp. W02–1, 2001.

[26] J M Tang, P S Spencer, and K A Shore, "Influence of Fast Gain Depletion on the Dynamic Response of TOAD's," *IEEE Journal of Lightwave Technology*, vol 16, no 1, pp 86–91, 1998

[27] S Kawanishi, "Ultrahigh-Speed Optical Time-Division-Multiplexed Transmission Technology Based on Optical Signal Processing," *IEEE Journal of Quantum Electronics*, vol 34, no 11, pp 2064–2079, 1998

[28] Physikalisch-Technische Bundesanstalt (PTB), "Ultra-fast optical sampling oscilloscopes" html document, 2004 http //www ptb de/en/suche/suche html

[29] R L Jungerman, G Lee, O Buccafusca, Y Kaneko, N Itagaki, and R Shioda, "Optical Sampling Reveals Details of Very High Speed Fiber Systems," pdf document, Agilent Technologies, www agilent com, 2004

[30] P Standt, "Getting the measure of ultrafast pulses," *Opto & Laser Europe Product Guide 2005*, pp 19–21, 2005

[31] A Yasa and M Amer, "A rapid scanning autocorrelation scheme for continuous monitoring of picosecond laser pulses," *Optics Communications*, vol 36, no 5, pp 406–408, 1981

[32] P Vasil'ev, *Ultrafast Diode Lasers, Fundamentals and Applications* Artech House Publications, 1st ed , 1995 ISBN 0-89006-736-8

[33] P Staudt, "Getting the measure of ultrashort pulses," *Opto and Laser Europe*, pp 33–35, 2004

[34] R Trebino, K W DeLong, D N Fittinghoff, John N Sweetser, M A Krumbugel, and B A Richman, "Measuring ultrashort laser pulses in the time-frequency domain using frequency-resolved optical gating," *Rev Sci Instrum - American Institute of Physics*, vol 68, no 9, pp 3277–3295, 1997

[35] L P Barry, J M Dudley, P G Bollond, J D Harvey, and R Leonhardt, "Complete characterisation of pulse propagation in optical fibres using frequency-resolved optical gating," *Electronics Letters*, vol 32, no 25, pp 2339–2340, 1996

[36] u2t Photonics, "1550nm Tunable Picosecond Laser Source (TMLL1550)" PDF Document, 2005 http //www u2t de/pdf/Datasheet_TMLL1550_V42 pdf

[37] M Westlund, P A Andrekson, H Sunnerud, J Hansryd, and J Li, "High-Performance Optical-Fiber-Nonlinearity-Based Optical Waveform Monitoring," *IEEE Journal of Lightwave Technology*, vol 23, no 6, pp 2012–2022, 2005

[38] P Andrekson, "Ultrahigh bandwidth optical sampling oscilloscope (OSO's)," in *OFC2004)*, 2004

[39] J A Valdmanis and G Mourou, "Subpicosecond Electrooptic Sampling Principles and Applications," *IEEE Journal of Quantum Electronics*, vol QE-22, no 1, pp 69–78, 1986

[40] R K Jain, "Electro-optic sampling of high-speed III-V devices and IC's," *IEEE/Cornell Conference on Advanced Concepts in High Speed Semiconductor Devices and Circuits*, pp 22–34, 1987

[41] B H Kolner and D M Bloom, "Electrooptic Sampling in GaAs Integrated Circuits," *IEEE Journal of Quantum Electronics*, vol QE-22, no 1, pp 79–93, 1986

[42] M Westlund, H Sunnerud, M Karlsson, and P Andrekson, "Software-Synchronised All-Optical Sampling for Fiber Communications Systems," *IEEE Journal of Lightwave Technology*, vol 23, no 3, pp 1088–1099, 2005

[43] B C Thomsen, L P Barry, J M Dudley, and J D Harvey, "Ultra-sensitive all-optical sampling at 1 5μm using waveguide two photon absorption," *Electronics Letters*, vol 35, no 17, pp 1483–1484, 1999

[44] T Kanada and D L Franzen, "Optical waveform measurement by optical sampling with a mode-locked laser diode," *Optics Letters*, vol 11, no 1, pp 4–6, 1986

[45] S Nogiwa, Y Kawaguchi, H Ohta, and Y Endo, "Highly sensitive and time-resolving optical sampling system using thin ppln crystal," *Electronics Letters*, vol 36, no 20, pp 1727–1728, 2000

[46] R L Jungerman, G Lee, O Buccafusca, Y Kaneko, N Itagaki, R Shioda, A Harada, Y Nihei, and G Sucha, "1-THz Bandwidth C- and L-Band Optical Sampling With a Bit Rate Agile Timebase," *IEEE Photonics Technology Letters*, vol 14, no 8, pp 1148–1150, 2002

[47] K Ketterer, E H Bottcher, and D Bimberg, "Picosecond optical sampling by semiconductor lasers," *Applied Physics Letters*, vol 50, no 21, pp 1471–1473, 1987

[48] S Kawanishi, T Yamamoto, M Nakazawa, and M M Fejer, "High sensitivity waveform measurement with optical sampling using quasi-phasematched mixing $LiNbO_3$ waveguide," *Electronics Letters*, vol 37, no 13, pp 842–844, 2001

[49] S Diez, R Ludwig, C Schmidt, U Feiste, and H G Weber, "160-Gb/s Optical Sampling by Gain-Transparent Four-Wave Mixing in a Semiconductor Optical Amplifier," *IEEE Photonics Technology Letters*, vol 11, no 11, pp 1402–1404, 1999

[50] J Li, M Westlund, H Sunnerud, B-E Olsson, M Karlsson, and P A Andrekson, "0 5-Tb/s Eye Diagram Measurement by Optical Sampling Using XPM-Induced Wavelength Shifting in Highly Nonlinear Fiber," *IEEE Photonics Technology Letters*, vol 16, no 2, pp 566–568, 2004

[51] J Li, J Hansryd, P O Hedekvist, P A Andrekson, and S N Knudsen, "300-Gb/s Eye-Diagram Measurement by Optical Sampling Using Fiber-Based Parametric Amplification," *IEEE Photonics Technology Letters*, vol 13, no 9, pp 987–989, 2001

CHAPTER 5

Two-Photon Absorption (TPA)

Introduction

Even though a number of experiments have demonstrated optical demultiplexing at data rates up to 640Gbit/s, a number of disadvantages including the need for speciality fibre and control of signal wavelengths in the NOLM, and gain depletion in the TOAD limit their performance. As such, it is necessary for consider an alternative optical nonlinearity to carry out optical signal processing tasks such as optical demultiplexing and pulse characterisation. One such nonlinearity present in semiconductors is Two-Photon Absorption, which is the main subject of this thesis. It will be shown that by incorporating a specially designed semiconductor, a Two-Photon Absorption-based device can be used to perform optical signal processing functions at optical power levels found in a typical telecommunications network.

5.1 Two-Photon Absorption

Standard semiconductor photodetectors generate a current when incident photons with energy greater than the band gap of the active region of the detector are absorbed. This results in the excitation of an electron from the ground state (valence band) to the excited state (conduction band), generating an electron-hole pair. This is a linear absorption process as one photon generates a single electron-hole pair. The generated electron-hole pair are then separated by the electric field present across the active region of the detector, resulting in a current (photocurrent) flowing in an external circuit.

Individual photons with energy less than the band gap of the photodetector, will not be absorbed, and will not contribute to the photocurrent generated. However, under certain operational conditions, two photons can be *simultaneously* absorbed to produce a single electron-hole pair. The resulting photocurrent generated is proportional to the square of the incident optical power falling on the detector. This nonlinear optical-to-electrical conversion process is known as Two-Photon Absorption (TPA) [1], and is considered a third-order nonlinearity in the material [2].

TPA was first theoretically proposed by German born physicist *Maria Göppert-Mayer* in 1929 [3], and later published in an article in *Annalen der Physik* in 1931 [4].

125

Göppert-Mayer, who later won a Nobel Prize for Physics in 1961 with J.Hans.D.Jensen, described the quantum mechanical interaction between electro-magnetic radiation and atoms using a second-order perturbation theory. This concept was used to explain the decay rate of metastable atomic states via two-photon spontaneous emission in 1940 [5], but as the probability of two-photon transitions was found to be a lot smaller than one photon emissions, it was not until the invention of the laser that TPA was first demonstrated. In 1961 Kaiser and Garrett [6] showed that when red light from a ruby laser operating at 649nm was passed through an Erbium-doped calcium fluoride crystal, blue fluorescent light at 425nm was observed emanating from the crystal. As the intensity of the red ruby light was increased, the blue fluorescent light intensity quadrupled, indicating a square dependence of the intensity of the incident light.

TPA is therefore a nonlinear optical-to-electrical conversion process where the addition of energy, momentum and angular momentum of *two photons* cause the transition of a *single electron* from one energy band to another [1]. For a transition from the valence band to the conduction band, the combined energy of the incident photons must exceed the semiconductor's band gap energy. In this work only degenerate TPA (photons of the same energy) will be considered.

5.1.1 Virtual State

The TPA process occurs when a photon of energy E_{ph} is incident on the active region of a semiconductor device with a band gap energy E_g exceeding E_{ph} but less than $2E_{ph}$. Under these conditions, individual photons do not possess sufficient energy to produce an electron-hole pair. However, as stated, an electron-hole pair can be produced by the simultaneous absorption of two photons, were the summation of the individual photon energies is greater than the band gap energy. The absorption of the two photons can be explained using a intermediate *virtual* state between the conduction band and the valence band within the band gap of the device. According to the Heisenberg uncertainty principle, population can reside in a virtual level for a time interval of the order of [7]:

$$\tau_{virtual} = \frac{\hbar}{\Delta E} \tag{5.1}$$

where ΔE is the energy difference between the virtual state and the nearest real level. This sets the timescale over which the TPA process can excite an electron from the valence band to the conduction band. This process is shown in Figure 5.1 (a-d). The energy of the incident photon, which is less that the band gap ($E_{ph} < E_g$) is absorbed causing an electron to be excited from the valence band to a virtual band somewhere in the band gap region of the semiconductor (Figure 5.1 (a), (b)). The electron is then almost instantaneously moved to the conduction band by the energy of a second photon
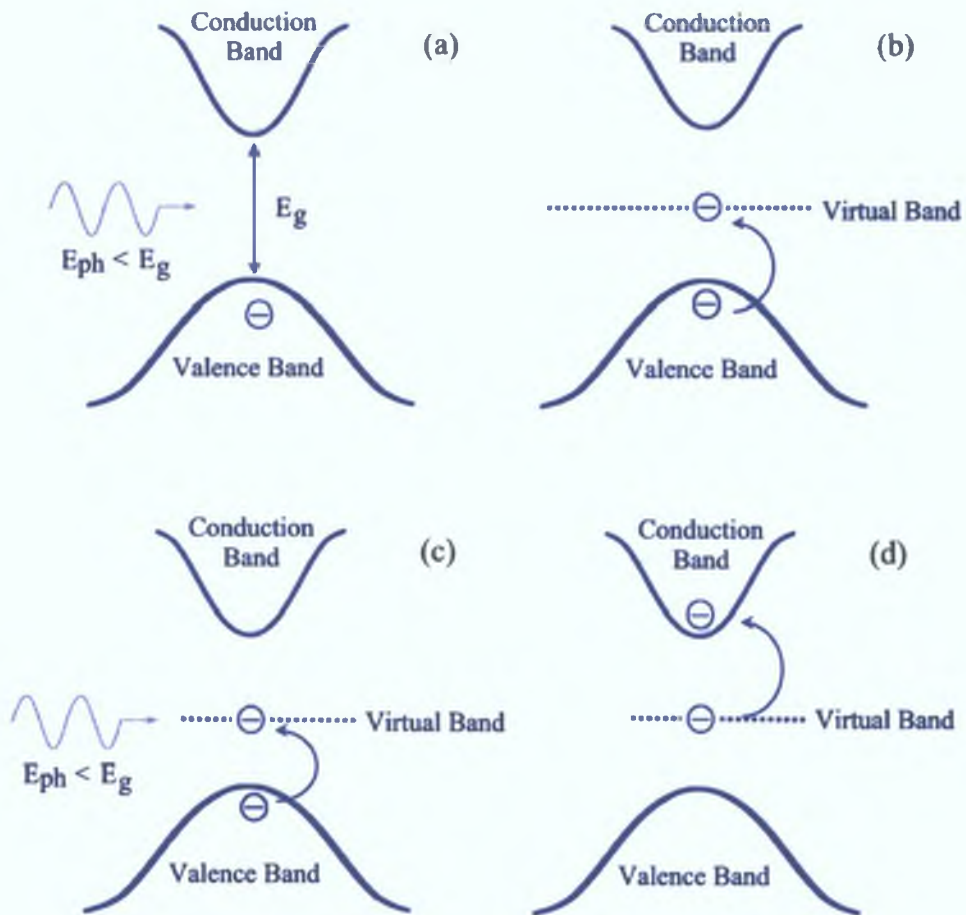
Figure 5.1: Illustration of the operation of Two-Photon Absorption using an intermediate virtual state with the energy band gap

(Figure 5.1 (c), (d)). By increasing the intensity of the light (increasing the number of incident photons per second on the material) the probability of the two-photon absorption will increase. The absorption coefficient of the medium is therefore proportional to the intensity of the light resulting in the photocurrent generated being proportional to the square of the incident optical power. Thus in order to observe the TPA process in a conventional photodetector, the peak power of the incident optical signal needs to be as high as possible.

The TPA process needs to be distinguished from a two-step absorption process in which photons are absorbed individually due to linear absorption. Such a process would require a real intermediate state, with a finite lifetime, and it would have a different intensity-dependent absorption relationship [8]. TPA involves the *simultaneous* absorption of two photons via a *virtual* state [9], which results in the generated photocurrent being proportional to the square of the optical intensity. It is this nonlinear response, combined with TPA's ultra-fast response time ($10^{-14}s$ at 1550nm [10]), that enables TPA to be considered for use in high-speed optical signal processing.

5.1.2 TPA Photocurrent

For linear absorption such as Single-Photon Absorption (SPA), the change in the intensity is determined by the linear absorption law [8]:

$$I(z) = I_0 e^{-\alpha z} \tag{5.2}$$

where $I(z)$ is the transmitted intensity, I_0 is the incident intensity, α is the absorption coefficient and z is the length of the transmission path. This linear absorption law is independent of the intensity I_0. However, if the absorption process is no longer linear, Equation 5.2 is no longer valid, and the absorption law becomes dependent on the instantaneous intensity. To take this into account, the differential equation for the intensity pulse propagation in the z direction, $I(r,z,t)$, is given by [11]:

$$\frac{dI(r,z,t)}{dz} = -\alpha I(r,z,t) - \beta I^2(r,z,t) \tag{5.3}$$

Solving for the optical intensity along the z-axis of a semiconductor results in [1]:

$$I(z) = I_0 \frac{e^{-\alpha z}}{1 + \left(\dfrac{\beta I_0}{\alpha}\right)(1 - e^{-\alpha z})} \tag{5.4}$$

The SPA and TPA contributions to the total absorption can be defined as:

$$I_{abs}^{SPA} = I_0 \left[1 - \frac{e^{-\alpha L}}{C}\right] \frac{\alpha L}{\alpha L + lnC} \tag{5.5}$$

and

$$I_{abs}^{TPA} = I_0 \left[1 - \frac{e^{-\alpha L}}{C}\right] \frac{lnC}{\alpha L + lnC} \tag{5.6}$$

with

$$C = 1 + \left(\frac{\beta I_0}{\alpha}\right)\left[1 - e^{-\alpha L}\right] \tag{5.7}$$

where L is the length of the semiconductor along the z-axis. If all the photon energy is used in creating electron-hole pairs within the semiconductor, the quantum efficiency of the photoconductivity is 100%, with the resulting photocurrent J given by:

$$J = \frac{eA}{\hbar v}\left(I_{abs}^{SPA} + \frac{1}{2}I_{abs}^{TPA}\right) \tag{5.8}$$

where A is the illuminated area of the semiconductor. Thus the TPA response is limited by SPA at low incident optical intensities and by total absorption in the semiconductor

on the high-intensity side. This is represented in the following equation:

$$\frac{\alpha}{\beta} \leq I \leq \frac{1}{\beta L} \qquad (5.9)$$

In order to make use of the TPA nonlinearity for high-speed optical signal processing, it is necessary to choose a semiconductor material so that the band gap is greater than the energy of the incident photons, but less than twice the photon energy. As a result, the TPA photogeneration will dominate, with only a residual amount of linear absorption occurring due to lattice imperfections or thermal excitations of carriers within the detector [1].

Figure 5.2 shows a theoretical log-log plot of the photocurrent generated versus vary-
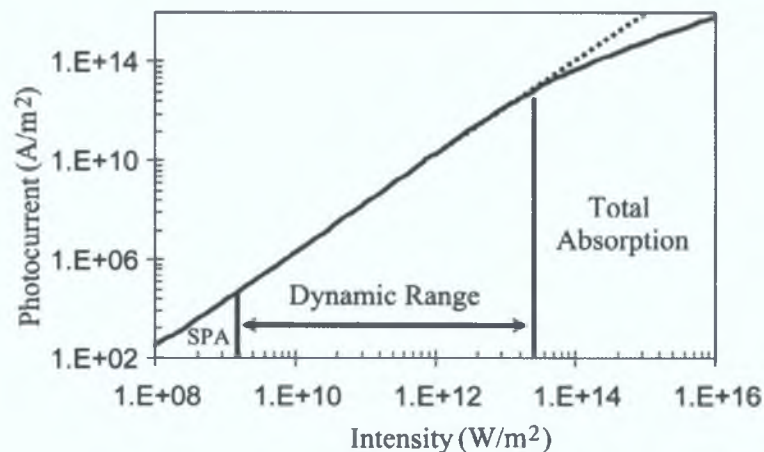
Figure 5.2: Plot of the simulated output current density as a function of the input optical power density for $\alpha = 0.01cm^{-1}$ and $\beta = 3 \times 10^{-10}m/W$

ing optical intensity of the input signal for a specially designed TPA detector (which will be discussed in more detail in the following chapter). The slope of 2 indicates the nonlinear TPA response, with a dynamic range over which this nonlinear response is active of about 40dB. At the extremities, the slope of the line decreases. At the lower incident optical intensities, SPA starts to dominate, while at higher intensities total absorption dominates [12].

5.2 Applications of TPA in High-Speed Optical Networks

Two-photon absorption based devices have found a number of different applications outside the optical communications field. These include infra-red image capture using a Si-CCD [13] and nonlinear optical spectroscopy [14]. This section however will focus on the applications of TPA for high-speed optical signal processing. These include:

- *Autocorrelation, Crosscorrelation and Sonogram*

- *Optical Thresholding*

- *Optical Clock Recovery*

- *Wavelength Conversion*

- *Optical Demultiplexing*

- *Optical Sampling*

5.2.1 Autocorrelation, Crosscorrelation and Sonogram

The first demonstration of a TPA-based autocorrelator took place in 1992 when Takago et al replaced the SHG crystal and photomultiplier tube of a conventional autocorrelator with a two-photon absorber [15] A number of different absorbers were used including a commercially available Si and GaAsP photodiode, and a CdS photoconductive cell These allowed easier construction and removed the need for phase matching when the incident wavelength was altered Since then, a number of different commercial devices have been demonstrated for use as a two-photon absorber These include semiconductor waveguides [16–18], photodiodes [19, 20], APD's [21, 22] and semiconductor microcavities [23] Crosscorrelation [24] and amplitude and phase analysis from a sonogram trace [25] have also been demonstrated using two-photon absorption Sonogram analysis involves utilising Fourier filtering and the intensity correlation of an optical pulse to retrieve information regarding the phase of that pulse [26] The sensitivity of these crosscorrelation and sonogram systems have been continuously improved over the years, with the latest results demonstrating an autocorrelation sensitivity of $9\ 3 \times 10^{-4}(mW)^2$ This is a two orders of magnitude improvement when compared to conventional second-harmonic generation-based autocorrelators [23] Thus not only do TPA-based autocorrelators remove the cost and complexity associated with the use of nonlinear crystals and a PMT, improved sensitivity and retrieval of phase information is also offered

5.2.2 Optical Thresholding

TPA-based devices may also find applications as optical thresholders in OCDMA systems [27] As already mentioned in Chapter 2 Section 2 4 4, OCDMA allocate each individual user a specific code that can be used to label bits that are transmitted by, or intended for that specific user The encoding of data can be carried out in a number of different ways, including the use of a FBG as an encoder and decoder The encoding grating imposes its shape onto the impulse response with code recognition accomplished by matching the transmitted code with a decoder grating which has the

exact time reversed impulse response to the encoding grating. If the encoder and decoder match, the filtering process results in the generation of a pulse which has the same shape as the code's autocorrelation function. Those pulses that do not match the decoding grating generates the crosscorrelation function.

One of the key requirements for an OCDMA receiver is the ability to discriminate between properly decided femtosecond pulses (autocorrelation pulse shape) and the equally energetic but improperly decoded picosecond interference signals (cross-correlation pulse shape) [28]. As the nonlinear TPA response is inversely proportional to pulse width (two pulses with equal average power but different pulse widths have different peak intensities) it permits the differentiation between correctly coded optical signals and pseudorandom noise bursts [27]. Also as the nonlinear optical process and electrical detection process are integrated in the same device, TPA-based thresholders are inherently compact and easy to integrate in optoelectronic systems [29]. The use of TPA for optical thresholding has been experimentally demonstrated using a 1.3μm InGaAsP laser diode [27] and GaAs P-i-N waveguide photodetector [29, 30].

5.2.3 Optical Clock Recovery

Another application for TPA devices is in high-speed optical clock recovery. The major advantage of using TPA is that the mixed clock product of the data signal and the clock signal can be directly measured as a photocurrent without the need for external detection [31]. Also as TPA is a nonresonant effect and does not require phase matching between the two input signals, its has a broad spectral bandwidth and ultrashort response time [32].

Figure 5.3 shows the experimental setup that was used in [31] to demonstrate a TPA-based optical clock recovery method. The data signal and the clock signal were optically
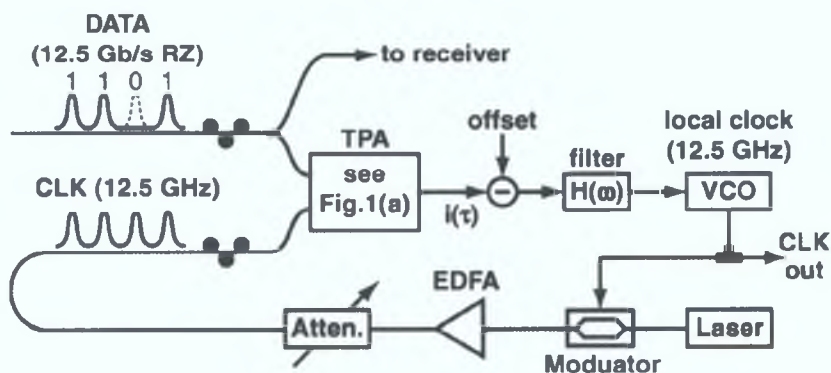
Figure 5.3: Schematic of experimental setup used for optical clock recovery via TPA [31]

combined in the TPA detector, which was a Si-APD, with a constant voltage offset

131

subtracted from the electrical TPA signal after the detector The resulting error signal passed through a feedback filter and is used to control the frequency of the VCO The resulting signal from the VCO is then used to drive an electro-optic modulator which generated the clock signal This allowed a locally generated 12 5GHz clock signal to be synchronised with a 12 5Gbit/s data signal A similar setup was used in [32] to synchronise a 10GHz clock signal to the 80Gbit/s RZ data signal

5.2.4 Wavelength Conversion

All-optical wavelength conversion via TPA in silicon wire waveguides has been demonstrated in [33] A mode-locked fibre ring laser was used to generate the pump pulses at 1550nm with a duration of 1 6ps at repetition rate of 1GHz An optical coupler then combined an optical amplified version of the pump signal with a weak CW signal at 1544nm, with the combined signal then coupled into the wire waveguide One photon from the pump signal and one photon from the CW signal were absorbed simultaneously within the pulse duration, as the sum of their electron energy exceeds the energy band gap of the waveguide This process is known as *non-degenerate* TPA as the pump and CW signal are at different wavelengths An optical bandpass filter was then used to filter out the pump pulses at the waveguide output It was shown that this non-degenerate absorption resulted in the wavelength conversion of the pump signal at 1550nm to 1544nm in the form of dark pulses, at the same repetition of the pump signal

5.2.5 Optical Demultiplexing

A TPA-based optical demultiplexer uses optical control pulses to switch out a single channel from a high-speed OTDM data signal The control pulses, which are at the repetition rate of the individual channels in the multiplex, are optically coupled together with the high-speed OTDM data signal and are incident on the TPA device The arrival time of the control pulses is varied using an optical delay line so that they arrive at the demultiplexer at a time corresponding to the data pulse to be switched out This is shown in Figure 5 4

The control pulse is adjusted to have a larger intensity than the signal pulse, for example a control-to-signal power ratio of 20 1 If there is a large relative delay between the control and signal pulses so that they arrive independently at the detector, then the TPA response due to the control pulse and data pulse are (assuming a 20 1 ratio) [34]

Control Pulses Arrive Independently (Constant Background Signal)	$\Rightarrow$	$(0 + 20)^2 = 400$
Data Pulses Arrive Independently	$\Rightarrow$	$\underline{(1 + 0)^2 = 1}$
Difference	$\Rightarrow$	$399(26dB)$
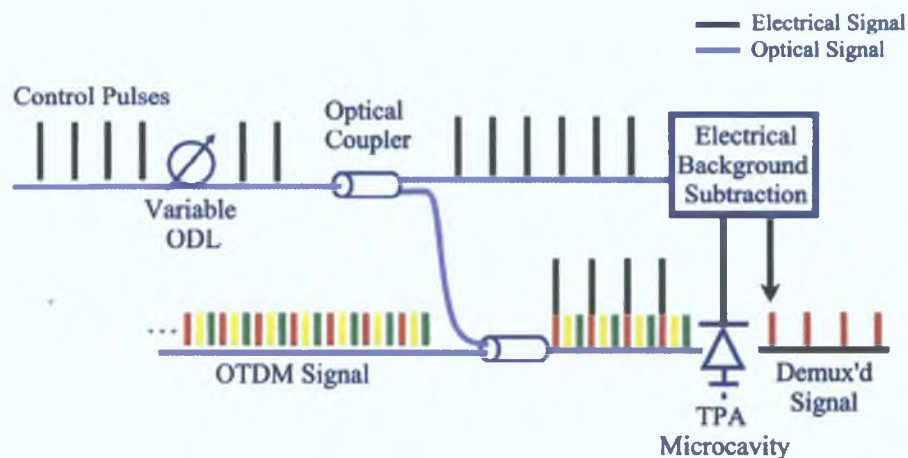
Figure 5.4: Schematic of optical demultiplexing via TPA in a semiconductor microcavity

showing that the TPA response from a data pulse unsynchronised with a control pulse is negligible (26dB) compared to the constant background signal generated by the arrival of the control pulse independently. If the relative delay between the control and signal is adjusted so that they arrive simultaneously at the detector, then the generated signals become:

$$\text{Synchronised} \quad \Rightarrow \quad (1+20)^2 = 441$$

$$\text{Control Pulse} \quad \Rightarrow \quad \underline{(0+20)^2 = 400(Background)}$$

$$\text{Difference} \quad \Rightarrow \quad 41(16dB)$$

As shown, after the subtraction background signal generated by the control pulse, a data signal representing a '1' generates a response of 41 times greater than the case when the data pulse arrives independently of a control pulse [35]. Thus the TPA effect in the semiconductor device leads to a delay-dependent response from the signal and the control pulses in the detector.

The TPA nonlinear response ensures that there is a strong contrast between the background electrical signal generated by the independent arrival of the control pulse and the electrical TPA signal generated when the control and the signal pulses are synchronised. The constant background generated by the control pulses may be removed by signal processing techniques, or by tapping off part of the optical signal, detecting it, and then subtracting this signal off the electrical output from the TPA demultiplexer. This would result in the required demultiplexed signal only [35].

There are a number of major advantages of using TPA for optical demultiplexing. These include that fact that since TPA is a near instantaneous nonlinearity, the maximum switching speed is determined by the duration of the data and control pulse, allowing successful optical demultiplexing of individual channels from an aggregate

data signal operating at 1Terabit/s and beyond Also the TPA demultiplexer is able to simultaneously carry out the process of channel selection and electrical detection in an optical communication system [1], reducing component count and allowing integration with other opto-electronic devices

TPA-based optical switching has been experimentally demonstrated using a GaAs /AlGaAs microring resonator [36, 37] and 1 3μm InGaAsP laser diode [34] [37] presented a TPA-based demultiplexer capable of switching speeds up to 100GHz using their microring resonator design for the switching device, with a switching on-off ratio of around 8dB [34] reported a switching window in the region of 650fs, allowing overall aggregate data rate in excess of 1Tbit/s The electrical response of their device, which determines the separation between data channels, was 200ps, permitting individual channel data rates of 2 5Gbit/s

Optical Sampling

The previous chapter highlighted the need to develop new performance monitoring techniques that can overcome the current speed limitations associated with using a photodetector in conjunction with a high-speed oscilloscope

Section 4 4 4 of Chapter 4 has already described the operation of optical sampling, with Figure 4 9 showing the basic operating principle of an optical sampling systems One of the key components of such a sampling scheme is the nonlinear sampling gate A number of different nonlinear effects are being investigated for use as the sampling gate One such effect takes advantage of SHG in optical crystals This method involves combining a high-power optical pulse tram to the data signal being analysed and generating the mixing product of both signals in the optical crystal The energy of the mixing product pulse represents the amplitude of the data signal and can be detected by a slow photodetector Unfortunately there are a number of disadvantages of using the SHG process which may limit its use for optical sampling in a high-speed network These include

- *High Optical Intensity* - Due to the poor efficiency of the SHG process, very high optical intensities for the sampling pulse are required

- *Free-Space Optics* - As this method relies on the use of free-space optics, associated stability problems can degrade performance

- *Phase Matching* - In order to operate at different wavelengths, the crystal employed has to be phase matched to that particular wavelength, increasing system complexity

As a result it is necessary to consider alternative optical nonlinearities for optical sampling One such nonlinearity is TPA in a semiconductor

134

To use TPA for optical sampling we require an optical sampling pulse $(I_{sam}(t - \tau))$ whose duration is significantly shorter than that of the optical signal pulses $(I_{sig}(t))$ under test. The signal and sampling pulses are then incident on the TPA device and the electrical signal $i(t)$ due to TPA in the device is measured as a function of the sampling delay (τ), to obtain an intensity crosscorrelation between signal and sampling pulse. For the practical implementation of a TPA sampling system, it is convenient to use a sampling pulse with a peak intensity much larger than the signal intensity. In this case, for a sufficiently short sampling pulse, the measured signal represents the signal pulse waveform on a constant background [38].

Kikuchi demonstrated in 1998 that TPA in a SiAPD could be used as the nonlinear sampling gate [39]. By replacing the nonlinear crystal and highly sensitive photodetector of conventional monitoring systems with a single device, the new sampling scheme greatly simplified construction and operation of the sampling scheme. It showed the successful sampling of a 10GHz optical signal, with a sampling temporal resolution of 2ps. In the following chapter, experimental results involving the use of our specially designed TPA detector will demonstrate optical sampling in excess of 100GHz, with a temporal resolution around 1ps.

5.3   Using a $1.3\mu m$ Laser Diode as TPA Detector

As already mentioned in the previous section, any semiconductor device with an energy band gap greater than 0.85eV will exhibit a TPA response if the intensity of an incident optical signal at $1.55\mu m$ is sufficient. The experimental setup shown in Figure 5.5 uses a commercially available NEL InGaAsP Fabry-Perot device, with a central wavelength of 1318nm, as a TPA detector (see Appendix A).
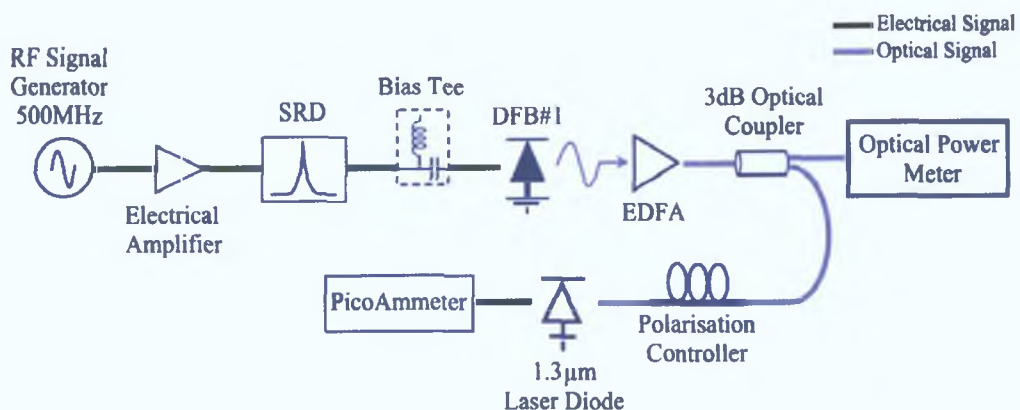
Figure 5.5: Schematic of the experimental setup using a $1.3\mu m$ laser diode as a TPA detector

A $1.55\mu m$ optical pulse train was generated using the exact same components as

135

shown in Figure 3.7 in 3.2.4 of Chapter 3. The gain-switched pulses, with a duration of 13.6ps, repetition rate of 500MHz and average power of -6.5dBm, were first amplified using a low-noise EDFA before entering a 3dB passive optical fibre coupler. One arm of the coupler was connected to an optical power meter, with the second arm connected to a Polarisation Controller (PC). The output from the PC was then incident on the $1.3\mu m$ laser diode via a GRIN lens, with the photocurrent generated by the device measured as a function of the incident optical power. A picoammeter, Keithley 6485 device with a 10fA resolution [40], was used to measure the photocurrent generated by the laser diode and an optical power meter was used to calculate the incident optical signal falling on the detector. The incident optical power was altered by varying the pump current of the EDFA.

Figure 5.6 shows a log-log plot of the photocurrent produced by the $1.3\mu m$ laser diode as a function of the incident optical power. It shows that at low incident optical
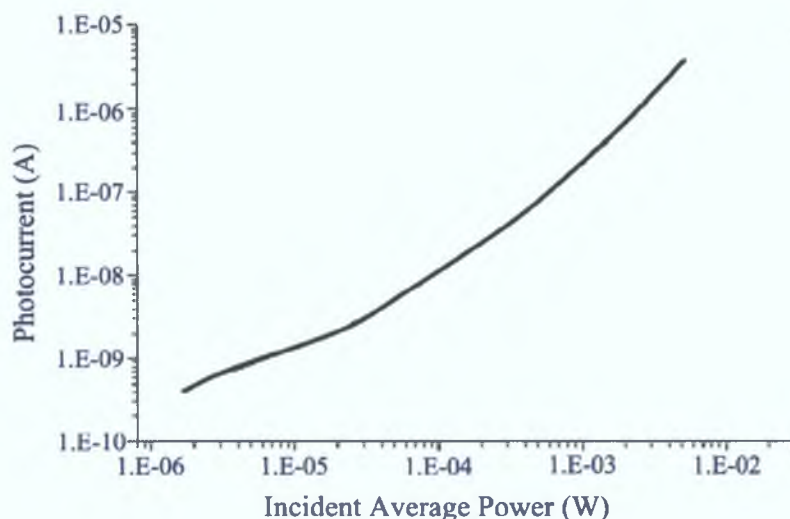
Figure 5.6: Logarithmic plot of the photocurrent produced against incident optical average power using 1.3μm laser diode as a TPA detector

powers, the slope is approximately one indicating linear absorption is the dominant process. As the power levels increase, the slope approaches 1.7, indicating that TPA is starting to dominate over SPA. It would be expected that the slope would continue to increase towards the ideal value of 2 for TPA, but the average optical power in this experiment was kept below 8dBm to prevent any damage from occurring to the 1.3μm device.

In order to demonstrate the dependency of the TPA response on optical peak power, the experimental setup was altered to that as shown in Figure 5.7, which is essentially the same as Figure 3.26 in 3.4.5 of Chapter 3. The major change is the inclusion of optical pulse compression stage, which reduces the gain-switched pulse duration from

12.8ps to 420fs at a repetition rate of 500MHz. As the average optical power was maintained, the reduction in pulse width will results in a 30 times increase in pulse peak power when compared to the case employing the 12.8ps pulse. The pulse compression technique employed here is the same technique that has already been described in 3.4.5 of Chapter 3.
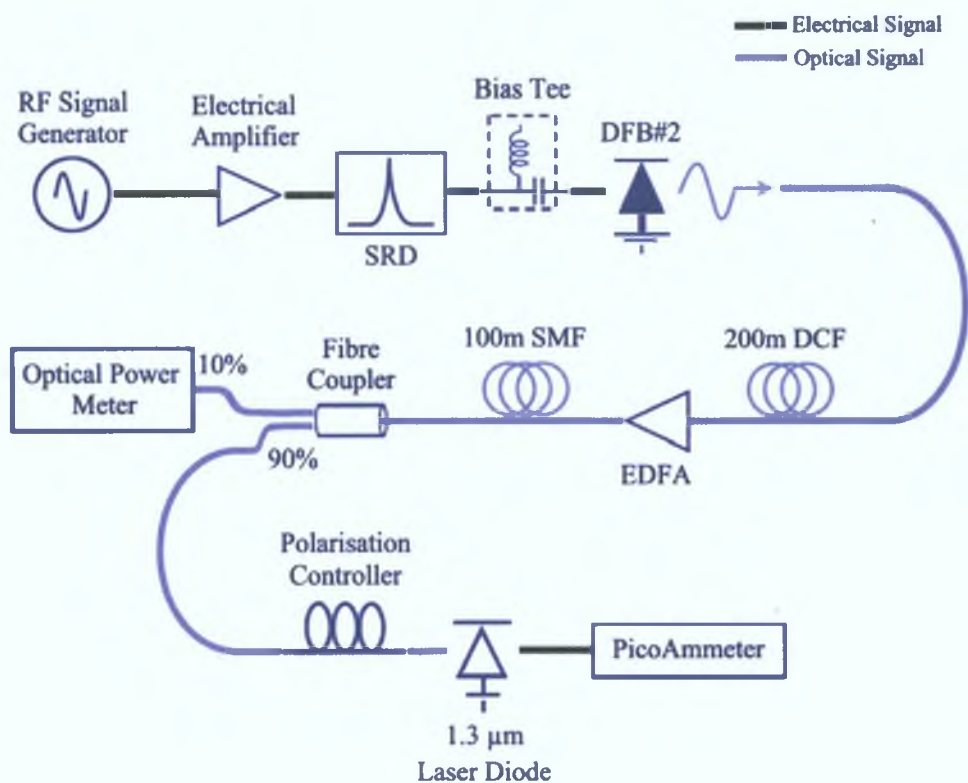
Figure 5.7: Schematic of the solitonic compression experimental setup used to demonstrate the peak intensity dependency of the TPA response

The photocurrent generated was again plotted against the incident optical signal as before, and this is shown in Figure 5.8. As the pulse width has been compressed to 420fs, the optical peak intensity of the signal should now be approximately 30 times greater than that for the 13.6ps signal, assuming the same average optical power in the signal. This is verified in Figure 5.8 by the increased dynamic range response of the TPA process within the detector, and the trace obtaining a slope of two at higher incident optical powers.

To verify that the nonlinear response was due to TPA, Figure 5.8 also shows a trace of the device response when the optical pulse train was turned off. As there was no signal entering the EDFA, the response from the detector arises from the ASE generated in the amplifier. As the peak power equals the average power for a CW signal, the dominant process for an ASE signal falling on the detector should be linear absorption. This is verified by the slope of 1 shown in Figure 5.8. This figure shows that TPA is indeed
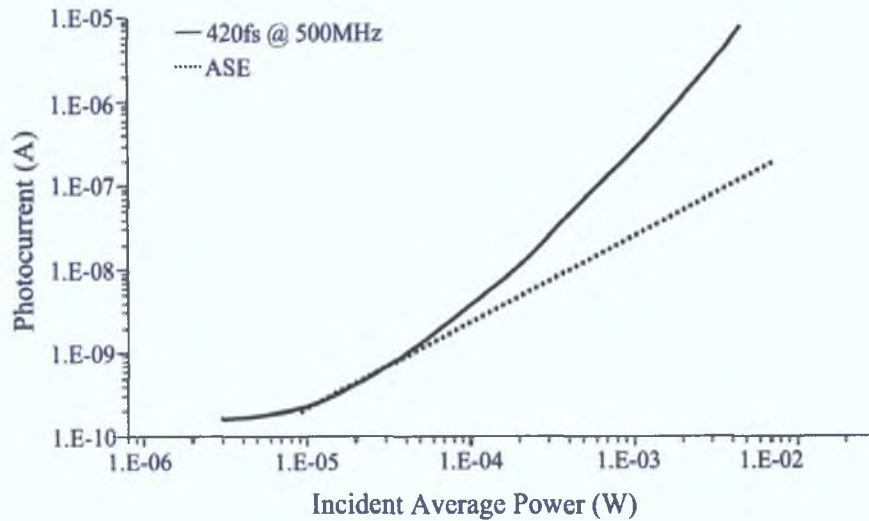
Figure 5.8: Comparison of the PI curves of the TPA response for an ASE incident signal and a 420fs optical pulse train

a peak intensity dependent process as the two signals, the ASE and optical pulse with 420fs pulse width, have the same average powers, but generate different responses due to the difference in the peak optical intensities of both signals.

5.4 Microcavity

It has already been shown that a number of different TPA devices are capable of performing various optical signal processing tasks. However in order to overcome the inherent inefficiency associated with TPA, high optical intensities or a long device were required, both of which makes those devices unsuitable for high-speed applications in an optical communications network. An alternative method to increase performance is to place the active device structure inside a FP resonant microcavity [41].

In conventional photodetectors, the quantum efficiency is limited by the absorption coefficient, the thickness of the active region and surface reflections [42]. Therefore, to achieve a high quantum efficiency, a thick active region and anti-reflection coatings applied to the surfaces of the device are essential. This results in a trade-off between high quantum efficiency and fast response time for conventional PIN photodiodes [43]. However, the required enhancement can be achieved by incorporating a multi-pass detection scheme, in which a single active layer serves many times in generating photocarriers [42]. This is the basis behind the operation of a Resonant Cavity Enhanced (RCE) photodetector.

Such RCE devices have a large wavelength-dependent increase in the optical field

within the cavity. This increased optical field allows RCE photodetector structures to be thinner and faster, while at the same time increasing the quantum efficiency at the designed resonant wavelength. This wavelength dependent operation allows RCE devices find many different applications in WDM and hybrid WDM/OTDM networks [44].

The fundamental physics behind the operation of RCE device has been known for over 100 years [44], with the first demonstration of a RCE semiconductor occurring in 1976 by Goedbloed and Joosten [45]. They showed that by varying the incident wavelength to a photodiode, interference ripples due to multiple reflections between the front and back contacts were formed.

As RCE devices allow high speeds, high quantum efficiency, narrow spectral linewidths (allowing the isolation of a single wavelength channel in a WDM system) and easy coupling of the incident signal [43], these devices are ideal for developing devices suitable for optical signal processing applications in high-speed optical communications networks. In addition, as growth of these structure can be carried out using Molecular Beam Epitaxy (MBE), fabricated devices can closely match the design specification [44]. Other uses for Fabry-Perot RCE devices include pressure and temperature sensors, optical filters and narrow spot-size lens in CD and DVD players [46, 47].

The cross-sectional diagram of the TPA microcavity device used in the sampling experiments described in the next chapter is shown in Figure 5.9. It was designed by our colleagues in the Semiconductor Optronics Group, based in the Physics Department, Trinity College Dublin, Ireland, with growth in the EPSRC National Centre for III-V Technologies, University of Sheffield, UK and packaging by Compound Semiconductor Technologies (CST) in Glasgow, UK. It consists of an undoped GaAs active region
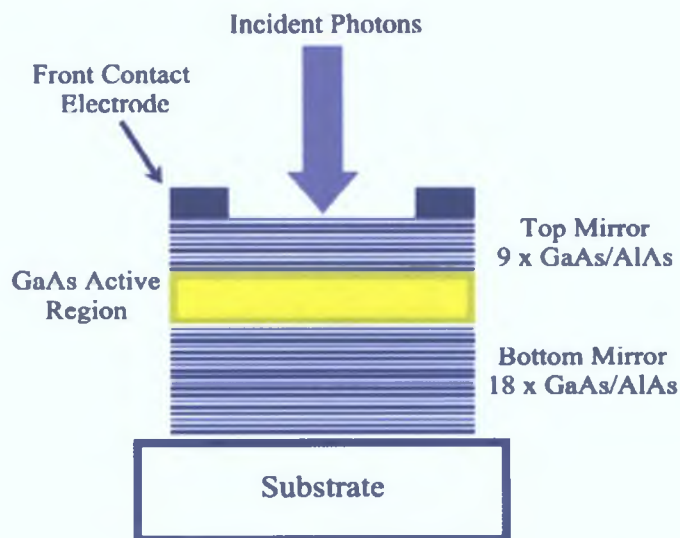
Figure 5.9: Schematic of the cross-sectional aspect of the TPA microcavity

approximately 460nm thick, sandwiched between multiple periods of alternating layers

of GaAs/AlAs, grown on a n-doped GaAs substrate. The multiple layers of GaAs/AlAs act as the front and back mirror (Distributed Bragg Reflector (DBR)) of the microcavity, with the number of periods and cavity size designed for optimal performance at 1550nm. The top layers of GaAs/AlAs was 2250nm thick, while the back layers were 4500nm. Further details regarding the device is given in later sections of this chapter. Enhancement is achieved from the formation of high intensity standing waves arising from multiple reflections from the top and bottom mirrors. This effectively increases the interaction length of the device and provides a large enhancement of the signal from a relatively thin active region at the resonance wavelength [43, 48]. A more precise description of the operation of the microcavity will be given in subsequent sections of this chapter. By using such a device design, the nonlinear TPA response of the GaAs is enhanced, increasing the TPA photocurrent level to allow optical signal processing applications at optical power levels found in a typical optical communications network.

5.5   Distributed Bragg Reflectors (DBR's)

In order to increase the quantum efficiency of a detector, a high level of reflectance is required from the top and bottom mirrors. A high-reflection coefficient at a particular wavelength can be achieved by using a mirror structure composed of multiple layers of two or more optically transparent materials, each with a different refractive index [49]. Interference occurs between the incident wave and one or more of the waves that are reflected from the multi-layer mirror stack. The phase and amplitude of these reflected waves will determine whether the resultant sum at the boundary of the mirror and the active region leads to constructive or destructive interference, and an increase or decrease in the reflectance or transmittance of the incident light [50]. If the waves interfere constructively at the boundary of the mirror stack and the active region, a high-reflection coefficient can be achieved. Such a mirror structure is known as a Distributed Bragg Reflector (DBR), and it was used to construct the front and back mirrors of the microcavity shown in Figure 5.9.

To ensure that constructive interference occurs at the boundary, each alternating layer is designed to have an optical thickness of one-quarter the wavelength of the desired reflected signal, that is:

$$\frac{L_H}{n_H} = \frac{L_L}{n_L} = \frac{\lambda_0}{4} \tag{5.10}$$

where L_L and L_H are the physical thickness of the low and high-index materials. Figure 5.10 shows a schematic of a Bragg reflector consisting of alternating layer of high (n_H) and low (n_L) refractive index material. The incident signal from the active region penetrates the different layers of the DBR, resulting in reflections from each layer. Light reflected from the high-index layer suffer no phase shift upon reflection, whereas those
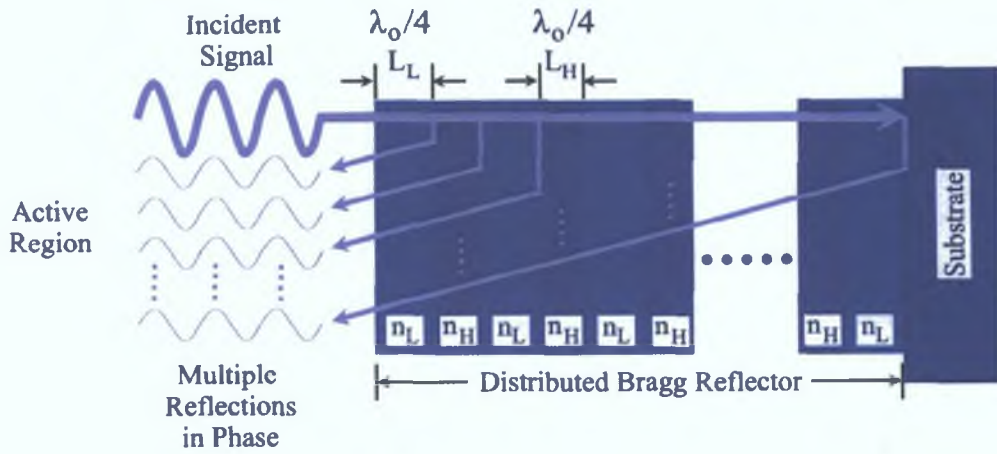
Figure 5.10: Schematic of the operating principle of a DBR

reflected within the low-index layers suffers a 180^0 phase shift [51]. The reflected components from each layer appear at the boundary of the active region and the mirror stack in phase, recombining constructively, providing a high reflection coefficient [49]. The reflectivity remains high over a limited range of wavelengths, with reflectance abruptly changing to a low value outside this zone. Such behaviour finds applications in optical filter design as well as a high reflectance coating [51]. The net reflectivity is determined by the refractive index step at each interface, the number of pairs in the mirror, the angle of incidence, and the polarisation of the incident light [52].

5.6 Operation of a Resonant Cavity Enhanced Device

A schematic of the basic Resonant Cavity Enhanced (RCE) photodetector is shown in Figure 5.11. The active region, with a thickness d, is sandwiched between two quarter-wave DBR's. The separation between the active region and the front and back DBR's are denoted as L_1 and L_2 respectively, with the overall cavity length defined as L. α is the absorption coefficient of the active region, with α_{ex} the absorption coefficient outside the active region. The field reflection co-efficients of the top and bottom mirror are given by $r_1 e^{-j\psi_1}$ and $r_2 e^{-j\psi_2}$, were ψ_1 and ψ_2 are the phase shifts experienced by the reflected components from each layer of the DBR's.

The input signal E_{in} is incident on the front DBR, with the transmitted signal into the device cavity denoted as $E_{in}.t_1$, where $t_1 = 0.9$ for a high Q-cavity [44]. For a propagation constant of:

$$\beta = \frac{2n\pi}{\lambda_0} \tag{5.11}$$

where λ_0 is the vacuum wavelength and n is the refractive index, the forward propagating Electro-magnetic (EM) field, denoted as E_{for}, at the interface between the front
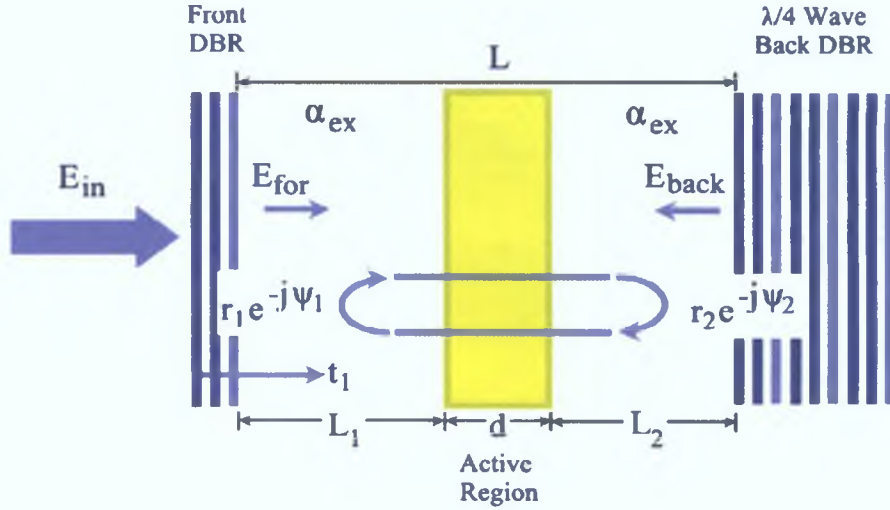
Figure 5.11: Schematic of the basic structure of a Resonant Cavity Enhanced (RCE) photodetector [44]

mirror and L_1 is given by [44]:

$$E_{for} = t_1 E_{in} + r_1 r_2 e^{-\alpha d - \alpha_{ex}(L_1+L_2)} e^{-j(2\beta L+\psi_1+\psi_2)} E_{for} \tag{5.12}$$

Equation 5.12 shows that E_{for} comprises of the signal transmitted through the top DBR ($t_1 E_{in}$), and the feedback signal from multiple reflections from both the top (r_1) and bottom (r_2) mirrors. It also takes into account the absorption encountered inside and outside the active region ($e^{-\alpha d - \alpha_{ex}(L_1+L_2)}$) and the phase shift experienced due to mirror and cavity penetration ($e^{-j(2\beta L+\psi_1+\psi_2)}$). Similarly the backward propagating electrical field, E_{back} can be written as [44]:

$$E_{back} = r_2 e^{-\alpha d/2} e^{-(\alpha_{ex}/2)(L_1+L_2)} e^{-j(\beta L+\psi_2)} E_{for} \tag{5.13}$$

Equations 5.12 and 5.13 show that by employing a RCE design, optical fields are formed within the cavity due to the signal undergoing multiple reflections at the top and bottom mirror. Such fields can lead to an increase in the quantum efficiency of the device, and this is discussed next.

5.6.1 Increased Quantum Efficiency

Assuming that there is negligible absorption in the areas outside the active region and within the mirrors, the quantum efficiency (η) within the active region can be defined

142

as [44]:

$$\eta = \left\{ \frac{(1 + R_2 e^{-\alpha d})}{1 - 2\sqrt{R_1 R_2} e^{-\alpha d} \cos(2\beta L + \psi_1 + \psi_2) + R_1 R_2 e^{-2\alpha d}} \right\} \times (1 - R_1)(1 - e^{-\alpha d})$$

(5.14)

R_1 and R_2 are the power reflectivity of the front and back mirror respectively, with $R_1 = r_1^2$ with $R_2 = r_2^2$, where r_1 and r_2 are the amplitudes of the reflection coefficients of the top and bottom mirror [42]. One interesting feature of Equation 5.14 that makes RCE devices suitable for WDM applications is that η is a function of the propagation constant β (see Equation 5.11). Therefore the quantum efficiency of RCE devices are enhanced periodically at a number of different resonant wavelengths (also called fringes) which occur at:

$$2\beta L + \psi_1 + \psi_2 = 2m\pi (m = 1, 2, 3 \ldots)$$

(5.15)

with the spacing between resonant cavity modes known as the *Free Spectral Range (FSR)* or the fringe interval. Figure 5.12 shows the quantum efficiency versus incident wavelength for a RCE photodetector ($L = 2\mu m$, $R_2 = 0.9$ and $\alpha d = 0.1$). The wavelength dependency is plotted for a number of different reflectivity values (R_1) of the front mirror. As can be seen, with an increase in the reflectivity of the top mirror,
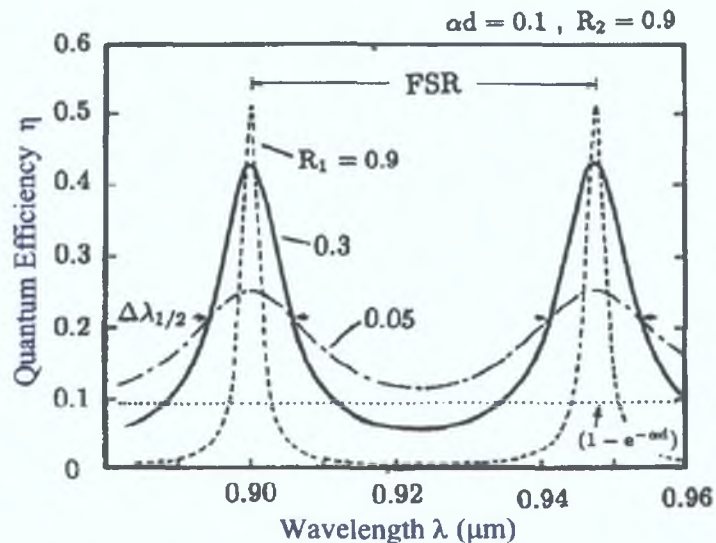
Figure 5.12: Wavelength dependence of the quantum efficiency for various top mirror reflectivities [42]

there is an increase in the quantum efficiency achieved with a corresponding decrease in the width of the resonant cavity mode. Also shown (flat dotted line) is the quantum efficiency of a conventional photodetector for the same active layer thickness. The conventional photodetector has a flat response over the entire wavelength range shown, whereas the RCE can be designed to have a maximum quantum efficiency at specific

wavelengths. This allows for the development of devices with enhanced response at specific wavelengths which would be suitable for WDM and hybrid WDM/OTDM applications.

For a thin active region, the peak quantum efficiency can be defined as [44]:

$$\eta_{max} \approx \left\{ \frac{(1 + R_2(1 - \alpha d))}{(1 - \sqrt{R_1 R_2}(1 - \alpha d)^2)} \right\} \tag{5.16}$$

which is dependent on the reflectivity of the front and back DBR (R_1, R_2), and the absorption and thickness of the active region (αd). Due the wavelength dependence of η (arising from its dependence on β and the wavelength dependence of the DBR's), off-resonance wavelengths will experience destructive interference, resulting in no cavity enhancement. Therefore, increased quantum efficiency only occurs at certain wavelengths which are defined by the structure and composition of the mirrors placed at either end of the device.

5.6.2 Formation of Standing Waves

It has been shown in the previous sections that by placing DBR mirrors at either end of the active region, optical fields are formed within the cavity due to an increase in the quantum efficiency at specific wavelengths. So far, the placement of the active region within the cavity has been ignored in Equation 5.14 for η. However, the formation of the forward and backward propagating waves (E_{for} and E_{back}) leads to a spatial distribution of the optical intensity within the cavity. This is known as the Standing Wave Effect (SWE). Therefore in order to maximise the quantum efficiency, the placement of the active region within the cavity needs to be taken into account.

For thick active regions, where the active region spans several periods of the standing wave, the SWE can be neglected. However, for thin active layers (which are necessary for high-speed operation) SWE has to be considered. Figure 5.13 shows the optical field distribution in a RCE detector as a function of wavelength and position. The top mirror consists of 5 period of GaAs/AlAs with the bottom mirror consisting of 15 periods of the same two materials. The central wavelength of the detector is 900nm.

The total electric field intensity $\left(|E|^2\right)$ within the cavity can therefore be defined as [44]:

$$|E|^2 = \left\{ \frac{|1 - r_1^2|}{|1 - r_1 r_2 e^{j(2\beta L + \psi_1 + \psi_2)}|^2} \right\} \times (1 + r_2^2 + 2r_2 cos(2\beta(L - z) + \psi_2)) |E_{in}|^2 \tag{5.17}$$

The first term in Equation 5.17 represents the enhancement effect of the resonant cavity, which as already mentioned is dependent on the reflectivity of the two mirrors and the phase shift encountered by the propagating signal. The second term takes into account
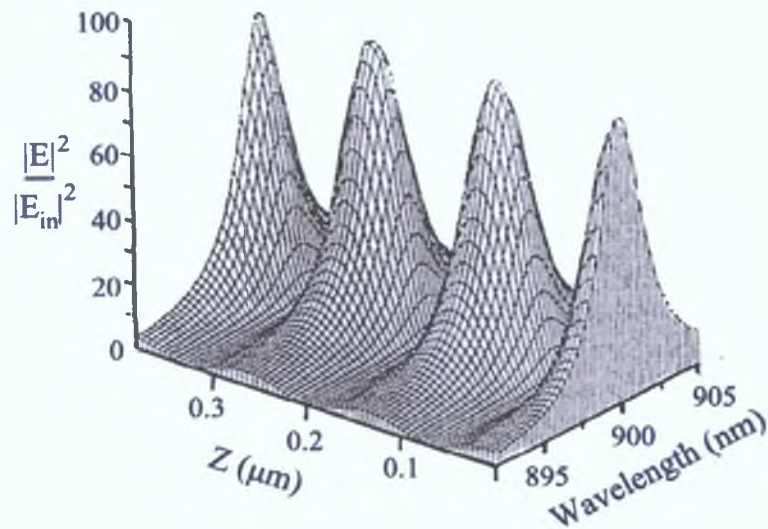
Figure 5.13: Optical field distribution in a RCE photodetector as a function of wavelength and position [44]

the reflectivity and phase due to light penetrating the back DBR and also the spatial dependence of the standing wave condition $(L - z)$.

5.7 Specially-Designed TPA Microcavity

The previous section showed that by incorporating a RCE design, the quantum efficiency of the device can be greatly enhanced. This should allow the TPA efficiency to be improved to such a level to allow practical optical signal processing at optical power levels found in a typical optical communications network. As the enhancement occurs within a shorter cavity length when compared to conventional detectors, higher bandwidths from a more compact device should also be possible. Finally, as the enhancement occurs only at specific wavelengths, a TPA-based device could be used for wavelength-selective operation in WDM and hybrid WDM/OTDM systems without the need for external filtering. This section will describe the microcavity and calculate a number of important parameters for device operation, for example the maximum channel rate at which the device can operate.

Figure 5.14 shows a cross-sectional schematic of the TPA microcavity that was specially designed for operation at 1550nm. It consists of an undoped GaAs active region, approximately 460nm thick, embedded between two quarter-wavelength DBR's, grown on a n-doped GaAs substrate.
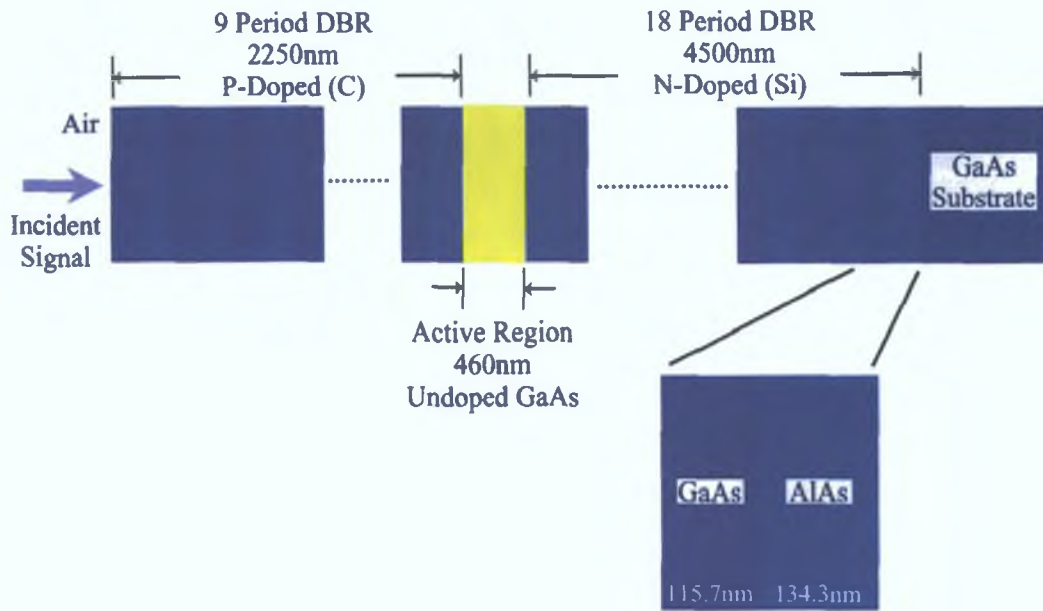
Figure 5.14: Schematic of the mirror composition of the TPA microcavity

Due to the penetration of the optical fields into the DBR's, the length of the cavity needs to be replaced by an effective cavity length [53]:

$$L_{eff} = L_{cav} + L_{DBR} \tag{5.18}$$

were L_{DBR} is the penetration length into the DBR's and L_{cav} is the physical length of the cavity. This penetration length is a function of the refractive indices of the mirror layers and is typically 3-4 times L_{cav} [53].

The front mirror consists of 9 periods of alternating layers of GaAs/AlAs. The uppermost GaAs layer of the front mirror was doped p++-doped with Carbon (C) to enable better contact with the contact electrode (not shown). The rest of the front mirror was again P-doped with Carbon to a concentration of $3 \times 10^{18} cm^{-3}$. This 9 period DBR provided an overall reflectivity of approximately 95% at $1.55 \mu m$. The back DBR consists of 18 periods of GaAs/AlAs, and was N-doped with Silicon (S) concentration of $1 \times 10^{18} cm^{-3}$. This mirror structure provided approximately 99.7% of back reflectance at $1.55 \mu m$. The microcavity was contacted on the highly p-doped top GaAs layer of the top mirror and the n-doped GaAs substrate, with the top contact being circular.

As mentioned, each period of the top and bottom DBR consists of alternating layers of GaAs and AlAs, with GaAs being the high-refractive index material ($n_H = 3.375$ at $1.55 \mu m$), and AlAs being the low-refractive index material ($n_L = 2.885$ at $1.55 \mu m$). It is worth remembering that in order to achieve a high overall reflectivity, a large number of layers are required, with every subsequent layer alternating in magnitude of the refractive index. The thickness of each layer (L_H, L_L) are chosen so that each layer

has the same optical thickness, that is $\frac{\lambda_0}{4}$. This results in $L_H(GaAs) = 115.7nm$ and $L_L(AlAs) = 134.3nm$. Taking into account the number of periods, and the thickness of each layer, the overall length of the top DBR is 2250nm, with the back DBR is 4500nm thick, which results in an overall device length of approximately 7.2μm.

5.7.1 Microcavity Material

In order to maximise the TPA response, the material must have a high TPA coefficient, β_2. The value of β_2 can be determined using [54]:

$$\beta_2 = K\sqrt{E_p}F\left(\frac{\frac{2\hbar\omega}{E_g}}{n^2 E_g}\right) \tag{5.19}$$

where K is a material-independent constant, n is the linear refractive index, and E_p (related to the Kane momentum parameter) is nearly material independent for a wide variety of semiconductors. The function F, whose exact form depends on the assumed band structure, is a function only of the ratio of the photon energy $\hbar\omega$ to E_g [54]. By using the expression given in 5.19, it is possible to predict the TPA of different materials at a variety of wavelengths.

As well as a high TPA coefficient, one of the major parameters for the selection of the substrate material is the wavelength range over which the device must operate. Thus in order to maximise the TPA response, the amount of SPA needs to be minimised. This can be achieved by carefully choosing the material so that the energy band gap is greater than the energy of the incident photons, but less than twice the photon energy. As these devices are intended for operation in the telecommunications wavelength window around 1.55μm, the energy band gap of the device must be greater than:

$$E_{photon} = \frac{\hbar c}{\lambda} = 0.85eV \tag{5.20}$$

where $\hbar$ is Planck's constant, c is the speed of light and λ is the wavelength of the incident photon (1.55μm). Other considerations for a suitable choice of material include the ease of growth and fabrication of the device, the ability to lattice match to other semiconductors for mirror construction, and to have a high TPA coefficient. An ideal candidate for an active region material is therefore Gallium Arsenide (GaAs).

GaAs has already been extensively used for the construction of RCE-based devices as GaAs based alloys and heterostructures can be grown by MBE [44]. It has an energy band gap in the region of 1.43eV, with an upper absorption wavelength of 880nm [55], making it ideal for TPA operation at 1550nm. It has good electronic properties, reasonably low carrier recombination rates (which reduces detector noise), allows low resistance ohmic contacts to be easily formed [44], and provides excellent lattice matching

to AlAs This final property allows a good refractive index contrast for the construction of the highly-reflective mirrors at either end of the cavity This minimises the number of defects introduced, which in turn decreases the contribution of SPA [44] GaAs also has a high TPA coefficient, which has been experimentally shown to be around 23(cm/GW) for bulk material, with theoretically predictions, using 5 19, of 19 7 (cm/GW) [54]

5.7.2 Reflectivity

In order to get a high quantum efficiency, the reflection coefficient from the top and bottom DBR's needs to be high This can be achieved by using multiple periods of alternating layers of materials with different refractive indices The total reflectivity of each DBR can be calculated using the following formula [53]

$$R = 1 - 4\frac{n_{ext}}{n_{cav}} \left(\frac{n_L}{n_H}\right)^{2N} \tag{5 21}$$

where n_{cav} is the refractive index of the cavity material, n_{ext} is the external medium on the other side the quarter-wave stack to the cavity, and n_L and n_H are the low- and high-index material comprising the quarter-wave stack N is the number of layers for each stack For the front Bragg mirror calculation, n_{ext} is the air interface (1 003), n_{cav} is the refractive index of the undoped GaAs active region (3 66), with n_L being the refractive index of AlAs (2 86), and n_H being the refractive index of GaAs (3 35) The front mirror comprises of 9 periods of alternating material, resulting in 18 layers ($N = 18$) By inserting these values in Equation 5 21, the total reflectivity of the top mirror is calculated to be 95% The calculation for the bottom DBR is the same process, except that in this case, n_{ext} is the refractive index of the GaAs substrate that the device is grown on, and $N = 36$ This results in the reflectivity of the rear mirror being 99 7% The difference in the values can be accounted for by the fact that the front mirror consists of 9 alternating periods, whereas the rear mirror consists of 18 alternating periods of GaAs/AlAs The refractive index of the alternating layers was calculated using the formula

$$nd = \frac{\lambda_0}{4} \quad \Rightarrow \quad n = \frac{\lambda_0}{4\,d} \tag{5 22}$$

where d is the physical thickness of each layer (GaAs=115 7nm, AlAs=134 3nm), and λ_0 is the cavity mode wavelength at normal incidence (1550nm)

Usually the overall reflectivity of the cavity is given, instead of separate values for

each mirror. The overall reflectivity is given by [51]:

$$\begin{aligned}
R_{cav} &= \sqrt{(R_{front})(R_{back})} \\
&= \sqrt{(95\%)(99.7\%)} \\
&= 97.3\%
\end{aligned}$$

(5.23)

5.7.3 Wavelength Selectivity

One of the main features of quarter-wave stacks is the fact that the reflectivity generated is wavelength dependent. This allows RCE devices to find applications in WDM and hybrid WDM/OTDM networks. The width of the reflectivity window is known as the *stop band* of the device and originates from the stop band of the two Bragg mirrors at either end of the cavity.
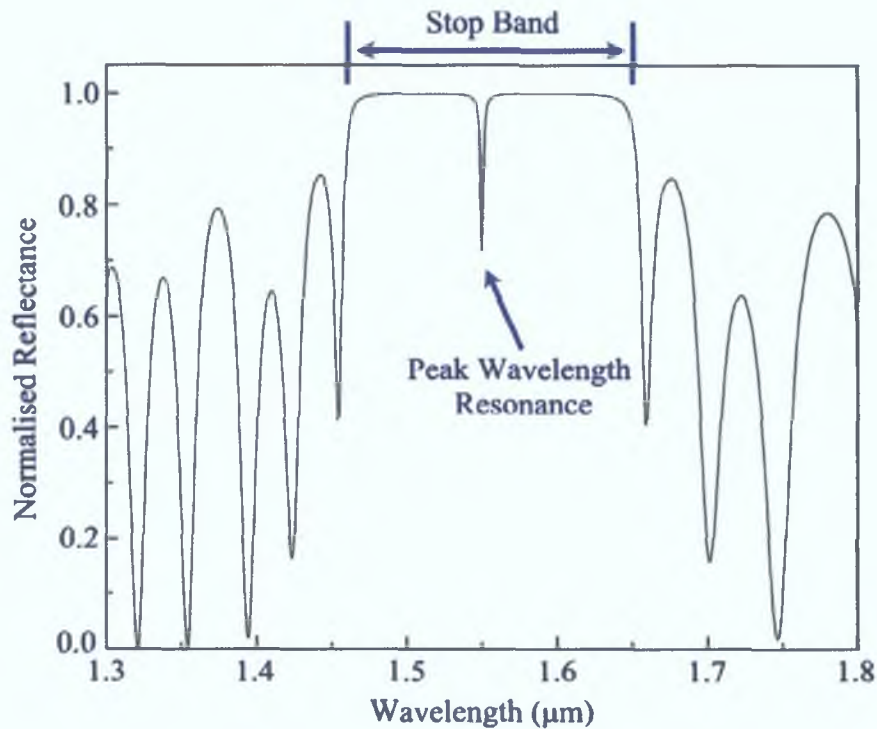
Figure 5.15: Plot of normalised reflectance against normalised wavelength for a DBR-based microcavity

Figure 5.15 shows the wavelength dependent reflectance response for a microcavity with a 10 period front DBR and 18 period rear DBR. The stop band is shown at the centre of the spectrum as the area with high reflectance, with the dip in the centre of the stop band corresponding the Bragg (central) frequency of the cavity [49]. The pronounced peak structures outside the stop band are known as *leaky modes*, and arise due to the low reflectivity of the DBR's at large angles [56].

Figure 5.12 showed the wavelength dependence of the quantum efficiency of a RCE detector as the mirror reflectivity of the top DBR was increased. As the reflectivity of the top mirror increased, the cavity modes became sharper, and the quantum efficiency of the device improved. The spectral width of the modes can be used to calculate the *Bandwidth* of the microcavity. The spectral width (σ_{cavity}) takes into account the refractance of the high- and low-index materials of the DBR's and can be calculated using [51]:

$$\sigma_{cavity} = \frac{4}{\pi} sin^{-1} \left(\frac{n_H - n_L}{n_H + n_L} \right)$$

(5.24)

$$\sigma_{cavity} = 5.7nm$$

where n_H (= 3.35($GaAs$)) and n_L (= 2.86($AlAs$)) are the refractive index of the high and low-index materials. Using the relationship $\Delta f = \frac{c\Delta\lambda}{\lambda^2}$, the optical bandwidth of the current device can be calculated to be in excess of 700GHz. This will determine the overall maximum aggregate data rates at which the device can operate at, and will be discussed in more detail later.

As already discussed in Section 5.6.1, the quantum efficiency of RCE devices is enhanced periodically at different resonant wavelengths, with the spacing between these modes known as the Free Spectral Range (FSR). The FSR can be calculated using [42]:

$$FSR = Finesse \times \sigma_{cavity}$$

(5.25)

where σ_{cavity} is the spectral width of the device (=5.7nm), and Finesse (F) is a dimensionless value used to quantify the performance of a Fabry-Perot device. The F is a function of the overall reflectivity of the microcavity and is given by [49]:

$$F = \frac{\pi}{2} \sqrt{\frac{4.R_{cav}}{(1 - R_{cav})^2}}$$

$$F = \frac{\pi}{2} \sqrt{\frac{4 \times (.973)}{(1 - 0.973)^2}}$$

(5.26)

$$F = 114$$

where R_{cav} = 97.3%, and is the overall reflectivity already calculated. Once the F of the device is known, the FSR is calculated to be 650nm. Thus as the active region of the microcavity was designed to be only 460nm thick, only one wavelength (determined by the Bragg frequencies of the DBR's) will experience cavity enhancement.

Equation 5.26 shows that the F is a function of the overall reflectivity of the cavity. Thus, in order to provide a high quantum efficiency, the finesse of the cavity should be as large as possible. However, Equation 5.25 shows that a high F will results in a narrow

spectral width of the cavity response, reducing the bandwidth of the device Therefore there exists a trade-off between the F (and thus overall reflectivity) and bandwidth of the device Generally, the number of periods of the top mirror is chosen to adjust the resonance width (and thus the bandwidth) of the device to match the channel spacing of the optical communications system in which the device is intend for [57]

5.7.4 Cavity Lifetime

As already discussed, by placing highly reflective mirrors at either end of the active region, an optical field builds up between the mirrors due to multiple reflections encountered by the incident signal Obviously a certain amount of time has to pass before the energy of the optical field exceeds the cavity losses, after which time the TPA response is enhanced by the microcavity This time period is known as the cavity (photon) lifetime (τ_p) [58] The cavity lifetime is given by [44]

$$\tau_p = \frac{\tau_{RT}}{Loss} \tag{5 27}$$

where τ_{RT} is the time required for the photons to make one round trip in the optical cavity, and $Loss$ is the total loss experienced during this round trip The $Loss$ is a function of mirror reflectivites (R_1, R_2) and absorption in the active region $(-\alpha d)$ The $Loss$ can be calculated using [44]

$$Loss \cong [1 - R_1 R_2 e^{(-2\alpha d)}] \tag{5 28}$$

Using the values for R_1 and R_2 already obtained, and $\alpha = 0$ $1cm^{-1}$ [23], the $Loss$ can be calculated In section 5 7, it was stated that due to the penetration of the optical fields into the DBR's at either end of the cavity, the length of the cavity needs to be replaced by an effective cavity length, which is the sum of the physical cavity length (L_{cav}) and the penetration length (L_{DBR}) of the two mirrors Thus in order for us to determine the value of d in Equation 5 28, the penetration length for each mirror needs to calculated, remembering that the front and back mirrors have different thickness, and hence should have different penetration depths The penetration depth can be calculated using [49]

$$L_{DBR} = \frac{c\tau}{2n_{cav}} \tag{5 29}$$

where τ equals [49]

$$\tau = \frac{n_{cav}}{c} \frac{tanh(kL)}{k} \tag{5 30}$$

151

with L being the mirror thickness and k being the coupling coefficient given by:

$$k = \frac{2\Delta n}{\lambda_0} \qquad (5.31)$$

Δn is the difference between the refractive index of the two materials of the mirror, and λ_0 is the design wavelength.

Using the values for the refractive indices of the different materials comprising the microcavity, the penetration depths were calculated for each mirror, with $L_{DBR\ Front} = 0.76\mu m$ and $L_{DBR\ Back} = 0.98\mu m$. This resulted in an effective cavity length of:

$$L_{DBR\ Front} + L_{DBR\ Back} + L_{cav} = 2.21\mu m \qquad (5.32)$$

Therefore the *Loss* of the cavity equals 0.0239.

Finally, in order to calculate the cavity lifetime, the time required for a photon to make one round trip in the optical cavity (τ_{RT}) is required. This is given by:

$$
\begin{aligned}
\tau_{RT} &= \frac{effective\ cavity\ length}{velocity} \\
&= \frac{2.21\mu m}{81.96 \times 10^6 ms^{-1}} \\
&= 24.9 fs
\end{aligned} \qquad (5.33)
$$

Therefore with the $Loss = 0.0239$ and $\tau_{RT} = 24.9fs$, Equation 5.27 gives:

$$
\begin{aligned}
\tau_p &= \frac{24.9 fs}{0.0239} \\
\tau_p &= 1.04 ps
\end{aligned} \qquad (5.34)
$$

This value for the cavity lifetime will place a limit on the minimum optical pulse duration that the device can operate with before the introduction of cavity-based pulse broadening. Thus for a cavity lifetime of 1.04ps, the minimum OTDM bit period would be approximately 3ps (assuming that the bit period is three times the pulse width to avoid ISI) resulting in an maximum overall OTDM aggregate data rate of 330Gbit/s ($Aggregate\ Data\ Rate{=}Bit\ Period^{-1}$). The value for the optical bandwidth has already been calculated from the spectral width of the stop band to be around 700GHz from the spectral width of the stop band. Therefore, a data rate in excess of 300Gbit/s should be possible with this detector which exhibits a bandwidth of 700GHz. It also clearly demonstrates the link between cavity lifetime of the device and the optical bandwidth (and hence spectral width of the resonance response) of the device, remembering that its the optical bandwidth that places a limit overall aggregate data rate, with the electrical bandwidth limiting the maximum speed at which the individual data channels can operate at. This will be covered in more detail in the following chapter.

5.8 Microcavity Characterisation

Figure 5.16 shows a photograph of the can structure packaging of the microcavity along with a diagram of various samples diameters contained within the sample. Bond wires are used to connect the various microcavity samples, of varying size, to the conducting wires, which are then connected to some external circuitry to allow the TPA photocurrent generated by the microcavity to be recorded. The current TPA device contains 11 different microcavity structures with diameters ranging from $25\mu m$ to $100\mu m$.
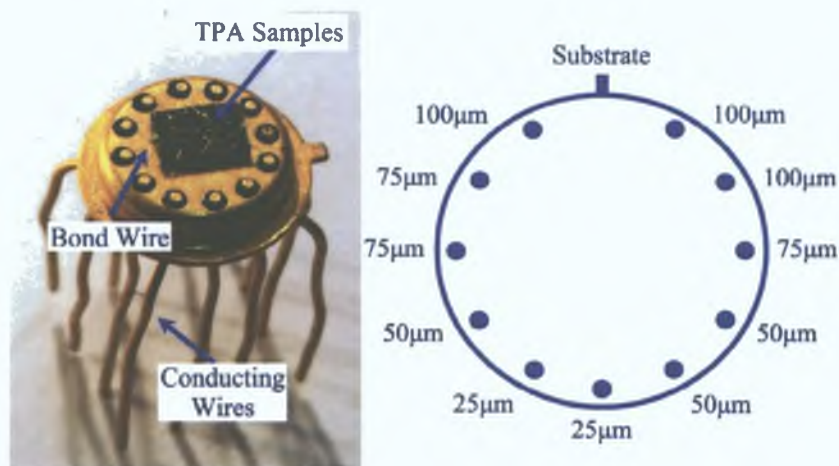
Figure 5.16: Photograph of the packaging of microcavity device used, with [left] a schematic of the top view of microcavity with device diameters marked

The characterisation of the microcavity can be divided into two separate categories - CW and dynamic testing. CW characterisation involves carrying out a wavelength response and PI curve for the current devices. This will allow the peak resonance response, spectral width of the response, dynamic range and minimum peak power required to generate a TPA response be determined. The dynamic testing will allow the electrical and optical bandwidth of the current device to be obtained. These will be important in order to evaluate the device for applications in optical processing functions in a high-speed communications network.

5.8.1 Wavelength Resonance

Small variations in the individual layers of the mirrors introduced during the growth process can shift the peak wavelength away from the design wavelength. As such, it is necessary to carry out a wavelength resonance sweep for each new sample used in order to determine the peak wavelength resonance. The experimental setup used to carry this out is shown in Figure 5.17, with the main components being a tunable pulse source, EDFA, OSA and picoammeter.

Initial alignment was performed by first forward biasing the TPA microcavity using a current source. This results in the device acting as a LED emitting light in the 850nm region. By placing the microcavity on a translation stage with micrometer variation in the x-y-z directions, the emitted light was coupled into a pigtailed GRIN lens with the optical power measured using an optical power meter. This provided a quick method for alignment, and ensured that the sample was connected (via bond wire) to the conducting legs of the sample.
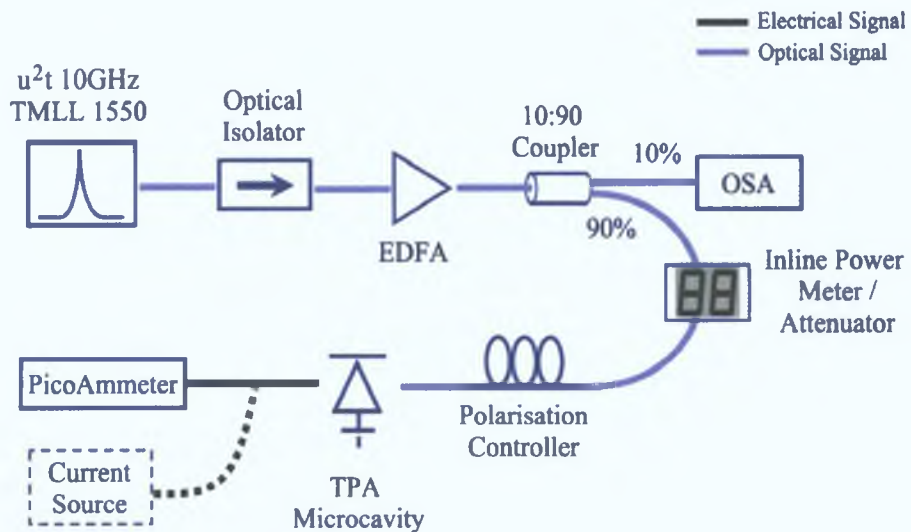
Figure 5.17: Schematic of the experimental setup for TPA wavelength sweep

The wavelength tunable signal was provided by a commercially-available ($u^2t\,photonics$, Germany) wavelength tunable pulse source [59], which has a continuous wavelength tuning range from 1480-1580nm. The 10GHz output pulse train first passed through an isolator to prevent any reflections from damaging the pulse source before entering a low-noise EDFA. The EDFA amplified the output power from the pulse source ($\approx -3dBm$) to 8dBm. The amplified signal than entered a 10:90 fibre coupler, with 10% of the optical signal sent to an OSA [60]. This allowed the output wavelength to be continuously monitored during the wavelength characterisation. The remaining 90% entered an in-line power meter/attenuator and a PC, before being incident on the microcavity. The PC was used to alter the polarization of the light incident upon the device and to maximise the photocurrent generated. The input signal was first tuned close to the design wavelength to optimise the alignment. Once completed, the wavelength of the tunable pulse source was tuned to 1520nm and varied in steps of 1nm to 1580nm. The photocurrent produced by the device was measured using the same picoammeter that was used for the previous tests involving the use of the 1.3μm laser diode as the TPA detector.

Figure 5.18 shows a plot of the photocurrent as a function of the incident optical

wavelength As shown, the cavity response is dependent on the incident wavelength, with a cavity wavelength resonance of 1556nm, and a measured linewidth of 5nm Figure 5 18 also shows that the photocurrent generated at the peak resonance wavelength is 3-orders of magnitude greater when compared to the photocurrent generated for off-resonance wavelengths Clearly this enhancement is due to the TPA enhancement at the resonant Bragg wavelength
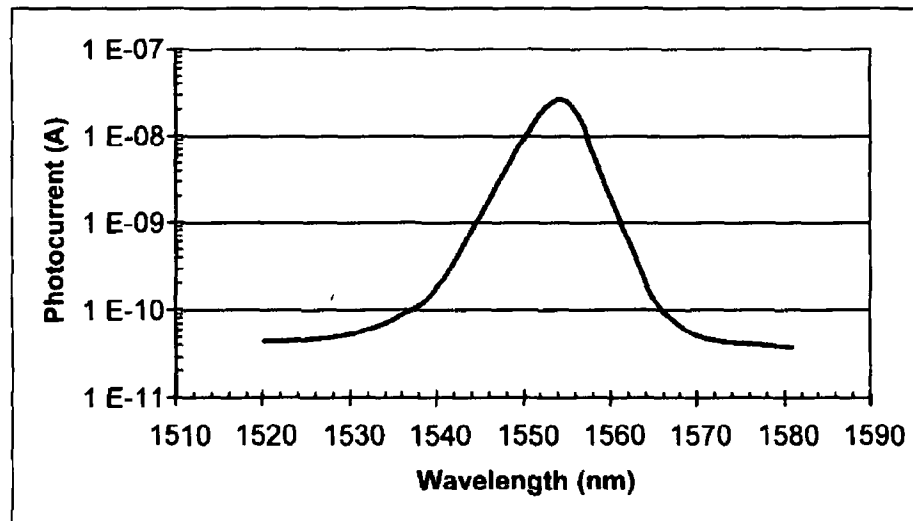
Figure 5 18 Plot of the wavelength response of 100μm diameter sample

5.8.2 PI Curve

Once the peak wavelength resonance of the sample has been determined, the next test involves obtaining an incident optical power versus photocurrent generated curve (PI curve) for the sample This allows the dynamic range over which the device has a nonlinear response to be ascertained, and determines the minimum power level at which TPA occurs

The experimental setup used is exactly the same as that shown in Figure 5 17 The wavelength of the tunable source was tuned to the wavelength resonance peak already determined As the TPA process is peak power dependent, any change in the pulse shape will alter the TPA response As such it was decided that the best method for altering the optical power of the incident signal was to operate the EDFA with a constant output power and vary the attenuation factor of the in-line power meter/attenuator The advantage of using the in-line power meter/attenuator was that the average optical power could be continuously monitored during the course of the experiment

Figure 5 19 shows a plot of the photocurrent generated as a function of incident optical peak power carried out at the cavity resonant wavelength It show that the photocurrent generated by the device is quadratically dependent on the incident optical

155
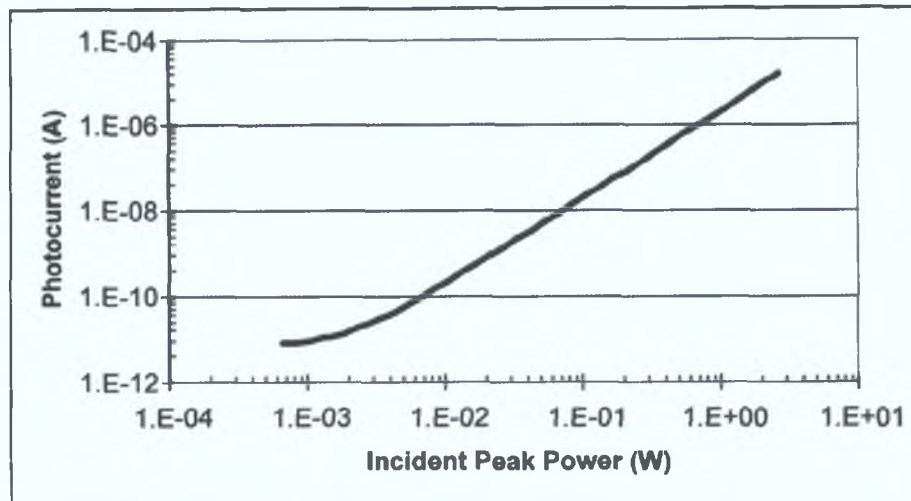
Figure 5.19: Plot of photocurrent as a function of incident optical peak power at the cavity wavelength resonance

intensity, which is evidence of the TPA process, with residual SPA occurring at low energies. However, there is over 3 orders of magnitude of nonlinear response with the current device. The maximum peak power applied to the device was in the order of 2.6W (average power $\approx 40mW$) which generated approximately $16.4\mu A$ of photocurrent. It is expected that by increasing the incident peak power, the dynamic range could be improved to nearly 40dB, before total absorption becomes the dominate process. However, in order to protect the device from any damage incurred from operating with a high optical intensity, the maximum pulse peak power applied was limited to 2.6W.

5.9 Device Bandwidth

In order to carry out a complete analysis of the bandwidth of the microcavity, it is possible to consider the *optical* and *electrical* bandwidths of the device separately. The optical bandwidth is a function of the optical-to-electrical TPA process, which is practically instantaneous, and the cavity (photon) lifetime of the device. The electrical bandwidth on the other hand is dependent on the time taken for the TPA generated photocarriers (carrier [electron] lifetime) to exit the device, and cause a current to flow in an external circuit. The electrical bandwidth is determined by the packaging, device structure and size as for any standard detector.

5.9.1 Optical Bandwidth

As mentioned, the optical bandwidth of the device is a determined primarily by the cavity (photon) lifetime of the cavity, which was calculated to be approximately 0.56ps (see Equation 5.34). As the TPA effect occurs on timescales of a few femtoseconds, the

cavity lifetime essentially determines the optical bandwidth of the device. The cavity lifetime can be defined as the amount of time which a photon resides within the cavity prior to absorption. During this time period, interference will build up within the cavity, sufficiently magnifying the intensity and enhancing the TPA response [48].

The microcavity has been designed to have a cavity lifetime $<$1ps making it suitable for operation in high-speed system operating at aggregate data rates beyond 100Gbit/s. To verify the cavity lifetime, an autocorrelation was carried out using optical pulses with durations less than 1ps. The resulting autocorrelation trace, which takes into account the shape of the optical pulses through the ACF, is therefore the convolution of the cavity lifetime and the actual duration of the optical pulses used. Thus the measured signal can be described as:

$$\tau_{measured} = \sqrt{\tau_{cavity}^2 + \tau_{actual}^2} \tag{5.35}$$

Therefore by rearranging Equation 5.35, the cavity lifetime can be determined by:

$$\tau_{cavity} = \sqrt{\tau_{measured}^2 - \tau_{actual}^2} \tag{5.36}$$

The experimental setup that was used is shown in Figure 5.20. It consists of a 10MHz
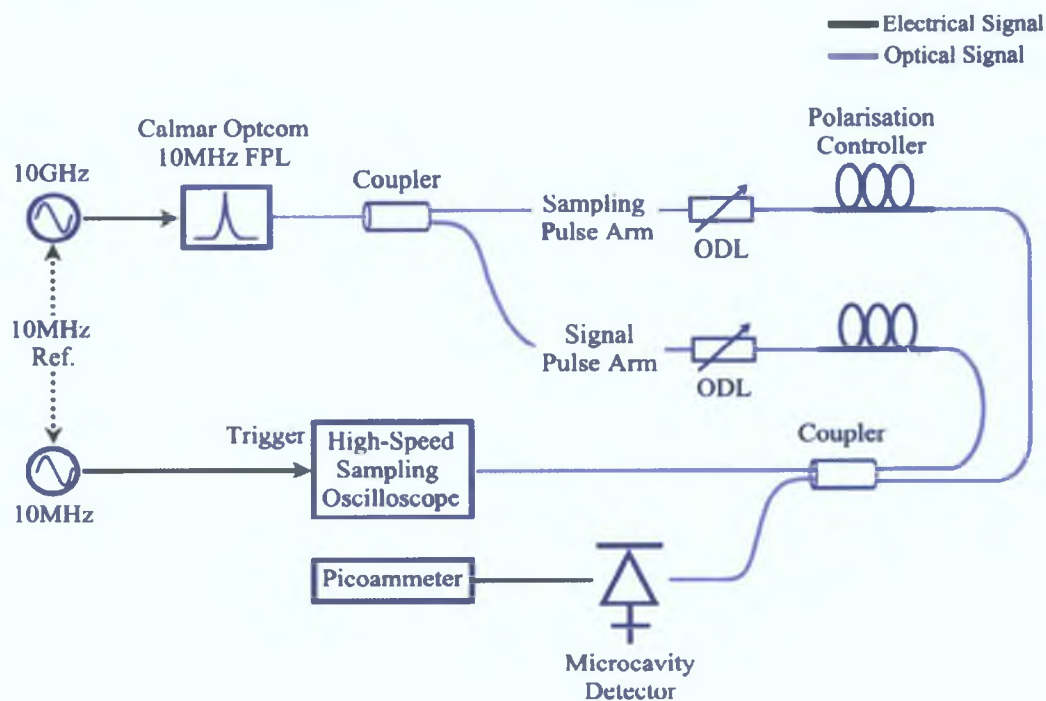
Figure 5.20: Schematic of the experimental setup used to measure the cavity lifetime of the microcavity

tunable pulse source, generating pulses with durations from 500fs to 2ps, over a wavelength tuning range from 1548-1558nm [61]. In order for the 10MHz pulse source to operate correctly, it must be locked to a 10GHz signal generator via a PLL. The 10MHz

optical pulse train was operated initially to generate pulses with durations of 500fs and an average power 0.5mW. The signal is then split in two by a 3dB optical coupler, with both copies passing through an variable ODL and polarisation controller before being recombined in a second 3dB coupler.

The variable ODL in the signal pulse arm is used to introduce the sampling delay between the signal pulse and the sampling pulse. The ODL in the sampling arm is used to align the pulses so that the sampling pulse is positioned just before the signal pulse prior to the scanning of the sampling pulse. This is required since the period of the pulse source is greater than the amount of time introduced using a single variable ODL. The photocurrent generated by the microcavity will then be measured using the picoammeter as a function of the sampling delay, resulting in an autocorrelation trace.

Figure 5.21 (a) shows the resulting TPA microcavity autocorrelation trace obtained for the 500fs pulses. The width of the optical pulse was verified using a SHG-based autocorrelator, with the pulse shown in Figure 5.21 (b). As expected the pulse width has been broadened to approximately 1.1ps. By using the pulse width determined from
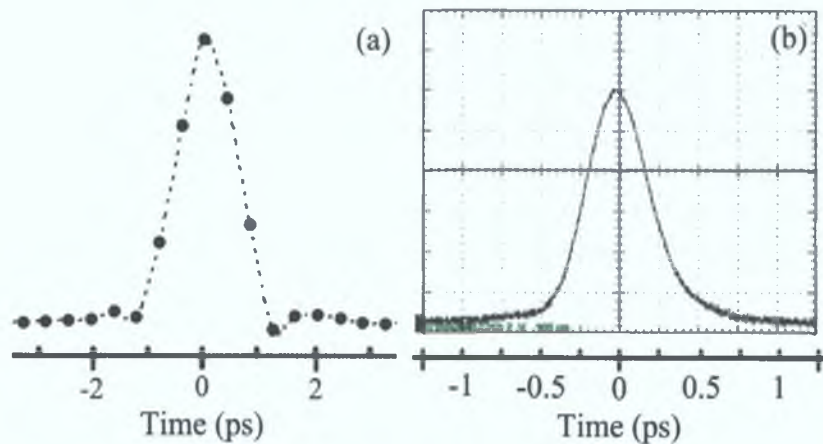
Figure 5.21: (a) TPA sampling of an 500fs optical pulse; (b) SHG autocorrelation trace of the same 500fs optical pulse

the TPA autocorrelation signal, the value of the duration as measured using the autocorrelation trace and Equation 5.35, the cavity lifetime is:

$$\tau_{cavity} = \sqrt{1.1ps^2 - 500fs^2}$$
$$= 0.979ps \qquad (5.37)$$
$$\approx 1ps$$

The experimentally determined value for the cavity lifetime of 1ps determined using Equation 5.37 is very close to the theoretically value of 1.04psps calculated in Section 5.7.4. This verifies that the microcavity tested has the same characteristics as that de-

scribed earlier in this chapter. Any deviation between the two can be accounted for slight variation in the thickness of the mirror layers, and localised variations in the refractive indices of the materials used.

5.9.2 Electrical Bandwidth

Figure 5.22 shows the experimental setup used to determine the electrical bandwidth of the microcavity. It consist of a tunable optical pulse source, modulator, pattern
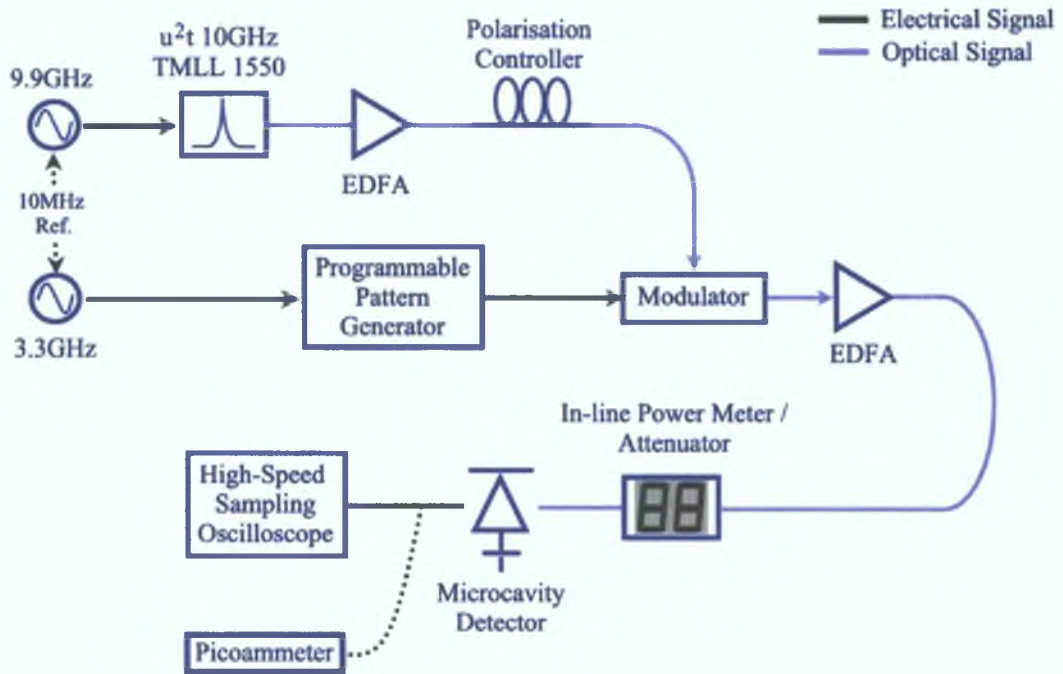
Figure 5.22: Schematic of the experimental setup used for the measurement of the electrical bandwidth of current microcavity device

generator and optical amplifiers. The 10GHz optical pulse generator (u^2t *photonics* TMLL1550) was actively mode-locked at 9.9GHz using an external signal generator. The 9.9GHz output optical pulse train from the source was first amplified using an EDFA before passing through a polarisation controller and entering a modulator. The electrical data signal to the modulator was provided by a Programmable Pattern Generator (PPG) driven by a 3.3GHz clock signal, which is the maximum repetition rate of the device. The 3.3GHz clock signal was phase locked to the 9.9GHz signal generator driving the optical pulse source. By varying the pattern of the PPG, the 9.9GHz pulse train can be reduced by using a programmable bit pattern comprising of a single 1 followed by a number of 0's, isolating three optical pulses from the 9.9GHz pulse stream. The principle of this is shown in Figure 5.23 where a 10GHz optical pulse train is combined with a 3.3GHz electrical bit pattern of alternating 1's and 0's.

159
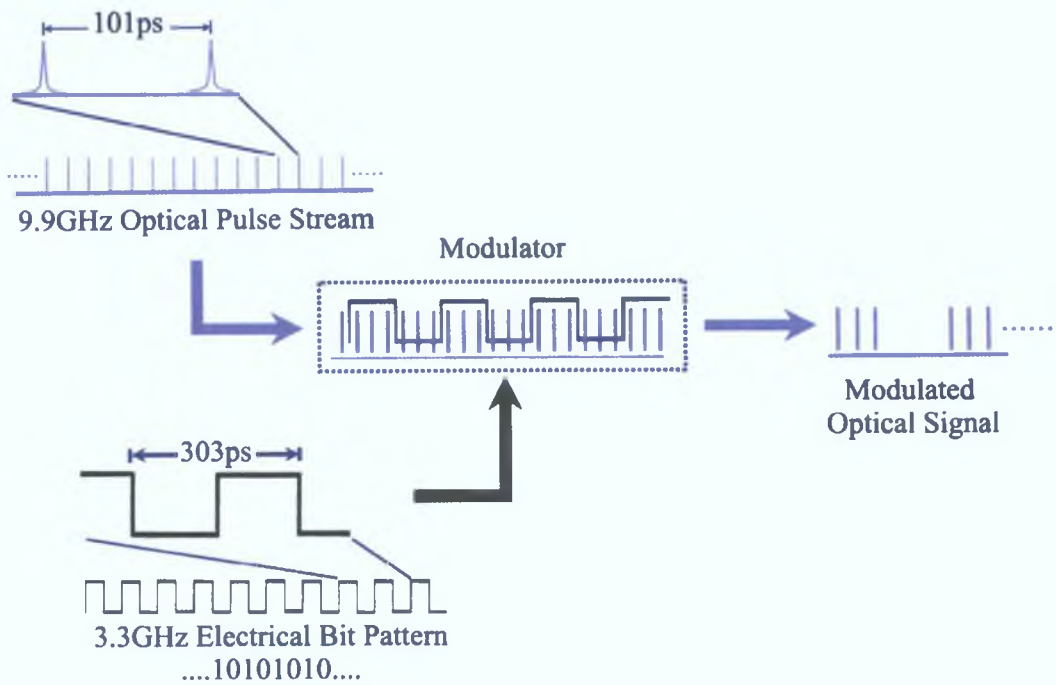
Figure 5.23: Schematic of the principle of operation of using a modulator and programmable pattern generator to reduce the repetition rate of an optical pulse train

Returning to Figure 5.22. Once the signal's repetition rate has been reduced by the appropriate amount, the lower repetition rate signal is amplified using a second EDFA and the amount of average optical output power monitored (and attenuated if required) using the in-line power meter/attenuator.

Figure 5.24 (a) shows a conceptual illustration of a 1-0-0-0-0-0-0-0-0-0 bit pattern
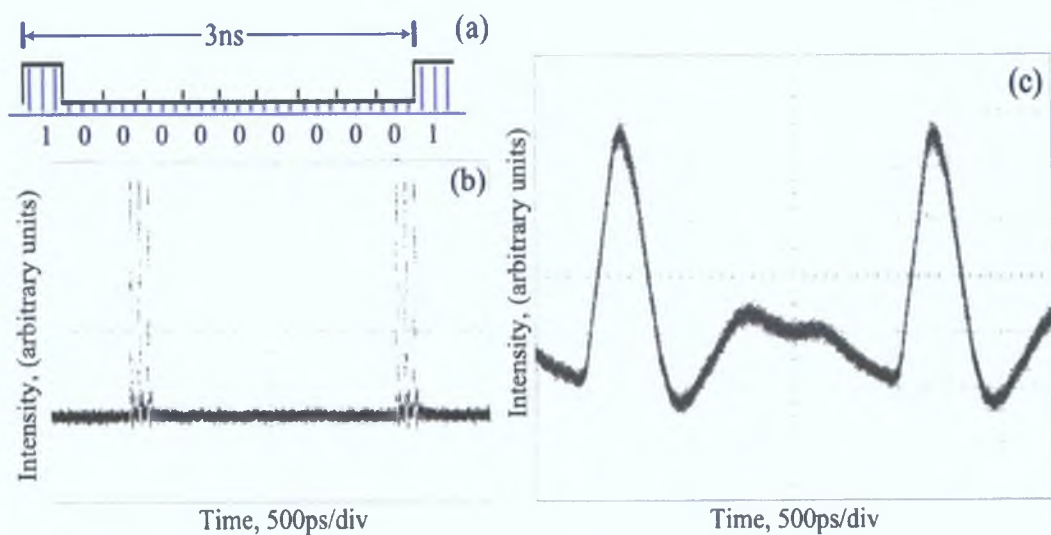
Figure 5.24: (a) Illustration of programmed bit pattern; (b) Oscilloscope trace after modulator; (c) Temporal response of microcavity for 1-0-0-0-0-0-0-0-0-0 bit pattern

160

with the actual bit pattern as displayed on the oscilloscope displayed in 5.24 (b). Finally 5.24 (c) shows the resulting temporal response as measured after the microcavity, which has a periods of 3ns corresponding to a repetition rate of 333MHz. Using:

$$Bandwidth_{3dB} = \frac{0.44}{T_{FWHM}} \qquad (5.38)$$

where T_{FWHM} is the measured pulse width (480ps), the bandwidth of the detector was just over 900MHz. In order to clarify the origins of the peaks between the two pulses in Figure 5.24 (c), the experiment was repeated at a lower repetition rate. The results of this are shown in Figure 5.25. The bit pattern used comprised of a 1 followed by 99 zeroes, effectively reducing the repetition rate by another order of magnitude, from 333MHz to 33MHz. Figure 5.25 (a) shows that the peaks are due to ringing being introduced into the measurement, probably due to some impedance mismatch between the input of the oscilloscope and the microcavity, and poor device packaging. A number of different chip resistors were inserted to try to improve performance and reduce the effects of the ringing, but they had no effect.
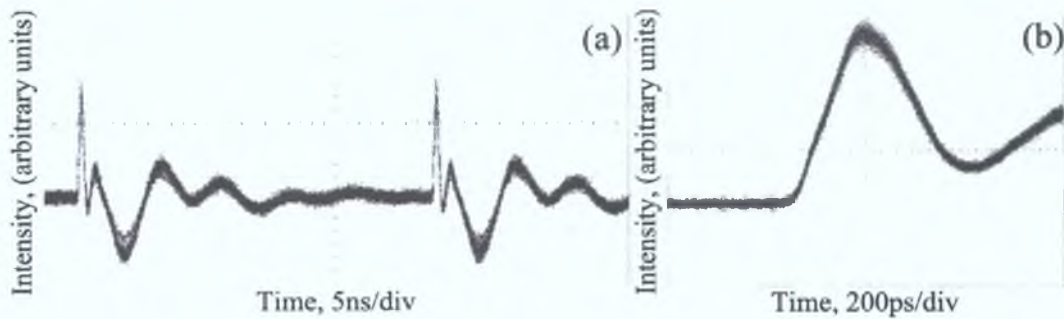
Figure 5.25: Temporal response of current microcavity device

Figure 5.26 again shows the current can design (left) and the aluminium mounting block that was used (right). As calculated, the electrical bandwidth of the current device was approximately 900MHz. As mentioned in Chapter 1, Section 1.3.3, the three factors that limit the speed of a detector are the diffusion of carriers, drift transit time in the depletion region, and capacitance of the depletion region [55]. The slowest of the three processes is the diffusion of carriers generated outside the depletion region. To minimise this, carriers should be generated close to the depletion region. The second process, transit time, is the time required for the carriers to drift across the depletion region and get swept out of the device. With a sufficient reverse bias, these carriers will drift at their saturation velocities, which is on the order of $3 \times 10^6 cm/s$ for GaAs [62]. Lastly, the capacitance of the device will determine its RC time constant, which R is the load resistance. Also as these devices were only intended for proof-of-concept experiments, they were not impedance matched or optimised for electrical response, and

161
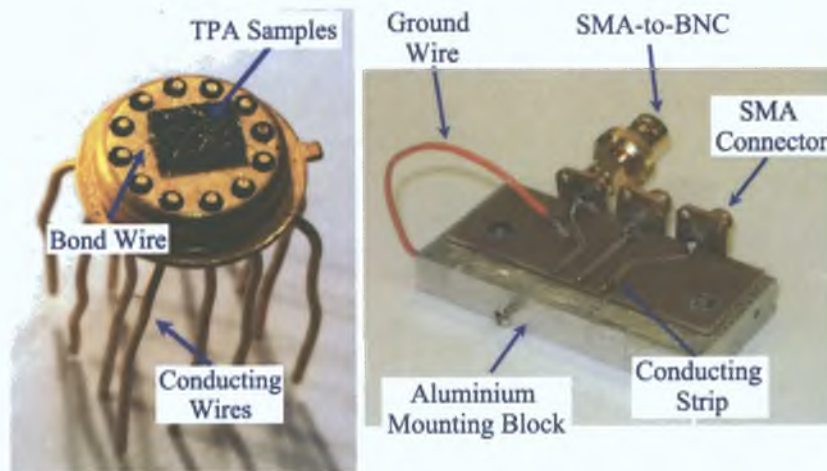
Figure 5.26: Photograph of microcavity device and optical mount used

we were reluctant to apply a reverse bias voltage to prevent any damage incurring. Significant improvements in the electrical bandwidth of the current device can be expected with the use of high-speed packaging [23], and the application of a reverse bias voltage.

5.10 Trade-Off Between Cavity Lifetime and Efficiency

In order to employ a microcavity for high-speed applications, the cavity lifetime of the device must be less than the optical pulses used to represent the data and carry out signal processing tasks such as switching and sampling. As shown in Section 5.7.4, in order to calculate the cavity lifetime the round trip time of a photon within the cavity and the loss of the cavity are required. The round trip calculations (Equations 5.29 to 5.33) involve a number of different parameters including the refractive index difference between the two materials comprising the front and back DBR, the length and penetration depth of the cavity and the reflectivity of the top and bottom mirrors. The cavity loss calculation (Equation 5.28) involves the effective length, cavity reflectivity and cavity absorption.

The current device, with a cavity lifetime of 1ps, is suitable for OTDM applications operating at aggregate data rates around 330Gbit/s. In order to operate at aggregate data rates approaching 1Tbit/s, the cavity lifetime needs to be in the order of 300fs. One way to alter the cavity lifetime is to change the number of layers of the top DBR of the microcavity. For a cavity lifetime in the order of 1ps, the top mirror consists of 18 layers of AlAs/GaAs. However, to reduce the cavity lifetime to around 300fs, the number of layers needs to be reduced to 6.5, which has the effect of reducing the overall reflectivity from 97.3% to 92.1%.

An alternative, albeit more difficult technique, is to change the refractive index difference between the two materials of the front and back DBR's. To reduce the cavity lifetime, the refractive index difference needs to be reduced. The current device has a

refractive index difference of 0 49 (n_L=2 86, n_H=3 35) For a cavity lifetime of 300fs, the refractive index difference would have to be reduced to 0 3 However, by altering the refractive indices of the mirror materials, the finesse, free-spectral range, cavity resonance width and reflectivity will also be altered The reflectivity of the device would be reduced from 97 3% (5 23) to 90 5%, with the resonant spectral width reducing to 3 4nm from 5 7nm

Regardless of which method is employed, both clearly demonstrate the trade-off between cavity lifetime and efficiency associated with utilising a microcavity structure

Summary

This chapter started with an introduction to TPA, a nonlinear optical-to-electrical conversion process found in semiconductors A number of applications for TPA in a high-speed OTDM network were then discussed, followed by some initial experimental work using a 1 3μm laser diode as a TPA detector Next the use of a specially-designed semiconductor microcavity in order to overcome the inherent inefficiency associated with TPA was examined in detail By using a microcavity, not only was the TPA response significantly enhanced allowing operation at optical power levels currently found in an optical communications network, but this enhancement occurred only a specific wavelengths This would allow the device find many applications in WDM and hybrid WDM/OTDM networks The chapter finished with characterisation results which were carried out on the fabricated devices, indicating its suitability for operation at aggregate data rates in excess of 100Gbit/s

The following chapter will present the results of a demultiplexing simulation and optical sampling experiments using the current microcavity design

Bibliography

[1] H Folliot, M Lynch, A L Bradley, T Krug, L A Dunbar, J Hegarty, J F Donegan, and L P Barry, "Two-photon-induced photoconductivity enhancement in semiconductor microcavities A theoretical investigation," *Journal of the Optical Society of America B Optical Physics*, vol 19, no 10, pp 2396–2402, 2002

[2] N Bloembergen, "Nonlinear Optics Past, Present, and Future," *IEEE Journal of Selected Topics in Quantum Electronics*, vol 6, no 6, pp 876–880, 2000

[3] M Goppert-Mayer, "Ueber die Wahrscheinlichkeit des Zusammenwirkens zweier Lichtquanten in einem Elementakrt," *Naturwissenshcaften*, vol 17, p 932, 1929

[4] M Goppert-Mayer, "Ueber Elementarakte mit zwei Quantenspruengen," *Annalen der Physik*, vol 9, no 2, pp 273–294, 1931

[5] G Breit and E Teller, "Metastability of hydrogen and helium levels," *Astrophysical Journal*, vol 91, no 2, pp 215–238, 1940

[6] W Kaiser and C G B Garrett, "Two-photon excitation in CaF_2 Eu^{2+}," *Physical Review Letters*, vol 7, no 6, pp 229–231, 1961

[7] R W Boyd, *Nonlinear Optics* Academic Press, 1st ed , 1992 ISBN 0-12-121680-2

[8] H P Weber, "Two-photon absorption laws for coherent and incoherent radiation," *IEEE Journal of Quantum Electronics*, vol 7, no 5, pp 189–195, 1971

[9] F R Laughton, J H March, D A Barrow, and E L Portnoi, "Demonstration of the use of a two-photon absorption waveguide detector as an autocorrelator," in *IEE Colloquium on Measurements on Optical Devices*, pp 10/1–10–4, 1992

[10] J Donegan, "Two-photon absorption speeds optical switching," *Lightwave europe*, p 31, 2002 July 2002

[11] J Reintjes and R C Eckardt, "Two-Photon Absorption in ADP and KD*P at 266 1nm," *IEEE Journal of Quantum Electronics*, vol 13, no 9, pp 791–795, 1977

[12] P J Maguire, L P Barry, T Krug, M Lynch, A L Bradley, J F Donegan, and H Folliot, "Simulation of a high-speed demultiplexer based on two-photon absorption in semiconductor devices," *Optics Communications*, vol 249, no 4-6, pp 415–420, 2005

164

[13] P.G.Chua, M.Takeda, and T.Kurokawa, "Infra-red image detection with a Si-CCD image sensor due to the two-photon absorption process," in *Pacific Rim Conference on Lasers and Electro-Optics (CLEO2001)*, vol. 1, pp. I–482–3, 2001.

[14] R.A.Negres, J.M.Hales, A.Kobyakov, D.J.Hagan, and E. Stryland, "Experiment and Analysis of Two-Photon Absorption Spectroscopy Using a White-Light Continuum Probe," *IEEE Journal of Quantum Electronics*, vol. 38, no. 9, pp. 1205–1216.

[15] K.Kikuchi, "Highly sensitive interferometric autocorrelator using Si avalanche photodiode as two-photon absorber," *Electronics Letters*, vol. 34, no. 1, pp. 123–125, 1998.

[16] F.R.Laughton, J.H.Marsh, D.A.Barrow, and E.L.Portnoi, "The Two Photon Absorption Semiconductor Waveguide Autocorrelator," *IEEE Journal of Quantum Electronics*, vol. 30, no. 3, pp. 838–845, 1994.

[17] H.K.Tsang, L. Chan, J. Soole, H. LeBlanc, M. Koza, and R.Bhat, "High sensitivty autocorrelation using two-photon absorption in InGaAsP waveguides," *Electronics Letters*, vol. 31, no. 20, pp. 1773–1775, 1995.

[18] T.K.Liang, H.K.Tsang, I.E.Day, J.Drake, A.P.Knights, and M.Asghari, "Silicon waveguide two-photon absorption detector at 1.5μm wavelength for autocorrelation measurements," *Applied Physics Letters*, vol. 81, no. 7, pp. 1323–1325, 2002.

[19] J.K.Ranka, A.L.Gaeta, A.Baltuska, M.S.Pshenichnikov, and D.A.Wiersma, "Autocorrelation measurement of 6-fs pulses based on the two-photon-induced photocurrent in a GaAsP photodiode," *Optics Letters*, vol. 22, no. 17, pp. 1344–1346, 1997.

[20] D.T.Reid, B.C.Thomsen, J.M.Dudley, and J.D.Harvey, "Sonogram characterisation of picosecond pulses at 1.5μm using waveguide two photon absorption," *Electronics Letters*, vol. 36, no. 13, pp. 1141–1142, 2000.

[21] C.Xu, J.M.Roth, W.H.Knox, and K.Bergman, "Ultra-sensitive autocorrelation of 1.5μm light with single photon counting silicon avalanche photodiode," *Electronics Letters*, vol. 38, no. 2, pp. 86–88, 2002.

[22] V.Mizrahi, K.W.DeLong, G.I.Stegeman, M.A.Saifi, and M.J.Andrejco, "Two-photon absorption as a limitation to all-optical switching," *Optics Letters*, vol. 14, no. 20, pp. 1140–1142, 1989.

[23] T.Krug, M.Lynch, A.L.Bradley, J.F.Donegan, L.P.Barry, H.Folliot, J.S.Roberts, and G.Hill, "High-Sensitivity Two-Photon Absorption Microcavity Autocorrelator," *IEEE Photonics Technology Letters*, vol. 16, no. 6, pp. 1543–1544, 2004.

[24] K.Kikuchi, F.Futami, and K.Katoh, "Highly sensitive and compact cross-correlator for measurement of picosecond pulse transmission characteristics at 1550nm using two-photon absorption in si avalanche photodiode," *Electronics Letters*, vol. 34, no. 22, pp. 2161–2162, 1998.

[25] I G Cormack, W Sibbett, and D T Reid, "Rapid measurement of ultrashort-pulse amplitude and phase from a two-photon absorption sonogram trace," *Journal of the Optical Society of America B Optical Physics*, vol 18, no 9, pp 1377–1382, 2001

[26] J L A Chilla and O E Martinez, "Direct determination of the amplitude and the phase of femtosecond light pulses," *Optics Letters*, vol 16, no 1, pp 39–41, 1991

[27] L P Barry, B C Thomsen, J M Dudley, and J D Harvey, "Autocorrelation and Ultrafast Optical Thresholding at 1 5μm using a Commercial ingaasp 1 3μm laser diode," *Electronics Letters*, vol 34, no 4, pp 358–360, 1998

[28] H P Sardesai and A M Weiner, "Nonlinear fibre-optic receiver for ultrashort pulse code division multiple access communications," *Electronics Letters*, vol 33, no 7, pp 610–611, 1997

[29] Z Zheng, S Shen, H Sardesai, C -C Chang, J H Marsh, M M Karkhanehchi, and A M Weiner, "Ultrafast two-photon absorption optical thresholding of spectrally coded pulses," *Optics Communications*, vol 167, pp 225–233, 1999

[30] Z Zheng, A M Weiner, J H Marsh, and M M Karkhanehchi, "Ultrafast optical thresholding based on two-photon absorption GaAs Waveguide Photodetectors," *IEEE Photonics Technology Letters*, vol 9, no 4, pp 493–495, 1997

[31] R Salem and T E Murphy, "Broad-Band Optical Clock Recovery System Using Two-Photon Absorption," *IEEE Photonics Technology Letters*, vol 16, no 9, pp 2141–2143, 2004

[32] R Salem, G E Tudury, T U Horton, G M Carter, and T E Murphy, "80Gb/s Optical Clock Recovery Using Two-Photon Absorption," in *Conference on Lasers and Electro-Optics (CLEO2005)*, 2005

[33] T L Liang, L R Nunes, H K Tsang, M Tsuchiya, D Van Thourhout, P Dumon, R Baets, and W Bogaerts, "All-Optical Wavelength Conversion in Silicon Wire Waveguide," in *European Conference on Optical Communications (ECOC2005)*, vol 4, pp 587–588, 2005

[34] B C Thomsen, L P Barry, J M Dudley, and J D Harvey, "Ultrahigh speed all-optical demultiplexing based on two-photon absorption in a laser diode," *Electronics Letters*, vol 34, no 19, pp 1871–1872, 1998

[35] L P Barry, B C Thomsen, J M Dudley, and J D Harvey, "All-optical demultiplexing based on two photon absorption in a laser diode," in *European Conference on Optical Communications (ECOC98)*, vol 1, pp 111–112, 1998

[36] T A Ibrahim, V Van, and P T Ho, "All-optical time-division demultiplexing and spatial pulse routing with a gaas/algaas microring resonator," *Optics Letters*, vol 27, no 10, pp 803–805, 2002

[37] A Villeneuve, C C Yang, G I Stegemen, C Lin, and H Lin, "Nonliner refractive index, two photon-absorption near half the band gap in algaas," *Applied Physics Letters*, vol 62, no 20, pp 2465–2467, 1993

166

[38] B.C.Thomsen, L.P.Barry, J.M.Dudley, and J.D.Harvey, "Ultra sensitive all-optical sampling at $1.5\mu m$ using waveguide two-photon absorption," *Electronics Letters*, vol. 35, no. 17, pp. 1483–1484, 1999.

[39] K.Kukuchi, "Optical sampling systme at $1.5\mu m$ using two photon absorption in Si avalanche photodiode," *Electronics Letters*, vol. 34, no. 13, pp. 1354–1355, 1998.

[40] Keithley, "Model 6485 picoammeter with 10fa resolution." http://www.keithley.com.

[41] V.Van, T.A.Ibrahim, K.Ritter, P.P.Absil, F.G.Johnson, R.Grover, J.Goldhar, and P.T.Ho, "All-Optical Nonlinear Switching in GaAs-AlGaAs Microring Resonators," *IEEE Photonics Technology Letters*, vol. 14, no. 1, pp. 74–76, 2002.

[42] K.Kishino, M. Unlu, J.-I. Chyi, J.Reed, L.Arsenault, and H.Morkov, "Resonant Cavity-Enhanced RCE Photodetectors," *IEEE Journal of Quantum Electronics*, vol. 27, no. 8, pp. 2025–2034, 1991.

[43] S.S.Murtaza, K. A. Anselm, I.-H. Tan, R. V. Chelakara, M. R. Islam, R. D. Dupuis, B. G. Streetman, J. E. Bowers, E. L. Hu, and J. C. Campbell, "Resonant-cavity avalanche photodiodes and narrow spectral response photodiodes," *IEEE/Cornell Conference on Advanced Concepts in High Speed Semiconductor Devices and Circuits*, pp. 333–342, 1995.

[44] M. Unlu and S. Strite, "Resonant cavity enhanced photonic devices," *Journal of Applied Physics*, vol. 78, no. 2, pp. 607–639, 1995.

[45] J. Goedbloed and J.Joosten, "Responsivity of Avalanche Photodiodes in the Presence of Multiple Reflections," *Electronics Letters*, vol. 12, no. 14, pp. 363–364, 1976.

[46] Y.Kim and D.P.Neikirk, "Micromachined Fabry-Perot Cavity Pressure Transducer," *IEEE Photonics Technology Letters*, vol. 7, no. 12, pp. 1471–1473, 1995.

[47] K.J.Vahala, "Optical microcavities," *Nature*, vol. 424, pp. 839–846, 2003.

[48] H.Folliot, M.Lynch, A.L.Bradley, L.A.Dunbar, J.Hegarty, J.F.Donegan, L.P.Barry, J.S.Roberts, and G.Hill, "Two-photon absorption photocurrent enhancement in bulk algaas semiconductor microcavities," *Applied Physics Letters*, vol. 80, no. 8, pp. 1328–1330, 2002.

[49] D.I.Babic and S.W.Corzone, "Analytic Expressions for the Reflection Delay, Penetration Depth, and Absorptance of Quarter-Wave Dielectric Mirrors," *IEEE Journal of Quantum Electronics*, vol. 28, no. 2, pp. 514–524, 1992.

[50] J.D.Rancourt, *Optical Thin Films*. SPIE Optical Engineering Press, 1st ed., 1996. ISBN 0-8194-2285-1.

[51] H. A. MacLeod, *Thin-Film Optical Filters*. Institute of Physics Publishing, 2nd ed., 2002. ISBN 0-7503-0688-2.

[52] S S Murtaza, K A Anselm, A Srinivasan, B G Streetman, J C Campbell, J C Bean, and L Peticolas, "High-Reflectivity Bragg Mirrors for Optoelectronic Applications," *IEEE Journal of Quantum Electronics*, vol 31, no 10, pp 1819–1825, 1995

[53] M S Skolnick, T A Fisher, and D M Whittaker, "Strong coupling phenomena in quantum microcavity structures," *Semiconductor Science and Technology*, vol 13, no 7, pp 645–669, 1998

[54] E Stryland, M A Woodall, H Vanherzeele, and M J Soileau, "Energy band-gap dependence of two-photon absorption," *Optics Letters*, vol 10, no 10, pp 490–492, 1985

[55] A Bar-Lev, *Semiconductors and Electronic Devices* Prentice/Hall International, 1st ed, 1984 ISBN 0-13-806265-X

[56] F Tassone, C Piermarocchi, V Savona, A Quattropani, and P Schwendimann, "Photoluminescence decay times in strong-coupling semiconductor microcavities," *Physical Review B*, vol 53, no 12, p R7642()R7645, 1996

[57] U Prank, M Mikulla, and W Kowalsky, "Metal-semiconductor-metal photodetector with integrated Fabry-Perot resonator for wavelenght demultipelxing high bandwidth receivers," *Applied Physics Letters*, vol 62, no 2, pp 129–130, 1993

[58] J T Verdeyen, *Laser Electronics* Prentice-Hall, 1st ed, 1981 ISBN 0-13-523738-6

[59] u2t Photonics, "1550nm Tunable Picosecond Laser Source (TMLL1550)" PDF Document, 2005 http //www u2t de/pdf/Datasheet_TMLL1550_V42 pdf

[60] Anritsu, "Optical Spectrum Analysers" http //www eu anritsu com

[61] Calmar Optcom, "Femtosecond Pulsed Fiber Laser (FPL Series)," 2005 http //www calmaropt com/pdf/FPL_Glossy pdf

[62] K Dessau and E Ginzton, "Insight into High-Speed Detectors and High Frequency Techniques," pdf document, New Focus, new focus website, 2001

CHAPTER 6

Optical Demultiplexing and Sampling via TPA in a Semiconductor Microcavity

Introduction

The previous chapter introduced the optical-to-electrical conversion process of Two-Photon Absorption (TPA) in a specially designed semiconductor microcavity By using the microcavity, a TPA-based device can be used for high-speed applications in WDM, OTDM and hybrid WDM/OTDM networks This chapter will examine the use of the TPA-based microcavity for optical demultiplexing and sampling in a high-speed OTDM network

6.1 Optical and Electrical Bandwidth

As mentioned in Section 5 9 in Chapter 5, in order to carry out a complete analysis of the bandwidth of the microcavity, it is possible to consider the optical and electrical bandwidth of the device separately A separate analysis is important as their affects on overall system performance will vary depending on the intended signal processing application for the device This section will examine the limitations imposed by the optical and electrical bandwidth on a TPA-based optical demultiplexing and optical sampling system

Theoretical and experimental values for the optical and electrical bandwidth of the current microcavity were determined in Chapter 5 A summary of the main points are

- *Optical Bandwidth* - The calculated optical bandwidth was determined by considering the cavity lifetime and the spectral width of the response, with an overall optical bandwidth value of approximately 700GHz for the current device As the optical bandwidth determines the maximum overall aggregate data rate at which the system can operate at, an optical bandwidth of 700GHz would allow a maximum data rate of 700Gbit/s for a system employing RZ [1]

- *Electrical Bandwidth* - The electrical bandwidth of the device was calculated ex-

perimentally by determining the impulse response of the device for an incident optical pulse with a duration of 1.8ps. The calculated electrical bandwidth was 900MHz, resulting in the maximum bit rate of just under 1Gbit/s for the individual OTDM channels if the current TPA microcavity design and packaging is used for optical demultiplexing (see Figure 5.26 in Chapter 5).

Next the impact that the optical and electrical bandwidth have on a TPA-based optical demultiplexer and optical sampling scheme will be discussed.

6.1.1 Bandwidth Effects on TPA-based Optical Demultiplexing

In order to explain the effects of optical and electrical bandwidth on a TPA-based optical demultiplexer, a system timing diagram for a microcavity-based TPA demultiplexer is shown in Figure 6.1.
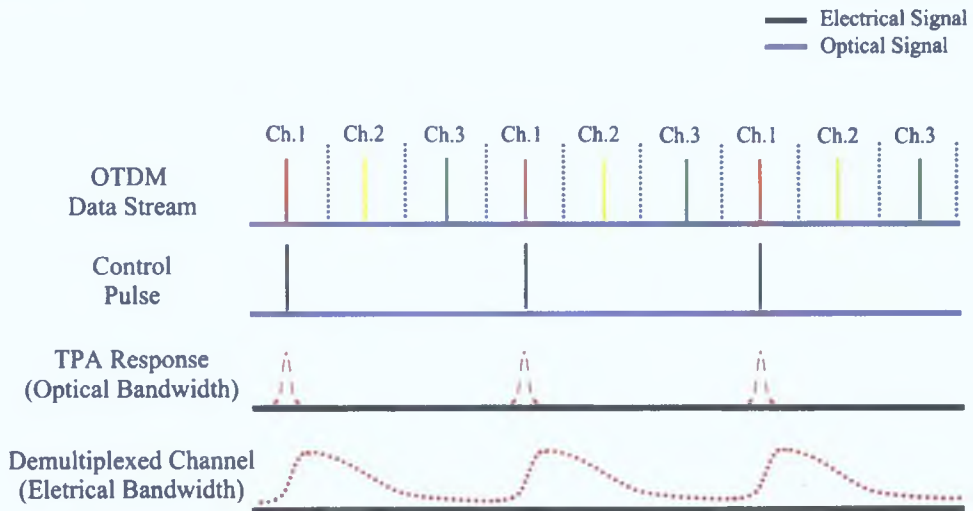
Figure 6.1: Optical demultiplexer system timings using a TPA-based microcavity as a nonlinear detector

The OTDM data signal consists of three individual channels; channel 1 (red), channel 2 (yellow) and channel 3 (green). As already explained in Chapter 5, a TPA-based optical demultiplexer uses high-power optical control pulses to optical demultiplex a single channel from a high-speed OTDM data signal. The control pulses are at a repetition rate of the individual channels in the aggregate signal, and have the same duration as the optical pulses used to represent the data being transmitted. The control pulses (black) are optically coupled together and the resulting signal is incident on the TPA device. The generated TPA response, shown as the red dashed line, is slightly broadened by the cavity lifetime of the device. Therefore the *optical bandwidth* of the TPA device determines the minimum temporal separation between channels.

170

The red dotted line represents the electrical bandwidth of the device, that is, the time associated with extracting the photocarriers generated by the TPA process from the cavity, resulting in the generation of a photocurrent in an external circuit. As shown in Figure 6.1 the electrical bandwidth determines the time taken for the microcavity's response to fully recover prior to the arrival of the next bit from the channel that is being demultiplexed.

Thus for an optical demultiplexer based on TPA in a semiconductor microcavity, the electrical bandwidth will affect the maximum speed at which the individual data channels can operate at, whereas the optical bandwidth will determine the overall data rate of the aggregate OTDM signal.

6.1.2   Bandwidth Affects on TPA-based Optical Sampling

As mentioned in Chapter 4, in order to accurately record a 10Gbit/s NRZ signal using a sampling rate of approximately 30GSample/s is required, which is a very challenging task. Therefore in order to operate at individual channel data rates in excess of 100Gbit/s, this bandwidth limitation must be overcome.

Sequential sampling circumvents the bandwidth limitations of conventional measurements techniques utilising a photodetector and oscilloscope combination by using the concept of equivalent time. Equivalent time samplers reconstruct the repetitive waveform by taking a single sample during each recognised trigger after a time delay which is incremented after each cycle [2]. The waveform slowly builds after a number of cycles, and allows the oscilloscope to capture signals whose frequency components are much higher than the oscilloscope's sample rate.

For TPA-based optical sampling, a very narrow optical pulse is used to sample the signal under test, which results in the crosscorrelation of the sampling pulse and signal under test. This crosscorrelation represents the original signal except that the time scale has been stretched, as shown in Figure 6.2. The sampling instant also shown in Figure 6.2 represents the narrow sampling gate that is opened by the sampling pulse.

As the principle of optical sampling employs time-averaging, the electrical bandwidth of the TPA microcavity will not be a limiting factor to performance. The repetition rate of the sampling pulse is kept low so that the peak power is high and also to allow the sampled signal to be displayed on a low bandwidth, high-impedance electrical oscilloscope.

However, the optical bandwidth of the microcavity will affect the performance of the sampling system. The temporal resolution of an optical sampling system is determined by the duration and jitter of the sampling pulse used in the setup. As the nonlinear detector being used here is the TPA microcavity, it is necessary to include the cavity lifetime when calculating the temporal resolution of the sampling system. This results in the

171
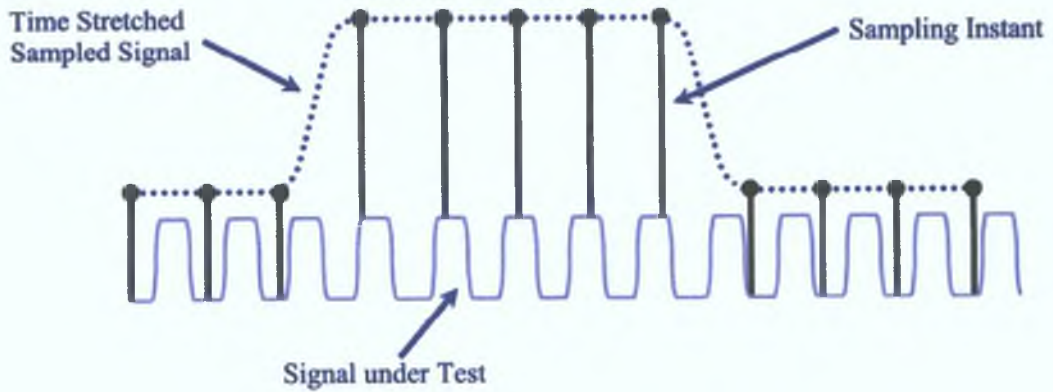
Figure 6.2: Principle of sequential sampling [2]

optical bandwidth (hence the cavity lifetime) of the microcavity limiting the maximum overall aggregate data rate that the system can operate at.

6.2 TPA Demultiplexing

Chapter 4 discussed how only optical switching methods based on optical nonlinearities in semiconductors, crystals and fibres will be fast enough to cope with the expected increase in future line rates. Those based on fibre generally require strict control of the wavelength of the signal and control pulses used, while gain depletion limits the maximum switching speed in SOA-based systems. This section will present a theoretical investigation into the use of TPA for high-speed demultiplexing in an OTDM communication system.
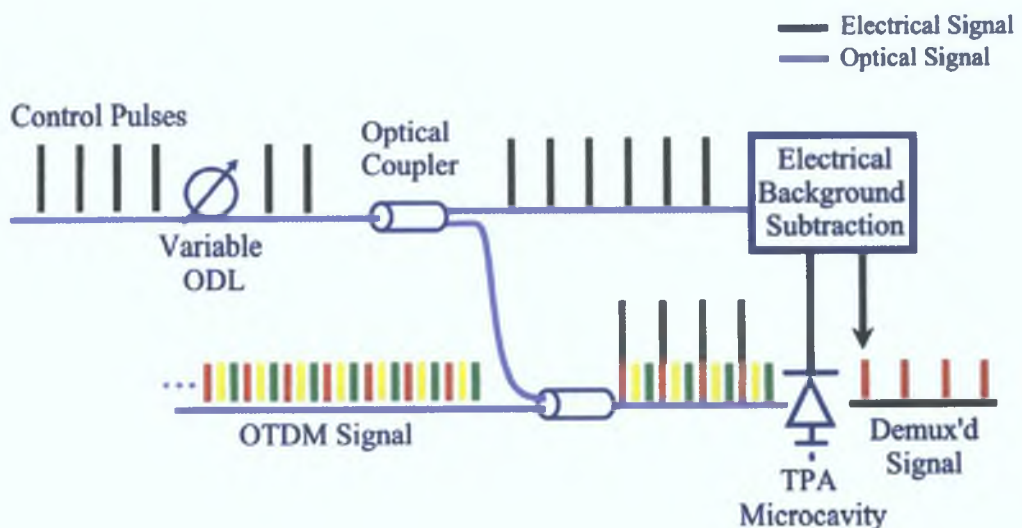
Figure 6.3: Schematic of the principle of TPA-based optical demultiplexing

Figure 6.3 shows a possible layout for optical demultiplexing via the TPA effect, and uses optical control pulses to switch out data from a single channel in a high-speed OTDM system. The control pulses, which are at the repetition rate of the individual channels in the multiplexed signal, are optically coupled together with the high-speed OTDM data signal and are incident on the device. The arrival time of the control pulses is varied using an optical delay line so that the control pulses arrive at the demultiplexer at a time corresponding to the data pulse to be switched out.

6.2.1 Demultiplexing Simulation

The purpose of the simulation is to determine how various system parameters affect the suitability of using a TPA device to switch a high-speed OTDM signal. The main device parameters used in the model, such as the TPA coefficient and cavity size, are taken from [3] and the characterisation of the microcavity carried out in the previous chapter. Using this model, the operation of the demultiplexer is examined when various system parameters were varied. The parameters were:

- *Number of channels in the OTDM network*

- *Ratio between the peak power of the control signal and data signal*

- *Electrical bandwidth of the TPA detector*

A flowchart of the programme is shown in Figure 6.4. The simulation programme starts by asking the user to enter parameters for the number of channels, data rate per channel and the peak power of the optical pulses used to represent the data. From this, a PRBS with a pattern length of $2^7 - 1$ is created for each channel in the system. These channels are then optical multiplexed together to create the OTDM data signal. The optical pulse width used was kept to one quarter of the bit period of the overall aggregate OTDM data rate in order to avoid any interference being introduced from adjacent data channels. Next a fixed level of noise is added to the signal which has the effect of limiting the optimum BER that can be achieved by the system. The OTDM data signal is then combined with optical control pulses. The control pulses, which are at the repetition rate of the individual channels in the OTDM signal, are synchronized with one of the OTDM channels to be demultiplexed. The duration of the control pulses are set to the same value as that of the signal pulses, with the peak power varied in steps of ten of the peak power of the signal pulse. The SNR and Optical Bit-Error Rate (OBER) are then calculated prior to the signal being incident on the detector.

When the combined signal (data pulse with noise and the control pulse with noise) is incident on the detector, a TPA photocurrent is generated. The TPA detector is modeled as described in [4]. For the model, the SPA coefficient (α) and a TPA coefficient (β)

173
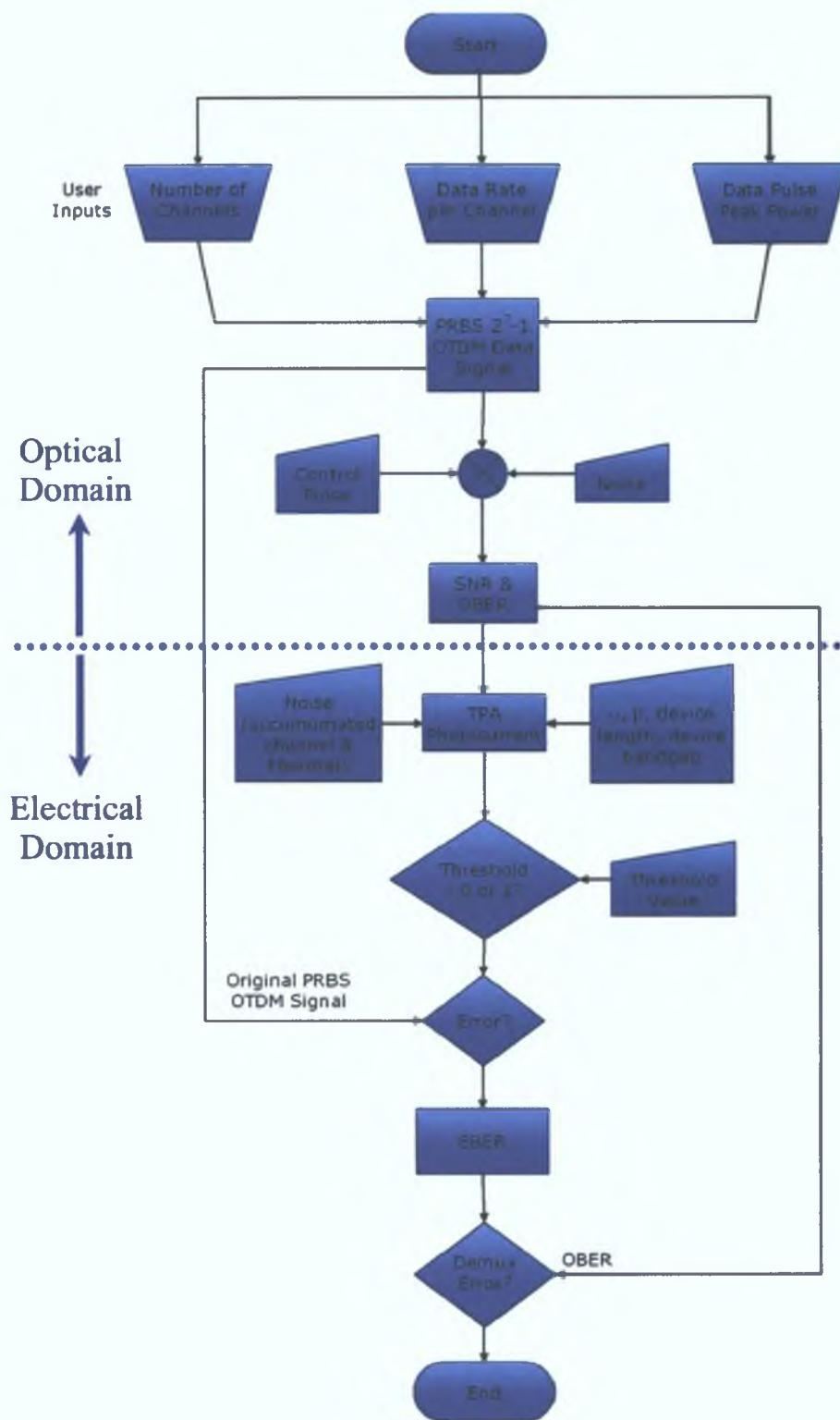
Figure 6.4: Flowchart of the simulation programme used to model TPA demultiplexing

are $0.01cm^{-1}$ and $3 \times 10^{-10} m/W$ respectively. These were taken from measurements carried out in [3]. Figure 6.5 shows a theoretical plot of the photocurrent generated
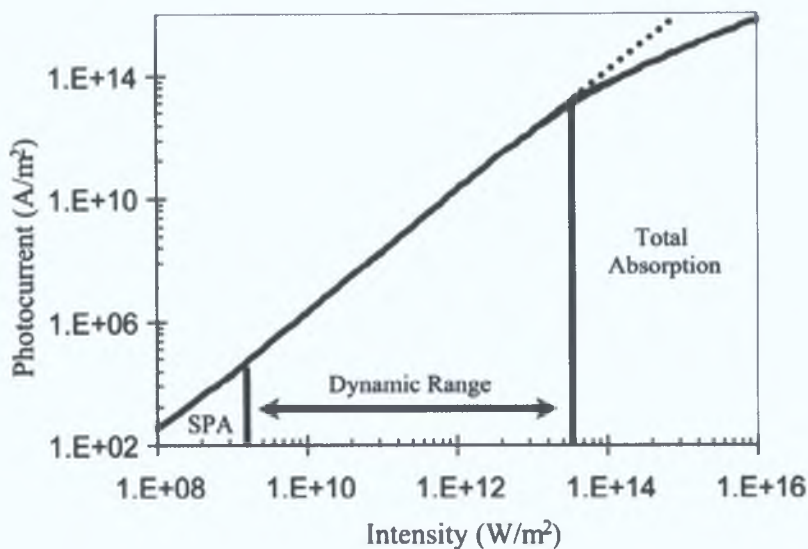
Figure 6.5: Plot of the simulated output photocurrent density as a function of the input optical power density for $\alpha = 0.01cm^-1$ and $\beta = 3 \times 10^{-10}$ m/W

versus the optical intensity using the parameters already mentioned and from the design specifications of the current devices, such as the thickness of the active region of the microcavity. This plot clearly shows that the nonlinear TPA response is limited on the lower side by SPA and on the higher side by total absorption. This gives the dynamic range ($\approx 40dB$) over which the TPA affect can be used for high-speed switching.

The TPA model also takes into account the electrical bandwidth of the TPA detector, which is varied in steps of 10 from 10GHz upwards during the simulation. The minimum electrical bandwidth required to temporally demultiplex one channel from the overall OTDM signal is 10GHz, assuming that the individual channel data rate is 10Gbit/s. However, even with this bandwidth, noise will be introduced on the demultiplexed channel from the electrical signals generated by the other OTDM channels that are not synchronized with the control pulse. To overcome this limitation it may be necessary to have a large control-to-signal pulse peak power ratio. This will increase the contrast ratio between the detected channel synchronized with the control, and unsynchronized channels, and thus increase the SNR of the demultiplexed channel. By increasing the bandwidth of the device, the noise contribution from the other OTDM channels is reduced.

The simulation model finally calculates the OBER of the signal before the detector and the Electrical Bit-Error Rate (EBER) after the TPA based demultiplexer. The overall goal is to determine the operating characteristics such that EBER of the demultiplexed/detected signal is the same as the OBER of the signal before the TPA detector,

indicating that the demultiplexing process is not introducing any additional errors to the system. The OBER takes into account any initial noise introduced by the transmitter in the system and is calculated from the SNR, taking into account the signal peak power and the level of noise added [5].

The EBER on the other hand takes into account noise introduced by the demultiplexing process. In order to calculate the EBER, the TPA photocurrent generated by the incident optical signal is first determined, taking into account the optical noise already present on the signal. The photocurrent takes into account the band gap of the device, which is optimized for TPA, the length of the detector (100μm as per the sample fabricated) and the SPA and TPA co-efficients [4]. Next the thermal noise introduced by the detector and the accumulated channel noise is added to the signal. The amount of thermal noise is user defined. The accumulated channel noise takes into account the other channels not synchronised with the control pulse and arises due to the demultiplexing process being dependent on the bandwidth of the detector. Once the noise has been added, the resultant electrical signal is compared to a threshold value, and assigned a bit value. This bit value is then compared to the original PRBS signal and the number of errors determined, resulting in the EBER. The values of the OBER and the EBER are then stored in output files.

6.2.2   Simulation Results

The initial parameter that was investigated was how a variation of the control-to-signal peak power ratio affects system performance as the number of channels that are multiplexed together increase. The number of channels were varied from 25 to 100, with an individual channel data rate of 10Gbit/s, offering aggregate OTDM data rate ranging from 250Gbit/s to 1Tbit/s. The signal peak power was kept constant at 80mW, and the detector bandwidth was set to 10GHz, the minimum required to prevent ISI between adjacent data bits in the demultiplexed channel. Figure 6.6 shows a plot of the received BER versus the control-to-signal ratio as the number of channels is varied. It can be clearly seen that as the control-to-signal ratio is increased, the EBER approaches the OBER. This results from the fact that as the control-to-signal peak power ratio is increased, the contrast ratio between the data signal synchronised with the control pulse and those not synchronised widens. Thus the noise level added to the demultiplexed signal, due the detection of all the adjacent channels, is reduced as the control-to-signal ratio increases. This improves the resultant SNR, and improves the BER of the received signal. For a given control-to-signal ratio, the BER is degraded as more channels are added to the system, due to the increased noise from these added channels on the received signal. It is worth noting that for the 25-channel system (250Gbit/s aggregate OTDM data rate), the EBER reached the OBER for a control to signal ratio beyond

Figure 6.6: Plot of BER against control-to-signal power as the number of channels (with base rate of 10Gbit/s per channel) is varied.

50:1, corresponding to a control pulse peak power of 4W. During the initial characterization of the microcavity samples that were fabricated, a maximum peak optical power of 20W was applied to the device without any damage being incurred. This suggests that a control pulse peak power of 4W is well within the operating range of the microcavity structure, even if it is slightly large for practical applications.

The second simulation investigated how the electrical bandwidth of the TPA detector affected demultiplexer operation. Once again the BER as function of the control-to-signal ratio was plotted, but this time the bandwidth of the device was also varied. These results are presented in Figure 6.7, and it should be noted that a 25-channel system was
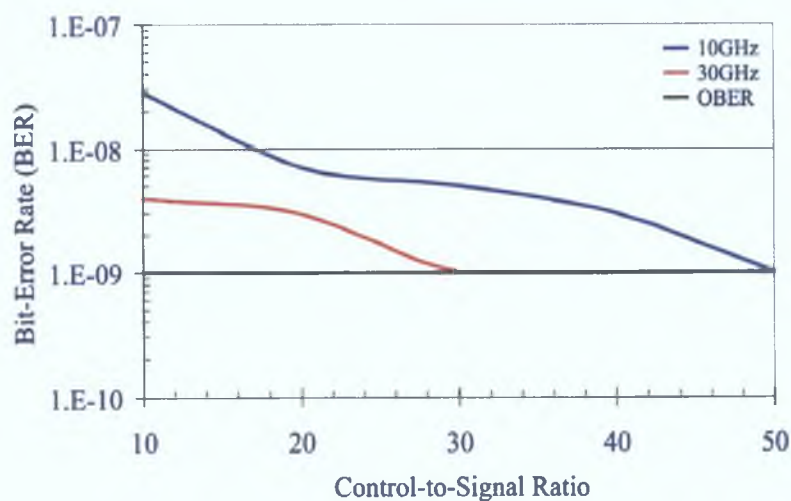
Figure 6.7: Plot of BER against control-to-signal power as electrical bandwidth is varied for a 250Gbit/s aggregate OTDM system.

177

employed (250Gbit/s aggregate OTDM data rate), as this was the only system that gave optimum performance at a reasonable control-to-signal ratio during the first simulation for varying channel number. As the bandwidth is increased, the BER of the received signal is improved. This is attributed to the fact that as the bandwidth is increased the number of adjacent channels that add noise to the detected channel decreases, improving the received BER. This allows a smaller control-to-signal ratio to be used to offer the same overall performance. For a 25-channel system, a bandwidth of 30GHz allows us to obtain good performance with a control-to-signal ratio of around 30:1.

To summarise the simulation results, it has been shown that with a device bandwidth of 30GHz, successfully TPA-based demultiplexing can be achieved with a control-to-signal ratio of 30:1 which corresponds to a control peak power of 2.4W and signal peak power of 80mW.

6.3 TPA Sampling

To successfully operate at data rates in excess of 100Gbit/s per channel, networks will require a sensitive and ultrafast technique for precise optical signal monitoring [6]. The standard way of characterising high-speed optical signals utilises a fast photodetector in conjunction with a high-speed sampling oscilloscope. However current electronic monitoring techniques are limited to bandwidths of approximately 80GHz [7] due to difficulties associated with the design of high-speed electronic components [8]. These are just capable of accurately measuring data rates of 40Gbit/s. Therefore, electrical sampling schemes are unable to accurately characterise high-speed data pulses used to represent data. Critical information such as pulse duration, pulse separation and pulse rise-time, which are crucial for the optimisation of the networks performance, are distorted.

As a result interest has focused on the development of an Optical Sampling Oscilloscope (OSO) for performance monitoring of high-speed signals. In these devices, the incident optical signal is not directly transformed into an electrical signal by a photodetector, but are first probed with a very short optical sampling pulse at a lower repetition rate. By means of a nonlinear optical process, the product of the data signal and the sampling pulse is formed. Repetitive scanning of the data signal at different points in time subsequently yields a highly-resolved temporal profile of the signal. This is known as sequential sampling (see Chapter 4, Section 4.4.3).

A number of commercial and research groups are investigating the use of SHG in optical crystals as the nonlinear process. This involves combining the high-power optical sampling pulse train to the data signal being analysed and generating the mixing product of both signals in the optical crystal. The energy of the mixing product pulse represents the amplitude of the data signal and can be detected by a slow photodetector.

Unfortunately there are a number of disadvantages of using the SHG process, including the need for high optical intensities, stability problems due to its reliance on free-space optics and the need to phase match the crystal for different operating wavelengths. As a result, it is necessary to consider utilising a different optical nonlinearity for developing an OSO, with a prime candidate being TPA in a semiconductor microcavity.

Figure 6.8 shows the operating principle of a TPA-based optical sampling system. Optical sampling pulses, with a duration $[I_{sam}(t - \tau)]$ significantly shorter than the optical signal pulse $[I_{sig}(t)]$, are combined with the optical signal under test, and incident on the microcavity. The electrical TPA signal generated $[i(t)]$ is measured as a function of the sampling delay τ, resulting in an intensity cross-correlation measurement between I_{sam} and I_{sig} [9]. This results in the measured signal representing the signal pulse waveform on a constant background [9]. By choosing a relative low scan frequency for the sampling pulses, the cross-correlation measurement can be easily displayed on a standard high-impedance oscilloscope.
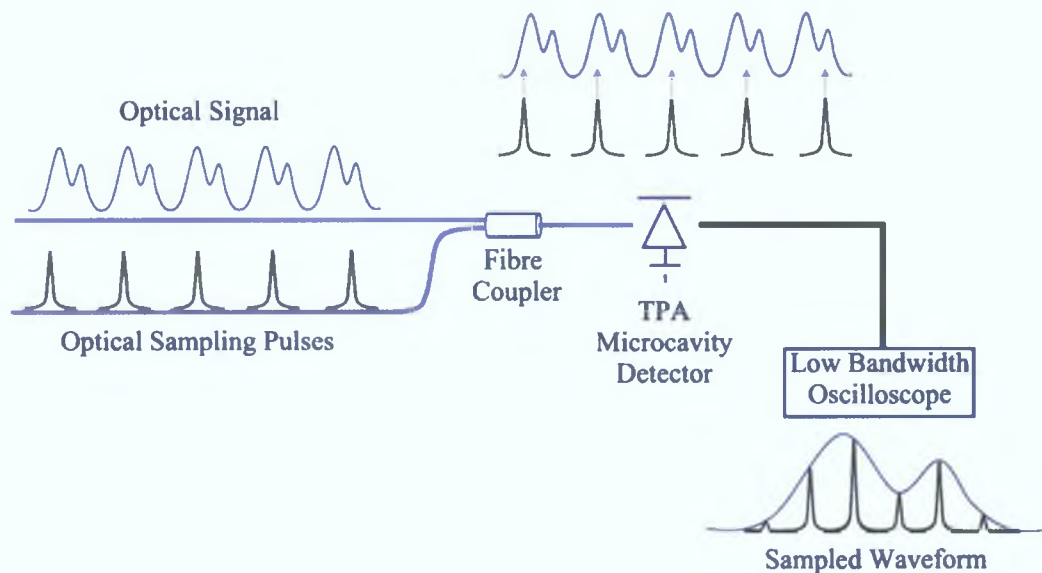
Figure 6.8: Schematic of the principle of TPA-based optical sampling

Two important measurements used to determine the performance of a sampling scheme are the temporal resolution and the sensitivity. Temporal resolution can be defined as a measure of the time increments between sampled points on the data signal. For TPA sampling employing a microcavity as a detector, it is necessary to include the cavity lifetime when calculating the temporal resolution of the system. This results in the temporal resolution being defined as:

$$t_{res} = \sqrt{\tau_{cavity}^2 + t_{sam}^2 + j_{sam}^2} \tag{6.1}$$

where t_{sam} and j_{sam} are the duration and jitter of the sampling pulse used, and τ_{cavity}

is the cavity lifetime, which was experimentally measured to be 1ps for the current microcavity design

The second performance measurement is the sensitivity of the optical sampling system. Sensitivity can be defined as minimum power necessary to achieve a given SNR, BER (typically 10^{-9} or another criteria [10] For electrooptic sampling systems, the sensitivity is given in terms of $V/\sqrt{Hz}$ [11] However for optical sampling systems, the sensitivity is defined a measurement of the minimum optical power required to successfully sample the signal pulse calculated at a particular SNR, given in units of $(mW)^2$ [12] It is calculated using [13]

$$Sensitivity = (P_{Signal\ Peak} \times P_{Sampling\ Average})_{min} \qquad (6\ 2)$$

where $P_{Signal\ Peak}$ is the peak power of the signal pulse and $P_{Sampling\ Average}$ is the average power of the sampling pulse Here all the calculations are carried out using a SNR=1 [3] The sensitivity depends on the TPA efficiency of the particular device and the sensitivity of the photocurrent detection electronics (picoammeter, lock-in amplifier, etc) [14]

6.4   TPA Sampling Experiments

The TPA sampling experiments that are described here all use the same microcavity sample that was characterised in the previous chapter, with the wavelength response and PI curve shown in Figure 6 9 Thus the cavity lifetime for all calculations will be 1ps The value of the sampling pulse width and jitter varies as different sampling pulse sources were employed Similarly as different measurements devices were used to determine the TPA photocurrent produced, the sensitivity of each system also differs
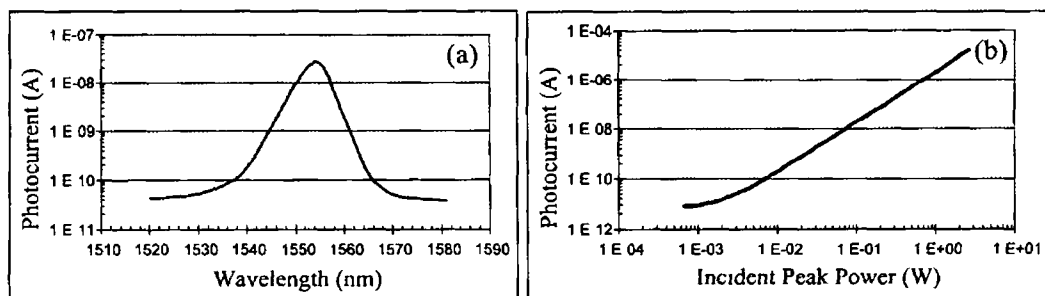
Figure 6 9   Plot of the (a) Wavelength response of microcavity, (b) Photocurrent as a function of optical peak power

180

6.4.1 Sampling Using Single Pulse Source

Figure 6.10 shows the experimental setup used during the initial optical sampling experiments using a single pulse source for both the single pulse and sampling pulse. The
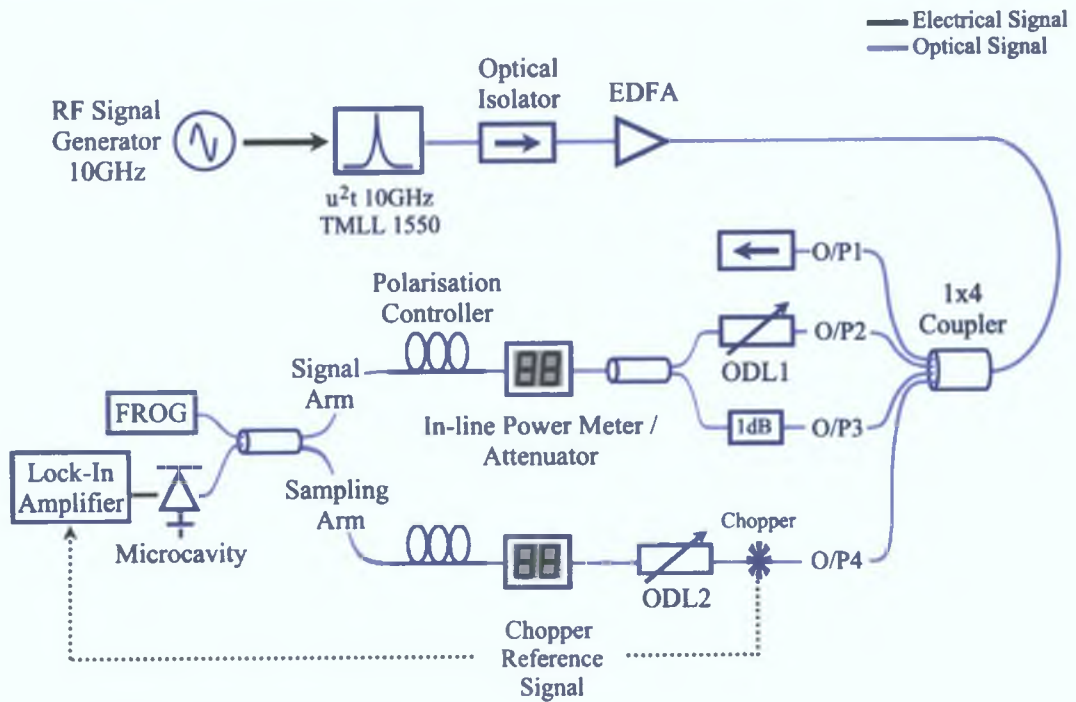
Figure 6.10: Schematic of the experimental setup for quasi-160GHz TPA sampling

pulse source employed was a u^2t TMLL1550 [15] tunable mode-locked laser, emitting 1.8ps optical pulses with a tunable repetition rate from 9.8-10.8GHz over a wavelength range from 1480-1580nm. An oscilloscope trace of the 10GHz optical pulse train (pulse separation 100ps) for the u^2t pulse source is shown in Figure 6.11 (a), while Figure 6.11 (b) shows the wavelength tuning range of the same pulse source.
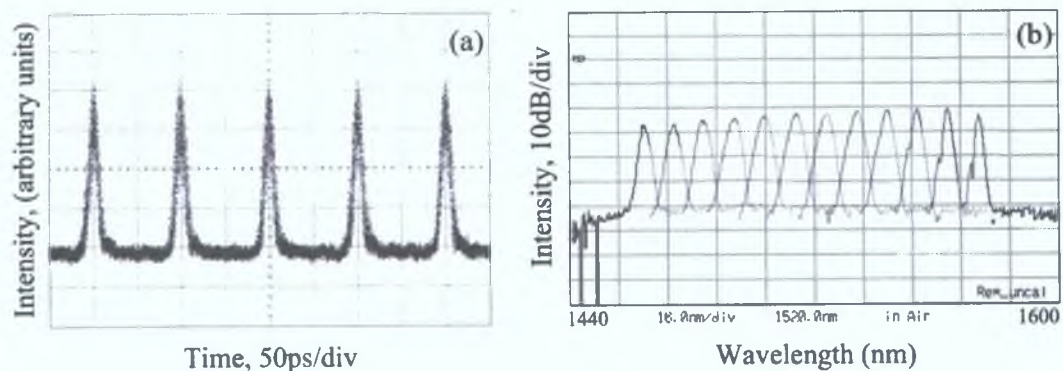
Figure 6.11: (a) 10GHz optical pulse train (pulse separation of 100ps) from u^2t tunable pulse source; (b) Composite of the wavelength tuning range of the u^2t tunable pulse source

181

The same pulse source was used to create both the signals and was tuned to a wavelength of 1556nm to coincide with the wavelength resonance of the microcavity, (see Figure 6 9 (a)) The 10GHz optical pulse train was first amplified using a low-noise EDFA before passing through a 1x4 passive optical fibre coupler Output 1 (O/P1) of the coupler was used as the signal pulse, while O/P2 and O/P3 were used for the creation of the quasi-160GHz signal O/P4 was used as the sampling pulse When not in use, O/P1 was connected to an optical isolator to prevent any backward reflections from occurring

In order to generate the quasi-160GHz, the 10GHz pulse train emerging from O/P2 was delayed by 7ps (corresponding to 160GHz) with respect to the pulse train from O/P3 by using an variable Optical Delay Line (ODL)1 To compensate for the insertion loss introduced by the ODL, O/P3 passed through a fixed in-line 1dB attenuator Both pulse trains (O/P2 and O/P3) were then recombined using a passive optical fibre coupler to form the quasi-160GHz signal An optical chopper was placed in the sampling arm (O/P4) to allow a lock-in amplifier to measure the TPA photocurrent after the microcavity The sampling pulse then passed through a second ODL (ODL2) in the sampling arm, which is used to introduce the sampling delay τ The signal and sampling pulse trains then passed through in-line power meters/attenuators and Polarisation Controller (PC) before being recombined at a coupler The power meters allow for easy measurement and attenuation of both signal and sampling pulses, allowing the sensitivity of the system to be continuously monitored The PC in each arm were optimised independently to generate the maximum amount of photocurrent after the detector Finally the sampling and signal pulse were combined using a fibre coupler before being incident on the microcavity The photocurrent generated by the device is fed into the lock-in amplifier to improve the SNR and recorded as a function of the sampling delay τ As shown in later experiments, it is also possible to directly measure the nonlinear photocurrent using a picoammeter, or show the cross-correlation trace directly on an oscilloscope The quality of the TPA sampling technique was independently verified by comparing the resulting output of the TPA sampling with the corresponding results from a Second Harmonic Generation - Frequency Resolved Optical Gating (SHG-FROG) [16] measurement of the same pulse

Figure 6 12 (a) shows the experimental result of TPA sampling (dotted line) versus the SHG-FROG measurement for a single pulse (continuous line) on the same plot From the TPA sampling, the optical pulse duration was calculated to be 2 7ps whereas from the SHG-FROG measurement the pulse width was 1 8ps The deviation between the two can be accounted for by the temporal resolution of the sampling setup The
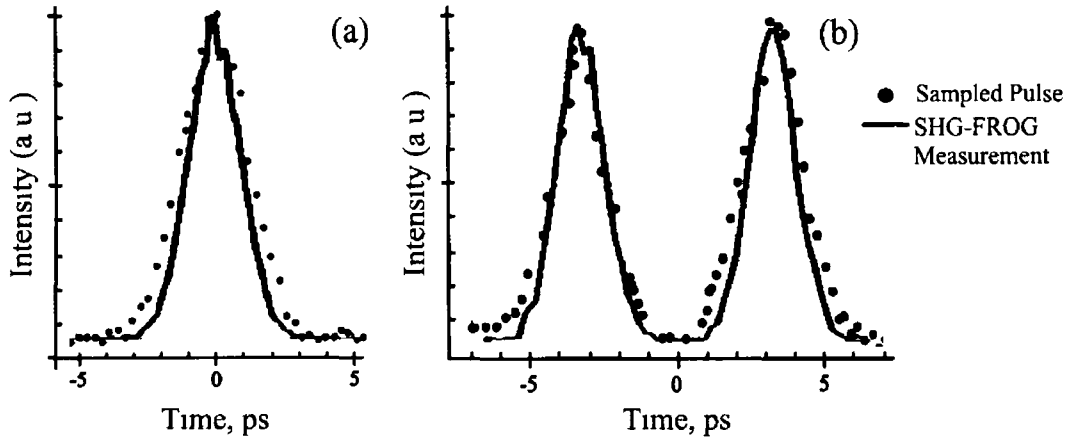
Figure 6 12   TPA sampling against SHG-FROG measurement for   (a) Single optical pulse , (b) Quasi-160GHz signal

temporal resolution was

$$\tau_{res} = \sqrt{1ps^2 + 1\ 8ps^2 + 500fs^2}$$
$$= 2\ 1ps$$
(6 3)

where 1ps is the cavity lifetime, 1 8ps the duration of the sampling pulse and 500fs was the sampling pulse jitter Deconvolving the temporal resolution and the measured pulse width gives

$$\tau_{actual} = \sqrt{\tau_{measured}^2 - \tau_{res}^2}$$
$$= \sqrt{2\ 7ps^2 - 2\ 1ps^2}$$
$$= 1\ 5ps$$
(6 4)

which taking into account that the specification for the jitter on the sampling pulse is given as $< 500fs$, is a close approximation to the SHG-FROG measurement of the signal pulse width

The peak powers of the signal and sampling pulses were 2 7mW and 8 6mW respectively Figure 6 12 (b) compares the TPA sampling (dotted) against the SHG-FROG measurement (continuous) of the quasi-160GHz signal again on the same plot As already stated, the deviation between the two can be accounted for by the temporal resolution of the system The pulse separation is approximately 7ps, highlighting that sampling of a 160Gbit/s signal should be possible The overall system sensitivity was calculated to be

$$Sensitivity = 1\ 6mW \times 62\ 5\mu W$$
$$= 0\ 1(mW)^2$$
(6 5)

183

where 1.6mW is the peak power of the signal pulse and 62.5μW is the average power of the sampling pulse. The peak power of the sampling pulse was 4mW.

6.4.2 TPA Sampling via Separate Data and Sampling Pulse Sources

As mentioned, the temporal duration of a TPA sampling system is determined by the cavity lifetime and the duration and jitter of the sampling pulses used. Therefore, as the microcavity sample used is the same for all the sampling experiments, the only way to improve the temporal resolution of the sampling system is to reduce the duration and jitter of the sampling pulse. Figure 6.13 shows the modified sampling experimental setup. The signal pulse is generated using the same u^2t pulse source as before, with the
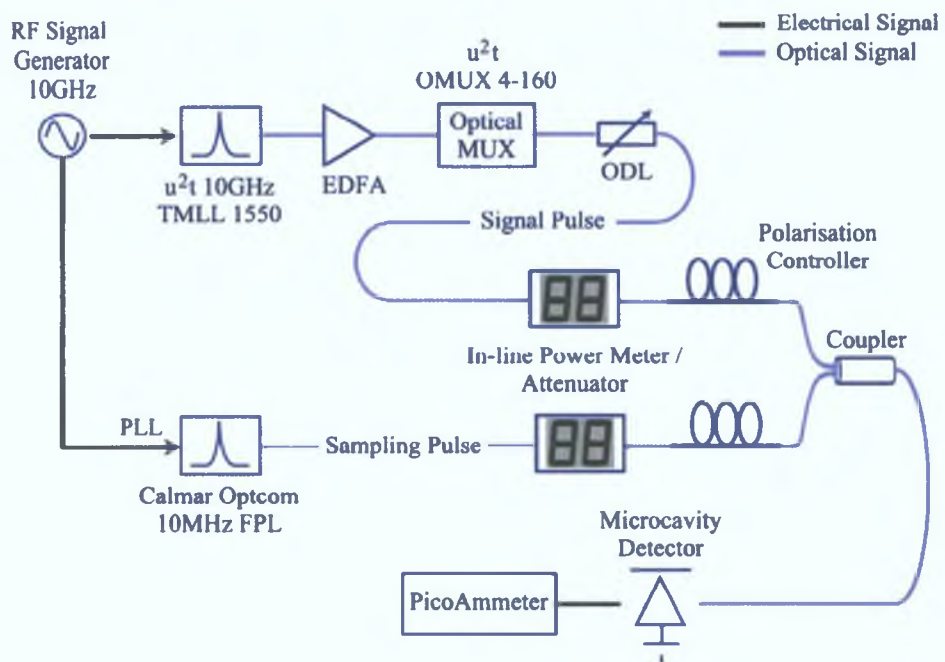
Figure 6.13: Schematic of the experimental setup for quasi-160GHz TPA sampling using separate sampling pulse source

sampling pulse provided by a Calmar Optcom Femtosecond Pulse Laser (FPL) [17]. The FPL has a repetition rate of 10MHz (to maximise the peak power and reduce the scan frequency) and emits optical pulses with durations ranging from 400fs to 1.4ps (jitter less than 150fs), over a tuning range of 1548-1558nm. Figure 6.14 (a) shows the spectrum of the 10MHz pulse source tuned to 1556nm, the resonance of the microcavity, while Figure 6.14 (b) shows an autocorrelation trace of the sampling pulse, with a measured duration of approximately 500fs.

Both pulse sources were tuned to 1556nm to coincide with the resonant wavelength of the microcavity. The signal pulse train was first amplified using a low-noise EDFA before entering a passive delay line multiplexer [18] which consists of a number of inde-
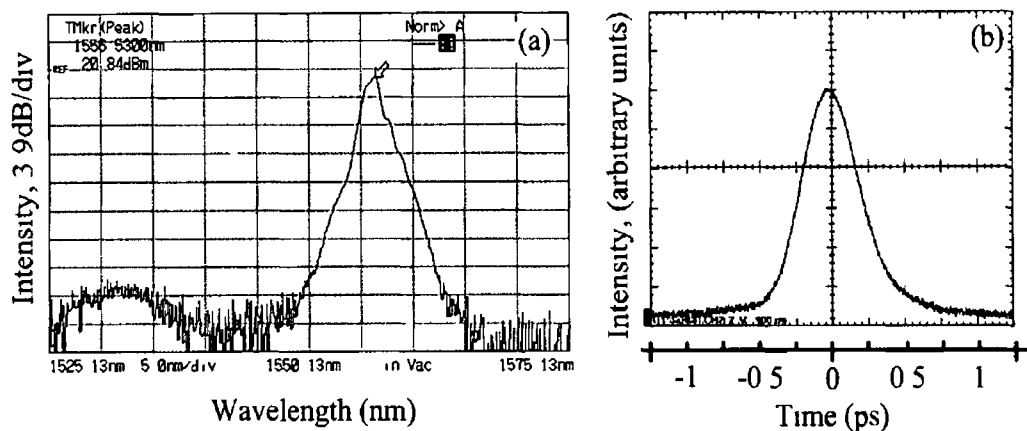
Figure 6 14 10MHz Calmar sampling pulse source (a) Optical spectrum at 1556nm, (b) Autocorrelation trace of 500fs optical sampling pulse

pendently switchable stages Figure 6 15 shows a number of different multiplexed pulse streams as measured using a fast photodetector and high-bandwidth oscilloscope with a combined rise-time of 11 4ps As shown, the optical multiplexer is able to generate a number of different data rates (20, 40, 80, 160GHz) depending on which of the four stages are open The input signal for the optical multiplexer was the u^2t tunable pulse source at a repetition rate of 9 95328GHz (STM-64) Figure 6 15 (c) and (d) graphically illustrates the limitation of using a photodetector and oscilloscope combination for the measurement of high-speed signals, as the separation between optical pulses above 80GHz become indistinguishable

Time, 20ps/div
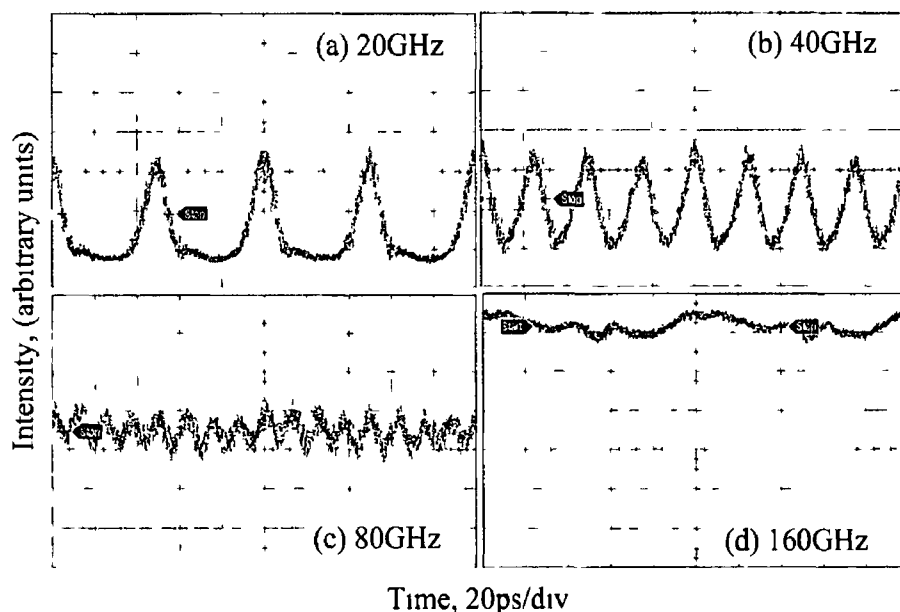
Figure 6 15 Oscilloscope traces of multiplexed data streams at (a) 20GHz, (b) 40GHz, (c) 80GHz, (d) 160GHz

Unfortunately, due to the narrow frequency locking range of the PLL of the 10MHz sampling pulse source, the repetition rate of the signal pulse source had to be set to exactly 10GHz. The major drawback was that as the optical fibre delay lengths in the multiplexer were fixed, a 160GHz data signal could not be produced as separation between adjacent pulses varied from the required 6.25ps. Figure 6.16 shows a comparison between two multiplexed data streams when the first and second stages of the multiplexer were open. Figure 6.16 (a) is for an input signal at exactly 9.95328GHz and clearly shows a signal with equal separation between pulses. The resulting multiplexed data stream for the same input signal but at a repetition rate of 10GHz is shown in Figure 6.16 (b). As shown there is unequal separation between pulses due to the fixed fibre delay lengths in the multiplexer. It was found that by operating the multiplexer with the first three stages open, a 100GHz optical pulse train could be generated and measured using the TPA sampling setup.
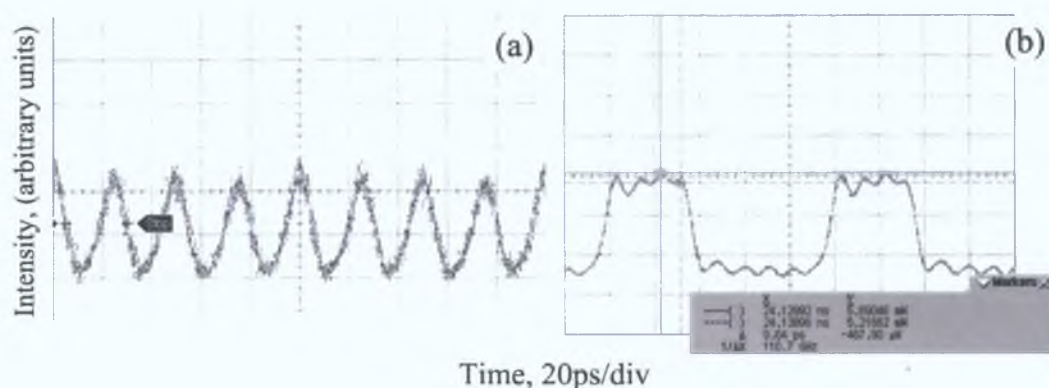
Figure 6.16: Oscilloscope trace of a 40GHz multiplexed data streams with base rate: (a) 9.95328GHz; (b) 10GHz

Returning to Figure 6.13, the 100GHz pulse train leaves the multiplexer and then passes through an variable ODL, which is used to introduce the sampling delay τ, as in the previous experiment. The 10MHz Calmar sampling pulse source was locked to the 10GHz clock signal driving the u^2t source via a PLL, with the drive current of the device adjusted to produce optical pulses with a duration of 500fs at 1556nm. As before, both the sampling and the signal pulse trains pass through in-line power meters/attenuators and PC's, before being combined at a coupler. The combined signals are then incident on the microcavity with the generated photocurrent recorded on a picoammeter [19] as a function of τ, the sampling delay. It was found that the picoammeter had a lower noise floor than the lock-in amplifier employed in the previous setup shown in Figure 6.10. As the sensitivity is a function of the microcavities efficiency and the photocurrent measurement system, an improvement in the system sensitivity was expected.

Figures 6.17 (a) and (b) shows the experimental results of the TPA sampling of a single optical pulse and a 100GHz optical pulse train. The TPA sampling is shown using
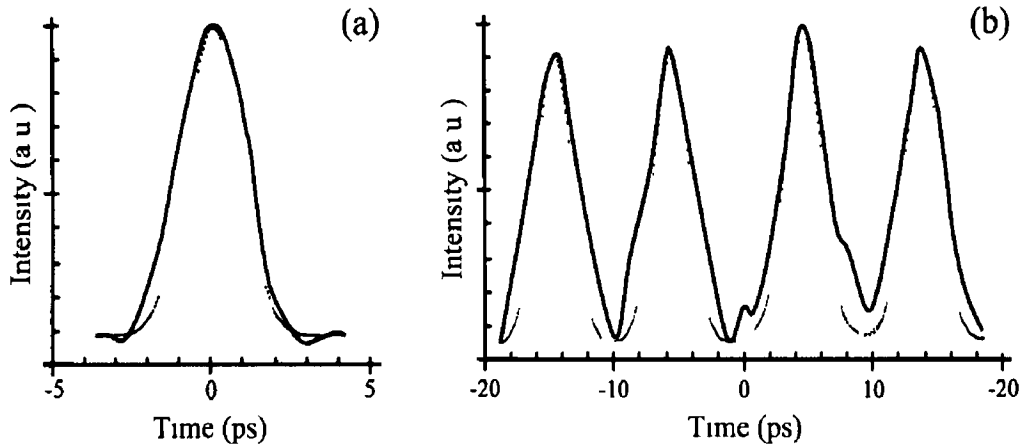
Figure 6 17 TPA sampling of (a) Single optical pulse, (b) 100GHz optical pulse train, plotted against a SHG-FROG trace

as the continuous line, with a SHG-FROG measurement for the same signal shown as the dotted line From (a), the optical pulse duration was calculated to be 2 5ps, with the expected pulse width being 1 8ps The deviation between the two can be accounted for by the temporal resolution of the sampling setup The temporal resolution for this system is

$$
\begin{aligned}
\tau_{res} &= \sqrt{1ps^2 + 500fs^2 + 140fs^2} \\
&= 1\ 1ps
\end{aligned}
\tag{6 6}
$$

where the duration and the jitter of the sampling pulse from the Calmar source is 500fs and 140fs respectively The peak powers of the signal and sampling pulses were 6 8mW and 1 2W, which corresponds to average powers of 105μW and 6μW respectively Figure 6 17 (b) displays the TPA sampling of a 100GHz data signal, as the separation between optical pulses is approximately 10ps The peak powers of the signal and sampling pulses were 10 3mW and 1 2W As before, to calculate the system sensitivity the signal power was reduced to the minimum value that still permitted accurate sampling of the pulse This resulted in a sensitivity of

$$
\begin{aligned}
Sensitivity &= 1\ 5mW \times 6\mu W \\
&= 0\ 009(mW)^2
\end{aligned}
\tag{6 7}
$$

where 1 5mW is the peak power of the signal pulse and 6μW is the average power of the sampling pulse To the best of our knowledge, this is the lowest system sensitivity reported for any TPA sampling system

6.4.3 Real-Time TPA Sampling

The previous experiment recorded the lowest sensitivity for any TPA-based sampling system, and with the temporal resolution calculated at 1.1ps, the fundamental limit seems to be the cavity lifetime of the current device. The major drawback of the two sampling system already described is their reliance upon a manual variation of an ODL to provide the sampling delay τ. This results in a step-wise sampling method, involving time-consuming manual recording of individual TPA photocurrent values.

Figure 6.18 shows a real-time TPA sampling scheme with the sampled pulse being displayed on a standard high-impedance low bandwidth oscilloscope. The sampling
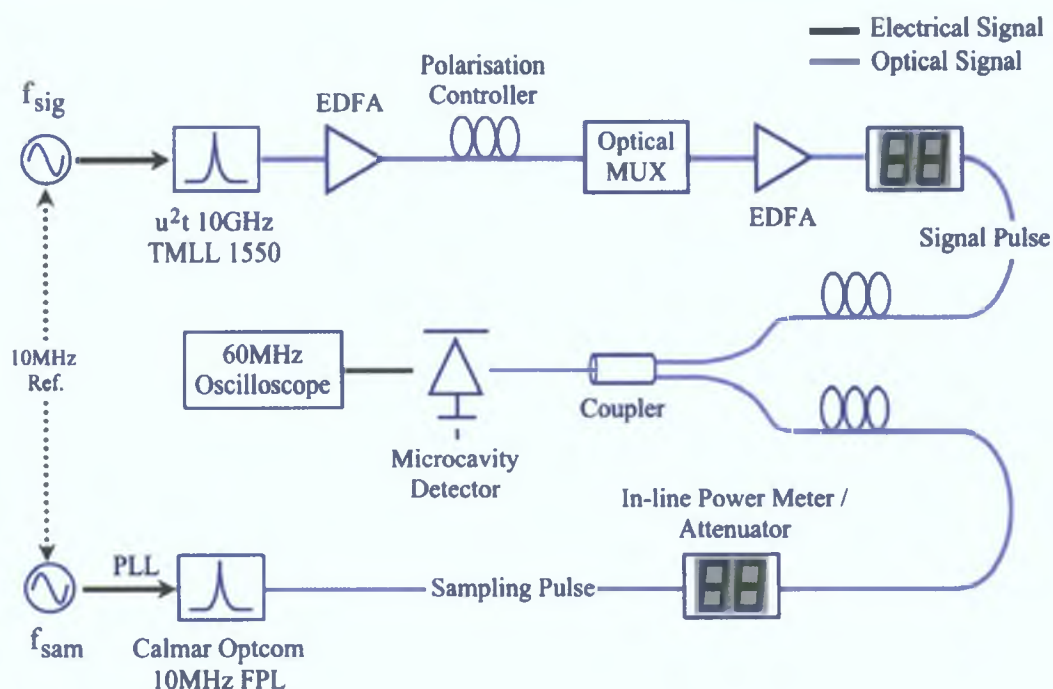
Figure 6.18: Schematic of the experimental setup used for real-time TPA sampling

and signal pulses were provided using the two separate pulse sources as before, but this time the sampling delay τ is generated by operating the sampling frequency (f_{sam}) slightly detuned from a sub-harmonic of the signal frequency (f_{sig}). This allows the sampling pulse to be automatically swept across the signal pulse at a scan frequency that is low enough to be directly detected and displayed on a standard high-impedance oscilloscope without the need for high-speed electronics or lock-in amplifier.

The signal pulse was again amplified before being multiplexed up to 100GHz with both pulses passing through in-line power meters/attenuators and polarisation controllers, before being recombined. The combined signals are then incident on the microcavity with the generated TPA photocurrent signal being displayed on a standard 60MHz high impedance digital oscilloscope.

The repetition rate of the signal pulse was set to 9 998991GHz (f_{sign}) with the sampling pulse operating at 9 998992MHz (f_{sam}) As mentioned already, the frequency lock range of the PLL of the sampling source places a limit on the operating frequency of the sampling system This value for f_{sam} represents the closest frequency value to 9 95328GHz (STM-64) at which the sampling pulse source will operate at, remembering that the optical multiplexer only works correctly at this frequency A value for δ and f_{scan} can be determined using the formulae 4 9 and 4 10 given in Chapter 4, where n is the ratio of f_{sig} to f_{sam}, which in this case is 1000 (approximately 10GHz for the signal pulse source and 10MHz for the sampling pulse source) Using these values, δ is calculated to be [20]

$$\delta = \frac{f_{sig} - nf_{sam}}{f_{sam}}$$
$$= \frac{9\ 998991e9 - [(1000)9\ 998992e6]}{9\ 998992e6} \tag{6 8}$$
$$= 0\ 0001$$

This value for δ results in a scan frequency of

$$f_{scan} = f_{sig} \left(\frac{\delta}{n + \delta} \right)$$
$$= 9\ 998991e9 \left(\frac{0\ 0001}{1000 + 0\ 0001} \right) \tag{6 9}$$
$$= 999\ 89Hz (\approx 1kHz)$$

which can be easily displayed on the 60MHz high-impedance oscilloscope

Figure 6 19 (a) shows the real-time measurement of a 10GHz optical pulse as displayed directly on the oscilloscope The optical pulse duration was measured to be approximately 2 5ps Again this deviation can be accounted for by the temporal resolution of the sampling setup (same as Equation 6 6), cavity lifetime of the device and the amplification of the signal pulse train twice using the two EDFAs The peak (average) powers of the signal and sampling pulses used were 11mW (160μW) and 25W (125μW) respectively Figure 6 19 (b) displays the real-time measurement of a 100GHz (pulse separation approximately 10ps) pulse train, with a signal peak (average) power of 9 6mW (145μW) and sampling peak power of 32W (160μW) The sensitivity of the sampling system was calculated as

$$Sensitivity = 5\ 6mW \times 62\ 5\mu W$$
$$= 0\ 35(mW)^2 \tag{6 10}$$

where 5 6mW is the peak power of the signal pulse, and 62 5μW is the average power of the sampling pulse The temporal resolution of the system is 1 1ps (same as Equa-

189
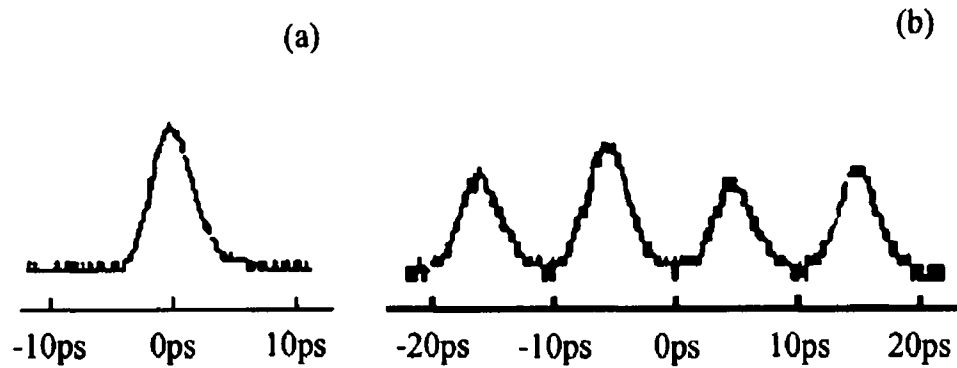
Figure 6 19   Real-time TPA sampling measurement of (a) 10GHz optical pulse, (b) 100GHz pulse train

tion 6 6), with the temporal resolution essentially limited by the cavity lifetime of the current microcavity design   The increase in the sensitivity can be accounted for by the replacement of the picoammeter in Figure 6 13 with the high-impedance oscilloscope shown in Figure 6 18

Summary

This chapter has examined the use of TPA in a specially designed microcavity for high-speed optical demultiplexing and sampling   The chapter started with a discussion regarding the impact that the optical and electrical bandwidth of the current microcavity and packaging used has on the demultiplexing and sampling processes   Next a theoretical model of an all-optical demultiplexer based on TPA in a microcavity for use in an OTDM was presented   Simulations suggested that it is possible to achieve error-free demultiplexing of a 250Gbit/s OTDM signal (25 × 10Gbit/s channels) using a control-to-signal peak pulse powers of 30 1, with a device electrical bandwidth of 30GHz   Following this three optical sampling experiments were presented   A temporal resolution of 1 $1ps$ (limited by the cavity lifetime) was calculated along with a sampling system sensitivity of 0 $009(mW)^2$ This value for sensitivity is the lowest ever reported for a TPA-based sampling system   The final experiment demonstrated sampling of a 100GHz optical pulse train and displayed the results on a high-impedance, low bandwidth electrical oscilloscope

190

Bibliography

[1] J.M.Senior, *Optical Fiber Communications - Principles and Practice*. Prentice Hall, 2nd ed., 1992. ISBN 0-13-635426-2.

[2] Tektronix, "XYZ's of Oscilloscopes Primer - The Systems and Controls of an Oscilloscope." PDF Document, 2005. http://www.tek.com/Measurement/App_Notes/XYZs/systems_controls.pdf.

[3] T.Krug, M.Lynch, A.L.Bradley, J.F.Donegan, L.P.Barry, H.Folliot, J.S.Roberts, and G.Hill, "High-Sensitivity Two-Photon Absorption Microcavity Autocorrelator," *IEEE Photonics Technology Letters*, vol. 16, no. 6, pp. 1543–1544, 2004.

[4] H.Folliot, M.Lynch, A.L.Bradley, T.Krug, L.A.Dunbar, J.Hegarty, J.F.Donegan, and L.P.Barry, "Two-photon-induced photoconductivity enhancement in semiconductor microcavities: A theoretical investigation," *Journal of the Optical Society of America B: Optical Physics*, vol. 19, no. 10, pp. 2396–2402, 2002.

[5] G. P. Agrawal, *Fiber-Optic Communication Systems*. Academic Press, 1st ed., 1997. ISBN 0-471-17540-4.

[6] S. Kawanishi, "Ultrahigh-Speed Optical Time-Division-Multiplexed Transmission Technology Based on Optical Signal Processing," *IEEE Journal of Quantum Electronics*, vol. 34, no. 11, pp. 2064–2079, 1998.

[7] Physikalisch-Technische Bundesanstalt (PTB), "Ultra-fast optical sampling oscilloscopes." html document, 2004. http://www.ptb.de/en/suche/suche.html.

[8] R.L.Jungerman, G.Lee, O.Buccafusca, Y.Kaneko, N.Itagaki, and R.Shioda, "Optical Sampling Reveals Details of Very High Speed Fiber Systems," pdf document, Agilent Technologies, www.agilent.com, 2004.

[9] B.C.Thomsen, L.P.Barry, J.M.Dudley, and J.D.Harvey, "Ultra sensitive all-optical sampling at $1.5\mu m$ using waveguide two-photon absorption," *Electronics Letters*, vol. 35, no. 17, pp. 1483–1484, 1999.

[10] M.Dinu and F.Quochi, "Amplitude sensitivity limits of optical sampling for optical performance monitoring," *Journal of Optical Networking*, vol. 1, no. 7, pp. 237–248, 2002.

[11] R.Hofmann and H.-J. Pfleiderer, "Electro-Optic Sampling System for the Testing of High-Speed Integrated Circuits Using a Free Running Solid-State Laser," *IEEE Journal of Lightwave Technology*, vol. 14, no. 8, pp. 1788–1793, 1996.

[12] M Westlund, P A Andrekson, H Sunnerud, J Hansryd, and J Li, "High-Performance Optical-Fiber-Nonlinearity-Based Optical Waveform Monitoring," *IEEE Journal of Lightwave Technology*, vol 23, no 6, pp 2012–2022, 2005

[13] K Kikuchi, "Optical sampling system at 1 5μm using two photon absorption in Si avalanche photodiode," *Electronics Letters*, vol 34, no 13, pp 1354–1355, 1998

[14] D T Reid, W Sibbett, J M Dudley, L P Barry, B Thomsen, and J D Harvey, "Commercial semiconductor devices for two photon absorption autocorrelation of ultrashort light pulses," *Optics and Photonics News*, vol 9, no 5, p 8142, 1998

[15] u2t Photonics, "1550nm Tunable Picosecond Laser Source (TMLL1550)" PDF Document, 2005 http //www u2t de/pdf/Datasheet_TMLL1550_V42 pdf

[16] R Trebino, K W DeLong, D N Fittinghoff, John N Sweetser, M A Krumbugel, and B A Richman, "Measuring ultrashort laser pulses in the time-frequency domain using frequency-resolved optical gating," *Rev Sci Instrum - American Institute of Physics*, vol 68, no 9, pp 3277–3295, 1997

[17] Calmar Optcom, "Femtosecond Pulsed Fiber Laser (FPL Series)," 2005 http //www calmaropt com/pdf/FPL_Glossy pdf

[18] u2t Photonics, "Four stage OTDM Multiplexer (OMUX 4-160/640)" PDF Document, 2005 http //www u2t de/pdf/Datasheet_OMUX-4_V42 pdf

[19] Keithley, "Model 6485 picoammeter with 10fa resolution" http //www keithley com

[20] B P Nelson and N J Doran, "Optical sampling oscilloscope using nonlinear fibre loop mirror," *Electronics Letters*, vol 27, no 3, pp 204–205, 1991

CHAPTER 7

Conclusions

By employing optical multiplexing techniques, network providers can better utilise their installed fibre network, and meet the demand for more bandwidth being driven by the continued growth of the Internet and the introduction of new broadband services. The main optical multiplexing techniques are WDM, OTDM and hybrid WDM/OTDM, and by taking advantage of these, total aggregate data rates in excess of 10Tbit/s will be feasible in the near future. In the next 5-10 years, it is anticipated that the individual channels will operate at data rates in excess of 100Gbit/s. This will require the development of new techniques for the generation of ultra-short optical pulses, optical demultiplexing and pulse characterisation for performance monitoring.

Important criteria that will have to be met by a suitable pulse source include the ability to generate ultra-short optical pulses, that are as spectrally pure as possible, have a low temporal jitter and high Side-Mode Suppression Ratio (SMSR), and are wavelength tunable. A prime candidate that can fulfil these is the gain-switching of a commercially available semiconductor laser diode. However, these gain-switched pulses possess high levels of temporal jitter, a poor SMSR and spectral broadening. If gain-switched optical pulses are to be used for high-speed optical communications these will have to be overcome. Two techniques that can be employed to achieve this are self-seeding and external injection. It was shown that by using either technique, optical pulses were generated with durations of 12-30ps, over a wavelength tuning range of 60nm with a SMSR exceeding 60dB. Thus a stable and compact wavelength tunable optical pulse source consisting of two or more gain-switched FP laser diodes could be produced.

A second important function for the development of high-speed systems is all-optical processing, which includes optical demultiplexing and pulse characterisation for performance monitoring. In order to carry out these functions at the very-high data rates anticipated, it is evident that only those techniques employing nonlinear optical effects, which are present in optical fibres, semiconductor devices and optical crystals, will be fast enough as these occur on time scales in the order of a few-femtoseconds ($10^{-15}s$). Under certain operating conditions, two photons can be simultaneously absorbed to produce a single electron-hole pair. The resulting photocurrent generated is proportional to the square of the incident optical power falling on the detector. This nonlinear optical-

to-electrical conversion process is known as Two-Photon Absorption (TPA)

The work presented in this thesis concentrated on the use of TPA for optical demultiplexing and optical sampling (pulse characterisation) For these applications we employ a specially designed semiconductor microcavity that overcame the inherent inefficiency associated with the TPA process The devices characterised had a resonance wavelength at 1556nm, with over 3 orders of magnitude enhancement in the photocurrent produced compared with off-resonance wavelengths Using these device parameters, a theorectical model was presented that demonstrated that error-free optical demultiplexing of a 250Gbit/s OTDM signal can be carried out using the microcavity Such an optical demultiplexing scheme would require a control-to-signal pulse peak power ratio of 30 1, corresponding to a signal peak power of 2 4W The device would require an electrical bandwidth of 30GHz It was also experimentally demonstrated that the current microcavity device can successfully sample an optical signal operating at a repetition rate in excess of 100GHz The sampling system had a temporal resolution of approximately $1ps$ (limited by the cavity lifetime) and a sampling system sensitivity of $0\ 009(mW)^2$ This value for sampling sensitivity is, to the best of our knowledge, the lowest ever reported for a TPA-based sampling system

In summary, the work undertaken and presented here has shown that TPA in a semiconductor microcavity is ideally suited for both switching and sampling of very-high data rates in an optical communications network Combined with the simultaneous filtering and detection that the device provides, TPA-based devices could be used for multiple signal processing applications in future high-speed systems

Appendix A: Laser Diode Data Sheets

The following pages contain data sheets for the following laser diodes

- 1 3FP ($\lambda_{central} = 1318\ 9nm$)

- 1 5DFB ($\lambda_{central} = 1537\ 4nm$)

- 1 5FP1 ($\lambda_{central} = 1569\ 9nm$)

- 1 5FP2 ($\lambda_{central} = 1570\ 1nm$)

I·3 FP #1

NEL

INSPECTION SHEET

Model Number	KELD1301CCC
Quantity	1
Serial Number	8A161
Data Attached	○ Laser Diode Test Data ○ I-L , I-V (@25℃) ○ FFP (@25℃) ○ Spectra (@25℃)
Order No	920099
Note	○ lead ⌇ 45Ω ⊲ ○ case

CAUTION

(a) Electrostatic surge causes a permanent damage to laser diodes Before connecting / disconnecting the laser diode to a power supply, set the output level of the power supply to zero
(b) These laser diodes are designed for use solely as components of buyer's products or systems and therefore do not comply with the appropriate requirements for complete laser products by U S Department of Health and Human Services

WARNING

1 Laser diodes emit invisible radiation which can be harmful to human eyes Do not look into the light emitted from the fiber
2 Semiconductor laser chip consists of In, Ga, As and P atoms When you dispose of it, to avoid environmental pollution, please follow the guidelines of your local government

                                          m   d   y
Inspection date   /2 / /4 / / 99 8

Inspected by   M Hashimoto

Approved by   Joshio Itoh

【　Laser Diode Test Data　】

Compound Semiconductor Device Division
NTT Electronics Corporation

Product Type	KELD1301CCC
Serial No.	8A161
Comment	

Test Condition　(Tcase=25℃)

Symbol	Parameter	Conditions	Specifications			Test Results (average)	Units	Judge
			Min.	Typ.	Max.			
VF	Forward Voltage	CW, IF=30mA		2.5		2.510	V	○
Ith	Threshold Current	CW		25	35	27.47	mA	○
Iop	Operation Current	CW, Po=5mW		55		55.85	mA	○
λc	Center Wavelength	CW, Po=5mW	1290	1310	1330	1318.9	nm	○
Δλ	Spectral Bandwidth	CW, Po=5mW		2		1.93	nm	○
θ ‖	Far Field Pattern(H)	CW, Po=5mW		30		25.4	deg	○
θ ⊥	Far Field Pattern(V)	CW, Po=5mW		35		25.9	deg	○

Inspection date :　12／14／1998

Tested by :　N. Hashimoto

Agreed by :　R. Kusaya

LD Characteristics

I-L

Ith1	: 27.47 [mA]
Iop	: 55.85 [mA]
Poi	: 6.15 [mW]
η	: 0.1741 [W/A]
Vop	: 3.854 [V]
Vf	: 2.510 [V]
Po	: 20.13 [mW]
Bv1	: 25.9 [deg]
Bh1	: 25.4 [deg]

Vf [V]   Po [mW]

Po

Vf

If [mA]

SPECTRUM

Level [dBm]   res=0.2nm   span=60.0nm   ADAPTIVE AVE=10   Po:5.00mW

λo = 1318.90 nm

Δλ = 1.93 nm

Wave Length [nm]

FFP

Intensity

Po:5.00mW

H 25.4
V 25.9

Angle [deg.]
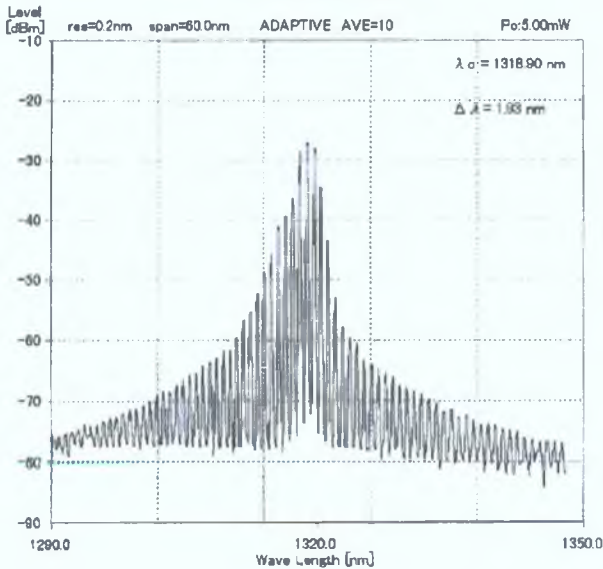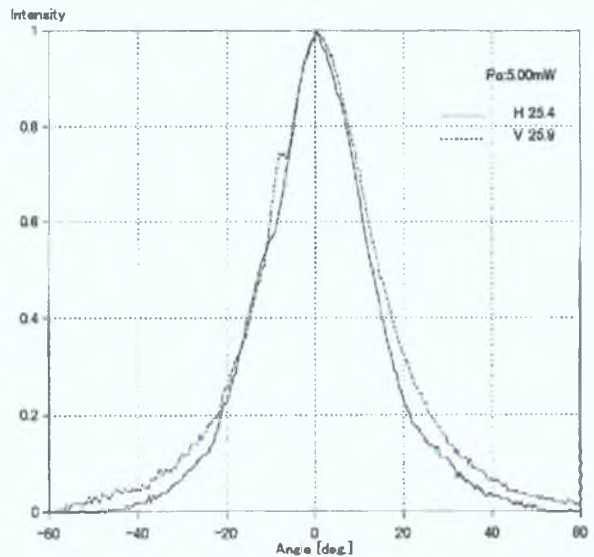
∠2831 ×6019

278.565 THz

226

2066 THz

NEL

⊙

NTT Electronics Corporation

3-1 Morinosato Wakamiya
Atsugi-shi, Kanagawa 243-0198 Japan
TEL +81 462 47 3717, FAX +81 462 47 5349

INSPECTION SHEET

Model Number	KELD1551CCC
Quantity	1
Serial Number	8D020
Data Attached	○ Laser Diode Test Data ○ I-L , I-V (@25℃) ○ FFP (@25℃) ○ Spectra (@25℃)
Order No.	820560
Note	lead 45 Ω case

CAUTION

(a) Electrostatic surge causes a permanent damage to laser diodes. Before connecting / disconnecting the laser diode to a power supply, set the output level of the power supply to zero.

(b) These laser diodes are designed for use solely as components of buyer's products or systems and therefore do not comply with the appropriate requirements for complete laser products by U.S. Department of Health and Human Services.

WARNING

1. Laser diodes emit invisible radiation which can be harmful to human eyes. Do not look into the light emitted from the fiber.
2. Semiconductor laser chip consists of In, Ga, As and P atoms. When you dispose of it, to avoid environmental pollution, please follow the guidelines of your local government.

⚠

Inspection date : 8 / 24 / 1998
                  m   d   y

Inspected by : N. Hashimoto

Approved by : Yoshio Itoh

NEL

【 Laser Diode Test Data 】

Compound Semiconductor Device Division
NTT Electronics Corporation

Product Type	KELD1551CCC
Serial No.	8D020
Comment	

Test Condition (Tcase=25℃)

Symbol	Parameter	Conditions	Specifications			Test Results (average)	Units	Judge
			Min.	Typ.	Max.			
VF	Forward Voltage	CW, IF=30mA		2.5		2.780	V	○
Ith	Threshold Current	CW		20	35	19.9	mA	○
Iop	Operation Current	CW, Po=5mW		55		59.31	mA	○
λ p	Peak Wavelength	CW, Po=5mW	1530	1550	1570	1537.4	nm	○
SMS	Side Mode Suppression Ratio	CW, Po=5mW	30			46.76	dB	○
θ ‖	Far Field Pattern(H)	CW, Po=5mW		30		25.1	deg	○
θ ⊥	Far Field Pattern(V)	CW, Po=5mW		35		33.0	deg	○

Inspection date : 8／24／1998

Tested by : *N. Hashimoto*

Agreed by : *R. Kosaya*

LD Characteristics

Sample No.   8D020   T-Case[°C]   24.5

I-L

Vf [V]   Po [mW]

Ith1	: 19.90	[mA]
Iop	: 59.31	[mA]
Poi	: 7.69	[mW]
η	: 0.1309	[W/A]
Vop	: 4.313	[V]
Vf	: 2.780	[V]
Po	: 15.88	[mW]
Bv1	: 33.0	[deg]
Bh1	: 25.1	[deg]

Vf

Po

If [mA]

FFP

Intensity   [V]   Po: 5.0mW

Angle [deg]

Intensity   [H]   Po: 5.0mW

Angle [deg]

LD Characteristics

Sample No.	8D020	T-Case[°C]	24.5

SPECTRUM

res=0.1nm span=25.0nm HIGH SENS1AVE=1 Po:5.00mW
λp = 1537.40 nm
SMSR= 46.76 dB

res=0.1nm span=25.0nm HIGH SENS1AVE=1 If:21.89mA
λp = 1536.80 nm
SMSR= 40.15 dB

res=0.1nm span=25.0nm HIGH SENS1AVE=1 If:29.90mA
λp = 1536.90 nm
SMSR= 43.64 dB

res=0.1nm span=25.0nm HIGH SENS1AVE=1 If:50.00mA
λp = 1537.20 nm
SMSR= 46.50 dB

res=0.1nm span=25.0nm HIGH SENS1AVE=1 If:100.00mA
λp = 1538.40 nm
SMSR= 48.07 dB

res=0.1nm span=25.0nm HIGH SENS1AVE=1 If:150.00mA
λp = 1540.10 nm
SMSR= 48.67 dB

NEL

INSPECTION SHEET

Model Number	KELD1501CCC
Quantity	1
Serial Number	8C1009
Data Attached	○ Laser Diode Test Data ○ I-L , I-V (@25℃) ○ FFP (@25℃) ○ Spectra (@25℃)
Order No	920099
Note	lead 45 Ω case

CAUTION

(a) Electrostatic surge causes a permanent damage to laser diodes Before connecting / disconnecting the laser diode to a power supply, set the output level of the power supply to zero

(b) These laser diodes are designed for use solely as components of buyer's products or systems and therefore do not comply with the appropriate requirements for complete laser products by U S Department of Health and Human Services

WARNING

1 Laser diodes emit invisible radiation which can be harmful to human eyes Do not look into the light emitted from the fiber

2 Semiconductor laser chip consists of In, Ga, As and P atoms When you dispose of it, to avoid environmental pollution, please follow the guidelines of your local government

Inspection date $\overset{m}{12}$ / $\overset{d}{14}$ / $\overset{y}{1998}$

Inspected by   M Hashimoto

Approved by   Yuchi Itoh

NEL

【 Laser Diode Test Data 】

Compound Semiconductor Device Division
NTT Electronics Corporation

Product Type	KELD1501CCC
Serial No.	8C1009
Comment	

Test Condition (Tcase=25℃)

Symbol	Parameter	Conditions	Specifications			Test Results (average)	Units	Judge
			Min.	Typ.	Max.			
VF	Forward Voltage	CW, IF=30mA		2.5		2.440	V	◯
Ith	Threshold Current	CW		15	30	21.32	mA	◯
Iop	Operation Current	CW, Po=5mW		45		64.89	mA	◯
λc	Center Wavelength	CW, Po=5mW	1520	1550	1580	1569.9	nm	◯
Δλ	Spectral Bandwidth	CW, Po=5mW		5		4.49	nm	◯
θ ‖	Far Field Pattern(H)	CW, Po=5mW		30		33.6	deg	◯
θ ⊥	Far Field Pattern(V)	CW, Po=5mW		35		38.8	deg	◯

Inspection date : 12／14／1998

Tested by : *N. Hashimoto*

Agreed by : *R. Kosaya.*

LD Characteristics

Sample No.   8C1009   T-Case[°C]   24.5

I-L

Vf [V]   Po [mW]

Ith1 : 21.32 [mA]
Iop : 64.89 [mA]
η   : 0.1075 [W/A]
Vop : 4.213 [V]
Vf   : 2.440 [V]
Poi : 5.66   [mW]
Po   : 12.71 [mW]
Bv1 : 38.8   [deg]
Bh1 : 33.6   [deg]

If [mA]

SPECTRUM

Level [dBm]   res=0.2nm   span=60.0nm   ADAPTIVE AVE=10   Po:5.00mW

λc = 1569.90 nm

Δλ = 4.49 nm

Wave Length [nm]

FFP

Intensity

Po:5.00mW

H 33.6
V 38.8

Angle [deg.]

NEL

INSPECTION SHEET

Model Number	KELD1501R-CCC
Quantity	1
Serial Number	8C1008
Data Attached	○ Laser Diode Test Data ○ I-L , I-V (@25°C) ○ Spectra (@25°C) ○ FFP (@25°C)
Order No.	920038
Note	lead 45 Ω case

CAUTION
(a) Electrostatic surge causes a permanent damage to laser diodes. Before connecting / disconnecting the laser diode to a power supply, set the output level of the power supply to zero.
(b) These laser diodes are designed for use solely as components of buyer's products or systems and therefore do not comply with the appropriate requirements for complete laser products by U.S. Department of Health and Human Services.

WARNING

1. Laser diodes emit invisible radiation which can be harmful to human eyes. Do not look into the light emitted from the fiber.
2. Semiconductor laser chip consists of In, Ga, As and P atoms. When you dispose of it, to avoid environmental pollution, please follow the guidelines of your local government.

Inspection date : 12 / 2 / 1998

Inspected by : R. Hashimoto

Approved by : Yoshida Itoh

NEL

【　Laser Diode Test Data　】

Compound Semiconductor Device Division
NTT Electronics Corporation

Product Type	KELD1501R-CCC
Serial No.	8C1008
Comment	

Test Condition　(Tcase=25℃)

Symbol	Parameter	Conditions	Specifications			Test Results (average)	Units	Judge
			Min.	Typ.	Max.			
Ith	Threshold Current	CW			35	21.28	mA	○
Po	Output Power	CW, ΔIF=50mA	5			5.54	mW	○
λ c	Center Wavelength	CW, Po=5mW	1510		1580	1570.1	nm	○
$\Delta \lambda$	Spectral Bandwidth	CW, Po=5mW		5		4.34	nm	○
θ ‖	Far Field Pattern(H)	CW, Po=5mW		35		30.5	deg	○
θ ⊥	Far Field Pattern(V)	CW, Po=5mW		40		40.4	deg	○

Inspection date :　12／1／1998

Tested by :　橋本典子

Agreed by :　嘗左和生

LD Characteristics

Sample No.   8C1008   T-Case[°C]   24.5

I-L

Vf [V] / Po [mW]
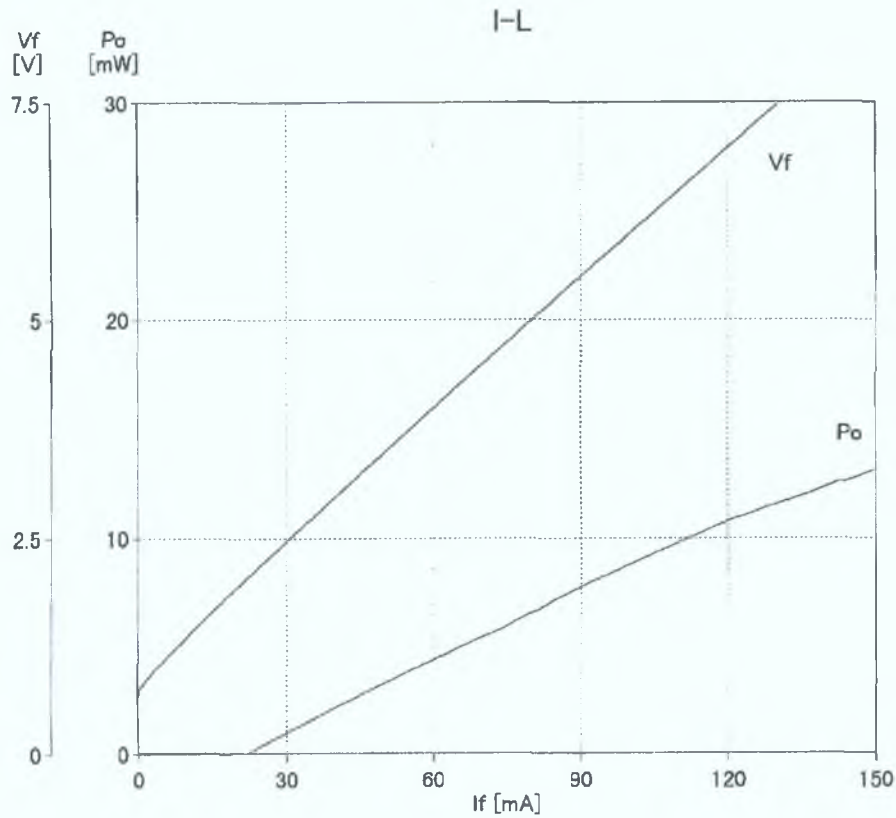
Ith1	: 21.28 [mA]
Iop	: 65.89 [mA]
η	: 0.1057 [W/A]
Vop	: 4.286 [V]
Vf	: 2.460 [V]
Poi	: 5.54 [mW]
Po	: 13.14 [mW]
Bv1	: 40.4 [deg]
Bh1	: 30.5 [deg]

If [mA]

SPECTRUM

Level [dBm]   res=0.2nm   span=60.0nm   ADAPTIVE AVE=10   Po:5.00mW

λo = 1570.10 nm

Δλ = 4.34 nm

Wave Length [nm]

FFP

Intensity

Po:5.00mW

H 30.5
V 40.4

Angle [deg]
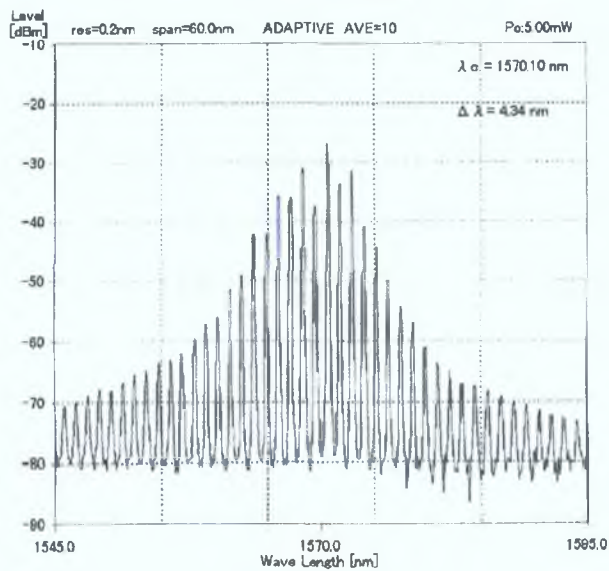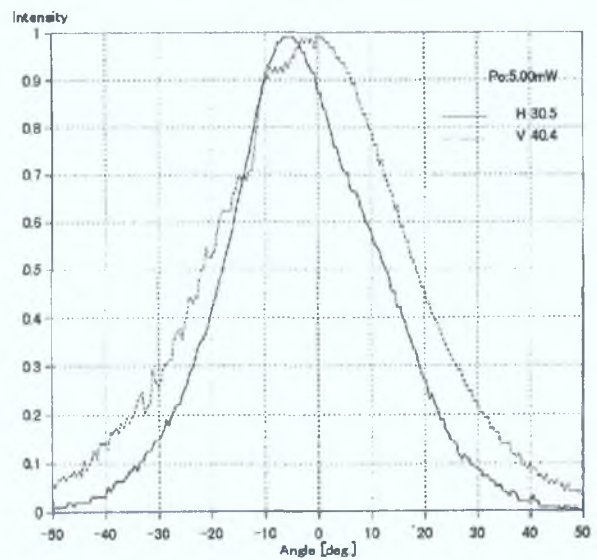
Appendix B: Publications Relating From This Thesis

The following is a list of the referred journals and reviewed conference papers arising from this work. Unless otherwise stated, the ideas, development and writing up of all the papers were the principal responsibility of myself, P.J.Maguire, working within the Radio and Optical Communications Laboratory under the supervision of Dr. Liam Barry. The inclusion of co-authors reflects the fact that the work came from active collaboration between researchers from the Semiconductor Photonics Group, University of Dublin, Trinity College, Ireland and the Laboratoire de Physique des Solides, INSA, Rennes, France.

Referred Journals

Optical signal processing via two-photon absorption in a semiconductor microcavity for the next generation of high-speed optical communications network, P.J.Maguire, L.P.Barry, T.Krug, W.H.Guo, J.O'Dowd, M.Lynch, A.L.Bradley, J.F.Donegan and H.Folliot, *IEEE Journal of Lightwave Technology, pending publication*, 2006
Summary of collabortive results over the last 3 years

Resonance tuning of two-photon absorption microcavities for wavelength-selective pulse monitoring, T.Krug, W.H.Guo, J.O'Dowd, M.Lynch, A.L.Bradley, J.F.Donegan, P.J.Maguire, L.P.Barry, H.Folliot, *IEEE Photonics Technology Letters*, vol.18, no.2, 2006
Experimentally collaboration only

Simulation of a high-speed demultiplexer based on two-photon absorption in semiconductor devices, P.J.Maguire, L.P.Barry, T.Krug, M.Lynch, A.L.Bradley, J.F.Donegan and H.Folliot, *Optics Communications*, vol.249, no.4-6, pp.415-420, 2005.

All-optical sampling utilising two-photon absorption in semiconductor microcavity, P.J.Maguire, L.P.Barry, T.Krug, M.Lynch, A.L.Bradley, J.F.Donegan and H.Folliot, *Electronics Letters*, vol.41, no.8, pp.489-490, 2005.

Self-Seeding of a Gain-Switched Integrated Dual-Laser Source for the Generation of Highly Wavelength-Tunable Picosecond Optical Pulses, P.Anandarajah, P.J.Maguire, A.Clarke and L.P.Barry, *IEEE Photonics Technology Letters*, vol. 16, no.2, pp.629-631, 2004

Experimentally collaboration only

Reviewed Conference Papers

Direct Measurement of a High-Speed >100Gbit/s OTDM Data Signal Utilising Two-Photon Absorption in a Semiconductor Microcavity, P.J.Maguire, L.P.Barry, T.Krug, J.O'Dowd, M.Lynch, A.L.Bradley, J.F.Donegan and H.Folliot, *Lasers and Electro-Optics Society Annual Meeting (LEOS2005)*, Paper ML3, Sydney, Australia, 23-28th October, 2005

Highly-Efficient Optical Sampling of a 100Gbit/s OTDM Data Signal via Two-Photon Absorption in a Semiconductor Microcavity, P.J.Maguire, L.P.Barry, T.Krug, J.O'Dowd, M.Lynch, A.L.Bradley, J.F.Donegan and H.Folliot, *European Conference and Exhibition on Optical Communication (ECOC2005)*, Paper Th1.3.5, Glasgow, UK, 25-29th September, 2005

Highly-Efficient Optical Sampling Based on Two-Photon Absorption in a Semiconductor Micro-Cavity Device, P.J.Maguire and L.P.Barry, T.Krug, M.Lynch, A.L.Bradley, J.F.Donegan and H.Folliot, *Conference on Lasers and Electro-Optics (CLEO2005)*, Paper CtuAA5, Baltimore, USA, 22-27th May, 2005

Simulation of All-Optical Demultiplexing utilizing Two-Photon Absorption in Semiconductor Devices for High-Speed OTDM Networks, P.J.Maguire and L.P.Barry, *Lasers and Electro-Optics Society Annual Meeting (LEOS2004)*, Puerto Rico, vol.2, pp.975-976, 2004

Generation of Wavelength Tunable Optical Pulses with SMSR Exceeding 50dB by Self-Seeding a Gain-Switched Source Containing Two FP Lasers, P.J.Maguire, P.Anandarajah, L.P.Barry and A.Kaszubowska, *Lasers and Electro-Optics Society Annual Meeting (LEOS2003)*, Tucson, Arizona, USA, vol.2, pp.471-472, 2003

Optical Signal Processing via Two-Photon Absorption in a Semiconductor Microcavity for the Next Generation of High-Speed Optical Communications Network

P.J.Maguire and L.P.Barry, T.Krug, W.H.Guo, J.O'Dowd, M.Lynch, A.L.Bradley, and J.F.Donegan, and H.Folliot

Abstract— Due to the introduction of new broadband services, individual line data rates are expected to exceed 100Gbit/s in the near future. In order to operate at these high-speeds, new optical signal processing techniques will have to be developed. This paper will demonstrate that Two-Photon Absorption in a specially designed semiconductor microcavity is an ideal candidate for optical signal processing applications such as autocorrelation, sampling and demultiplexing in high-speed WDM and hybrid WDM/OTDM networks.

I. INTRODUCTION

Due to the continued growth of the Internet and the introduction of new broadband services such as video-on-demand and mobile telephony, there will be a need to better exploit the enormous bandwidth that optical fibre provides in the network. The conventional method employed by many network providers is to use optical multiplexing techniques to increase the number of carriers per optical fibre, with Wavelength Division Multiplexing (WDM) being the most common. In order to increase capacity in WDM networks, new transmitter/receiver pairings (operating at different wavelengths) can be added but this can be expensive. A second option is to increase the data rate transmitted per channel, but this is limited by speed of commercially available electronics. An alternative is to use Optical Time Division Multiplexing (OTDM) [1] to enhance the data rate of a number of different wavelengths channels in a WDM network by putting OTDM coding on top of the channels provided by WDM. This hybrid WDM/OTDM approach would result in a smaller number of channels operating at much higher data rates [2].

Optical Time Division Multiplexing uses short optical pulses to represent data and multiplexes in the time domain by allocating each channel specific bit slots in the overall multiplexed signal. The basic configuration for a bit-interleaved OTDM transmitter is shown in Figure 1. The main component in a bit-interleaved OTDM system is an ultrashort optical pulse source. The optical pulse train generated is at a repetition rate R and is split into N copies by a passive optical coupler, where N corresponds to the number of electrical channels to be multiplexed. Each copy is then modulated by electrical data which is at a data rate R. The resulting output from the modulator is an optical data channel where the electrical data is represented using short optical pulses. The modulated Return-to-Zero (RZ) optical signal then passes through a fixed fibre

delay length, which delays each channel by 1/RN relative to adjacent channels in the system. This ensures that the optical data channels arrive at the output at a time corresponding to its allocated bit slot in the overall OTDM signal. The N modulated and delayed optical data channels are then recombined using a second passive optical coupler to form the OTDM data signal.
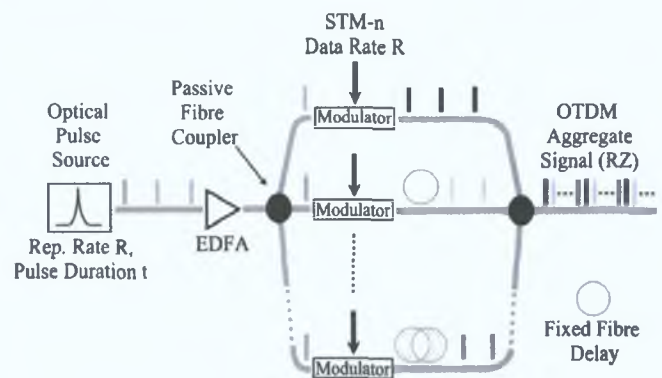
Fig. 1. Bit-interleaved OTDM transmission system

In order to successfully operate at data rates in excess of 100Gbit/s per channel, new optical signal processing techniques, such as optical demultiplexing [1] and optical sampling [3] will have to be developed. The majority of research has focused on taking advantage of optical nonlinearities that are present in fibres, semiconductors and crystals, as these occur on timescales in the order of a few femtosecond making them ideal for high-speed applications. However there are a number of factors that may limit their performance for high-speed optical signal processing. For those based on the Kerr effect in optical fibres, speciality fibres are required and precise control of the wavelength of the control pulse and signal pulse around the zero dispersion wavelength are necessary [4]. Gain depletion in Semiconductor Optical Amplifier's (SOA's) limits the control pulse width and thus the maximum switching speed [5], while those techniques employing Second Harmonic Generation (SHG) in optical crystals require high optical intensities and adjustment of the crystal orientation for phase matching [6]. Due to these disadvantages, it is necessary to consider alternative optical nonlinearities for high-speed

optical signal processing. This work will focus on the use of Two-Photon Absorption (TPA) in a semiconductor for high-speed signal processing applications such as switching [7], sampling [8], autocorrelation [9], and optical thresholding [10].

This paper examines the use of Two-Photon Absorption in a specially designed semiconductor microcavity for high-speed optical signal processing applications of autocorrelation, optical sampling and optical switching. Section II presents a brief overview of the TPA process, with the specially designed microcavity presented in Section III. High-speed optical signal processing applications of autocorrelation, sampling and switching via the TPA process in the semiconductor microcavity are demonstrated in Sections IV, V and VI respectively. Section VII shows how the resonance response of the microcavity can be alted by angle tuning thus providing wavelength selectivity for WDM and hybrid WDM/OTDM applications. Finally Section VIII provides a summary of the experimental work carried out, followed by some conclusions.

II. TWO-PHOTON ABSORPTION

Two-Photon Absorption (TPA) is a nonlinear optical-to-electrical conversion process that occurs in semiconductors when two photons are absorbed to generate a single electron-hole pairing. It occurs when a photon of energy E_{ph} is incident on the active region of a semiconductor device with a band gap energy exceeding E_{ph} but less than $2E_{ph}$. Under these conditions, individual photons do not possess sufficient energy to produce an electron-hole pair. However an electron-hole pair can be produced by the simultaneous absorption of two photons, were the summation of the individual photon energies is greater than the band gap energy. The resulting photocurrent produced is proportional to the square of the incident optical power falling on the detector [11]. It is this nonlinear response, combined with TPA's ultra-fast response time ($10^{-14}s$ at 1550nm [12]), that enables TPA to be considered for use in high-speed optical signal processing. The photocurrent produced via the TPA process in a semiconductor with Single-Photon Absorption (SPA) coefficient α and Two-Photon Absorption coefficient β may be represented by:

$$ J = \frac{eS}{h\nu}\left(I_{abs}^{SPA} + \frac{1}{2}I_{abs}^{TPA}\right) \qquad (1) $$

where S is the illuminated area, $h\nu$ the photon energy and I_{abs}^{SPA} and I_{abs}^{TPA} are the SPA and TPA contribution in the total absorption [13]. Therefore to observe the TPA process, the semiconductor material is chosen so that the band gap is greater than the energy of the incident photons but less than twice the photon energy. The nonlinear two photon response is limited on the lower intensity side by SPA and on the high intensity side by the total absorption. The dynamic range where TPA can be usefully exploited for autocorrelation and demultiplexing applications is given by:

$$ \frac{\alpha}{\beta} \leq I \leq \frac{1}{\beta L} \qquad (2) $$

where L is the length of the absorption region and I is the intensity of the light falling on the detector. As a result TPA

photogeneration will dominate, with only a residual amount of linear absorption due to lattice imperfections or the thermal excitations of carriers within the detector [11].

III. MICROCAVITY DEVICE STRUCTURE

One of the major problems associated with the use of TPA for optical signal processing applications such as autocorrelation, switching and sampling, is its inherenet inefficiency, requiring either high optical intensities typically not found in an optical communications network, or a long interaction length for response enhancement [11]. One way in which the efficiency of the TPA process can be greatly enhanced is to place the active region within a semiconductor microcavity structure [14].

The microcavity works by placing mirrors at either end of the active region of the semiconductor, resulting in the formation of very strong optical fields within the cavity. This can be viewed as an increase in the interaction length of the active region. This leads to a reduction of the device length when compared with waveguide structures, as well as a significant enhancement of the TPA generated photocurrent by four orders of magnitude when compared to non-cavity devices [14]. Such an increase in the photocurrent should allow the development of a simple and compact device for constructing high-speed optical processing components in an optical communications system. An illustration of the structure
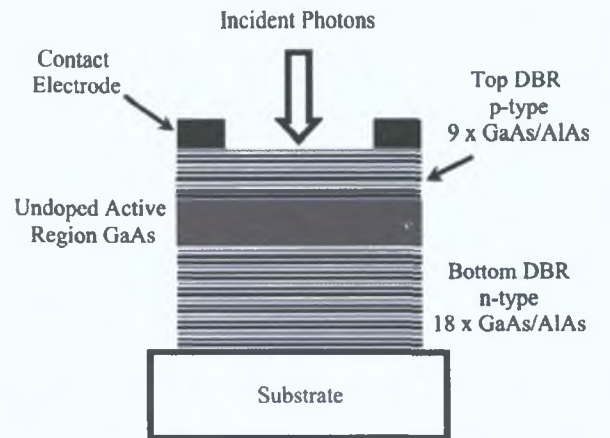
Fig. 2.   Schematic of microcavity device structure

of the specially fabricated TPA microcavity is shown in Figure 2. It consists of two GaAs/AlAs distributed Bragg reflector (DBR) surrounding an undoped GaAs active region. The active region is 460nm thick with a bandgap energy of 1.428eV. The mirrors consist of alternating $\lambda/4$ AlAs and $\lambda/4$ GaAs layers, with the top p-doped (C$\approx 10^{18}cm^{-3}$) mirror consisting of 9 periods of AlAs/GaAs whereas the bottom n-doped (Si$\approx 10^{18}cm^{-3}$) mirrors consists of 18 periods of AlAs/GaAs. The device length is designed to an integral of the absorption wavelength to enhance the TPA efficiency within the 1.5μm wavelength range. The cavity lifetime of the device structure, which takes into account the reflectivity of the Bragg mirrors at either end of the device [15], is in the order of 1ps.

Prior to carrying out an optical processing experiments using the devices fabricated, some initial characterisation of the TPA microcavity samples was carried out. Figure 3 shows a plot of the photocurrent generated from the microcavity as a function of the incident optical wavelength. The incident
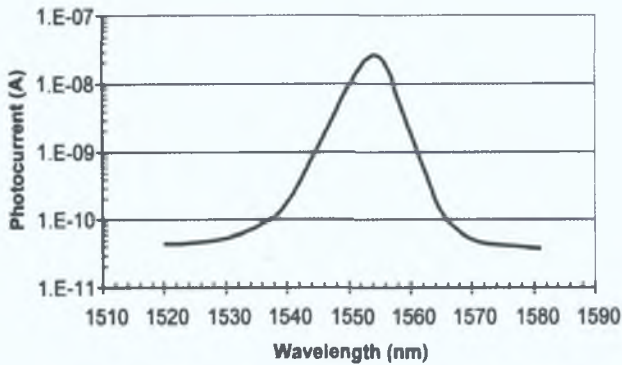
Fig. 3. Plot of the photocurrent generated as a function of incident optical wavelength

optical signal was generated from a commercially available 10GHz u^2t TMLL 1550 pulse source (pulse duration 2ps, jitter < 500fs, tunable wavelength range 1480-1580nm). The average optical output power was 0.5mW, which was then optical amplified using a low noise EDFA to result in an incident peak power of 2W falling on the TPA microcavity. The wavelength of the incident signal was then altered in steps of 0.5nm, with the photocurrent generated by the TPA microcavity recorded using a picoammeter as a function of the incident wavelength. As can be seen in Figure 3, the cavity response is dependent on the incident wavelength, with a cavity wavelength resonance of 1556nm, with a measured spectral linewidth of 4.2nm. Figure 3 also shows that the peak wavelength resonance is 3-orders of magnitude greater when compared to the photocurrent generated for off-resonance wavelengths.

Figure 4 shows a plot of the photocurrent generated as a function of the incident peak optical power. The character-
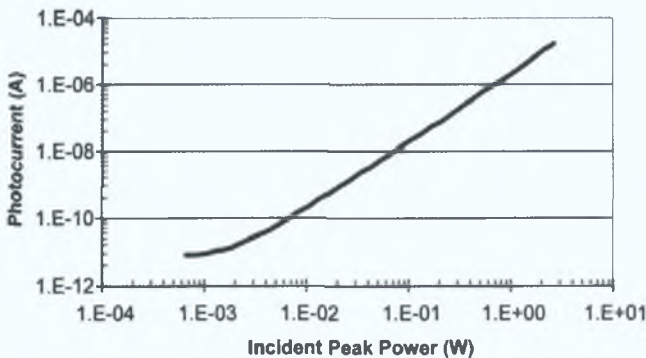
Fig. 4. Plot of the photocurrent as a function of incident optical peak power at the cavity wavelength resonance

isation was carried out using the same 10GHz u^2t tunable

optical pulse source as used before, with the output wavelength tuned to coincide with the resonance peak wavelength of the cavity (1556nm). The optical pulse train was then amplified using a low-noise EDFA (as before) before passing through an in-line power meter/attenuator, which allowed simultaneous power monitoring and attenuation of the optical signal. The incident signal was then attenuated from 16.4dBm (average power) to -20dBm in steps of 1dB, with the TPA photocurrent generated measured using a picoammeter as a function of incident optical power. Figure 4 shows a square dependence of the photocurrent generated on the incident optical intensity, which is evidence of the TPA process, with residual SPA occurring at low energies. However, there is over 3 orders of magnitude of nonlinear response with the current device.

IV. TPA-BASED AUTOCORRELATION

The technique of autocorrelation allows the detection and characterisation of ultrashort optical pulses. Here results are presented that use a TPA microcavity as an unbiased PIN diode, which exhibits nonlinear power-dependent response, to detect and charcterise modelocked picosecond pulses as part of an autocorrelator. The use of the TPA microcavity completely replaces the nonlinear crystal and photomultiplier tube or photodetector needed for second harmonic autocorrelation.

A. Principle of TPA Autocorrrelation

Two-Photon Absorption in semiconductors is an attractive alternative to second harmonic generation for autocorrelation [16], [17], because of lower cost and increased sensitivity. TPA in photodiodes [9], [18] and AlGaAs light emitting diodes [19] for autocorrelation measurement of picosecond and femtosecond laser pulses has been previously demonstrated. Also waveguide TPA in commercial laser diodes has also been used to fully characterize picosecond pulses in the temporal and phase domain [20]. However the low efficiency of the TPA process and resulting requirement for high peak powers have to be overcome before it can be satisfactorily exploited in practical optical communications systems. We have recently demonstrated that the TPA photocurrent can be hugely enhanced, by four orders of magnitude, by placing the active material in a microcavity structure as described in Section 3. Therefore in optical telecommunication, as opposed to laser diagnostics, where there is a requirement to measure low peak powers, the presented 1.5 μm TPA microcavity device is an excellent candidate for a detector. The enhancement of the TPA-induced photocurrent due to the cavity finesse greatly improves the sensitivity of the autocorrelation measurement. There are numerous additional advantages of using a TPA microcavity in an autocorrelator. The growth of these devices will also be significantly cheaper due to the vertical device orientation compared with waveguide TPA structures. The vertical nature and the relatively large area of the structure allow for easier fibre coupling than waveguide strucrures. In addition, the fact that the device is thin means there are no phase matching problems compared with SHG crystals and free space optics. In this section, we measured the sensitivity of the TPA microcavity devices in an autocorrelation config-uration.

B. TPA Autocorrelation Experimental Setup

The non-interferometric autocorrelation is measured using a standard Michelson interferometer configuration. The configuration of a second harmonic crystal followed by a highly sensitive photodetector used in the conventional schemes was simply replaced by the Two-Photon Absorption microcavity photodetector. The experimental setup is shown in Figure 5.
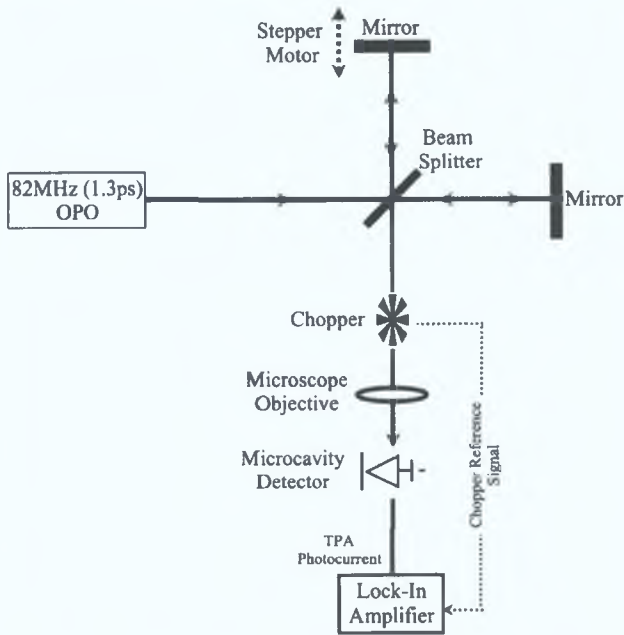
Fig. 5. The configuration of the TPA autocorrelator setup.

The optical pulses were generated by an optical parametric oscillator (OPO) synchronously pumped by an Ti:Sapphire laser system, at a repetition rate of 82 MHz. At a wavelength of $1.5\mu m$ the typical temporal pulsewidth was 1.3 ps. After traversing the two arms of the interferometer the two beams are co-linearly focused to a 12 μm-diameter spot on the microcavity device using a $\times 10$ microscope objective. The Two-Photon Absorption photocurrent was measured using a lock-in technique. The best sensitivity is achieved using the shunt resistance, $R_{SHUNT} = 10M\Omega$, of the microcavity device as the load resistor.

C. TPA Autocorrelation Experimental Results

The sensitivity of the TPA microcavity autocorrelator was measured by inserting neutral density filters in the beam path to control the signal-to-noise (SNR) levels. Figure 6 shows the microcavity device photocurrent as a function of delay for an incident average power of 0.77 mW and peak power of 3.6 mW.

The quadratic response of the TPA photocurrent (versus incident average power) of the devices was verified down to 1mW peak power. Given the nonlinear response of the photocurrent with incident power it is possible to extrapolate the incident power to a SNR of 1 [21]. The sensitivity of the autocorrelator defined as the product of the peak and average power of the minimum detectable signal (SNR=1) is found to
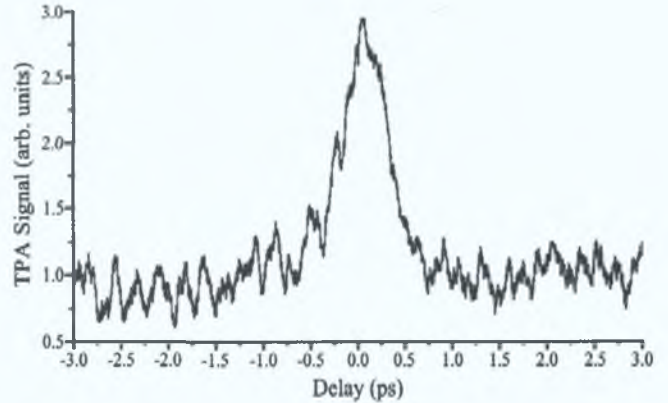
Fig. 6. Microcavity device photocurrent as a function of delay

be $9.3\times10^{-4}(mW)^2$ at a bandwidth of 1Hz. For a given shunt-resistance R_{SHUNT}, the limit for the detectable photocurrent is governed by the thermal noise $I_{th}^2 = 4kTB_N/R_{SHUNT}$, where k is the Boltzmann constant, T the temperature and B_N =1.6Hz the measurement bandwidth. Comparing the theoretical value of the thermal noise, I_{th}=0.16pA, with the standard deviation of the data in the side arms of the autocorrelation trace in Figure 6, I_{th}=0.1pA, we observe good agreement. To show the enhancement in sensitivity due to the microcavity, the autocorrelation measurement has also been performed at a wavelength of $1.46\mu m$ off the stop-band of the microcavity DBRs reflectivity spectrum. The magnitude of photocurrent measured offband, $I_{TPA} = 220pA$, is consistent with the theoretical values obtained by assuming TPA in bulk material with the same thickness as the active region of the microcavity device, given a TPA coefficient of $\beta = 3 \times 10^{-10}$m/W. A sensitivity of $1.5 \times 10^3(mW)^2$ is determined corresponding to an average-power of 330mW and peak-power of 1.5W. The sensitivity of the TPA microcavity autocorrelation measurements presented here compares very favourably with conventional autocorrelators based on second harmonic generation techniques which typically have a sensitivity of $1(mW)^2$ [22]. Compared to commercially available GaAsP photodiodes, AlGaAs LEDs and GaAs LEDs recently used for TPA autocorrelation at $1.5\mu m$, the microcavity device is found to be more sensitive by at least a factor of 10 [23] at a bandwidth of 1Hz. However, waveguide devices and photomultiplier tubes are still more sensitive due to a much longer active region and direct-detection photon counting, respectively.

V. OPTICAL SAMPLING

In order to measure current high-speed optical signals, a fast photodetector in conjunction with a high-speed sampling oscilloscope is commonly employed. However, such a measurement scheme is limited by the design of high-speed electronic component allowing bandwidths of approximately 80GHz [24], permitting the accurate measurement of data rates approaching 40Gbit/s. Therefore, as individual channel data rates are expected to exceed this in the next 5-10 years, current electrical sampling techniques will be inadequate. Critical information such as pulse duration, pulse separation and pulse

rise-time, which are crucial for the optimisation of optical network performance, will be distorted.

A. Principle of TPA Sampling

TPA sampling employs a separate optical sampling pulse to monitor the performance criteria of a high-speed OTDM signal. The optical sampling pulse has a higher intensity and shorter duration $[I_{sam}(t - \tau)]$ than the duration of the signal under test $[I_{sig}(t)]$. The signal and sampling pulses are then incident on the microcavity, with the electrical TPA signal generated $[i(t)]$ measured as a function of the sampling delay τ, resulting in an intensity cross-correlation measurement between I_{sam} and I_{sig} [25]:

$$i(\tau) \propto \langle I_{sam}(t - \tau) I_{sig}(t) \rangle \tag{3}$$

where $\langle\rangle$ denotes time averaging. The sampling delay τ is generated by operating the sampling frequency (f_{sam}) slightly detuned from a sub-harmonic of the signal frequency (f_{sig}). The sampling frequency is calculated using [25]:

$$f_{sam} = \frac{f_{sig}}{n + \delta} \tag{4}$$

where n is an integer and $\delta << 1$. This results in a scan frequency of:

$$f_{scan} = f_{sig} \frac{\delta}{\delta + n} \tag{5}$$

which can be easily displayed on a standard high-impedance oscilloscope, with the measured signal representing the signal pulse waveform on a constant background [25].

B. TPA-based Optical Sampling Experimental Setup

The TPA sampling setup is shown in Figure 7. The signal pulse, I_{sig}, is generated using the 10GHz u^2t TMLL 1550 pulse source already described in Section III. The sampling pulse I_{sam} was generated using a Calmar Optcom Femtosecond Pulse Laser (pulse duration 500fs, jitter < 140fs, tunable range 1548-1558nm). Both sources were tuned to the resonance wavelength of the TPA microcavity ($\lambda = 1556nm$), and were phase locked together via the 10MHz reference signal provided by the signal generators and the Phase Lock Loop (PLL) input to the Calmar source. The repetition rate of the signal pulse (f_{sig}) was set to 9.998991GHz with the sampling pulse (f_{sam}) operating at 9.998992MHz, resulting in a scan frequency (f_{scan}) of 1kHz. The 10GHz optical pulse train used to create the data signal was first amplified using a low-noise Erbium Doped Fibre Amplifier (EDFA) before entering a passive delay line multiplexer. The OTDM multiplexer is a commercially available u^2t 4-160 OMUX, consisting of a four independently switchable stages with fixed fibre delay lengths within each stage. This results in the need to have an input signal at a repetition rate of exactly, or a multiple of 9.95328GHz (STM-64). Due to the narrow frequency locking range of the sampling pulse generator, it was not possible to generate a multiplexed optical signal at 160GHz. However, by operating the signal and sampling pulse sources at the lowest repetition frequency possible (f_{sig} and f_{sam}), it was possible to generate a 100GHz optical multiplexed pulse stream. This
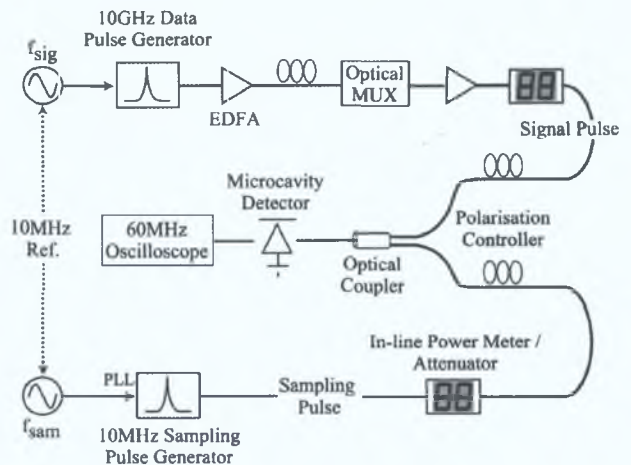
Fig. 7. Experimental setup for optical sampling based on TPA in a semiconductor microcavity

signal was then amplified a second time in order to overcome the 18dB insertion loss associated with the passive multiplexer. The sampling and the signal pulses then pass through separate in-line power meters/attenuators and polarisation controllers before being recombined at a passive optical fibre coupler. The power meters allow easy power measurement and attenuation of both pulse trains, while allowing the system sensitivity to be continuously monitored. The combined signals are then incident on the microcavity with the generated TPA photocurrent signal being displayed on a standard 60MHz high impedance digital oscilloscope.

C. TPA Sampling Results
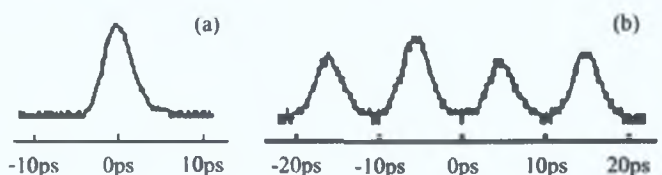
Fig. 8. Real-time TPA sampling measurement of (a) single optical pulse before multiplexing; (b) 100GHz multiplexed pulse train

Figure 8 (a) shows the real-time measurement of a single optical pulse as displayed on the high-impedance oscilloscope. The signal was measured prior to any optical multiplexing taking place. The optical pulse duration was measured to be 2.5ps, with a pulse width of 2ps expected. This deviation is due to the temporal resolution of the sampling set up. The temporal resolution is defined as:

$$t_{res} = \sqrt{\tau_{cavity}^2 + t_{sam}^2 + j_{sam}^2} \tag{6}$$

and takes into account the cavity lifetime of the device (τ_{cavity}= 1ps) and the duration (t_{sam}=500fs) and jitter (j_{sam} <140fs) of the sampling pulse used. This gives a minimum temporal resolution of 1.1ps. The average powers of the signal and sampling pulses used were 0.2mW and 0.12mW respectively. Figure 8 (b) displays the real-time measurement of a

100GHz (pulse separation 10ps) optically multiplexed pulse train, with a signal average power of 0.17mW and sampling average power of 0.16mW. The variation in the amplitude of the optical pulses can be accounted for by the propagation of each pulse over a different transmission path within the passive delay line multiplexer. The sensitivity of the sampling system, which is defined as being the product of the peak power of the signal pulse and the average power of the sampling pulse [25] was calculated as $0.35(mW^2)$, corresponding to a signal peak power of 5.6mW. This was obtained without any post-amplification of the TPA photocurrent. With the addition of a low-noise amplifier after the microcavity, further improvements in the sensitivity are expected.

VI. OPTICAL SWITCHING

In this section a theoretical investigation into the possibility of high-speed optical demultiplexing using TPA in a microcavity is carried out. The main device parameters used in the model, such as the Two-Photon Absorption coefficient, are taken from results obtained from the characterisation of the microcavity samples used in the previous experimental work. Using this model, the operation of the demultiplexer is examined when various system parameters are varied.

A. TPA Optical Demultiplexer

The demultiplexer uses optical control pulses, operating at a different wavelength, to switch out data from a single high-speed OTDM system via the TPA effect in the microcavity [7]. By operating the control pulses at a different wavelength, interference between control and data signal can be minimised [26]. The control pulses, which are at the repetition rate of the individual channels in the multiplexed signal, are optically combined with the high-speed OTDM data signal and are incident on the device. The arrival time of the control pulses is varied using an optical delay line so that they arrive at the demultiplexer at a time corresponding to the data to be switched out. A schematic of TPA demultiplexing is shown in Figure 9. The TPA effect in the microcavity leads to a delay-
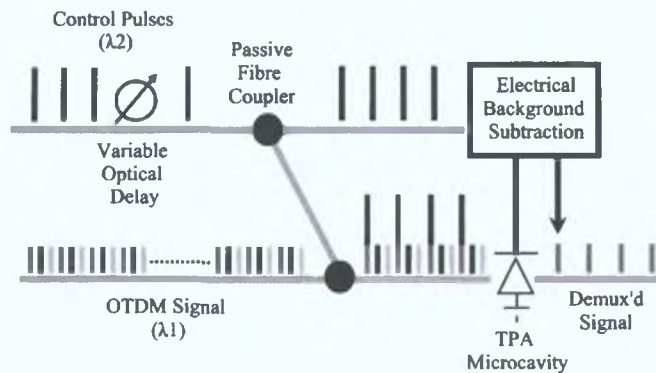
Fig. 9. Schematic of TPA demultiplexing

dependent response between the OTDM data signal and the control pulses in the detector. Due to TPA's nonlinear quadratic response, there is a strong contrast between the electrical TPA

signal generated when the control and data pulses overlap on the detector and that generated when the adjacent channels arrive independently. The constant background signal due to the control pulses can be conveniently subtracted electrically, resulting in a high contrast demultiplexing output signal. Thus, the TPA demultiplexer is able to carry out simultaneous channel selection and electrical detection in an OTDM optical communications system [7], [27].

Since the generation of TPA electron-hole pairs is essentially instantaneous, the maximum switching speed is determined by the duration of the data and control pulses, allowing Tbit/s data rates to become feasible [27]. It also allows for simpler optical alignment since it does not require phase-matching as required for applications utilising nonlinear crystals [28]. In addition, by making use of semiconductor microcavities, the inefficiency associated with TPA can be overcome.

B. Optical Demultiplexing Model

A simulation was carried out to determine the suitability of using a TPA microcavity for high-speed demultiplexing when a number of system parameters were varied. These parameters included:

- Number of OTDM channels
- Ratio between peak power of control pulse and OTDM data pulse
- Electrical bandwidth of the TPA detector

With reference to the electrical bandwidth of the TPA detector, it is necessary to differentiate between the optical bandwidth and the electrical bandwidth of the detector. The optical bandwidth of the microcavity, which determines the overall aggregate OTDM data rates that the device can operate at, is a function of the optical-to-electrical TPA process and the cavity (photon) lifetime of the device. The TPA process is essentially instantaneous, while the cavity lifetime is a function of the reflectivity of the Bragg mirrors [15], which is in the order to 1ps for the devices used in the experimental work described. This would allow aggregate data rates in excess of 100Gbit/s to be demultiplexed. The electrical bandwidth of the detector is determined by the extraction time (carrier/electron lifetime) of the photogenerated carriers from the device and is a function of the packaging, device structure and device size. This carrier lifetime determines the maximum speed of the individual channels in the multiplexed signal. Thus for individual channel data rate of 10Gbit/s, the minimum required electrical bandwidth would be 10GHz. However, even with this bandwidth, noise will be introduced on the demultiplexed channel from the electrical signals generated by the other OTDM channels that are not synchronized with the control pulse. This can be overcome by operating with a large control-to-signal ratio, but at the expense of operating with higher optical intensities. By increasing the bandwidth of the device, the noise contribution from the other OTDM channels is reduced.

The simulation models the switching scheme described in Figure 9. An OTDM data signal is created, which consists of a number of individual data channels, each transmitting

a Pseudo Random Bit Stream (PRBS) signal. The optical pulse width used was kept to one quarter of the bit period of the overall aggregate OTDM data rate in order to avoid interference in adjacent channels. The number of channels, individual data rate, and peak power of the optical pulses used to represent the data are user defined. Noise is then added to limit the optimum Bit Error Rate (BER) that can be achieved. The control pulses, which have the same duration as the data signal pulse are combined and then incident on the TPA detector, which is modeled as per [11]. The peak power of the control pulses can be set to any value. From the resulting SNR [29], the Optical Bit-Error Rate (OBER) before the detector is calculated, which takes into account any noise in the transmitter, and the Electrical Bit-Error Rate (EBER), which is a function of device structure and device noise. The OBER is then compared to the EBER, with the overall goal being to determine the operating conditions such that the EBER is the same as the OBER. A more detailed description of the model can be found in [30].

C. Simulation Results

The first system parameter that was varied was the control-to-signal power ratio, as the number of channels were varied from 25 to 100, each with a data rate of 10Gbit/s per channel (250Gbit/s to 1Tbit/s aggregate OTDM data rates). The signal peak power was kept constant at 80mW, and the detector bandwidth was set to 10GHz, the minimum required to prevent ISI between adjacent data bits in the demultiplexed channel.
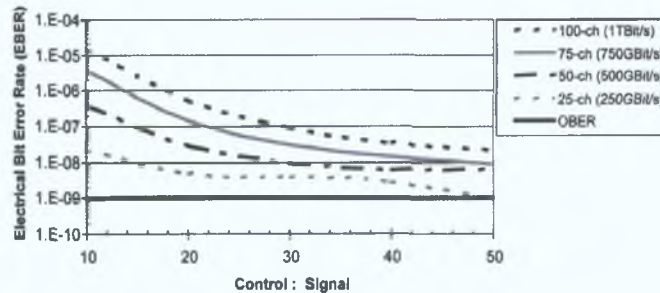
Fig. 10. BER Vs. control-to-signal power as the number of channels (with base rate of 10Gbit/s per channel) is varied.

Figure 10 clearly shows that as the control-to-signal ratio is increased, the EBER approaches the OBER. This results from the fact that as the control-to-signal power is increased, the contrast ratio between the data signal synchronised with the control pulses, and those not synchronised widens. This reduces the amount of noise introduced by the adjacent channels, improving the SNR and the EBER. For a given control-to-signal power ratio, the EBER is degraded as the number of channels increases from 25 to 100. This results from the increased noise levels introduced from the increased number of channels. For a 25-channel system, the EBER reached the OBER for a control-to-signal ratio of 50:1, corresponding to a control pulse peak power of 4W. During the initial characterization of the microcavity samples that were fabricated, a maximum peak optical power of 20W was applied to the

device without any damage being incurred. This suggests that a control pulse peak power of 4W is well within the operating range of the microcavity structure, even if it is slightly large for practical applications.

Figure 11 shows how the control-to-signal ratio is affected by the electrical bandwidth of the TPA microcavity. As already mentioned, by increasing the bandwidth of the device, the noise contribution due to the TPA photocurrent generated by adjacent OTDM channels falling within the response time of the device is reduced. This allows the same performance to be achieved, but at a reduced control-to-signal ratio. Hence for the same system that is displayed in Figure 10, the control-to-signal ratio can be reduced from 50:1 to 30:1, corresponding to a control pulse peak power of 2.4W.
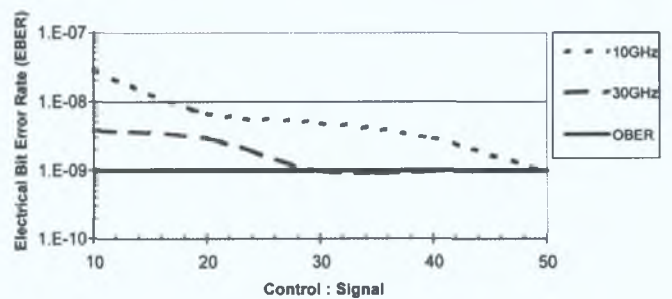
Fig. 11. BER Vs. control-to-signal power as electrical bandwidth is varied for a 250Gbit/s aggregate OTDM system.

From recent experimental work carried out on the characterization of the microcavities, the device bandwidth of the 100μm sample was determined to be 1GHz. It is hoped that with smaller device size, an improved cavity design and the use of high-speed packaging, the device bandwidth can be improved. As the device is based on a PIN structure, bandwidths in excess of 10GHz should be readily feasible.

VII. ANGLE-TUNING OF TPA MICROCAVITY

Optoelectronic devices whose performance is enhanced by placing the active device structure inside a Fabry-Perot resonant microcavity benefit from wavelength selectivity and the large increase of the resonant optical field introduced by the cavity. This resonance response makes the device suitable for WDM and hybrid WDM/OTDM applications as the selection and optical signal processing functions (optical thresholding, switching, sampling, autocorrelation) of a high-speed optical data channel can be carried out simultaneously using a single device. In addition by angle tuning the device, it is possible to vary the peak of the wavelength resonance. This technique would remove the need for expensive re-growth of different detectors for different WDM channels, as tilting the device alters the selected channel.

A. Principle of Angle Tuning

The angular dependence of resonance cavity enhanced photodetectors is well known and has been extensively studied [31], [32]. Tilting of a DBR based resonator will change the resonant wavelength, as the resonant conditions are strictly

satisfied only for the normal component of the propagation constant. Using the transfer matrix model (TMM) we have analysed the reflection and transmission spectrum of the microcavity structure and compare these with experimental results.

B. Angle Tuning Experimental Setup

A schematic cross-section view of the GaAs/AlAs microcavity structure is shown in Figure 2. The cavity resonance full width half maximum (FWHM) was 4.2nm with a finesse of 96. The created TPA photocurrent was measured using a standard lock-in amplifier technique. TPA photocurrent spectra are measured with various light incidence angle with a tunable OPO system. The light was focused onto the device using a 0.20 NA lens. The angle contribution due to the focusing effect is smaller than the accepting angle of the microcavity device.

Fig. 13. Measured and simulated peak wavelength response of TPA microcavity versus incident light angle. The error bars show the variations in TPA and angles associated with the measurement system.

Fig. 12. Schematic view of the angle tuning setup including a TPA microcavity and translation stage.
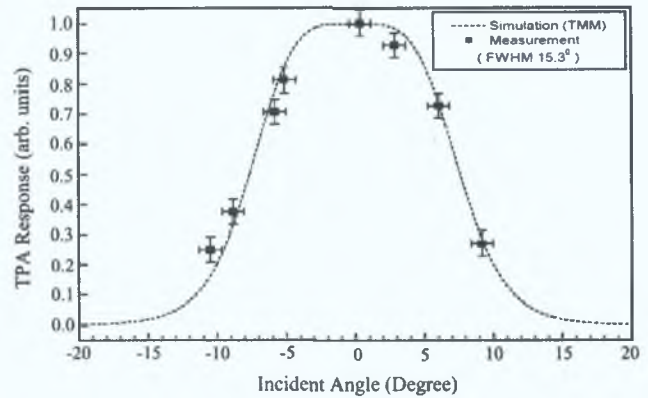
Fig. 14. Measured and simulated response of TPA microcavity at 1.52 μm versus incident light angle.

C. Angle Tuning Experimental Results

Figure 13 shows the resonance wavelength of the TPA microcavity as a function of incident angle. The resonance wavelength at normal incident for this device was 1.512 μm. By rotating the TPA microcavity by an angle θ the resonance wavelength changes to lower wavelengths. The agreement between theoretically predicted and the experimental results is excellent for θ less than $\sim 45°$. A tuning range of 35 nm is achieved by rotating the TPA microcavity over 45°. Angle tuning beyond 45° is possible but we were limited to 45° by the tuning range of our rotation stage.

In Figure 14 the incident wavelength was tuned to cavity resonance, corresponding to peak TPA induced photocurrent and kept constant while the incident angle was varied. The change in angle of incidence off normal leads to a decrease of the TPA response that can be easily explained by the TMM approach. The FWHM of the angular response of the TPA device for a constant wavelength λ_0 is 15.3°. Here λ_0 is the resonant wavelength for normal incident. The results agree well with the theoretical predictions made for plane waves using the TMM.

VIII. SUMMARY OF RESULTS

It has been shown that by using a specially designed semiconductor microcavity, the TPA efficiency can be improved to enable optical signal processing applications using optical power levels that are typically found in an optical communications network. The microcavity used during in our experiments had a wavelength resonance in the 1550nm telecommunications transmission window, with measured spectral line widths of approximately 5nm. The TPA photocurrent produced at the cavity wavelength resonance is 3 orders of magnitude higher nonlinear response when compared to the photocurrent generated by off-resonance wavelength signals falling on the detector. By using the microcavity design, the nonlinear crystal and the photomultiplier tube can be replaced in a conventional SHG autocorrelation with a single device, lowering cost, while at the same time increasing the sensitivity by at least a factor of ten. Real-time optical sampling of a 2ps optical pulse and a 100GHz optical pulse train was then demonstrated using the microcavity device. This was carried out using an average signal pulse power of 0.2mW and an average sampling pulse power of 0.12mW, corresponding to a system sensitivity of $0.35(mW)^2$. The temporal resolution of the TPA sampling

system was calculated to be 1.1ps, with further improvement in the system sensitivity anticipated with the inclusion of a low-noise amplifier after the detector. A theoretical investigation into the use of the microcavity for optical demultiplexing was then carried out. It showed that successful demultiplexing of a 25-channel OTDM data signal, with individual channel data rates of 10Gbit/s, could be achieved with a control-to-signal ratio of 30:1 and an electrical device bandwidth of 30GHz. This bandwidth should be feasible with a smaller device size, improved cavity design and use of a high-speed packaging as the microcavity is based on a PIN structure. Finally it was reported that with the use of device angle tuning, the wavelength resonance of the microcavity could be shifted by up to 35nm with a rotation of $45°$. This ability to alter the peak wavelength resonance of a single device would make it suitable for WDM and hybrid WDM/OTDM applications without the need for growth of different devices for different wavelength channels.

CONCLUSIONS

This paper has shown that by incorporating a microcavity design, Two-Photon Absorption efficiency can be improved to allow practical optical signal processing at power levels typically found in an optical communications network. Therefore, by developing a specially designed microcavity device, TPA-based elements could form one of the major building blocks of an optical sub-system designed to carry out optical signal processing tasks in the next gneration of optical systems.

ACKNOWLEDGMENTS

REFERENCES

[1] D.M.Spirit, A.D.Ellis, and P.E.Barnsley, "Optical time division multiplexing: systems, networks," *IEEE Communications Magazine*, vol. 32, no. 12, pp. 56–62, 1994.

[2] M.Attygalle, H.F.Liu, and A.Nirmalathas, "An all-optical WDM to TDM conversion scheme with simultaneous all-optical synchronization for WDM/OTDM network nodes," *Optical and Quantum Electronics*, vol. 33, pp. 827–840, 2001.

[3] S. Kawanishi, "Ultrahigh-Speed Optical Time-Division-Multiplexed Transmission Technology Based on Optical Signal Processing," *IEEE Journal of Quantum Electronics*, vol. 34, no. 11, pp. 2064–2079, 1998.

[4] M. Saruwatari, "All-Optical Signal Processing for Terabit/Second Optical Transmission," *IEEE Journal of Selected Topics in Quantum Electronics*, vol. 6, no. 6, pp. 1363–1374, 2000.

[5] G. P. Agrawal, *Applications of Nonlinear Fiber Optics*. Academic Press, 1st ed., 2001. ISBN 0-12-045144-1.

[6] P. Staudt, "Getting the measure of ultrashort pulses," *Opto and Laser Europe*, pp. 33–35, 2004.

[7] B.C.Thomsen, J.D.Harvey, and L.P.Barry, "Error Free Demultiplexing in High-Speed OTDM Systems using a Two-Photon Absorption Based Switch," in *Optical Fibre Communication Conference*, pp. W02–1, 2001.

[8] K.Kikuchi, "Optical sampling system at $1.5\mu m$ using two photon absorption in Si avalanche photodiode," *Electronics Letters*, vol. 34, no. 13, pp. 1354–1355, 1998.

[9] Y.Takagi, T.Kobayashi, and K.Yoshihara, "Multiple- and single-shot autocorrelator based on two-photon conductivity in semiconductors," *Optics Letters*, vol. 17, no. 9, pp. 658–660, 1992.

[10] Z.Zheng, A.M.Weiner, J.H.Marsh, and M.M.Karkhanehchi, "Ultrafast optical thresholding based on two-photon absorption GaAs Waveguide Photodetectors," *IEEE Photonics Technology Letters*, vol. 9, no. 4, pp. 493–495, 1997.

[11] H.Folliot, M.Lynch, A.L.Bradley, T.Krug, L.A.Dunbar, J.Hegarty, J.F.Donegan, and L.P.Barry, "Two-photon-induced photoconductivity enhancement in semiconductor microcavities: A theoretical investigation," *Journal of the Optical Society of America B: Optical Physics*, vol. 19, no. 10, pp. 2396–2402, 2002.

[12] J. Donegan, "Two-photon absorption speeds optical switching," *Lightwave europe*, p. 31, 2002. July 2002.

[13] F.R.Laughton, J.H.Marsh, D.A.Barrow, and E.L.Portnoi, "The Two Photon Absorption Semiconductor Waveguide Autocorrelator," *IEEE Journal of Quantum Electronics*, vol. 30, no. 3, pp. 838–845, 1994.

[14] H.Folliot, M.Lynch, A.L.Bradley, L.A.Dunbar, J.Hegarty, J.F.Donegan, L.P.Barry, J.S.Roberts, and G.Hill, "Two-photon absorption photocurrent enhancement in bulk algaas semiconductor microcavities," *Applied Physics Letters*, vol. 80, no. 8, pp. 1328–1330, 2002.

[15] T.Krug, M.Lynch, A.L.Bradley, J.F.Donegan, L.P.Barry, H.Folliot, J.S.Roberts, and G.Hill, "High-Sensitivity Two-Photon Absorption Microcavity Autocorrelator," *IEEE Photonics Technology Letters*, vol. 16, no. 6, pp. 1543–1544, 2004.

[16] H.K.Tsang, L.Y.Chan, J.B.D.Soole, H.P.LeBlanc, M.A.Koza, and R.Bhat, "High sensitivity autocorrelation using two-photon absorption in ingaasp waveguides," *Electronics Letters*, vol. 31, no. 20, pp. 1773–1775, 1995.

[17] Y.Takagi, "Simple autocorrelator for ultraviolet pulse width measurements based on the nonlinear photoelectric effect," *Applied Optics*, vol. 33, no. 27, pp. 6328–6332, 1994.

[18] J.K.Ranka, A.L.Gaeta, A.Baltuska, M.S.Pshenichnikov, and D.A.Wiersma, "Autocorrelation measurement of 6-fs pulses based on the two-photon-induced photocurrent in a gaasp photodiode," *Optics Letters*, vol. 22, no. 17, pp. 1344–1346, 1997.

[19] D.T.Reid, M.Padgett, C.McGowan, W.E.Sleat, and W.Sibbett, "Light-emitting diodes as measurement devices for femtosecond laser pulses," *Optics Letters*, vol. 22, no. 4, pp. 233–235, 1997.

[20] D.T.Reid, B.C.Thomson, J.M.Dudley, and J.D.Harvey, "Sonogram characterisation of picosecond pulses at 1.5 mm using waveguide two photon absorption," *Electronics Letters*, vol. 36, no. 13, pp. 1141–1142, 2000.

[21] T.Krug, M.Lynch, A.L.Bradley, and J.F.Donegan, "Two-photon absorption in microcavities for optical autocorrelation and sampling," *Technical proceedings, CLEO/Europe-EQEC Conference, Munich, Germany*.

[22] APE, *Autocorrelator PulseScope Manual*. 1st ed., 2001.

[23] L.P.Barry, B.C.Thomsen, J.M.Dudley, and J.D.Harvey, "Autocorrelation and Ultrafast Optical Thresholding at $1.5\mu m$ using a Commercial ingaasp $1.3\mu m$ laser diode," *Electronics Letters*, vol. 34, no. 4, pp. 358–360, 1998.

[24] R.L.Jungerman, G.Lee, O.Buccafusca, Y.Kaneko, N.Itagaki, and R.Shioda, "Optical Sampling Reveals Details of Very High Speed Fiber Systems," pdf document, Agilent Technologies, www.agilent.com, 2004.

[25] B.C.Thomsen, L.P.Barry, J.M.Dudley, and J.D.Harvey, "Ultra sensitive all-optical sampling at $1.5\mu m$ using waveguide two-photon absorption," *Electronics Letters*, vol. 35, no. 17, pp. 1483–1484, 1999.

[26] Y.Tanaka, N.Sako, S.Imoto, and T.Kurokawa, "Profilometry Using Optical Microwaves With Different Carrier Frequencies and Two-Photon Absorption Process of Photodetector," *IEEE Photonics Technology Letters*, vol. 17, no. 12, pp. 2682–2684, 2005.

[27] B.C.Thomsen, L.P.Barry, J.M.Dudley, and J.D.Harvey, "Ultrahigh speed all-optical demultiplexing based on two-photon absorption in a laser diode," *Electronics Letters*, vol. 34, no. 19, pp. 1871–1872, 1998.

[28] T.Hori, N.Nishizawa, M.Yoshida, and T.Goto, "Cross-correlation measurement without mechanical delay scanning using electronically controlled wavelength-tunable femtosecond soliton pulse," *Electronics Letters*, vol. 37, no. 17, pp. 1077–1078, 2001.

[29] G. P. Agrawal, *Fiber-Optic Communication Systems*. Academic Press, 1st ed., 1997. ISBN 0-471-17540-4.

[30] P.J.Maguire, L.P.Barry, T.Krug, M.Lynch, A.L.Bradley, J.F.Donegan, and H.Folliot, "Simulation of a high-speed demultiplexer based on two-photon absorption in semiconductor devices," *Optics Communications*, vol. 249, no. 4-6, pp. 415–420, 2005.

[31] Z. Ruikang, Z. Yuan, Z. Wei, X. Yingqiang, D. Yun, H. Yongqing, R. Xiaomin, N. Zhichuan, and W. Ronghan, "Angular dependent characteristics of a 1.3- mu m gainnas/gaas quantum-well resonant cavity enhanced photodetectors," *Microwave and Optical Technology Letters*, vol. 34, no. 5, pp. 333–336, 2002.

[32] M. Unlu and S. Strite, "Resonant cavity enhanced photonic devices," *Journal of Applied Physics*, vol. 78, no. 2, pp. 607–639, 1995.

Resonance Tuning of Two-Photon Absorption Microcavities for Wavelength-Selective Pulse Monitoring

T. Krug, W. H. Guo, J. O'Dowd, M. Lynch, A. L. Bradley, J. F. Donegan, P. J. Maguire, L. P. Barry, and H. Folliot

Abstract—We show the potential use of a single photodetector for multichannel pulse monitoring. Two-photon absorption in a microcavity structure is used as the nonlinear optical technique for pulse monitoring. Angle tuning of the device allows the resonance to be tuned. For the device studied here that is optimized for 2-ps pulses, a possible tuning range of 55 nm is shown.

Index Terms—Cavity resonator filters, cavity resonators, demultiplexing, detectors, photodetectors, tuning, wavelength-division multiplexing (WDM).

I. INTRODUCTION

MULTIWAVELENGTH detectors for ultrafast pulse monitoring in dense wavelength-division-multiplexing (DWDM) systems are in high demand due to rapid progress of high-capacity optical networks. The precise measurement of a signal pulse with high spectral and temporal resolution is an important requirement for realizing >100-Gb/s optical transmission in the near future. Two-photon absorption (TPA) in semiconductors as an optical nonlinear effect is an attractive candidate for optical autocorrelation of short pulses and all-optical switching and sampling of high-speed optical data signals in optical time-division-multiplexed systems [1], [2]. In this letter, we demonstrate a simple approach for accurately detecting different wavelengths in a DWDM system using a single detector. The addressed detector is a TPA microcavity, optimized for 2-ps pulses as this is the pulsewidth available from our pulse source. The TPA detector can be optimized for the pulsewidth of any particular system by adjusting the cavity finesse [3]. Such a detector will find use in 160-Gb/s communications systems which operate with 2-ps pulses. The enhancement of the TPA-induced photocurrent (by a factor of 10 000) due to the cavity finesse greatly improves the sensitivity and enables the implementation of the TPA microcavity as a practical monitoring element in high-speed optical systems characterized by low peak power pulses [4]. The cavity nature of the device allows the resonance frequency to be tuned as a

function of angle [5]. Therefore, each channel, corresponding to a different wavelength, in a 160-Gb/s DWDM system can be selected by angle tuning the TPA microcavity. The resonance wavelength is a maximum at normal incidence and the resonance of the optical sampling system can be tuned to lower wavelengths over a wide wavelength range.

II. EXPERIMENTAL SETUP

The TPA microcavity structure, performance, response, and use as an single wavelength autocorrelator has been described in detail previously [6]. This letter addresses specifically the angle dependent TPA response and potential use in DWDM systems. Our experimental setup allowed us to tune the incident angle of the light on the device from minus to plus 45° with respect to normal incidence. The angle tuning was done in the $z - x$ plane and rotational symmetry around the growth axis of the device was assumed. The light was focused onto the device using a 0.20-NA lens. Using such a lens, the angle contribution due to the focusing effect is smaller than the acceptance angle of the microcavity device. The diameter of the focused beam waist was about 5 μm. The generated TPA photocurrent was measured using a standard lock-in amplifier technique.

III. MODELLING AND EXPERIMENTAL RESULTS

Using the transfer matrix model (TMM), we have analyzed the reflection and transmission spectrum of our microcavity structure. The total phase shift ψ inside the cavity for one round-trip is the important quantity, which determines the resonance behavior of the TPA cavity. We outline a novel approach below in which analytic expressions are an approximation to the TMM for the cavity layout and are presented in order to clearly compare the experimental results with theoretical predictions, as well as to extrapolate the signal TPA response beyond the experimentally available range. It is also worth noting that this analytic treatment has been compared with the results of the TMM approach and good correspondence between the two approaches has been found for simple cavity structures. For the modeling results in Figs. 1–3, the numerical results for the two models are within 1%. For a plane wave incident at angle θ onto the planar microcavity, the TPA inside the cavity can approximately be expressed as

$$A_{\text{TPA}} \approx \beta I_{\text{in}}^2 \varsigma F^2 \cos^2(\theta) \tag{1}$$

where β is the TPA coefficient, I_{in} is the intensity of the incident plane wave, ς is the TPA enhancement factor for the plane

wave of normal incidence with the wavelength equal to λ_0, the resonant cavity wavelength at normal incidence, and

$$F = [1 + 2R(1-R)^{-2}[1 - \cos(\psi)]]^{-1} \quad (2)$$

where $R = (R_t R_b)^{1/2}$, $R_{t,b}$ is the reflectivity of the top/bottom quarter-wavelength Bragg mirror, and

$$\psi(\lambda, \theta) = 4\pi \lambda^{-1} d \sqrt{n_a^2 - \sin^2(\theta)} + \phi_t(\lambda, \theta) + \phi_b(\lambda, \theta) \quad (3)$$

where d and n_a are the active layer thickness and the active layer refractive index, respectively, λ is the incident wavelength on the device; $\phi_{t,b}$ is the phase shift of the front/back distributed Bragg reflection (DBR). The equation $\psi(\lambda, 0) = 2m\pi$ determines the cavity mode wavelength at normal incidence, λ_0. As the active refractive index used is $n_a \approx 3$, for angles $\theta < 70°$ the term $\sin(\theta)/n_a^2$ is smaller than 0.1 and we use the following approximation: $(n_a^2 - \sin^2(\theta))^{1/2} \approx n_a - \sin^2(\theta)/2n_a$. The same approximation has been used to calculate the phase shift of the front/back DBR. As the incident wavelength deviates from λ_0 or the incident angle deviates from the normal incidence, we have the phase shift ψ deviating from $2m\pi$ by

$$\Delta\psi \approx -\frac{4\pi n_a d}{\lambda_0^2}\Delta\lambda - \frac{2\pi d}{\lambda_0 n_a}\sin^2(\theta) + \Delta\phi_t + \Delta\phi_b \quad (4)$$

where the refractive index dispersion is neglected and

$$\Delta\phi_{t,b} \approx -\frac{4\pi D_{t,b}^\lambda}{\lambda_0^2}\Delta\lambda - \frac{2\pi D_{t,b}^\theta}{\lambda_0}\sin^2(\theta) \quad (5)$$

where $D_{t,b}^{\lambda,\theta}$ is in units of length and is determined by the DBR structure. In the approximation of the limiting case where the number of the DBR mirror pairs goes to infinity, we have

$$D_t^\lambda = D_b^\lambda = \frac{n_l \lambda_0}{4(n_h - n_l)} \quad (6a)$$

$$D_t^\theta = D_b^\theta = \frac{\lambda_0}{4(n_h^2 - n_l^2)}\left(\frac{n_h}{n_l} + \frac{n_l^2}{n_h^2}\right) \quad (6b)$$

where the refractive index dispersion is also neglected, $n_{h,l}$ is the high/low refractive index of the composition material of the DBRs. This approximation is used because we consider a cavity with high finesse and a large number of DBR mirror pairs. Combining (4) and (5) we obtain

$$\Delta\psi \approx -\frac{4\pi(n_a d + D_t^\lambda + D_b^\lambda)}{\lambda_0^2}\Delta\lambda$$
$$- \frac{2\pi\left(dn_a^{-1} + D_t^\theta + D_b^\theta\right)}{\lambda_0}\sin^2(\theta)$$
$$\equiv -\frac{4\pi D^\lambda}{\lambda_0^2}\Delta\lambda - \frac{2\pi D^\theta}{\lambda_0}\sin^2(\theta). \quad (7)$$

The case $\Delta\psi = 0$ determines the modification of the cavity mode wavelength at the incidence angle of θ. According to (7), we have

$$\Delta\lambda = -\frac{D^\theta \lambda_0}{2D^\lambda}\sin^2(\theta) \quad (8)$$

which clearly shows that the modification of the cavity mode wavelength is proportional to $\sin^2(\theta)$ and the larger the angle of incidence, the shorter the resonant wavelength.

Fig. 1 shows the resonant wavelength of the TPA microcavity as a function of incident angle. The resonant wavelength at normal incidence for this device was 1.512 μm. By rotating
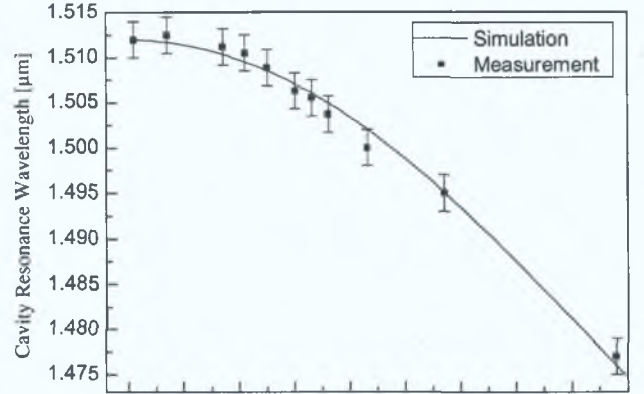
Fig. 1. Peak TPA response wavelength of the microcavity versus the incident angle, measurement, and simulation. Cavity resonance at normal incident is 1512 nm.

the TPA microcavity by an angle θ, the resonant wavelength changes, in accordance with (8). The agreement between (8) and the experimental results is excellent for θ up to 45°. A tuning range of 35 nm is achieved by rotating the TPA microcavity over 45°. Angle tuning beyond 45° is possible but we were limited to 45° by the range of our rotation stage. Extrapolating these results to a DWDM system a TPA microcavity with a normal incidence resonance at 1565 nm would, therefore, be able to scan over the entire C-band (1530–1565 nm) for an angular range of 45°. In a potential 160-Gb/s system, the 2-ps pulsewidth will result in 5-nm spacing between channels to prevent crosstalk. Thus, the microcavity structure would allow seven channels to be monitored with the same detector. In a customized setup tuning over 60° would certainly be possible corresponding to a channel selection bandwidth of 55 nm. This would, for instance, allow for tuning into the L-band beyond 1570 nm. Again with a channel spacing of about 5 nm, this would allow for approximately 11 channels with 2-ps pulses at 160 Gb/s to be monitored.

For the factor F in (1), we can make the following approximation by using (7):

$$F \approx [(1-R)^2 + R\Delta\psi^2]^{-1} = R$$
$$\times \left\{\left(\frac{1-R}{\sqrt{R}}\right)^2 + \left[\frac{4\pi D^\lambda}{\lambda_0^2}\Delta\lambda + \frac{2\pi D^\theta}{\lambda_0}\sin^2(\theta)\right]^2\right\}^{-1}. \quad (9)$$

It can be seen that F has a Lorentzian lineshape if $\Delta\lambda$ or $\sin^2(\theta)$ is taken as the argument. Under the condition of normal incidence but varying the incident wavelength, F as a function of λ has a full-width at half-maximum (FWHM) of

$$\lambda_{\text{FWHM}} = \frac{1-R}{\sqrt{R}}\frac{\lambda_0^2}{2\pi D^\lambda} \quad (10)$$

which is just the linewidth of the cavity reflection or transmission spectrum. If the incident wavelength is kept as λ_0 but the incident angle increases, F as a function of $\sin^2(\theta)$ has an FWHM of

$$[\sin^2(\theta)]_{\text{FWHM}} = \frac{1-R}{\sqrt{R}}\frac{\lambda_0}{\pi D^\theta} = \frac{2D^\lambda}{D^\theta \lambda_0}\lambda_{\text{FWHM}}. \quad (11)$$

The formula shows that the angle dependence is connected to the cavity bandwidth. This dependence is shown in Fig. 2, the TPA response decreases with increasing angle, and the FWHM of the angular response of the TPA device for a constant wavelength λ_0
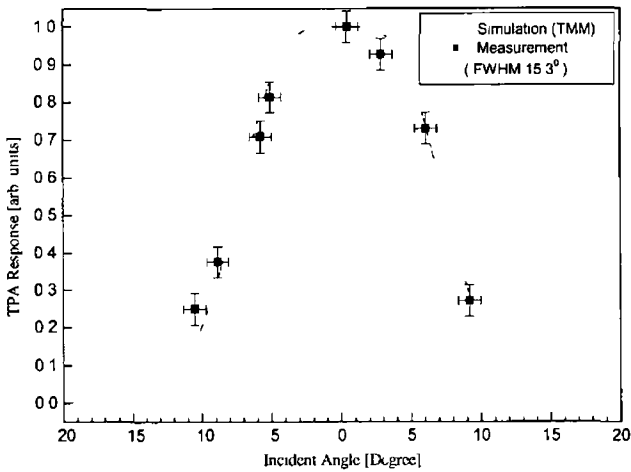
Fig 2   Simulated and measured results for the TPA response at fixed resonance wavelength as a function of angle   If normally incident the resonance wavelength is 1512 nm and the FWHM of the reflectivity spectrum is 4 nm
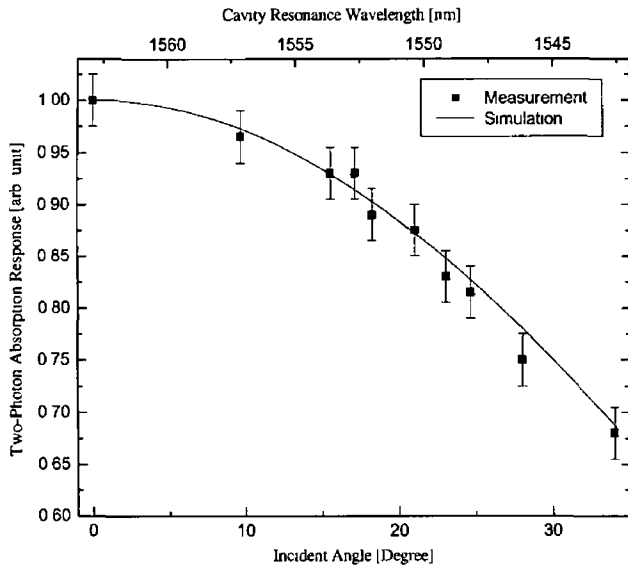
Fig 3   Peak TPA response as a function of cavity resonance wavelength and incident angle   Cavity resonance at normal incidence is 1566 nm

is 15 3°   These analytic results agree well with the simulations based on plane waves using the full TMM approach   From (1), it can also be seen that the TPA inside the cavity is dependent on F squared, e g , if F drops to $1/\sqrt{2}\,F$, the corresponding width is 64% of its original value given by (10)   Fig 3 shows the dependence of the peak TPA response at the resonance wavelength

on the tuning angle   Here a different sample has been used with a cavity resonance for normal incident of 1566 nm   The TPA response at cavity resonance frequency for an incident angle of 45° should be half that of the TPA response at normal incident   This is expected from (1), which indicates that if the resonance conditions are always satisfied as the incident angle increases, i e , $\Delta\psi = 0$, the TPA will drop as $\cos^2(\theta)$ The measured electronic signals for different wavelengths in a multichannel WDM system could be accordingly amplified and/or normalized for further analysis as the $\cos^2(\theta)$ functional variation is straightforward   Experimental data at angles greater than 35° is not available due to mode hopping in the source laser below 1540 nm   Excellent agreement between the predicted and measured values is obtained over the 35° range which could be measured

IV CONCLUSION

We have demonstrated the practicality of a TPA microcavity structure for pulse characterization measurements at a range of wavelengths   This form of pulse monitoring technique lends itself to convenient experimental implementation in DWDM   Since TPA is a nonphasematched process, pulse characterization can be performed over a wide wavelength range (>50 nm) with a single detector by simply exploiting the angular response of the microcavity

REFERENCES

[1]   Y Takagi   Simple autocorrelator for ultraviolet pulse width measurements based on the nonlinear photoelectric effect   *Appl Opt* vol 33 no 27 pp 6328–6332 1994
[2]   B C Thomsen   L P Barry   J M Dudley and J D Harvey   Ultra sensitive all optical sampling at 1 5 μm using waveguide two photon absorption ' *Electron Lett* , vol 35 pp 1483–1484 1999
[3]   H Folliot M Lynch L P Barry, A L Bradley L A Dunbar J Hegarty, J F Donegan J S Roberts and G Hill   Two photon absorption pho tocurrent enhancement in bulk AlGaAs semiconductor microcavities   *Appl Phys Lett* vol 80 pp 1328–1330 2002
[4]   P J Maguire L P Barry T Krug M Lynch A L Bradley J F Donegan and H Folhot   All optical sampling utilising two photon absorption in semiconductor microcavity   *Electron Lett* vol 41 no 8 pp 489–490 2005
[5]   N E J Hunt E F Schubert and G J Zydzik   Resonant cavity p i n photodetector utilizing an electron beam evaporated Si/SiO2 microcavity   *Appl Phys Lett* vol 63 no 3 pp 391–393 Jul 1993
[6]   T Krug M Lynch A L Bradley J F Donegan L P Barry J S Roberts and G Hill   High sensitivity two photon absorption micro cavity autocorrelator   *IEEE Photon Technol Lett* vol 16 no 6 pp 1543–1545 Jun 2004

Simulation of a high-speed demultiplexer based on two-photon absorption in semiconductor devices

P.J. Maguire [a,*], L.P. Barry [a], T. Krug [b], M. Lynch [b], A.L. Bradley [b], J.F. Donegan [b], H. Folliot [c]

[a] *Research Institute for Networks and Communications Engineering, School of Electronic Engineering, Dublin City University, Glasnevin, Dublin 9, Ireland*
[b] *Semiconductor Optronics Group, Physics Department, Trinity College, Dublin 2, Ireland*
[c] *Laboratoire de Physique des Solides, INSA, Rennes, France*

Abstract

In this paper, we present a theoretical model of an all-optical demultiplexer based on two-photon absorption in a specially designed semiconductor micro-cavity for use in an optical time division multiplexed system. We show that it is possible to achieve error-free demultiplexing of a 250 Gbit/s OTDM signal (25 × 10 Gbit/s channels) using a control-to-signal peak pulse power ratios of around 30:1 with a device bandwidth of approximately 30 GHz.
© 2005 Elsevier B.V. All rights reserved.

1. Introduction

The future development of high capacity optical time division multiplexed (OTDM) networks will require a stable and ultra-fast switch for demultiplexing ultra-high bit rate signals [1]. The majority of all-optical switching techniques for OTDM take advantage of non-linear effects that are present in optical fibres and semiconductor devices. Since these non-linear effects occur on timescales in the order of a few femtoseconds they are ideal for high-speed switching. Two all-optical demultiplexers that are based on these non-linear effects are the non-linear optical loop mirror (NOLM) [2], based on the Kerr effect in optical fibres, and the terahertz optical asymmetric demultiplexer (TOAD) [2], based on the non-linearities associated with carrier depletion in semiconductor opti-

* Corresponding author. Tel.: +35317005884; fax: +35317005508.
E-mail address: maguirep@eeng.dcu.ie (P.J. Maguire).

cal amplifiers (SOAs). There are a number of factors that limit the performance of these devices for high-speed switching. The NOLM requires speciality fibre and precise control of the wavelength of the control and signal pulses around the zero dispersion wavelength, while the gain depletion in the SOA limits the control pulse width and thus may limit the maximum switching speed of the TOAD [3]. Due to these limitations, it is necessary to consider alternative optical non-linearities for ultra-fast switching. One such method is to use the non-linear optical-to-electrical process of two-photon absorption (TPA) in a semiconductor device to carry out all-optical switching at data rates above 100 Gbit/s [4,5]. The main difficulty with using the TPA effect for high-speed demultiplexing is its inherent inefficiency, however, we have recently undertaken work aimed at significantly enhancing the TPA response by using a micro-cavity device [6,7]. In this paper, we present a TPA micro-cavity device with enhanced TPA efficiency that may be used for high-speed demultiplexing, and we theoretically investigate an optical demultiplexer (based on TPA in a micro-cavity device) for use in an OTDM communication system. The main device parameters used in the model, such as the Two-Photon Absorption coefficient, are taken from results obtained from the characterization of a specially fabricated micro-cavity sample received. Using this model, the operation of the demultiplexer is examined when various system parameters are varied.

2. TPA micro-cavity device

As already mentioned, the TPA process is a very inefficient, non-linear process. In order to utilise this non-linearity, high optical intensities are required, which makes it unsuitable for applications, such as optical sampling and switching, in high-speed telecommunications networks. One possible way to overcome this efficiency problem is to use a Fabry–Perot micro-cavity to greatly enhance the optical intensity by increasing the interaction length in the device. It is hoped that such a simple and compact device will improve the TPA efficiency to a level that may enable the implementation of practical switching and sampling elements for high-speed optical systems.

The device that is specially fabricated for TPA at 1550 nm is a GaAs/AlAs PIN micro-cavity photodetector grown on a GaAs substrate. It comprises a 0.459 μm GaAs active region embedded between two GaAs/AlAs Bragg mirrors. The front p-doped (C $\sim 10^{18}$ cm^{-3}) mirror consists of 9 pairs while the back n-doped (Si $\sim 10^{18}$ cm^{-3}) mirror contains 18 pairs designed for reflectivity at 1550 nm. The device studied was a 100 μm diameter vertical structure [7,8]. The cavity lifetime of the device structure, taking into account the reflectivity of the Bragg mirrors, is in the order of 1 ps.

In order to initially characterize the device, a tunable mode-locked laser source, producing 1.5 ps pulses at 10 GHz over 100 nm wavelength range, was employed. Firstly, we performed a photocurrent measurement as a function of the incident optical power close to the cavity resonance (Fig. 1(a)). As clearly shown there is a square dependence of the photocurrent on the incident optical intensity, evidencing the TPA process. Fig. 1(b) shows how the cavity resonance response is dependent on the incident wavelength, with a cavity resonance of 1554 nm and a measured cavity linewidth of 5 nm.

3. Principle of TPA demultiplexer operation

The phenomenon of TPA is a non-linear optical-to-electrical conversion process where two photons are absorbed in the generation of a single electron–hole carrier pair [4]. The generated photocurrent is proportional to the square of the intensity, and it is this non-linear response that enables the use of TPA for optical switching. The demultiplexer uses optical pulses to switch out data from a single channel in a high-speed OTDM system via the TPA effect in a semiconductor device. The control pulses, which are at the repetition rate of the individual channels in the multiplex, are optically coupled together with the high-speed OTDM data signal and are incident on the device. The arrival time of the control pulses is varied using an optical delay line so that they arrive at the demultiplexer at a time corresponding to the
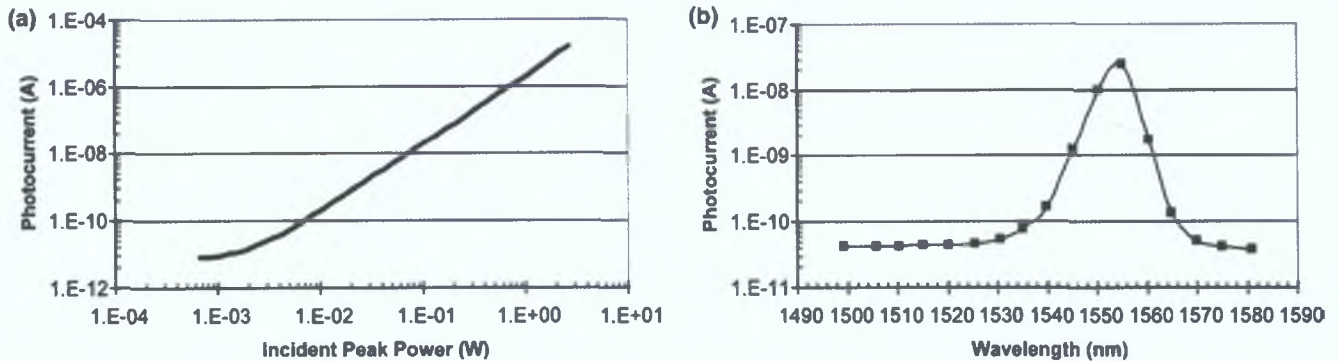
Fig. 1. (a) Photocurrent as a function of incident optical power (b) Micro-cavity resonance.

data pulse to be switched out (Fig. 2). The TPA effect in the semiconductor device leads to a delay-dependent response from the signal and the control pulses in the detector. Due to TPAs non-linear quadratic response, there is a strong contrast between the electrical TPA signal generated when the control and data pulses overlap on the detector and that generated when the adjacent channels arrive independently. The constant background signal due to the control pulse can be conveniently subtracted electrically, resulting in a high contrast demultiplexed output signal. Thus, the TPA demultiplexer is able to simultaneously carry out the process of channel selection and electrical detection in an OTDM communication system [4,5].

Since the generation of electron-hole pairs by the TPA effect is essentially instantaneous, the maximum switching speed is determined by the duration of the data and control pulses, allowing

Tbit/s data rates to become feasible [4]. It also allows for simpler optical alignment since it does not require phase-matching as required for applications utilizing non-linear crystals [9]. In addition, by making use of semiconductor micro-cavities [6,7], we can now overcome the problem of TPA inefficiency.

4. Simulation model

The purpose of the simulation is to determine how various system parameters affect the suitability of using a TPA device to switch a high-speed OTDM signal. The system parameters that are examined are as follows:

- Number of channels in the OTDM network.
- Ratio between the peak power of the control signal and data signal.
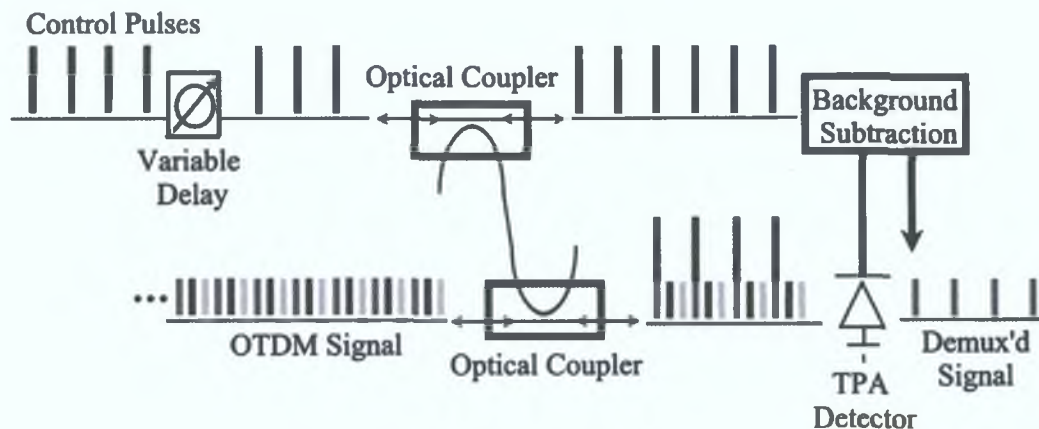
Fig. 2. Schematic of TPA Demultiplexing.

• Bandwidth of the TPA detector.

The model initially creates a certain number of channels, each consisting of a pseudo random bit stream (PRBS) with a pattern length of 2^7-1, which are then multiplexed together using optical pulses (representing the data bits) to create an OTDM data signal. The optical pulse width used was kept to one quarter of the bit period of the overall aggregate OTDM data rate in order to avoid interference in adjacent channels. The number of channels used and the data rate of each channel can be set in the model. The peak power of the data pulses can be set to a specific value with a fixed level of noise then added. This has the effect of limiting the optimum bit error rate (BER) that can be achieved by the system. The OTDM data signal is then combined with optical control pulses, which are at the repetition rate of the individual channels in the OTDM signal, with the control pulses synchronized with one of the OTDM channels. The duration of the control pulses is set to the same value as that of the signal pulses, and the peak power of the control pulses can be set to any value. The OTDM signal and the control pulses are then incident on the TPA detector. The TPA detector is modeled as described in [6]. For our model, we have chosen a single-photon absorption (SPA) coefficient (α) and a TPA coefficient (β) of 0.01 and 3×10^{-10} m/W, respectively, from measurements carried out in [9]. Fig. 3 is a theoretical plot of the photocurrent generated versus the optical intensity using the parameters taken from experiments carried out on the devices fabricated. This plot clearly shows that the non-linear TPA response is limited on the lower side by single-photon absorption and on the higher side by total absorption. This gives the dynamic range (~40 dB) over which the TPA affect can be used for high-speed switching.

The TPA model also takes into account the bandwidth of the TPA detector. As previously mentioned, the TPA effect (generation of electron-hole pairs) is essentially instantaneous which allows any overall data rate possible and is limited only by the duration and jitter of the optical pulses used for the signal and control, and the cavity lifetime of the device (which is dependent on the
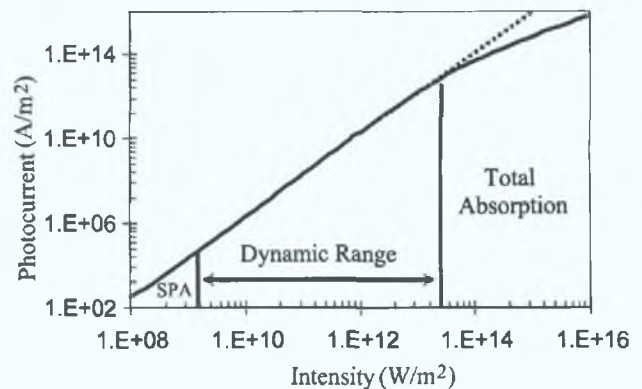
Fig. 3. Simulation of the output photocurrent density as a function of the input optical power density for $\alpha = 0.01$ cm^{-1} and $\beta = 3 \times 10^{-10}$ m/W.

reflectivity of the Bragg mirrors [8]). However, the extraction of the carriers (current produced) is affected by the carrier lifetime of the micro-cavity, which affects the maximum data rate of the individual channels in OTDM signals. Therefore, the bandwidth of the TPA detector will be restricted by the carrier lifetime of the device. The minimum bandwidth required to temporally demultiplex one channel from the overall OTDM signal is 10 GHz, assuming that the individual channel data rate is 10 Gbit/s. However, even with this bandwidth, noise will be introduced on the demultiplexed channel from the electrical signals generated by the other OTDM channels that are not synchronized with the control pulse. To overcome this limitation, it may be necessary to have a large control-to-signal ratio which will increase the contrast ratio between the detected channel synchronized with the control, and unsynchronized channels, and thus increase the signal-to-noise ratio (SNR) of the demultiplexed channel. By increasing the bandwidth of the device, the noise contribution from the other OTDM channels is reduced. As can be seen, it is vitally important to consider all the parameters in order to achieve optimum performance.

The simulation model finally calculates the optical bit-error-rate (OBER) of the signal before the detector and the electrical bit-error-rate (EBER) after the TPA based demultiplexer. The overall goal is to determine the operating characteristics such that EBER of the demultiplexed/detected signal is the same as the OBER of the signal before

the TPA detector, indicating that the demultiplexing process is not introducing additional errors. The OBER takes into account any initial noise introduced by the transmitter in the system and is calculated from the signal power and the noise power inputted at the start of the simulation. From the resulting SNR, the OBER is calculated [10]. The EBER on the other hand takes into account noise introduced by the demultiplexing process. In order to calculate the EBER, the TPA photocurrent generated by the incident optical signal is first determined, taking into account the optical noise already present on the signal. The photocurrent takes into account the band gap of the device, which is optimized for TPA, the length of the detector (100 μm as per the sample fabricated) and the SPA and TPA coefficients [6]. Next, the thermal noise introduced by the detector and the accumulated channel noise is added to the signal. The amount of thermal noise is user defined. The accumulated channel noise takes into account the other channels not synchronized with the control pulse and arises due to the demultiplexing process being dependent on the bandwidth of the detector. Once the noise has been added, the resultant electrical signal is compared to a threshold value, and assigned a bit value. This bit value is then compared to the original PRBS signal and the number of errors determined, resulting in the EBER.

5. Simulation results

The initial parameter that was investigated was the ratio of the control-to-signal pulse power, and we examined how this parameter affected system performance as a function of the number of channels multiplexed together. The number of channels were varied from 25 to 100, with a data rate of 10 Gbit/s per channel (250 Gbit/s to 1 Tbit/s aggregate OTDM data rates). The signal peak power was kept constant at 80 mW, and the detector bandwidth was set to 10 GHz, the minimum required to prevent ISI between adjacent data bits in the demultiplexed channel. Fig. 4 illustrates the received BER vs. control- to-signal ratio as the number of channels is varied. It can be clearly
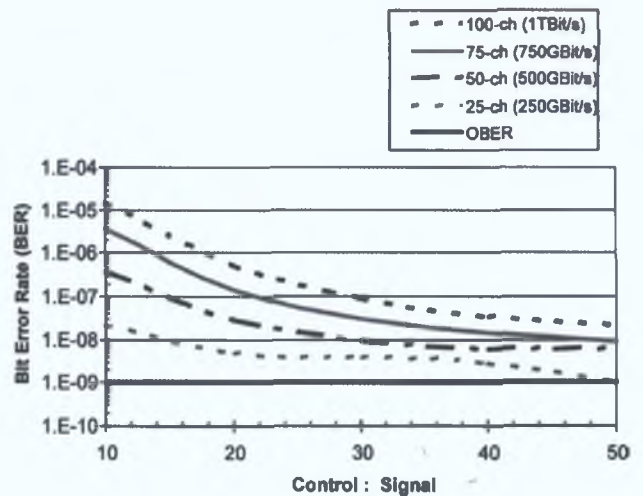
Fig. 4. BER vs. control-to-signal power as the number of channels (with base rate of 10 Gbit/s per channel) is varied.

seen that as the control-to-signal ratio is increased, the EBER approaches the OBER. This occurs due to the fact that as the control-to-signal peak power ratio is increased, the contrast ratio between the data signal synchronized with the control pulse and those not synchronized widens. Thus, the noise level added to the demultiplexed signal, due the detection of all the adjacent channels, is reduced as the control-to-signal ratio increases. This improves the resultant SNR, and improves the BER of the received signal. For a given control-to-signal ratio, the BER is degraded as more channels are added to the system, due to the increased noise from these added channels on the received signal. It is worth noting that for the 25-channel system (250 Gbit/s aggregate OTDM data rate), the EBER reached the OBER for a control to signal ratio beyond 50:1, corresponding to a control pulse peak power of 4 W. During the initial characterization of the micro-cavity samples that were fabricated, a maximum peak optical power of 20 W was applied to the device without any damage being incurred. This suggests that a control pulse peak power of 4 W is well within the operating range of the micro-cavity structure, even if it is slightly large for practical applications.

We subsequently went on to examine how the bandwidth of the TPA detector affected its operation as a demultiplexer in an OTDM system. Once again we plot the BER as function of the control-to-signal ratio, but this time we also vary the band-
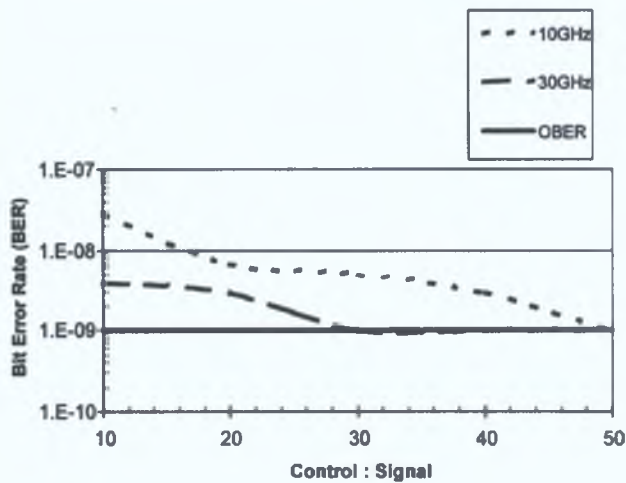
Fig. 5. BER vs. control-to-signal power as the temporal response is varied for a 250 Gbit/s (25 channel × 10 Gbit/s) OTDM System.

width of the device. These results are presented in Fig. 5, and it should be noted that a 25-channel system is employed (250 Gbit/s aggregate OTDM data rate), as this was the only one that gave optimum performance at a reasonable control-to-signal ratio. As the bandwidth is increased, the BER of the received signal is improved. This is attributed to the fact that as the bandwidth is increased the number of adjacent channels that add noise to the detected channel decreases, thus improving the received BER. This allows a smaller control-to-signal ratio to be used to offer the same overall performance. For a 25-channel system, a bandwidth of 30 GHz allows us to obtain good performance with a control-to-signal ratio of around 30:1. From recent experimental work carried out on the characterization of the micro-cavities, the device bandwidth of the 100 μm sample was determined to be 1 GHz. It is hoped that with smaller device size, an improved cavity design and the use of high-speed packaging, the device bandwidth can be improved. As the device is based on a PIN structure, bandwidths in excess of 10 GHz should be readily feasible.

6. Conclusion

We have modeled the performance of a TPA based demultiplexer in an OTDM communication system. The performance of the demultiplexer was evaluated by comparing the electrical BER (EBER) of the demultiplexed/detected channel after the detector to the optical BER (OBER) of the signal before the demultiplexer. Our results have shown how the ratio of the control-to-signal pulse power, number of OTDM channels, and bandwidth can affect the performance of a TPA based demultiplexer for use in a practical OTDM system. Using the parameters, we have chosen for the TPA device, (including SPA coefficient, TPA coefficient, and temporal response) which we have taken for measurements of newly developed samples, we have shown that it should be possible to achieve error-free demultiplexing of a 250 Gbit/s OTDM signal (25 × 10 Gbit/s channels), using a control-to-signal ratio of around 30:1, for a TPA device with a bandwidth of 30 GHz. By further optimizing the existing cavity design, it is hoped that the device can be further improved to allow for the successful demultiplexing of higher-speed data signals approaching 1 Tbit/s.

References

[1] D.M. Spirit, A.D. Ellis, P.E. Barnsley, IEEE Commun. Mag. 32 (1994) 56.

[2] M. Saruwatari, IEEE J. Sel. Top. Quant. 6 (2000) 1363.

[3] G.P.Agrawal, Applications of Non-linear Fiber Optics, first ed. vol. 135, Academic Press, New York, 2001.

[4] B.C. Thomsen, L.P. Barry, J.M. Dudley, J.D. Harvey, Electron. Lett. 34 (1998) 1871.

[5] B.C. Thomsen, J.D. Harvey, J.M. Dudley, L.P. Barry, in: Conference on Optical Fiber Communications, Technical Digest Series Anaheim, USA, vol. 54, 2001, WO2/1–WO2/3.

[6] H. Folliot, M. Lynch, A.L. Bradley, T. Krug, L.A. Dunbar, J. Hegarty, J.F. Donegan, L.P. Barry, J. Opt. Soc. Am. B 19 (2002) 2396.

[7] L.P. Barry, P. Maguire, T. Krug, H. Folliot, M. Lynch, A.L. Bardley, J.F. Donegan, J.S. Robert, and G. Hill, in: Lasers and Electro-Optics Society Annual Meeting-LEOS, Conference Proceedings Glasgow, vol. 2, 2002, p. 839.

[8] T. Krug, M. Lynch, A.L. Bradley, J.F. Donegan, L.P. Barry, H. Folliot, J.S. Roberts, G. Hill, IEEE Photonic. Tech. L. 16 (2004) 1543.

[9] T. Hori, N. Nishizawa, M. Yoshida, T. Goto, Electron. Lett. 37 (2001) 1077.

[10] G.P.Agrawal, Fiber-Optic Communication Systems, second ed., vol. 175, Wiley, New York, 1997.

High-Speed Measurement of 100GHz Optical Pulse Train via Two-Photon Absorption in a Semiconductor Microcavity

P.J.Maguire and L.P.Barry, T.Krug, J.O'Dowd, M.Lynch, A.L.Bradley, and J.F.Donegan, and H.Folliot

Abstract— This paper presents a highly-efficient all-optical sampling technique based upon the nonlinear optical-to-electrical conversion process of Two-Photon Absorption (TPA) in a semiconductor microcavity. By incorporating a microcavity design, the TPA response is enhanced to allow the successful real-time measurements of optical pulses at repetition rates in excess of 100GHz, with a temporal resolution of approximately 1ps, and a system sensitivity of $0.35mW^2$

Index Terms— Optical Time Division Multiplexing (OTDM), Optical Signal Processing, Optical Sampling, Two-Photon Absorption (TPA), Microcavity

Fig. 1. Schematic of Microcavity Device Structure

I. INTRODUCTION

Future Optical Time Division Multiplexed (OTDM) networks operating at aggregate data rates in excess of 100Gbit/s will require a sensitive and ultra-fast method for precise signal characterisation [1], [2]. The standard way of measuring high-speed signals involves using a fast photodetector in conjunction with a high-speed oscilloscope. However, this method is limited to a maximum data rate of around 40Gbit/s. Therefore in order to monitor signals at data rates of 100Gbit/s and beyond, it is necessary to employ all-optical sampling techniques based on optical nonlinearities. Nonlinear optical effects that are present in fibres, crystals and semiconductors, are ideal for optical sampling as these occur on timescales in the order of a few femtoseconds ($10^{-15}s$). One such nonlinearity is the optical-to-electrical conversion process of Two-Photon Absorption (TPA) in semiconductors [3].

TPA occurs when a photon of energy E_{ph} is incident on the active area of a semiconductor device with a bandgap exceeding E_{ph} but less than $2E_{ph}$, and results in two photons being simultaneously absorbed to generate a single electron-hole pair [3]. The generated photocurrent is proportional to the square of the intensity, and it is this nonlinear response that enables the use of TPA for optical sampling. One of the main difficulties associated with employing TPA is its inherent inefficiency, meaning that either high optical intensities, or a very long detector, are required making it unsuitable for high-speed telecommunications applications.

One way to overcome this is employ a specially designed semiconductor microcavity as a TPA detector. By placing the active materials within a microcavity structure, the interaction length within the device is increased, enhancing the optical intensity within the device. The TPA photocurrent produced can be increased by up to four orders of magnitude [4], allowing the development of practical sampling and switching
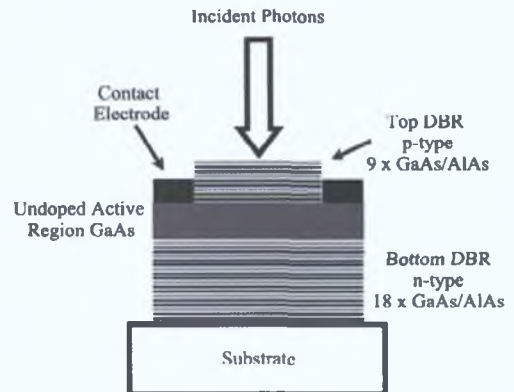
elements for high-speed optical communications. Previous work has already demonstrated the suitability of using TPA in a semiconductor microcavity for autocorrelation [5], switching [6] and sampling [7] applications. The aim of this work is to carry out real-time measurements of optical pulses at a repetition rates in excess of 100GHz.

II. TPA BASED OPTICAL SAMPLING

The specially fabricated devices are shown in Figure 1 and have been optimised for TPA performance using optical pulses with durations in the region of 1ps in the 1550nm wavelength region. The microcavity consists of two GaAs/AlAs distributed Bragg reflectors (DBR) surrounding an undoped GaAs active region. The active region is 460nm thick with a bandgap energy of 1.428eV. The mirrors consist of alternating 134.3nm AlAs and 115.7nm GaAs layers, with the top p-doped (C≈ $10^{18}cm^{-3}$) mirror consisting of 9 periods of AlAs/GaAs with the bottom n-doped (Si≈ $10^{18}cm^{-3}$) mirrors consisting of 18 periods of AlAs/GaAs. The device studied was a 100μm diameter vertical structure, with a cavity lifetime, taking into the account the reflectivity of the Bragg mirrors, in the order of 1ps [5]. It is possible to design the microcavity mirrors the match to cavity lifetime to the pulsewidth, therefore allowing the maximum enhancement of the TPA photocurrent generated. The vertical orientation of the devices and relatively large area allows for significant cost saving in the growth process and easier coupling of light when compared to waveguide TPA structures [5]. During the initial characterisation of the fabricated devices, a plot of the TPA photocurrent generated

versus incident optical wavelength around the microcavity resonance was carried out which showed a cavity resonance of 1554nm and a measured cavity linewidth of 5nm [7]. A photocurrent measurement against incident optical power close to the cavity resonance was also carried out. It showed that there was a square dependence of the photocurrent against the incident optical intensity evidencing the TPA process. It has been theoretically proven [6] that the dynamic range extends over 40dB, with limitations due to single-photon absorption on the lower side and total absorption on the higher side.

For TPA optical sampling, the duration of the sampling pulse $[I_{sam}(t - \tau)]$ must be significantly shorter than the optical signal pulse $[I_{sig}(t)]$ under test. The signal and sampling pulses are then incident on the microcavity, with the electrical TPA signal generated [i(t)] measured as a function of the sampling delay τ, resulting in an intensity cross-correlation measurement between I_{sam} and I_{sig} [8]. For practical implementation, the sampling pulse has a shorter duration and higher peak intensity than the signal pulse, with the measured signal representing the signal pulse waveform on a constant background [8]. The sampling delay τ is generated by operating the sampling frequency (f_{sam}) slightly detuned from a harmonic of the signal frequency (f_{sig}). This allows the sampling pulse to be automatically swept across the signal pulse at a scan frequency that is low enough to be directly detected and displayed on a standard high-impedance oscilloscope without the need for high-speed electronics or lock-in amplifier. The sampling frequency is calculated using [8]:

$$f_{sam} = \frac{f_{sig}}{n + \delta} \tag{1}$$

where n is an integer and $\delta << 1$. This results in a scan frequency of:

$$f_{scan} = f_{sig}\frac{\delta}{\delta + n} \tag{2}$$

which can be easily displayed on a standard high-impedance oscilloscope.

III. Experimental Setup

The experimental setup is shown in Figure 2, and consists of two tunable optical pulse sources. The signal pulse (I_{sig}) is generated using a 10GHz u2t TMLL 1550 pulse source,(pulse duration $\approx$ 2ps, tunable wavelength range of 1480-1580nm). A Calmar Optcom Femtosecond Pulse Laser (pulse duration 500fs, jitter < 140fs, tunable wavelength range 1548-1558nm) was used to provide the sampling pulse (I_{sam}). Both sources were tuned to the resonance wavelength of the TPA microcavity (1554nm), and were phase locked together via the 10MHz reference signal provided by the signal generators and the Phase Lock Loop (PLL) input to the Calmar source. The repetition rate of the signal pulse (f_{sig}) was set to 9.998991GHz with the sampling pulse (f_{sam}) operating at 9.998992MHz. This results in a scan frequency (f_{scan}) of 1kHz which can be easily displayed on a standard high-impedance oscilloscope. The signal pulse train was first amplified using a low-noise Erbium Doped Fibre Amplifier (EDFA) before entering a passive delay line multiplexer which
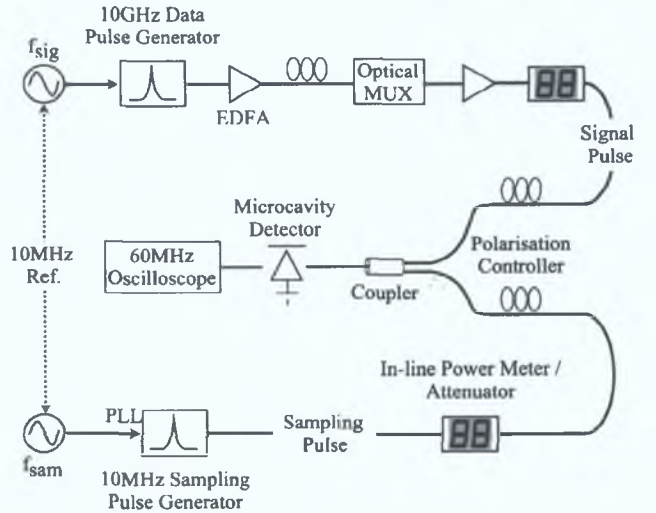
Fig. 2. Experimental setup of TPA-based optical sampling using a semiconductor microcavity

consists of a number of independently switch-able stages. Using the passive multiplexer a 100GHz optical pulse stream was obtained, which was then amplified again with a second EDFA to overcome the 18dB insertion loss associated with the multiplexer. The sampling and the signal pulses then pass through in-line power meters/attenuators and polarisation controllers before being recombined at a coupler. The power meters allow easy power measurement and attenuation of both pulse trains, while allowing the system sensitivity to be constantly monitored. The combined signals are then incident on the microcavity with the generated TPA photocurrent signal being displayed on a standard 60MHz high impedance digital oscilloscope.

IV. Experimental Results

Figure 3 (a) shows the real-time measurement of a single optical pulse as displayed on the high-impedance oscilloscope. The optical pulse duration was measured to be 2.5ps, with a pulse width of 2ps expected. This deviation is due to the temporal resolution of the sampling set up. The temporal resolution is defined as:

$$t_{res} = \sqrt{\tau_{cavity}^2 + t_{sam}^2 + j_{sam}^2} \tag{3}$$

and takes into account the cavity lifetime of the device (τ_{caity}= 1ps), which is dependent on the reflectivity of the Bragg mirrors, and the duration (t_{sam}=500fs) and jitter (j_{sam} <140fs) of the sampling pulse used.

This gives a minimum temporal resolution of 1.1ps. The average powers of the signal and sampling pulses used were 0.2mW and 0.12mW respectively. Figure 3 (b) displays the real-time measurement of a 100GHz (pulse separation 10ps) pulse train, with a signal average power of 0.17mW and sampling average power of 0.16mW. The variation in the amplitude of the optical pulses can be accounted for by the propagation of each pulse over a different transmission path within the passive delay line multiplexer. The sensitivity of
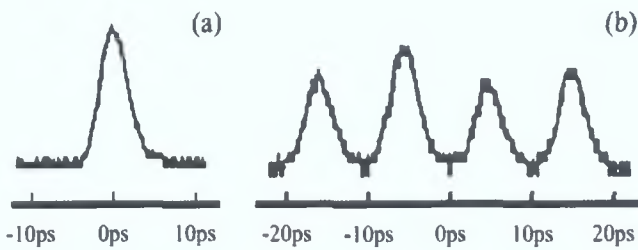
Fig. 3. Real-Time TPA Sampling Measurement of (a) Single Optical Pulse; (b) 100GHz Optical Pulse Train

the sampling system, which is defined as being the product of the peak power of the signal pulse and the average power of the sampling pulse [8] was calculated as $0.35mW^2$. This was obtained without any post-amplification of the TPA photocurrent and with the addition of a low-noise amplifier after the microcavity, further improvements in the sensitivity are expected.

V. CONCLUSION

This work has demonstrated the suitability of using TPA for optical sampling of data rates in excess of 100Gbit/s. By employing a semiconductor microcavity, the TPA efficiency has been enhanced to a level that would enable the implementation of a real-time sampling element using optical powers levels found in current optical communications networks. The system sensitivity is calculated to be $0.35mW^2$ (corresponding to a signal peak power of 5.6mW) and temporal resolution around 1ps. With the addition of a low-noise electrical amplifier after the TPA detector, further improvement in the system sensitivity can be achieved.

REFERENCES

[1] S. Kawanishi, "Ultrahigh-Speed Optical Time-Division-Multiplexed Transmission Technology Based on Optical Signal Processing," *IEEE Journal of Quantum Electronics*, vol. 34, no. 11, pp. 2064–2079, 1998.

[2] K.Kikuchi, F.Futami, and K.Katoh, "Highly sensitive and compact cross-correlator for measurement of picosecond pulse transmission characteristics at 1550nm using two-photon absorption in si avalanche photodiode," *Electronics Letters*, vol. 34, no. 22, pp. 2161–2162, 1998.

[3] F.R.Laughton, J.H.Marsh, D.A.Barrow, and E.L.Portnoi, "The Two Photon Absorption Semiconductor Waveguide Autocorrelator," *IEEE Journal of Quantum Electronics*, vol. 30, no. 3, pp. 838–845, 1994.

[4] H.Folliot, M.Lynch, A.L.Bradley, L.A.Dunbar, J.Hegarty, J.F.Donegan, L.P.Barry, J.S.Roberts, and G.Hill, "Two-photon absorption photocurrent enhancement in bulk algaas semiconductor microcavities," *Applied Physics Letters*, vol. 80, no. 8, pp. 1328–1330, 2002.

[5] T.Krug, M.Lynch, A.L.Bradley, J.F.Donegan, L.P.Barry, H.Folliot, J.S.Roberts, and G.Hill, "High-Sensitivity Two-Photon Absorption Microcavity Autocorrelator," *IEEE Photonics Technology Letters*, vol. 16, no. 6, pp. 1543–1544, 2004.

[6] P.J.Maguire, L.P.Barry, T.Krug, M.Lynch, A.L.Bradley, J.F.Donegan, and H.Folliot, "Simulation of a high-speed demultiplexer based on two-photon absorption in semiconductor devices," *Optics Communications*, vol. 249, no. 4-6, pp. 415–420, 2005.

[7] ——, "All-optical sampling utilising two-photon absorption in semiconductor microcavity," *Electronics Letters*, vol. 41, no. 8, pp. 489–490, 2005.

[8] B.C.Thomsen, L.P.Barry, J.M.Dudley, and J.D.Harvey, "Ultra sensitive all-optical sampling at $1.5\mu m$ using waveguide two-photon absorption," *Electronics Letters*, vol. 35, no. 17, pp. 1483–1484, 1999.

Self-Seeding of a Gain-Switched Integrated Dual-Laser Source for the Generation of Highly Wavelength-Tunable Picosecond Optical Pulses

P. Anandarajah, P. J. Maguire, A. Clarke, and L. P. Barry

Abstract—The authors demonstrate the generation of nearly transform-limited optical pulses that are wavelength tunable over almost 50 nm. The wide tuning range is obtained by self-seeding a gain-switched source containing two Fabry–Perot lasers, and employing a widely tunable Bragg grating in the feedback loop. The generated pulses exhibit Side-mode suppression ratios of 50 dB above and across the full tuning range.

Index Terms—Optical fiber communications, optical pulse generation, self-seeding, semiconductor laser, wavelength tunable.

I. INTRODUCTION

THE USE OF wavelength tunability as a means of providing dynamic provisioning, in next-generation photonic systems, is currently a key area that is attracting much attention [1]. This interest could be attributed to the convergence of data networking with multiwavelength optical networking, a natural outcome driven by the impending needs of the Internet. In addition to this development, current trends and technology maturity favor the deployment of optical communication systems, operating at line rates 40 Gb/s and beyond, thereby making it more likely that return-to-zero (RZ) coding be used for data transmission, as it is easier to compensate for dispersion and non-linear effects in the fiber by employing soliton-like propagation [2]. Taking into account these moves toward tunable optical systems employing RZ coding, it is obvious that the development of a wavelength tunable source of short optical pulses will be of paramount importance for future wavelength division multiplexed (WDM), optical time division multiplexed (OTDM), and hybrid WDM/OTDM optical communication systems [3].

One of the simplest and most reliable techniques available to generate wavelength-tunable picosecond optical pulses involves the self-seeding of a gain-switched Fabry–Perot (FP) laser, and many experimental schemes have been reported [4], [5]. Self-seeding entails the use of a wavelength selective external cavity to reinject a small fraction of the output light back into the gain-switched FP laser at only one longitudinal mode frequency. Provided that the optical signal reinjected into the laser arrives during the buildup of an optical pulse in the FP laser, then a single-moded output pulse is obtained. An important charac-
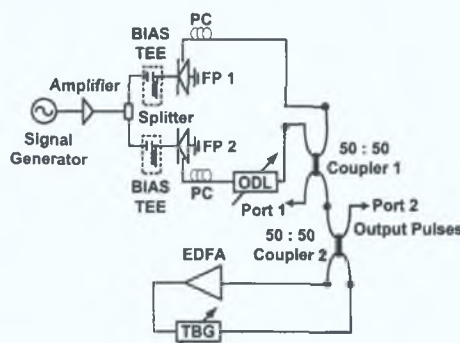
Fig. 1. Experimental setup for the generation of widely tunable optical pulses using the SSGS FP lasers.

teristic of these Self-Seeded Gain-Switched (SSGS) sources is the variation in the side-mode suppression ratio (SMSR) as the wavelength is tuned [6], as this may ultimately affect their usefulness in optical communication systems. In particular, recent work has demonstrated that, as the number of channels in a WDM system using SSGS pulse sources increases, the specifications on the required SMSR, due to cross-channel interference, may become very stringent [7]. It is thus likely that SMSRs in excess of 30 dB will be required for error-free operation of such systems.

Recent work in the development of wavelength tunable SSGS pulse sources has resulted in the generation of 90–130-ps optical pulses with SMSRs of around 32 dB that are tunable over 19–26 nm [8], [9]. The tunability of these systems was limited by factors such as the tunable range of the fiber Bragg grating (FBG) and the gain profile of the laser. In this letter, we show the generation of shorter pulses ($\sim$20 ps) that exhibit SMSRs greater than 50 dB over a tuning range approaching 50 nm. Our technique is based on the self-seeding of a gain-switched source containing two FP lasers, and the use of a widely tunable Bragg grating (TBG) filter. As we use two FP lasers with different gain curves, we can achieve a very large wavelength tuning range, and the high SMSR is essentially obtained by passing the self-seeded gain-switched pulses through the Bragg filter before the output.

II. EXPERIMENTAL SETUP

Fig. 1 illustrates the experimental configuration. It essentially consists of two gain switched FP laser diodes that are self-seeded using a single external cavity. The two FP lasers were chosen in such a way as to ensure that there was only

a very small overlap between their gain profiles, and finer placement of the gain profiles of the two lasers could be achieved by temperature controlling the diodes. The peak of the gain curve for FP 1 is at 1524 nm, while the peak of the gain curve for FP 2 is at 1561 nm. The incorporation of two gain-switched FP lasers enhances the wavelength tuning range that can be achieved using this self-seeding setup, as will be demonstrated below.

The FP lasers used were commercial 1.5-μm InGaAsP devices with threshold currents of approximately 26 mA, and mode spacings of 1.12 nm. Gain switching of both lasers was carried out by applying a dc-bias current of 17 mA and a 2.5-GHz sinusoidal modulation signal with a power of 29 dBm to both devices. The gain-switched output from both lasers were then coupled together before the composite signal was fed into an external loop cavity, which was used to self-seed both lasers. The external cavity contained a polarization controller (PC), a 3-dB coupler, a TBG (bandwidth: 0.23 nm, wavelength tuning range: 1460–1575 nm, rejection ratio: 40 dB, insertion loss: 5 dB) and an erbium-doped fiber amplifier (EDFA). An optical isolator in the EDFA ensures that light only propagates in one direction around the feedback loop, and the tunable filter eliminates unwanted amplified spontaneous emission from the EDFA in addition to selecting the laser mode to be seeded. The external cavity for self-seeding FP 2 also contains a tunable optical delay line (just at the output of the laser) to ensure that simultaneous self-seeding of FP 1 and FP 2 can be achieved. The EDFA in the external cavity is required to overcome the high losses obtained in the TBG (which has an insertion loss of approximately 5 dB across the tuning range and a very narrow linewidth compared to the spectral width (~63 GHz) of the modes from the gain-switched laser), and ensure that there is sufficient light reinjected into either laser to obtain suitable SMSRs on the output pulses.

To achieve optimum SSGS pulse generation, the Bragg grating was initially tuned to one of the longitudinal modes of the gain-switched FP-1 laser. The frequency of the modulation was then varied to ensure that the signal reinjected into the laser, from the external cavity, arrives as an optical pulse is building up in the laser. An operating frequency of 2.498 GHz was found to be suitable. The grating was then tuned to one of the longitudinal modes of FP 2 and, in this case, the tunable optical delay line was varied to ensure that the signal fed back into FP 2 arrives at the correct instant. The bias currents of FP 1 and FP 2 were then slightly changed to obtain the minimum pulsewidth. By subsequently tuning the grating across the gain curves of the lasers, we can achieve single-moded optical pulses over a very wide range of wavelengths. The output pulses, from the return arm of the second 50 : 50 fiber coupler (port 2) were characterized using a 50-GHz photodiode in conjunction with a 50-GHz digitizing oscilloscope, and a 0.05-nm resolution spectrum analyzer.

III. RESULTS AND DISCUSSION

The optical spectrum of the dual-wavelength signal from the gain-switched lasers without self-seeding is shown in Fig. 2(a). It can clearly be seen that, by combining the output of the gain
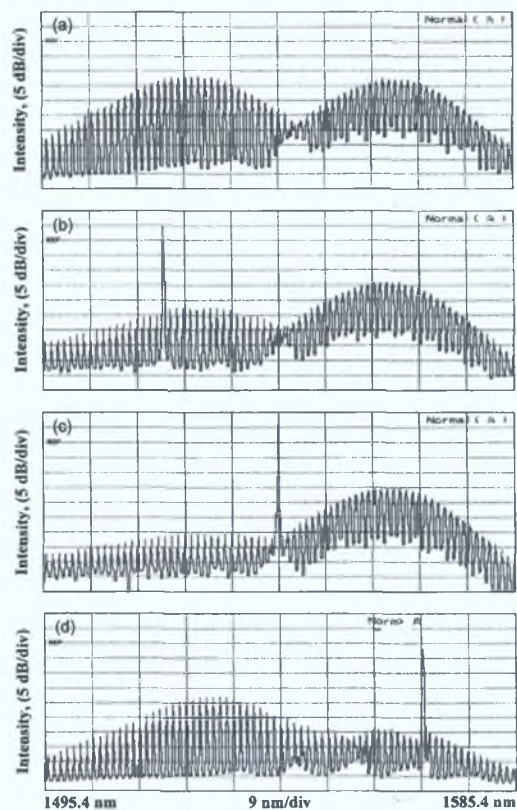
Fig. 2. Output optical spectra at port 1 of: (a) dual-wavelength signal. (b) Shortest wavelength that can be obtained: 1517.73 nm. (c) Central wavelength at 1540.4 nm. (d) Longest wavelength that can be obtained: 1566.64 nm.

switched lasers in the wavelength domain, the composite span of the gain profile that could be used for seeding has been greatly increased. The gain spectra of the two lasers overlap at approximately 16 dB down from the peak of their gain curves. This overlap corresponds to the maximum wavelength of FP 1, and the minimum wavelength of FP 2, for which we can achieve suitable SMSRs using the self-seeding configuration.

Different longitudinal modes of each FP laser were selectively excited when the seeding wavelength was tuned near the center of any desired mode. To obtain more continuous wavelength tuning with this setup, it is possible to use temperature tuning of the diodes in conjunction with tuning the Bragg grating. Fig. 2(b)–(d) shows in respective order the shortest, central, and longest wavelengths that could be seeded. The seeded spectra shown are the composite output (port 1) of the two SSGS lasers before passing through the optical filter and amplifier to be output to port 2.

By taking the output pulses at port 2, we thus pass the composite signal from the SSGS lasers through the external cavity before being outputted. The effect of this is to eliminate the signal from the unseeded laser, and greatly improve the SMSR of the generated optical pulses from the seeded laser [as shown below in Fig. 3(b) and (d)]. The output pulses, and their associated spectra, generated at two specific wavelengths (1524 and 1560 nm) are shown in Fig. 3. The deconvolved pulsewidth for the 1524-nm signal was 16 ps, while that of the 1560-nm signal was 18.5 ps. The associated spectral widths of these two
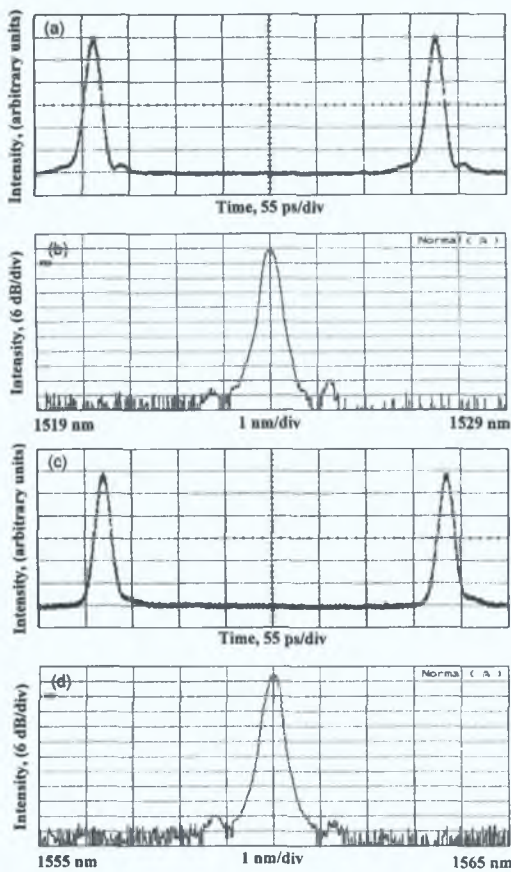
Fig. 3. (a) and (c) Output optical pulses and (b) and (d) associated spectra from port 2 for signal generation at 1524 nm [(a) and (b)] and 1560 nm [(c) and (d)].

Fig. 4. SMSR (left-hand-side axis) and deconvolved pulsewidth (right-hand-side axis) against tunable range in the wavelength.

SMSR is 56 dB with 20-mW EDFA pump power, the SMSR is reduced to 49 dB and 44 dB at pump powers of 15 and 10 mW, respectively. Also presented in Fig. 4 is the pulsewidth variation as the wavelength is tuned. The point where the pulsewidth exhibits a sudden increase is the juncture when the seeded wavelength is moved from FP 1 to FP 2.

IV. CONCLUSION

The generation of widely tunable ($\sim$50 nm) self-seeded gain-switched short optical pulses that exhibit very high SMSR (in the order of 50 dB) has been demonstrated. Such pulses (widely tunable and high SMSR) play a vital part in ensuring the optimal performance of high-speed WDM/OTDM optical communication networks [7]. Using an integrated dual laser source, it may be possible to develop a compact and highly stable SSGS wavelength tunable pulse source suitable for use in future high-speed optical networks.

signals were 27 and 26 GHz, respectively, while the SMSR of the generated pulses were 54 and 56 dB, respectively. The measured pulsewidth remained reasonably constant (16–20 ps) as the output pulses were tuned across the entire tuning range, with slight increases at the limits of tunability, and the time-bandwidth product of the generated pulses remains in the 0.43–0.49 range over the tuning range [which is close to that of a transform limited Gaussian pulses (0.44)]. The average output power of the optical pulses is approximately 1.8 mW. The main limitation on the wavelength tuning of the generated pulses was imposed by the gain bandwidth of the EDFA used in our experimental setup.

The dependence of the SMSR on the seeding wavelength was plotted and is shown in Fig. 4. It can be clearly seen that we were able to obtain an SMSR of 50 dB and above within a range of 48.91 nm (1517.73–1566.64 nm). As the seeding power was increased, due to higher pump powers from the EDFA, the achievable SMSR was enhanced and the possible tuning range became wider; however, pulse deformation and instabilities were observed. The results shown are taken at the optimum level of EDFA pump power (around 20 mW) to ensure maximum SMSR is achieved without pulse deformation and instabilities. Reduction of the EDFA pump power leads to a degradation in pulse SMSR, but this relationship is heavily dependent on the operating wavelength, and its position relative to the gain curve of the EDFA and FP laser being self-seeded. For example, at an operating wavelength of 1560 nm, where the

REFERENCES

[1] C.-K. Chan, K. L. Sherman, and M. Zirngibl, "A fast 100-channel wavelength-tunable transmitter for optical packet switching," IEEE Photon. Technol. Lett., vol. 13, pp. 729–731, July 2001.
[2] R. Ludwig, U. Feiste, E. Dietrich, H. G. Weber, D. Breuer, M. Martin, and F. Küppers, "Experimental comparison of 40 Gbit/s RZ and NRZ transmission over standard single mode fiber," Electron. Lett., vol. 35, pp. 2216–2218, 1999.
[3] T. Morioka, H. Takara, S. Kawanishi, O. Kamatani, K. Takiguchi, K. Uchiyama, M. Saruwatari, H. Takahashi, M. Yamada, T. Kanamori, and H. Ono, "1 Tbit/s (100 Gbit/s times 10 channel) OTDM/WDM transmission using a single supercontinuum WDM source," Electron. Lett., vol. 32, pp. 906–907, 1996.
[4] L. P. Barry, R. F. O'Dowd, J. Debeau, and R. Boittin, "Tunable transform limited pulse generation using self-injection locking of an FP laser," IEEE Photon. Technol. Lett., vol. 5, pp. 1132–1134, Oct. 1993.
[5] D. Huhse, M. Schell, W. Utz, J. Kassner, and D. Bimberg, "Dynamics of single-mode formation in self-seeded Fabry–Perot laser diodes," IEEE Photon. Technol. Lett., vol. 7, pp. 351–353, Apr. 1995.
[6] L. P. Barry and P. Anandarajah, "Effect of side mode suppression ratio on the performance of self-seeded, gain-switched optical pulses in lightwave communications systems," IEEE Photon. Technol. Lett., vol. 11, pp. 1360–1363, Nov. 1999.
[7] P. Anandarajah, L. P. Barry, and A. Kaszubowska, "Performance issues associated with WDM optical systems using self-seeded gain-switched pulse sources due to mode partition noise," IEEE Photon. Technol. Lett., vol. 14, pp. 1202–1204, Aug. 2002.
[8] J. W. Chen and D. N. Wang, "Self-seeded gain switched optical short pulse generation with high side mode suppression ratio and extended wavelength tuning range," Electron. Lett., vol. 39, pp. 679–681, 2003.
[9] X. Fang and D. N. Wang, "Mutual pulse injection seeding by the use of two Fabry–Perot laser diodes to produce wavelength tunable optical short pulses," IEEE Photon. Technol. Lett., vol. 15, pp. 855–857, June 2003.

Direct Measurement of a High-Speed (>100Gbit/s) OTDM Data Signal Utilising Two-Photon Absorption in a Semiconductor Microcavity

P.J.Maguire and L.P.Barry,
Research Institute for Networks and Communications Engineering, Dublin City University, Dublin 9, IRELAND.
Tel: +353 (0)1 700 5884, Fax: +353 (0) 1 700 5508,   maguirep@eeng.dcu.ie

T.Krug, J. O'Dowd, M.Lynch, A.L.Bradley and J.F.Donegan,
Semiconductor Optronics Group, Physics Department, Trinity College, Dublin 2,IRELAND.

H.Folliot,
Laboratoire de Physique des Solides, INSA, Rennes, FRANCE.

The future development of high-speed optical data channels, operating at individual data rates in excess of 100Gbit/s, will require a sensitive and ultra-fast method for pulse measurement [1]. Current high-speed signals are usually characterized using a fast photodetector in conjunction with a high-speed oscilloscope, but are limited to maximum data rate of approximately 40Gbit/s. An alternative is to employ all-optical sampling techniques based on ultra-fast optical nonlinearities present in optical fibres, crystals and semiconductors. One such nonlinearity is the optical-to-electrical process of Two-Photon Absorption (TPA) in a semiconductor [2].

TPA is a nonlinear process where two photons are absorbed in the generation of a single electron-hole pair [2]. It occurs when a photon of energy E_{ph} is incident on the active area of a semiconductor device with a bandgap exceeding E_{ph} but less than $2E_{ph}$. The generated photocurrent is proportional to the square of the intensity, and it is this nonlinear response that enables the use of TPA for optical sampling. As TPA is an instantaneous nonlinearity, the temporal resolution is limited only by the duration and jitter of the sampling pulses [3]. However, the main difficulty of employing TPA is its inherent inefficiency, which requires either high optical intensities or a very long detector, making it unsuitable for high-speed telecommunications applications. By incorporating a semiconductor microcavity, the optical intensity, and hence the TPA response, should be greatly enhanced due to the increased interaction length within the device. Therefore it should be possible to use these specially fabricated microcavity devices [2], which are optimized for TPA at 1550nm, in the development of practical sampling and switching elements for high-speed optical communications.

For the practical implementation of optical sampling via TPA, the duration of the sampling pulse [$I_{sam}(t-\tau)$] must be significantly shorter than the optical signal pulse [$I_{sig}(t)$] under test. The signal and sampling pulses are then incident on the microcavity, with the electrical TPA signal generated [$i(\tau)$] measured as a function of the sampling delay τ. This results in an intensity cross-correlation measurement between I_{sam} and I_{sig} [4]. By operating the sampling pulse with a higher peak intensity than the signal pulse, the resulting cross-correlation trace represents the signal pulse waveform on a constant background [4]. Previous TPA sampling experiments [5] involved a manual variation of an Optical Delay Line (ODL) in the sampling arm to provide the sampling delay, resulting in a laborious stepwise measurement of the signal under test. Here the sampling delay between the sampling pulses and the signal under test is generated by operating the frequency of the sampling pulse (f_{sam}) slightly detuned from a sub-harmonic of the signal frequency (f_{sig}) [4]. This allows the sampling pulse to be automatically swept across the signal pulse at a scan frequency that is low enough to be directly detected and displayed on a standard high-impedance oscilloscope without the need for high-speed electronics or a lock-in amplifier [5].

Figure 1 shows the experimental set up of the real-time TPA optical sampling. It consists of two tunable optical pulse sources; a 10GHz u^2t TMLL 1550 (pulse duration ~ 2ps with a tuneable range 1480-1580nm) used for the signal pulses and a 10MHz Calmar Optcom Femtosecond Pulse Laser (pulse duration 400fs-1.4ps, jitter < 140fs, tunable range 1448-1558nm) used as the sampling pulse. By assuming that the sampling pulse has the same average output power as the signal pulse, the lower repetition rate (10MHz) allows a higher peak power, and hence a higher nonlinear TPA response. The repetition rate of the signal pulse (f_{sig}) was set to 9.998991GHz with the sampling pulse (f_{sam}) operating at 9.998992MHz, which results in a scan frequency of 1KHz [4], which can be easily displayed on the 60MHz high impedance oscilloscope used. The stability of the scan frequency was maintained by feeding the 10MHz reference clock signal from synthesiser 1 to synthesiser 2, and by using a Phase Locked Loop (PLL) to synchronise the 10GHz signal of synthesiser 2 to the 10MHz output optical signal of the sampling pulse source. The u^2t signal pulse train is first amplified using a low-noise Erbium Doped Fibre Amplifier (EDFA) before entering a passive delay line multiplexer (u^2t OMUX 4-160) which consists of a number of independently switchable stages. Using the passive multiplexer a 100GHz pulse stream was obtained at the output of the device, which was then amplified via a second EDFA to overcome any losses encountered in the OMUX. Next the sampling and
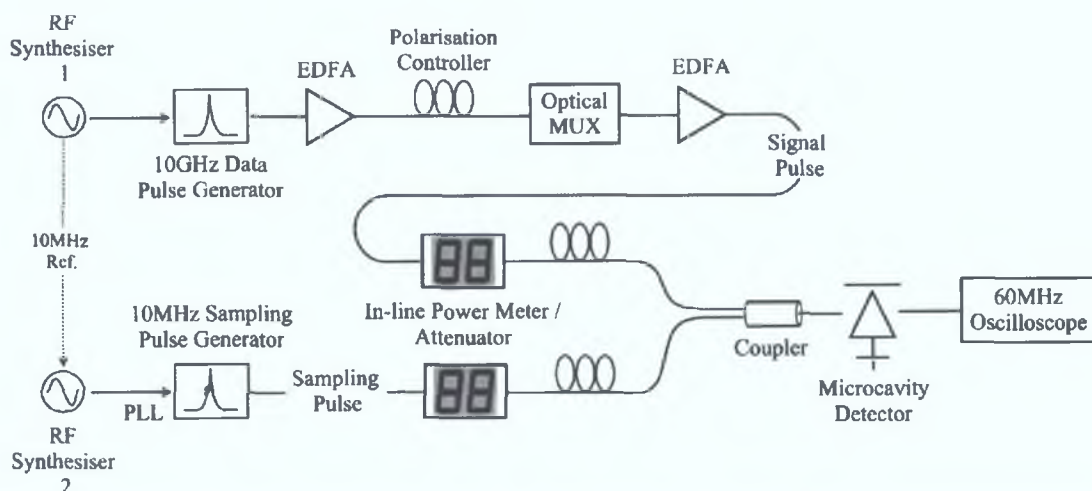
Figure 1: Experimental Set Up for Optical Sampling based on TPA in a Semiconductor Microcavity

the signal pulse trains pass through in-line power meters/attenuators and polarisation controllers before being recombined at a coupler. The power meters allow easy power measurement and attenuation of both pulse trains, while allowing the system sensitivity to be monitored. The combined signals are then incident on the microcavity with the generated TPA photocurrent signal being directly displayed on a standard 60MHz high impedance digital oscilloscope.

Figure 2 (a) shows the real-time measurement of a 10GHz optical pulse as displayed directly on the oscilloscope. The optical pulse duration was measured to be ~2.5ps, with a pulse width of ~2ps expected. This deviation can be accounted for by the temporal resolution of the sampling set up, cavity lifetime of the device and the amplification of the signal pulse in the EDFA's. The peak powers of the signal and sampling pulses used were 11mW and 25W respectively. Figure 2 (b) displays the real-time measurement of a 100Gbit/s (pulse separation ~ 10ps) pulse train, with a signal peak power of 9.6mW and sampling peak power of 32W. The sensitivity of the sampling system, which is defined as being the product of the peak power of the signal pulse and the average power of the sampling pulse [4] was calculated as $0.35mW^2$, with the temporal resolution of the system being < 500fs.

(a)   (b)

-10ps   0ps   10ps   -20ps   -10ps   0ps   10ps   20ps
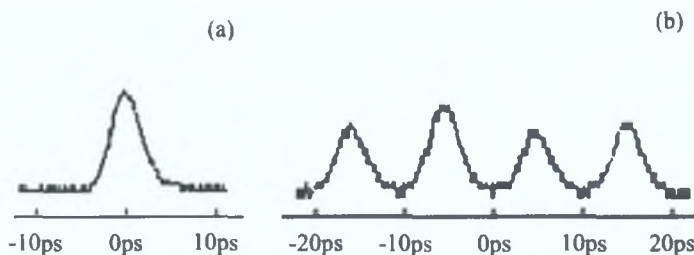
Figure 2: Real-Time TPA Sampling Measurement of (a) 10GHz Optical Pulse; (b) 100Gbit/s Pulse Train

Our results demonstrate that the TPA efficiency is enhanced using the microcavity to a level that allows the successful real-time direct detection of a 100Gbit/s data stream. The system sensitivity is calculated to be $0.35mW^2$, with a signal peak power of 5.6mW, and temporal resolution less than 500fs. This higher temporal resolution, combined with the low sampling rate, allows the direct monitoring of high data rates (>100Gbit/s) without the need for high-speed electronics. By optimising the existing cavity design, it is hoped that the device can be further improved to allow operation at higher data rates approaching 1Tbit/s.

[1] S. Kawanishi, *IEEE Journal of Quantum Electronics*, vol. 34, no. 11, pp.2064-2079, 1998
[2] H.Folliot et al., *Journal of Optical Society Of America B*, vol. 19, no. 10, pp. 2396–2402, 2002.
[3] K.Kikuchi, *Electronics Letters*, vol. 34, no.13, pp. 1354-1355, 1998
[4] B.C.Thomsen et al., *Electronics Letters*, vol. 35, no. 17, pp. 1483-1484, 1999
[5] P.J.Maguire et al., *Electronic Letters*, vol. 41, no. 8, pp. 489-490, 2005

Highly-Efficient Optical Sampling of a 100Gbit/s OTDM Data Signal via Two-Photon Absorption in a Semiconductor Microcavity

P.J.Maguire(1) and L.P.Barry (1), T.Krug (2), J. O'Dowd(2), M.Lynch(2), A.L.Bradley(2) and J.F.Donegan (2), H.Folliot (3)

1 : Research Institute for Networks and Communications Engineering, Dublin City University, Dublin 9, IRELAND; maguirep@eeng.dcu.ie

2 : Semiconductor Optronics Group, Physics Department,Trinity College, Dublin 2,IRELAND; krugt@tcd.ie

3 : Laboratoire de Physique des Solides, INSA, Rennes, FRANCE;

Abstract By incorporating a semiconductor microcavity device, a highly-efficient Two-Photon Absorption based sampling system, with a system sensitivity of $0.009mW^2$ and temporal resolution <500fs is presented.

Introduction

Future high-speed optical networks employing Optical Time Division Multiplexing (OTDM) will require a sensitive and ultra-fast technique for precise optical signal monitoring [1]. Currently high-speed optical signals are characterised using a fast photodetector in conjunction with a high-speed oscilloscope. Unfortunately such a system is limited to a maximum data rate of approximately 40Gbit/s. Optical nonlinearities in optical fibres, crystals and semiconductors, which occur on timescales in the order of a few femtoseconds (10^{-15}s), are thus being considered for the accurate monitoring of data rates in excess of 100Gbit/s. One example of such a nonlinearity is Two-Photon Absorption (TPA) in a semiconductor.

TPA Based Sampling

As TPA is an instantaneous optical nonlinearity, the temporal resolution is limited only by the duration and the jitter of the sampling pulses used [2], making it an ideal candidate for use in a high-speed all-optical sampling scheme. The main difficulty with using TPA is its inherent inefficiency resulting in the need for either high optical intensities, or a very long detector, making them unsuitable for practical applications. One way to overcome this problem is to employ a semiconductor microcavity [3]. This should significantly enhance the TPA response of the device enabling the implementation of practical sampling elements for high-speed optical communications.

The phenomenon of TPA is a nonlinear optical-to-electrical conversion process where two photons are absorbed in the generation of a single electron-hole pair [4]. It occurs when a photon of energy E_{ph} is incident on the active area of a semiconductor device with a bandgap exceeding E_{ph} but less than $2E_{ph}$. The generated photocurrent is proportional to the square of the intensity, and it is this nonlinear response that enables the use of TPA for optical sampling. The semiconductor microcavity used in this work [3] was specifically fabricated for TPA at 1550nm, and greatly enhances the optical intensity by increasing the interaction length in the device [4]. The

TPA photocurrent plotted as a function of wavelength around the microcavity resonance is shown in Figure 1. It clearly shows how the cavity response is dependent on the incident wavelength, with a cavity resonance of 1556nm and a measured cavity linewidth of 5nm.
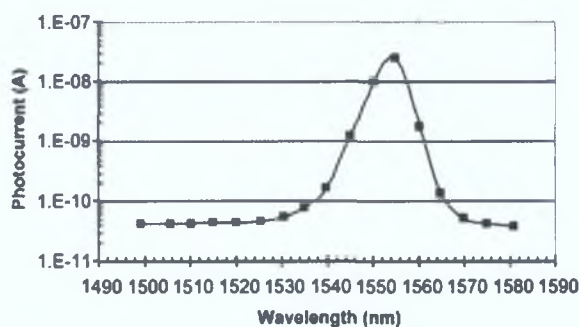
Figure 1: TPA photocurrent as a function of the incident optical wavelength across the microcavity resonance.

In order to use TPA for optical sampling, the duration of the optical sampling pulse $I_{sam}(t-\tau)$ used must be significantly shorter than the optical signal pulses $I_{sig}(t)$ under test. The signal and sampling pulses are then incident on the microcavity device and the electrical signal $i(\tau)$ generated by the TPA process in the device is measured as a function of the sampling delay τ. This results in an intensity cross-correlation measurement between I_{sam} and I_{sig}. For practical implementation, the peak intensity of the sampling pulse is larger and sufficiently shorter than the signal pulse. Therefore the measured signal represents the signal pulse waveform on a constant background [5].

Experimental Set-Up

Figure 2 shows the experimental set-up used. It consists of two tunable pulse sources; a 10GHz u^2t TMLL 1550 (pulse duration ~ 2ps with a tuneable range 1480-1580nm) used for the signal pulses and a 10MHz Calmar Optcom Femtosecond Pulse Laser (pulse duration 400fs-1.4ps, jitter < 140fs, tunable range 1448-1558nm) used as the sampling pulse. Both pulse sources were tuned to 1556nm, the

resonant wavelength of the microcavity device used during the experiment.
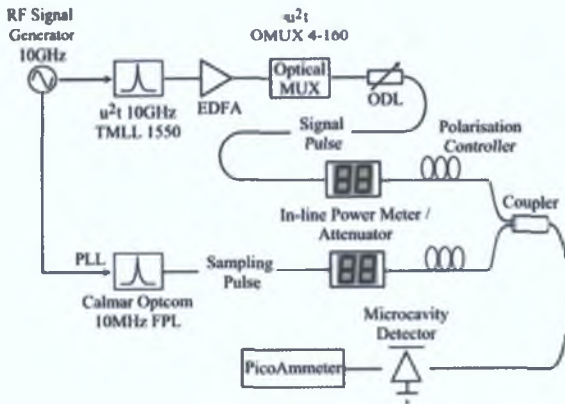
Figure 2: Experimental set-up for TPA Sampling

The signal pulse train from the u^2t source was first amplified using a low-noise Erbium Doped Fibre Amplifier (EDFA) before entering a passive delay line multiplexer which consists of a number of independently switch-able stages. Using the passive multiplexer and operating at a data rate of 10GHz, a 100 GHz stream of pulses was obtained at the output of the device. The 100 GHz pulse train then passes through an Optical Delay Line (ODL), which is used to introduce the sampling delay τ.

As mentioned, the sampling pulse was generated using the Calmar Optcom pulse source. This pulse source was locked to the 10GHz clock signal driving the u^2t source the using a Phase Locked Loop (PLL), and generated pulses with durations ~500fs at 1556nm. Both the sampling and the signal pulse trains pass through in-line power meters/attenuators and polarisation controllers before being recombined at a coupler. The power meters allow easy measurement and attenuation of both pulse trains, while allowing the system sensitivity to be monitored. The combined signals are then incident on the microcavity with the generated photocurrent recorded on a picoammeter as a function of τ, the sampling delay.

Experimental Results

Figures 3(a) and (b) shows the experimental results of the TPA sampling of a single optical pulse and a 100Gbit/s pulse train. From 3(a), the optical pulse duration was calculated to be ~2.5ps, with the expected pulse width being ~2ps. The deviation between the two can be accounted for by the temporal resolution of the sampling set-up, cavity lifetime of the device and amplification of signal pulse in the EDFA. The peak powers of the signal and sampling pulses were 6.8mW and 1.2W respectively. Figure 3(b) displays the TPA sampling of a 100Gbit/s

data signal, as the separation between optical pulses is approximately ~10ps. The peak powers of the signal and sampling pulses were 10.3mW and 1.2W. To calculate the system sensitivity, which is the product of the peak power of the signal pulse and the average power of the sampling pulse [5], we reduced the signal power to levels at which we can just still accurately sample the pulses. In this case the signal peak power was 1.5mW and a sampling peak power was 1.2W, resulting in a system sensitivity of $0.009mW^2$.
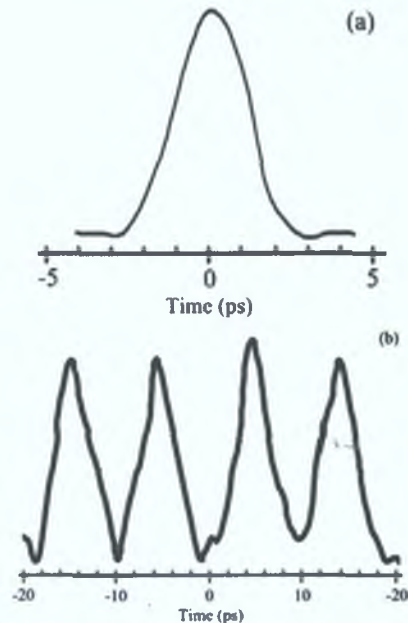
Figure 3: (a) TPA Sampling of a Single Optical Pulse; (b) TPA Sampling of a 100Gbit/s Optical Pulse Train

Conclusions

This papers shows that by employing a microcavity device the TPA efficiency can be improved to a level that allows successful sampling of a 100Gbit/s optical signal with a system sensitivity of $0.009mW^2$, corresponding to a signal peak power of 1.5mW, and a temporal resolution <500fs. These represent the most sensitive ultra-fast TPA optical sampling reported. With the addition of a low-noise amplifier after the detector, it is anticipated that further improvement in the system sensitivity can be acheived.

References

1 S.Kawanishi, IEEE J. Quan. Electron., 34 (1998), 2064-2079

2 K.Kikuchi, Electron. Lett., 34 (1998), 1354-1355

3 T.Krug et al. IEEE Photon. Technol. Lett., 16 (2004) 1543-1544

4 H.Folliot et al. J. Opt. Soc. America B, 19 (2002), 2396-2402

5 B.C.Thomsen et al. Electron. Lett., 35 (1999) 1483-1484

Highly-Efficient Optical Sampling Based on Two-Photon Absorption in a Semiconductor Micro-Cavity Device

P.J.Maguire and L.P.Barry,
Research Institute for Networks and Communications Engineering, Dublin City University, Dublin 9, IRELAND.
Tel: +353 (0)1 700 5884, Fax: +353 (0) 1 700 5508,   maguirep@eeng.dcu.ie

T.Krug, M.Lynch, A.L.Bradley and J.F.Donegan,
Semiconductor Optronics Group, Physics Department,Trinity College, Dublin 2,IRELAND.

H.Folliot,
Laboratoire de Physique des Solides, INSA, Rennes, FRANCE.

Abstract: We demonstrate a highly-efficient optical sampling system based upon the nonlinear process of Two-Photon Absorption in a specially designed semiconductor microcavity. The sensitivity of the system is around $0.1 mW^2$ and the temporal resolution is 2ps.
© 2005 Optical Society of America
OCIS codes: (060.4510) Optical communications; (190.4360) Nonlinear optics, devices

1. Introduction

The future development of high capacity Optical Time Division Multiplexed (OTDM) networks operating at aggregate data rates greater than 100Gbit/s will require a sensitive and ultrafast technique for precise measurement of the optical signal pulse [1]. Presently, the characterisation of such systems is usually performed using fast photodetectors in conjunction with high-speed oscilloscopes. However, this method of characterisation is limited to a maximum bit rates of about 40Gbit/s. Thus for systems operating at aggregate data rates in excess of 100Gbit/s all-optical sampling based on instantaneous optical nonlinearities is required [2].

One such method is to use the nonlinear optical-to-electrical process of Two-Photon Absorption (TPA) in a semiconductor device [3]. Since TPA is an instantaneous nonlinearity, the temporal resolution is limited only by the duration and jitter of the sampling pulses used. The main difficulty with using TPA for high-speed applications, such as optical sampling and switching, is its inherent inefficiency. In order to utilise this nonlinearity, either high optical intensities or very long detectors are required, which may make it unsuitable for high-speed telecommunications applications. However we have recently undertaken work aimed at significantly enhancing the TPA response by using a micro-cavity structure [4,5].

2. TPA Micro-cavity Device

In order to overcome the efficiency problem associated with TPA, a Fabry-Perot micro-cavity was used to greatly enhance the optical intensity by increasing the interaction length in the device [6]. It is hoped that such a device will improve the TPA efficiency to a level that may enable the implementation of practical switching and sampling elements for high-speed optical communications systems.

In order to initially characterise the device, a tunable 10GHz mode-locked laser source, producing 1.8ps pulses over 100nm wavelength range, was employed. Firstly, we performed a photocurrent measurement as a function of the incident optical power close to the cavity resonance (Fig.1a). As clearly shown there is a square dependence of the photocurrent on the incident optical intensity, evidencing the TPA
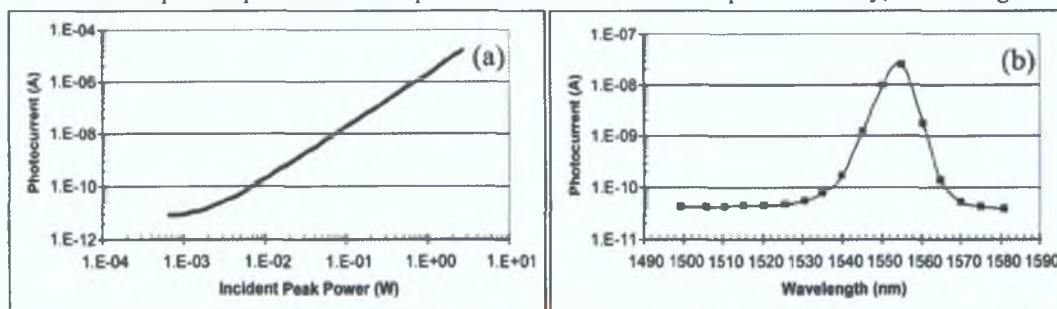
Fig. 1. (a) Photocurrent as a function of Incident Optical Power (b) Micro-cavity Resonance

process. Fig.1b. shows how the cavity resonance response is dependent on the incident wavelength, with a cavity resonance of 1554nm and a measured cavity linewidth of 5nm.

3. Principle of TPA Sampling Operation

The phenomenon of TPA is a nonlinear optical-to-electrical conversion process where two photons are absorbed in the generation of a single electron-hole carrier pair [3]. It occurs when a photon of energy E_{ph} is incident on the active area of a semiconductor device with a bandgap exceeding E_{ph} but less than $2E_{ph}$. The generated photocurrent is proportional to the square of the intensity, and it is this nonlinear response that enables the use of TPA for optical sampling.

To use TPA for optical sampling we require an optical sampling pulse $I_{sam}(t-\tau)$ whose duration is significantly shorter than that of the optical signal pulses $I_{sig}(t)$ under test. The signal and sampling pulses are then incident on the microcavity device and the electrical signal $i(\tau)$ due to TPA in the device is measured as a function of the sampling delay τ, to obtain an intensity cross-correlation between I_{sig} and I_{sam}. For the practical implementation of a TPA sampling system, it is convenient to use a sampling pulse with a peak intensity much larger than the signal intensity. In this case, for a sufficiently short sampling pulse, the measured signal represents the signal pulse waveform on a constant background [7].

4. Experimental Set-Up

Fig.2 shows the experimental set-up used for all-optical sampling based on TPA in a semiconductor microcavity. The tunable pulse source that was used for the initial characterization was also used for the sampling experiments. The pulse duration was approximately 1.8ps (Jitter <500fs) and the operating wavelength was set to 1554nm to coincide with the wavelength resonance of the microcavity. The 10GHz optical pulse train was then amplified and passed through a 1x4 optical coupler. O/P 1 and O/P 4 were used as signal and sampling pulse respectively for the sampling of a single optical pulse, whereas O/P 2 and 3 were used for the creation of a quasi 160GHz pulse train. When O/P 1 was not in use it was connected to an
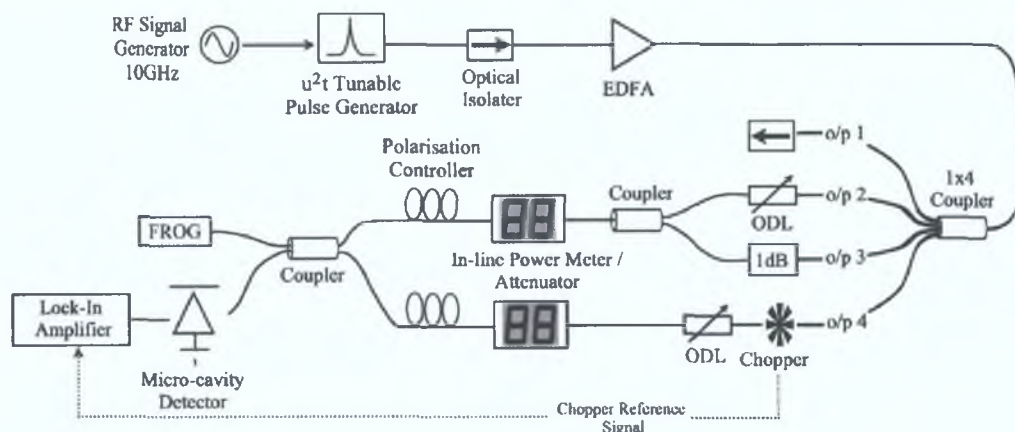
Fig. 2. Experimental Set-Up for Synthesised 160Gbit/s Sampling

optical isolator to prevent any backward reflections. An optical chopper was placed in the sampling arm to allow a lock-in amplifier to measure the TPA photocurrent after the micro-cavity. The sampling pulse then passes through an Optical Delay Line (ODL), which is used to introduce the sampling delay τ. To synthesise the quasi 160GHz signal, the pulse train from O/P 2 was delayed by approximately ~7ps (corresponding to the pulse separation of 160GHz pulse train) by the ODL. To compensate for any insertion loss associated with ODL, the pulse train from O/P 3 was attenuated using a fixed inline optical attenuator. Both pulse trains were then recombined at the coupler to form the quasi 160GHz signal. The signal and sampling pulse trains then pass through inline power meters/attenuators and polarisation controllers before being recombined at a coupler. The power meters allow for easy measurement and attenuation of both signal and sampling pulses allowing the sensitivity of the system to be monitored. Finally the sampling and signal pulse are incident on the micro-cavity with the photocurrent generated by the device fed into the lock-in amplifier. The electrical output was then recorded as a function of the sampling delay τ. The quality of the TPA sampling technique is

independently verified by comparing the resulting output of the TPA sampling with the corresponding results from an SHG-FROG [8] measurement of the same pulse.

5. Experimental Result

Fig.3a shows the TPA sampling output for a single pulse (dotted line) and the SHG-FROG measurement (solid line). The pulse duration from the TPA sampling was calculated as ~2.4ps whereas the SHG-FROG measurement carried out indicated a pulsewidth of ~1.8ps. This deviation can be accounted for by the cavity lifetime, and the temporal resolution of the sampling set-up as determined by the jitter and duration of the sampling pulse. The average peak power of the signal and sampling pulses were 2.7mW and 8.6mW respectively. Fig.3b shows the sampling and SHG-FROG trace of the quasi 160GHz signal. Again the deviation between the measured and SHG-FROG can be accounted for as described above. As the pulse
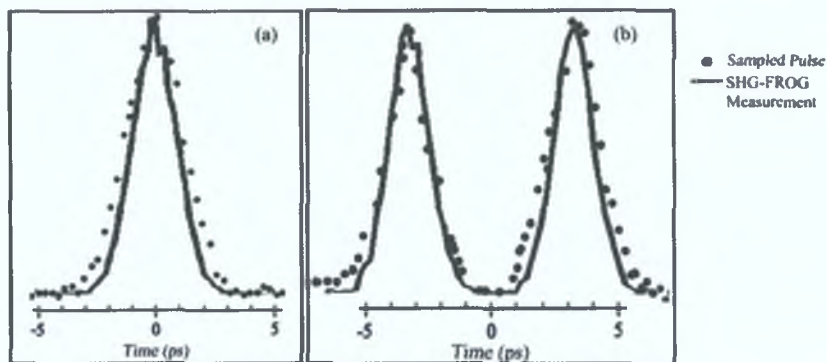
Fig. 3. (a) TPA Sampling versus FROG measurement for single pulse (b) TPA Sampling versus FROG measurement for synthesized 160GHz signal.

separation is approximately 7ps, this highlights that sampling of a 160Gbit/s signal should be possible. An overall system sensitivity was calculated to be $0.1mW^2$ by determining the minimum optical power levels required to successfully sample the pulse.

6. Conclusion

We have shown that by using a micro-cavity device, we are able to enhance the TPA efficiency to a level that can be used for high-speed optical sampling. Our initial results show that TPA can be used for sampling of a 160Gbit/s signal, with a sensitivity of ~ $0.1mW^2$. In our set-up this equates to peak pulse power level around 1 mW. It should be noted that the sensitivity of the TPA sampling system was achieved without any post-amplification of the electrical TPA photocurrent. It is anticipated that the sensitivity could be improved with the addition of a low noise amplifier. Also with a sampling pulse duration and jitter of 1.8ps and 500fs respectively, the minimum temporal resolution possible is ~2ps. Thus by reducing the pulse duration of the sampling pulse, it is hoped that the temporal resolution can be further reduced.

7. References

[1] S.Kawanishi, "Ultrahigh-Speed Optical Time-Division-Multiplexed Transmission Technology Based on Optical Signal Processing", IEEE Quan. Elec. 34, 2064-2079 (1998)

[2] S.Kawanishi, T.Yamamoto, M.Nakazawa and M.M.Fejer, "High sensitivity waveform measurement with optical sampling using quasi-phasematched mixing LiNbO₃ waveguide", Electron. Lett, 37, 842-844 (2001)

[3] B.C.Thomsen and L.P.Barry and J.M.Dudley and J.D.Harvey, "Ultrahigh speed all-optical demultiplexing based on two-photon absorption in a laser diode", Electron. Lett, 34, 1871-1872 (1998)

[4] H.Folliot, M.Lynch, A.L.Bradley, T.Krug, L.A.Dunbar, J.Hegarty, J.F.Donegan and L.P.Barry, "Two-photon-induced photoconductivity enhancement in semiconductor microcavities: A theoretical investigation", J. Opt. Soc.America B, 19, 2396-2402 (2002)

[5] L.P.Barry, P.Maguire, T.Krug, H.Folliot, M.Lynch, A.L.Bardley, J.F.Donegan, J.S.Robert and G.Hill, "Design of microcavity semiconductor devices for highly efficient optical switching, sampling applications", in Lasers and Electro-Optics Society Annual Meeting-LEOS 2002, (Insititute of Electrical and Electronics Engineers, New York, 2002) pp.839.

[6] T.Krug, M.Lynch , A.L.Bradley, J.F.Donegan, L.P.Barry , H.Folliot , J.S.Roberts and G.Hill, "High-Sensitivity Two-Photon Absorption Microcavity Autocorrelator", IEEE Photon. Technol. Lett, 16, 1543-1544, 2004

[7]B.C.Thomsen, L.P.Barry, J.M.Dudley and J.D.Harvey, "Ultra Sensitive All-Optical Sampling Scheme for use in high capacity telecommunication systems at 1.5μm", Electron. Lett, 35, 1483-1484 (1999)

[8] Rick Trebino, Kenneth W.DeLong, David N.Fittinghoff , John.N.Sweetser, Marco A.Krumbugel and Bruce A.Richman, "Measuring ultrashort laser pulses in the time-frequency domain using frequency-resolved optical gating", Rev. Sci. Instrum, 68, 3277-3295, 1996

Simulation of All-Optical Demultiplexing utilizing Two-Photon Absorption in Semiconductor Devices for High-Speed OTDM Networks

P. J. Maguire, and L.P. Barry

Research Institute for Networks and Communications Engineering, School of Electronic Engineering,
Dublin City University, Dublin 9, IRELAND.
Phone: + 353 1 700 5883, Fax: + 353 1 700 5508, Email: maguirep@eeng.dcu.ie

SUMMARY

A stable and ultra-fast switch for the demltiplexing of a ultra-high bit rate data signal will be vital for the development of future high-capacity Optical Time Division Multiplexed (OTDM) networks [1]. Nonlinear effects present in fibres and semiconductors are used in the majority of all-optical switching techniques for OTDM since they occur in time scales of a few femto-seconds. Current all-optical demultiplexers for OTDM suffer from a number of factors that limits their performance for high-speed switching. An alternative is to use the nonlinear optical-to-electrical process of Two-Photon Absorption (TPA) in a semiconductor, where two photons are absorbed in the generation of a single electron-hole carrier pair [2,] to carry out all-optical switching at data rates above 100Gb/s [3]. The generated photocurrent is proportional to the square of the intensity, and it is this nonlinear response that enables the use of TPA for optical switching. Recent work undertaken has been aimed at significantly enhancing the TPA response by using a micro-cavity device [4], which overcomes the inherent inefficiency associated with TPA, and enables the implementation of practical switching and sampling elements of high-speed optical systems. The device that we specially fabricated for TPA at 1550nm is a GaAs/AlAs PIN micro-cavity photodetector grown on a GaAs substrate. It comprises a 0.459μm GaAs active region embedded between two GaAs/AlAs active region embedded between two GaAs/AlAs Bragg mirrors. The front p doped (C~10^{18}cm^{-3}) mirror consists of 9 pairs while the back n (Si~10^{18}cm^{-3}) mirror contains 18 pairs designed for reflectivity at 1550nm. The device studied was a 100μm diameter vertical structure. The characteristics of these devices are shown in Figure 1. The measured photocurrent as a function of incident optical power is shown in Figure 1 (a) and clearly shows the square dependence of the photocurrent on the incident intensity, indicating Two-Photon Absorption. Figure 1 (b) shows how the TPA response is dependent on the incident wavelength, with a cavity resonance of 1554 nm and a measured cavity linewidth of 5nm.
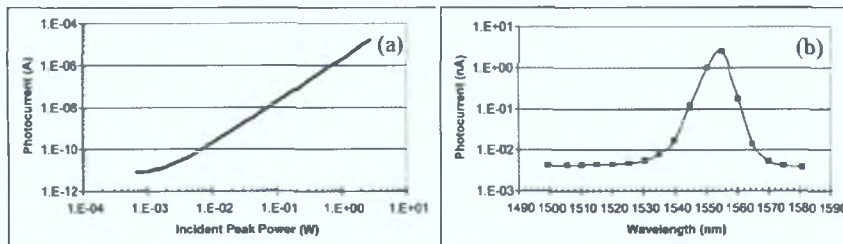
Figure 1: (a) Photocurrent as a function of Incident Optical Peak Power (b) Micro-Cavity Resonance

From these characteristics, the Single-Photon Absorption (SPA) coefficient (α) and the TPA coefficient (β) of 0.01cm^{-1} and 3x10^{-10} m/W were chosen respectively. To use these devices as optical demultiplexers we normally use a setup as shown in Figure 2, in which the TPA device uses optical control pulses to demultiplex a high-speed OTDM channel via TPA in the semiconductor device. The high speed OTDM signal and the control pulses (at the repetition rate of the individual channels) are optically coupled together and are incident on the device with their relative arrival time adjusted via a variable optical delay in the control arm. The nonlinear quadratic nature of the TPA
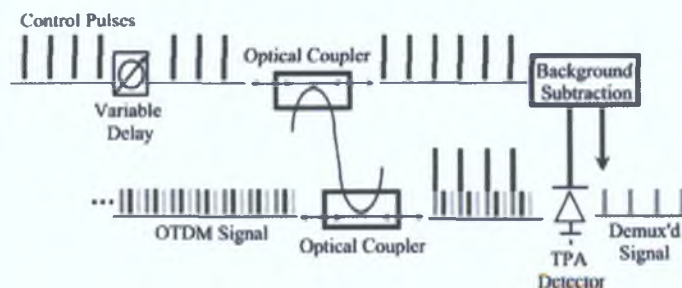
Figure 2: Schematic of TPA Demultiplexing

response ensures that there is a strong contrast between the electrical TPA signal generated when the control and selected channel pulses overlap, and that generated when the adjacent channels arrive independently. Background subtraction of the constant signal due only to the control pulse can then be conveniently carried out to result in a high contrast demultiplexed signal output.

The purpose of the simulation was to investigate the suitability of using a TPA device to switch a high-speed OTDM signal. System parameters that were examined include: 1) Number of channels in the OTDM network 2) Ratio between the peak power of the control signal and data signal 3) Temporal response of the TPA detector.

The model creates an OTDM data signal by multiplexing together a number of specified channels, each consisting of random data, using short optical pulses. The peak power of the data pulses can be set to a specific value with a fixed level of noise added, which has the effect of limiting the optimum BER achievable. Control pulses are synchronized with one of the OTDM channel and are then incident on the TPA device. The TPA model also takes into account the temporal response of the TPA detector, and this is set to a percentage of the bit slot duration of the individual data channels in the OTDM signal in order to minimize the amount of noise from adjacent channels. The simulation model finally calculates the Bit-Error-Rate (BER) of the demultiplexed and detected signal after the TPA device. The overall goal is to determine the operating characteristics such that BER of the demultiplexed/detected signal (EBER) is the same as the optical BER (OBER) on the signal before the TPA detector (due to noise on the signal pulses), indicating that the demultiplexing process is not introducing additional errors.
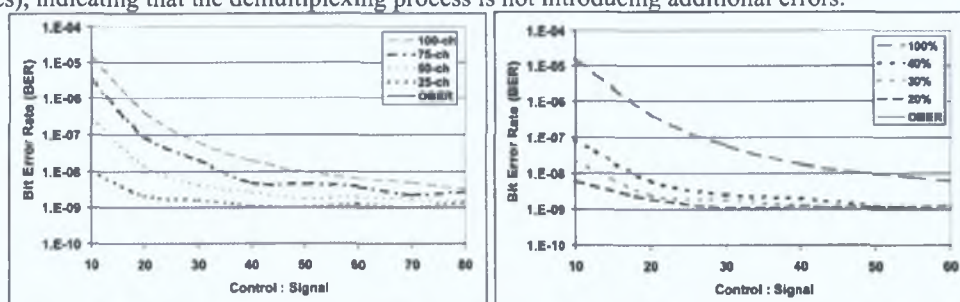
Figure 3: (a) BER Vs. Control-to-Signal Power as the number of channels is varied (b) BER Vs. Control-to-Signal Power as the temporal response is varied.

Figure 3 (a) illustrates the received BER vs. control-to-signal ratio as the number of channels is varied. It can be clearly seen that as the control-to-signal ratio is increased, the EBER approaches the OBER. This results from the fact that as the control-to-signal peak power ratio is increased, the contrast ratio between the data signal synchronised with the control pulse and those not synchronised widens. This reduces the amount of noise due to the detection of all adjacent channels (since the temporal response is set to 100%), which improves the resultant signal-to-noise ratio, and improves the BER of the received signal. We subsequently went on to examine how the temporal response of the TPA detector affected its operation. Figure 3 (b) plots the BER as a function of the control-to-signal ratio as the temporal response of the device is varied from 100% to 10%. The 25-channel system is employed, as this was the only one that gave optimum performance at a reasonable control-to-signal ratio. As the temporal response is reduced (enhancing device bandwidth), the BER of the received signal is improved since the number of adjacent channels that add noise to the detected channel decreases, thus improving the received BER. This allows a smaller control-to-signal ratio to be used to offer the same overall performance. For a 25-channel system, a temporal response of 20% allows us to obtain good performance with a control-to-signal ratio of around 30:1. Assuming a data rate for each channel of 10Gbit/s, and thus a bit period of 100ps, a 20% temporal response (20ps) would correspond to a device bandwidth of approximately 20GHz.

We have modeled the performance of a TPA based demultiplexer in an OTDM communication system. The performance of the demultiplexer was evaluated by comparing the electrical BER of the demultiplexed and detected channel to the optical BER of the signal before the demultiplexer. Using the parameters we have chosen for the TPA device, we have shown that error-free demultiplexing of a 250 Gbit/s OTDM signal (25 x 10 Gbit/s channels), using a 30:1 control-to-signal peak power ratio, with a TPA device with a bandwidth of 20Ghz should be possible.

[1] D.M.Spirit et al., *IEEE Communications Magazine*, vol. 32, no. 12, pp. 56–62, 1994.

[2] B.C.Thomsen et al., *Electronics Letters*, vol. 34, no. 19, pp. 1871–1872, 1998.

[3] B.C.Thomsen et al., *Conference on Optical Fiber Communications*, vol. 54, no. 3, pp. WO2/1-WO2/3, Anaheim, USA, 2001.

[4] H.Folliot et al., *Journal of Optical Society Of America B*, vol. 19, no. 10, pp. 2396–2402, 2002.

Generation of Wavelength Tunable Optical Pulses with SMSR Exceeding 50 dB by Self-Seeding a Gain-Switched Source Containing Two FP Lasers

P. J. Maguire, P. Anandarajah, L.P. Barry and A. Kaszubowska

Research Institute for Networks and Communications Engineering, School of Electronic Engineering, Dublin City University, Dublin 9, Ireland. Phone: + 353 1 700 5883, Fax: + 353 1 700 5508, Email: liam.barry@dcu.ie

SUMMARY

The development of transform-limited optical pulse sources with broad wavelength tunability and short pulse widths is extremely important for use in future high-speed communication systems, especially in applications such as Wavelength Division Multiplexing (WDM), Optical Time Division Multiplexing (OTDM), Hybrid WDM/OTDM and soliton systems [1]. One of the simplest, and most reliable, techniques available to generate wavelength tunable, picosecond optical pulses involves the self-seeding of a gain-switched Fabry-Perot (FP) laser, and many experimental schemes have been reported [2-4]. Self-seeding entails the use of a wavelength selective external cavity to re-inject a small fraction of the output light back into the gain-switched laser at only one longitudinal mode frequency. Provided that the optical signal re-injected into the laser arrives during the build-up of an optical pulse in the FP laser, then a single-moded output pulse is obtained.

Recent reports have revealed wavelength tunable Self-Seeded Gain-Switched (SSGS) pulses with widths of about 90-130 ps and Side Mode Suppression Ratios (SMSR) of 32 dB that are tunable between 19 and 26 nm [5, 6]. Their tunability was limited by various factors such as the tunable range of the Fibre Bragg Grating (FBG). In this letter, we show the generation of shorter pulses (~ 20 ps) that exhibit SMSR's greater than 50 dB and wider tuning range (48.91 nm). Our technique is based on the self-seeding of a gain-switched source containing two FP lasers.

Figure 1 illustrates our experimental set up used. The FP lasers used were commercial 1.5 μm InGaAsP devices, with threshold currents of about 26 mA, and a longitudinal mode spacing of 1.12 nm. Gain-switching of both lasers was carried out by applying a DC bias current of 17 mA, and a sinusoidal modulation signal with a power of 29 dBm. The sinusoidal modulation signal had a frequency around 2.5 GHz. Self-seeding of the gain-switched lasers was achieved by using an external cavity containing a polarization controller (PC), a 3 dB coupler, a Tunable Bragg Grating (TBG) with a bandwidth of 0.23 nm and an Erbium Doped Fibre Amplifier (EDFA). The external cavity for self-seeding FP 2 also contained a tunable optical delay line to ensure simultaneous self-seeding of FP 1 and FP 2.
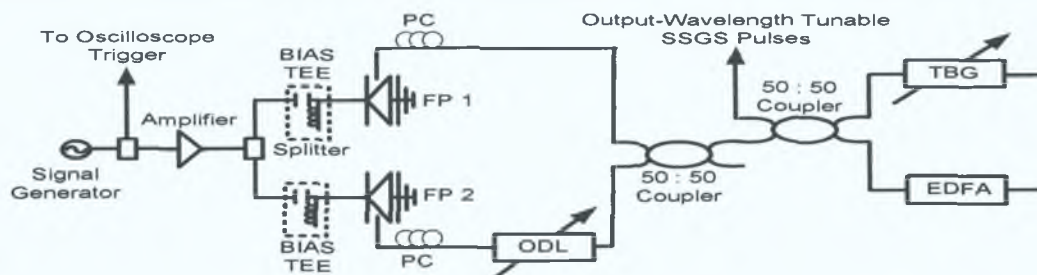
Figure 1: Experimental set up used for the generation of widely tunable SSGS pulses

To achieve optimum SSGS pulse generation, the grating was initially tuned to one of the longitudinal modes of the two gain-switched lasers. The frequency of the sinusoidal modulation was then varied to ensure that the signal re-injected into the laser, from the external cavity, arrives as an optical pulse is building up in the laser. An operating frequency of 2.498 GHz was found to be suitable. The bias current of FP 1 and FP 2 was also changed (reduced to about 12 mA) in order to obtain the minimum pulsewidth. The output pulses, from the return arm of the second 50:50 fiber coupler, were characterized in the temporal domain using a 50 GHz photodiode in conjunction with a 50 GHz HP digitizing oscilloscope. Pulse characterization in the spectral domain was carried out using an optical spectrum analyzer with a resolution of 0.07 nm.
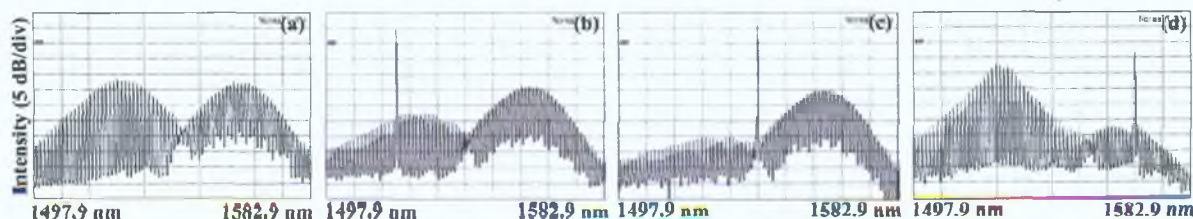
Figure 2: Optical spectra (a) Dual wavelength signal (b) 1517.73 nm (c) 1540.4 nm (d) 1566.6 nm

The optical spectrum of the dual wavelength signal from the gain-switched lasers without self-seeding is shown in Figure 2 (a). Different longitudinal modes of each FP laser were selectively excited when the seeding wavelength was tuned near the centre of the desired mode. Figure 2 (b, c, & d) shows in respective order the shortest, central and longest wavelengths that could be seeded. The seeded spectra shown are the composite output of the two self-seeded gain-switched lasers before passing through the amplifier and optical filter. By taking the output pulses as the signal that is fed back into the lasers we thus pass this signal through the filter again, which greatly improves the SMSR of the generated optical pulses (as shown below in Fig. 3 (b) and (d)).

The output pulses, and their associated spectra, generated at two specific wavelengths (1524 and 1560 nm) are shown in Figure 3. The pulse duration and spectral width of the signal at 1524 nm are 16 ps and 27 GHz respectively, while for the 1560 nm pulse the temporal duration and spectral width are 18.5 ps and 26 GHz respectively. The measured pulsewidth remained almost constant right through the entire tuning range, with slight increases at the limits of tunability, and the time-bandwidth product of the generated pulses remains in the range 0.43 to 0.49 over the tuning range (which is close to that of a transform limited Gaussian pulses (0.44)). The main limitation on the tuning was imposed by the gain-bandwidth of the EDFA used in our experimental set-up. It is important to note that the spectra of the pulses after going through the filter for the second time, eliminates any effect from the unseeded laser while enhancing the SMSR of the seeded laser (generated pulses). We can thus achieve an SMSR greater than 50 dB for the generated optical pulses over the entire tuning range.
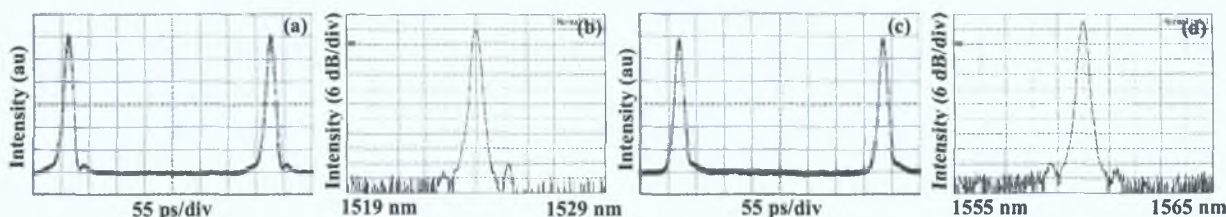
Figure 3: (a) SSGS Pulse FP 1 @ 1524 nm (b) Spectrum of pulse @1524 nm with SMSR of 54 dB (c) SSGS Pulse FP 2 @ 1560 nm (d) Spectrum of pulse @1560 nm with SMSR of 56 dB

The dependence of the SMSR on the seeding wavelength was plotted and is shown in figure 4. It can be clearly seen that we were able to obtain a SMSR of 50 dB and above within a range of 48.91 nm. Also shown in the same plot is the pulse width variation as the wavelength is tuned. The point where the pulse width increases slightly is the juncture when the seeded wavelength is moved from FP 1 to FP 2. As the seeding power was increased, due to higher pump powers from the EDFA, the achievable SMSR was enhanced and the possible tuning range became wider, however pulse deformation and instabilities were observed.
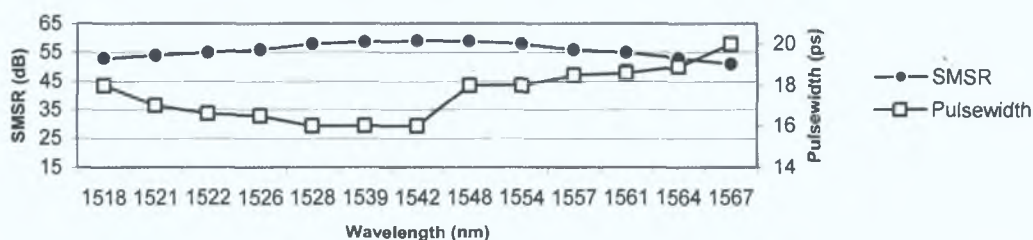
Figure 4: SMSR (left axis) and Deconvolved pulsewidth (right axis) against tunable range in wavelength

The generation of widely tunable (~ 50 nm) self-seeded gain switched short optical pulses that exhibit very high SMSR in the order of 50 dB has been demonstrated. Such pulses (widely tunable and high SMSR) play a vital part in ensuring the optimal performance of high-speed WDM/OTDM optical communication networks [7]. By using an integrated dual laser source it may be possible to develop a compact and highly stable tunable pulse source based on this technique.

[1]   S. Kawanishi, *IEEE J. Quantum Electron.*, vol. 34, pp. 2064-2079, 1998.
[2]   M. Cavelier et al, *Electron. Lett.*, vol. 28, pp. 224-226, 1992.
[3]   L.P. Barry et al, *IEEE Photonics Technol. Lett.*, vol. 5, pp. 1132-1134, 1993.
[4]   D. Huhse et al, *IEEE Photonics Technol. Lett.*, vol. 7, pp. 351-353, 1995.
[5]   J. W. Chen et al, *Electron. Lett.*, Vol. 39, pp. 679–681, 2003.
[6]   X. Fang et al, *IEEE Photon Technol. Lett.*, vol. 15, pp. 855-857, 2003.
[7]   P. Anandarajah et al, *IEEE Photon Technol. Lett.*, vol. 14, pp. 1202-1204, 2002.

Appendix C: Computer Code for TPA Demultiplexing Simulation

```c
#include <stdio.h>
#include<math.h>


#define MAX 20          /*lfsr*/
#define m 2147483647

double g1,g2;                    /*canale*/
long cont,v;


        int main();
        void riempi(int *),riempi1(int
*),copia(int,int*,int*),putint(double),shift(int,int*); /*lfsr*/
        int compare(int,int*,int*),reazione(int,int*,int*),getint();
        double rumore(long,double,double),modula(int,double);long genera_unif(long);

        void
genera_gauss(double,double,double),in_v_out(),ber_v_control(),ber_v_signal(),ber_v_c
ontrol2(),ber_v_signal2(),run_ber(),signal_v_time();
        int decidi(double,double), confronta(int,int);           /*canale*/
        double TPA(double),time_delay();

/*Used to calculate settings for the use of the random number generator
  for accumulative channel noise*/

        double thr_optim(),STD(double);

/*used for random number generation*/

        int iseed =10000;
        double pi=3.14,ran1=0,ran2=0;
        double ranf();
        double fill_in(double,double,double*);

/*used to determine if the result of the device output is a 1 or 0*/

        double soglia;

        void shift_arr(double*);

        FILE *out,*graph1,*graph2,*graph3,*graph4;


/* made external to run graph mode*/

         float N0_det=8.5,pulse_power,ratio,percentage,bit_r;    /*N0det is device
thermal noise,5 is best value*/
        int chan_number,loop;
        long p;
        double errori,ber,N0_d,erroro,ber_optical,N0=40;  /*N0 is optical noise 18 is
best value*/
        double Alpha=0.01,B,bit_rate=1,max_delay,total_bit_rate,td;
                                                /*Alpha value changed from
0.1*/
int main()
{

char plot;
int graph,graphc;


printf("Do you wish to plot a graph (Y/N)?\n - no will allow you to enter values for
all variables\n and simply output the BER for that arrangement-\n  ");
scanf("%c",&plot);

        if(plot=='y')
```

```c
                {
                loop=11;
                printf("\nchoose one of the following...\n1. INPUT V's OUTPUT of TPA
devise:\n2. BER V's CONTROL Power:\n3. BER V's SIGNAL Power (before/after
devise):\n4. PLOT SIGNAL OUTPUT - (plots output of all channels on a time scale):
");
                scanf("%d",&graph);
        if(graph==1)
                        {
                        graph1=fopen("in_v_out.dat","w");
                        fprintf(graph1, "INPUT(watt)\ta=0.1\ta=1\ta=10\ta=100\n");
                        in_v_out();
                        }
        if(graph==2)
                        {
                        printf("\n\n\n\n\n\nYou have 2 choices :\n1. BER v CONTROL -
for varying values of channels 20 to 100:\n2. BER v CONTROL - for varying values of
devise time delay 10_percent to 100_percent:\n\n");
                        scanf("%d",&graphc);

                        if(graphc==1)
                                {
                                graph2=fopen("ber_v_control_ch.dat","w");
                                fprintf(graph2, "RATIO\tCONTROL\t25-ch\toptical\t50-
ch\toptical\t75-ch\toptical\t100-ch\toptical");

                                printf("insert bit rate for individual channels:(G/s)
");
                                scanf("%f",&bit_r);

                                printf("\ninsert the signal peak power (W):(approx = 1,
for dynamic range of device)      ");
                                scanf("%f",&pulse_power);

                                ratio=10;
                                percentage=100;
                                td=time_delay();

                                bit_rate=bit_r*pow(10,9);/* Giga bits per second*/
                                max_delay=1/bit_rate;

                                ber_v_control();


        for(chan_number=20;chan_number<101;chan_number=chan_number+40)
                                        {
                                        fprintf(graph2,"\nCHANNELS\tDEVICE-
DELAY\n%d\t%e",chan_number,((percentage/100)*max_delay));
                                        }


                                }

                        if(graphc==2)
                                {
                                graph2=fopen("ber_v_control_dl.dat","w");
                                fprintf(graph2, "RATIO\tCONTROL\tBER-10\tBER-40\tBER-
70\tBER-100");

                                printf("insert bit rate for individual channels:(Gb/s)
");
                                scanf("%f",&bit_r);

                                printf("\ninsert the signal peak power (W):(approx = 1,
for dynamic range of device)      ");
                                scanf("%f",&pulse_power);
```

```c
                                    ratio=10;
                                    chan_number=100;

                                    bit_rate=bit_r*pow(10,9);/* mega bits per second*/
                                    total_bit_rate=chan_number*bit_rate;
                                    max_delay=1/bit_rate;

                                    ber_v_control2();

                for(percentage=10;percentage<101;percentage=percentage+30)
                                            {
                                            td=time_delay();
                                            fprintf(graph2,"\nPERCENTAGE\tDEVICE-
DELAY\n%f\t%e",percentage,((percentage/100)*max_delay));

                                            }


                                }


                        }
                if(graph==3)
                        {

                        printf("\n\n\n\n\n\nYou have 2 choices :\n1. BER v PULSE - both
optical/electrical ber for 20 and 100 channels:
                        \n2. BER v PULSE - for 100 channels varying Control ratio and
delay percentage:");
                        scanf("%d",&graphc);

                        if(graphc==1)
                                {

                                graph3=fopen("ber_v_signal_ch.dat","w");
                                fprintf(graph3, "SIGNAL\tBER-20\tOPT-BER-20\tEFF-
20\tBER-100\tOPT-BER-100\tEFF-100");

                                printf("insert bit rate for individual channels:(Gb/s)
");
                                scanf("%f",&bit_r);

                                bit_rate=bit_r*pow(10,9);/* Giga bits per second*/
                                max_delay=1/bit_rate;

                                ratio=10;      /*typically 10*/
                                percentage=100;       /*typically 100*/
                                pulse_power=0.5;
                                td=time_delay();

                                ber_v_signal();
                                }


                        if(graphc==2)
                                {

                                graph3=fopen("ber_v_signal_mul.dat","w");
                                fprintf(graph3, "SIGNAL\t10R-10D\topt_10R-10D\t10R-
100D\topt_10R-100D\t100R-10D\topt_t100R-10D\t100R-100D\topt_100R-100D");


                                printf("insert bit rate for individual channels:(Gb/s)
");
```

```c
                        scanf("%f",&bit_r);

                        chan_number=100;
                        ratio=10;
                        percentage=10;
                        pulse_power=0.1;
                        td=time_delay();

                        bit_rate=bit_r*pow(10,9);/* Giga bits per second*/
                        total_bit_rate=chan_number*bit_rate;
                        max_delay=1/bit_rate;

                        ber_v_signal2();

                        for(ratio=10;ratio<101;ratio=ratio*10)
                            {

       for(percentage=10;percentage<101;percentage=percentage*10)
                                    {
                                    td=time_delay();

                                    fprintf(graph3, "\nDevice delay for ratio
%f and Percentage %f = %e",ratio,percentage,(max_delay*percentage/100));

                                    }
                              }

                            }


                    }
        if(graph==4)
                    {
                    graph4=fopen("signal_v_time.dat","w");
                    fprintf(graph4,"TIME\tSIGNAL");

                    loop=2;

                    printf("\nhow many channels are to be used :   ");
                     scanf("%d",&chan_number);

                    printf("\nEnter bit rate per channel:(Gb/s) ");
                     scanf("%f",&bit_r);

                     printf("\ninsert the receiver thermal noise : (0.01 - 10)");
                     scanf("%f",&N0_det);

                     printf("\ninsert the signal peak power (W):(approx = 1, for
dynamic range of device)     ");
                    scanf("%f",&pulse_power);

                     printf("\ninsert the control to signal ratio:(0 - 100)  ");
                     scanf("%f",&ratio);

                    printf("\nEnter percentage of max delay for device output:(0-
150) ");
                     scanf("%f",&percentage);

                    bit_rate=bit_r*pow(10,9);/* Giga bits per second*/
                    total_bit_rate=chan_number*bit_rate;
                    max_delay=1/bit_rate;
                    td=time_delay();

                    signal_v_time();
```

```
                /*      fprintf(out "\n\n\nCHANNELS\tO-NOISE(db)\tT-
NOISE\tCONTROL/RATIO\tT  BIT RATE(Gb/s)\t  Ch  BIT RATE(Gb/s)\tMAX
DELAY(s)\tPERCENTAGE(%)\tDEVICE DELAY(s)\n"),

                fprintf(graph4  "%d\t%e\t%e\t%d\t%f\t%f\t%e\t%f\t%e\n
",chan_number,NO NO_det ratio (bit_r*chan_number) (bit_r) max_delay percentage,(perc
entage*max_delay)),
                */

                printf("\n\nCOMPLETE '' - check file signal_v_time dat for
details - ")




                }

        }
    else
        {

        loop=2

        printf("\nhow many channels are to be used      ")
         scanf("%d",&chan_number)

        printf("\nEnter bit rate per channel (Gb/s) ")
         scanf("%f" &bit_r)

         printf("\ninsert the receiver thermal noise    (0 01 - 10)")
         scanf("%f" &NO_det)

         printf("\ninsert the signal peak power (W) (approx = 1  for dynamic
range of device)      "),
             scanf("%f" &pulse_power)

         printf("\ninsert the control to signal ratio (0 - 100)   ")
         scanf("%f",&ratio),

        printf("\nEnter percentage of max delay for device output   ")
         scanf("%f",&percentage),

        bit_rate=bit_r*pow(10,9) /* Giga bits per second*/
        total_bit_rate=chan_number*bit_rate,
        max_delay=1/bit_rate
        td=time_delay()

        out=fopen("BER dat" "w")
        fprintf(out "CHANNELS\tO-NOISE(db)\tT-NOISE\tCONTROL/RATIO\tOPT-
BER\tBER\tEFFECIENCY\tT  BIT RATE(Gb/s)\t  Ch  BIT RATE(Gb/s)\tMAX
DELAY(s)\tPERCENTAGE\tDEVICE DELAY(s)\n"),
             run_ber(),

        fprintf(out  "%d\t%e\t%e\t%d\t%f\t%f\t%f\t%f\t%f\t%e\t%f\t%e\n
" chan_number,NO NO_det,ratio ber_optical ber (ber*100/ber_optical) (bit_r*chan_numb
er) (bit_r),max_delay percentage (percentage*max_delay)),
             printf("noise %f db\nerrors %e\nBER %e\n "  NO,errori ber)
             printf("\n\nCOMPLETE '' - check file BER dat for details - ")
             }

        printf("\n\n\aDone\n"),

return 0,
}
```

```c
void run_ber()
{
        int j,k=16,w;
        int c;
        long p2;
        int x;
        int flag;
        int stato[MAX];
        int s0[MAX];
        int connessioni[MAX];
         int decisione,confronto,temp,decisiono,compares;
         long i;

         double pulse,uscita1,uscita2,rum,rum2,sum,electr_pulse;
         double E,control,intensity,sol,electr_out,mult,pulse_power_d,signal;
         double ref,S_N,S_N_dB;

        /* used for calc channel noise on device*/

        double chan_no_avg,chan_no_std,chan_no_sum;

         float N;
         int chan_dem,chan_count;
         double pulse_arr[1000];

        /* used to check optical BER before the devise converts to electrical*/

        double optical_decision;

        /* alters power to intensity */

         mult=pow(10,12);
        intensity=pulse_power*mult;
         pulse_power_d=pulse_power;



        /* this setsup the random number generator for the noise from other
channels*/
        /* avg has the added td to ensure that the rate of decay of effect of other
        channels is proportional to the percnetage of max delay allowable*/
        /* noise is include in the STD to ensure accountability of N0_det */

        chan_no_sum=thr_optim();
        chan_no_avg=TPA(intensity)*chan_no_sum;
        chan_no_std=STD(chan_no_avg);



        riempi(stato);
        copia(k,stato,s0);
        riempi1(connessioni);
        flag=1;
        c=compare(k,stato,s0);



         temp=1;
         cont=0;v=0;
        signal= 1.647412*pow(10,9);

        sol=intensity*ratio+(intensity)/2;
         soglia=TPA(sol)+(chan_no_avg);
```

```
optical_decision=(intensity/2)+(intensity*ratio);

erroro=0;
errori=0;
p2=0;/* used to chooes one of the 2 random numbers generated by the gaussian
RNDG*/
p=0;

N0_d=pow(10,N0/10);
w=1;
chan_count=0;

        for(;p<1*pow(10,7);p++)
                {

                        /* converts digital to watts intensity */

                        pulse=modula(stato[k-1],intensity);
                        p2++;

                        /* noise for a signal of 1, used for 0 also
                        should not be but used regardless */

                        rum=rumore(p2,N0_d,pulse_power_d)*mult;

                        /* if 1 add pulse */

                        if(stato[k-1]==1)
                                {
                                                uscita1=pulse+rum;
                                }
                        else
                                {
                                        rum=rumore(p2,N0_d,0)*mult;
                                        uscita1=0+rum;
                                }


                        p2++;

                        control=intensity*ratio;

                        /* add noise for the control signal at same S/N as pulse
divided by 10 to
                        reduce ratio noise as we have a poor corolation to
control noise so we must reduce it*/
                        rum2=rumore(p2,N0_d,(pulse_power_d))*mult;/*
*(1+(ratio/1000))*/


                        uscita2=control+rum2;
                        sum=uscita1+uscita2;

                        decisiono=decidi(sum,optical_decision);
                        compares=confronta(stato[k-1],decisiono);
                        erroro=erroro+compares;


                        electr_pulse=TPA(sum);/* converting watts optical to
current amps */
                        p2++;

                        /*printf("\n%e\t%d",electr_pulse,stato[k-1]); */
```

```c
                                /* electrical pulse +control + thermal noise */


        pulse_arr[0]=electr_pulse+rumore(p2,N0_det*mult,signal)*signal;

                                /* add on channel accumulative noise, did not use
thermal noise on accum.
                                as thermal noise is gaussian distributed around 0 ie
averages out at zero*/


        electr_out=fill_in(chan_no_avg,chan_no_std,pulse_arr);

/*printf("\ncont  %e  \t optical+n  %e \toptical+signal  %e \t elect  %e \t elect+n
%e \t elect+n+c  %e \t soglia  %e
",control,uscita2,sum,electr_pulse,pulse_arr[0],electr_out,soglia);*/



                                /* decision process is out put of TPA a 1 or a zero*/

                                decisione=decidi(electr_out,soglia);
                                confronto=confronta(stato[k-1],decisione);
                                errori=errori+confronto;


                                /* fprintf(out,"1 intensity  %e \n 2 optical power sol
%e  \n 3 decider soglia   %e   \n 4 control and pulse sum   %e \n 5 electrical sum
%e \n 6 elec sum and noise thermal %e \n 7 elec and noise and other channels %e\n 8
pulse   %e  \n 9 noise rum  %e  \n 10 optical pulse uscita1   %e  \n 11 control  %e
\n 12 noise2 rum2  %e \n  13 optical control uscita2 %e \n 14 original bit stato
%d\n 15 what is it decision %d\n  16 are they the same confronto %d \n 17 error %e
\n
",intensity,sol,soglia,sum,electr_pulse,pulse_arr[0],electr_out,pulse,rum,uscita1,co
ntrol,rum2,uscita2,stato[k-1],decisione,confronto,errori);*/

                                /*setting up the next bit - some of this is not needed*/

                                x=reazione(k,connessioni,stato);
                                shift(k,stato);
                                stato[0]=x;    c=compare(k,stato,s0);
                                flag=0;
                        }


        ber=errori/p;
        ber_optical=erroro/p;




    /*       ref=TPA(control+intensity);
        S_N= 2*mult*N0_det*pow(ref,2)/pow(signal,3);
        S_N_dB= 10*log(S_N);
        printf(" the S/N ratio of the receiver is: %f", S_N_dB);*/
        /*printf("signal:    %e   %e  %e  \n",electr_pulse,electr_out,soglia); */


}




void in_v_out()
{
/*for a range of Alpha outputs the input and output of the devise*/
```

```c
        double i,j;
        int x;
        double in,out;

        for(i=1;i<100000000001;i=i*10)
                {
                j=i;
                for(x=1;x<10;x++)
                        {
                        in=j*pow(10,8);
                        fprintf(graph1,  "\n%e",in);
                        for(Alpha=0.01;Alpha<101;Alpha=Alpha*10)
                                {
                                out=TPA(in);
                                fprintf(graph1,  "\t%e",out);
                                }

                        j=j+(i*10*0.1);
                        }
                }

printf("COMPLETE !!   - check file in_v_out.dat for details - ");
}




void ber_v_control()
{
/* this part of the program outputs the ber v control for different numbers of
channels*/


        int i;
        for(i=1;i<loop;i++)
                {
                fprintf(graph2,  "\n%f\t%f\t",ratio,(pulse_power*ratio));
                for(chan_number=25;chan_number<101;chan_number=chan_number+25)
                        {
                        run_ber();
                        fprintf(graph2,"%e\t%e\t",ber,ber_optical);
                        printf("\n\n\n%e\t%e\t\n",ber,ber_optical);
                        printf("\n\t\tsub-loop %d-%d complete \n",i,chan_number);
                        }
                ratio=ratio+10;
                printf("\nloop %d of %d complete \n", i,loop-1);
                }
                fprintf(graph2,"\nPercentage delay %f\nthermal noise %f\noptical noise
%f\npulse power %f\nDevice delay %e s\nChannel bit rate %f Gb/s\n
",percentage,N0_det,N0,pulse_power,(max_delay*percentage/100),bit_r);

printf("\nCOMPLETE !!  - check file ber_v_control_ch.dat for details - ");
}




void ber_v_control2()
{
/* this part of the program outputs the ber v control for different values of device
time delay*/


        int i;

        for(i=1;i<loop;i++)
                {
```

```c
                fprintf(graph2, "\n%f\t%f\t",ratio,(pulse_power*ratio));
                for(percentage=10;percentage<50;percentage=percentage+10)/* typically
percentage+30*/
                        {
                        td=time_delay();
                        run_ber();
                        printf("\n%e\n",ber_optical);
                        fprintf(graph2,"%e\t",ber);
                        printf("\n\t\tsub-loop %d-%3.0f complete \n",i,percentage);
                        }
                ratio=ratio+10;
                printf("\nloop %d of %d complete \n", i,loop-1);
                }
                fprintf(graph2,"\nnumber of channels %d\nthermal noise %f\noptical
noise %f\npulse power %f\nTotal Bit Rate %f Gb/s\nChannel bit rate %f
Gb/s",chan_number,N0_det,N0,pulse_power,(bit_r*chan_number),bit_r);

printf("\nCOMPLETE !!  - check file ber_v_control_dl.dat for details - ");
}




void ber_v_signal()
{
/* this outputs the BER v Signal power for both optical and electrical signal allows
us to compare the effieiency of the device*/

        double i;
        for(i=1;i<loop;i++)
                {
                fprintf(graph3, "\n%f",pulse_power);
                for(chan_number=20;chan_number<101;chan_number=chan_number+80)
                        {
                        run_ber();
                        fprintf(graph3,
"\t%e\t%e\t%3.3f",ber,ber_optical,100*ber_optical/ber);
                        }
                pulse_power=pulse_power+0.1;
                printf("loop %f of %d complete \n", i,loop-1);
                }
        fprintf(graph3,"\nthermal noise %f\noptical noise %f\ncontrol
ratio%f\nPercentage %f\nDevice delay %e s\n
",N0_det,N0,ratio,percentage,(max_delay*percentage/100));
        printf("COMPLETE !!  - check file ber_v_signal_ch.dat for details - ");


}




void ber_v_signal2()
{
/* this outputs the BER v Signal power for both optical and electrical signal allows
us to compare the effieiency of the device*/

        int i;
        for(i=1;i<loop;i++)
                {
                fprintf(graph3, "\n%f",pulse_power);
                for(ratio=10;ratio<101;ratio=ratio*10)
                        {
                        for(percentage-10;percentage<101;percentage-percentage*10)
                        {
```

```c
                             td=time_delay();
                             run_ber();
                             fprintf(graph3, "\t%e\t%e",ber,ber_optical);
                             printf("\n\t\t\tsub-loop %3.0f-%3.0f of %d complete
\n",ratio,percentage,loop+4);
                         }
                     }
                 pulse_power=pulse_power+0.1;
                 printf("loop %d of %d complete \n", i,loop-1);
             }
         fprintf(graph3,"\nnumber of channels %d\nthermal noise %f\noptical noise
%f\nTotal Bit Rate %f Gb/s\nMax device delay %e s\n
",chan_number,N0_det,N0,(bit_r*chan_number),max_delay);
         printf("COMPLETE !!  - check file ber_v_signal_mul.dat for details - ");


}




void signal_v_time()
{
         double bit_slot,overlap,time,max_time,sub_time,output,step,sample;
         int i,diagram;

         int j,k=16,z;
         int c;
         long p2;
         int x,counter=0;
         int flag;
         int stato[MAX];
         int s0[MAX];
         int connessioni[MAX];

         double pulse,uscita1,uscita2,rum,rum2,sum,electr_pulse;
         double E,control,intensity,electr_out,mult,pulse_power_d,signal;
         double ref,S_N,S_N_dB;

         float N;
         int chan_dem,chan_count,bits;
         double pulse_arr[1000],pulse1_arr[1000],sum_arr,control_arr[500];


         /* zero all pulse arays*/
         for(z=0;z<1000;z++)
         {
         pulse_arr[z]=0;
         pulse1_arr[z]=0;
         }


         /* calculating timing for data collection*/


         overlap = chan_number*(percentage/100);


         /* alters power to intensity */

         mult=pow(10,12);
         intensity=pulse_power*mult;
         pulse_power_d=pulse_power;

         /*set up bits*/

         riempi(stato);
```

```
        riempil(connessioni),
        flag=1,                                                        •

        cont=0,v=0,
        signal= 1 647412*pow(10,9)

        p2=0,/* used to chooes one of the 2 random numbers generated by the gaussian
RNDG*/

        N0_d=pow(10,N0/10)
        chan_count=1


        printf("Do you require \n1  EYE DIAGRAM or \n2  BIT v TIME DIAGRAM\n"),
        scanf("%d",&diagram),


        for(bits=1 bits<((chan_number*500)+1) bits++)
                {

                /* converts digital to watts intensity */

                pulse=modula(stato[k-1],intensity)
                 p2++,

                /* noise for a signal of 1, used for 0 also
                should not be but used regardless */

                rum=rumore(p2 N0_d,pulse_power_d)*mult


                /* if 1 add pulse */

                        if(stato[k-1]==1)
                                {
                                 uscita1=pulse+rum,
                                }
                          else
                                    {
                                     rum=rumore(p2,N0_d stato[k-1])*mult,
                                 uscita1=rum
                                        }

                p2++
                        if(chan_count==1)
                                {

rum2=rumore(p2 N0_d,(pulse_power_d*(1+(ratio/100))))*mult
                                control=intensity*ratio
                                uscita2=control+rum2
                                }
                          else
                                {
                                uscita2=0 0
                                }




                sum=uscita1+uscita2
                electr_pulse=TPA(sum) /* converting watts optical to current amps */
                if(chan_count==1)
                                {
                                printf("\n%e\t%e\t%d" sum,electr_pulse stato[k-1]),
                                }



                ▾
```

```
                p2++;

                /* electrical pulse +control + thermal noise */
                sum_arr=0;



/*the effect of the last bit containd the effect of the bit before it and the bit
before it and so on
so we only add on the effect of the bit before the one of interest the difference is
the point at which i is degrading
ex. if it effect 8 post bits the next bit has 1/8 the effect if 16 the next bit is
1/16 as an exponential
1/16 is much larger*/

                    sum_arr=(pulse_arr[1]*exp(-4*1/(overlap)));


                /* pulse size based on the previous signals included - controlled by
percentage*/

        pulse_arr[0]=electr_pulse+sum_arr+rumore(p2,N0_det*mult,signal)*signal;
                pulse1_arr[0]=sum_arr;
                if(chan_count==1)
                        {
                        control_arr[counter]=pulse_arr[0];
                        counter++;
                        }


/*printf("\nFIRST pulse 1 = %e\t stato = %d\t chan count =
%d\t%d",pulse_arr[1],stato[15],chan_count,k);*/



                chan_count=(chan_count+1)%chan_number;
                x=reazione(k,connessioni,stato);
                shift_arr(pulse_arr);
                shift_arr(pulse1_arr);
                shift(k,stato);
                stato[0]=x;
                flag=0;



                }
printf("\n all arrays are now assigned\n\n Expanding pulses in time domain");

        bit_slot=1/total_bit_rate;
        bits=chan_number*3+2;
        counter=400;
        max_time=(bits)*bit_slot;


        for(time=bit_slot;time<max_time+bit_slot;time=time+bit_slot)
                {

                sample=bit_slot/10;


                /* choice of eye diagram or time*/
                if(diagram==1)
                        {
                        step=3*sample;

                        /* Rise of signal */
```

```c
                          for(sub_time=(step-
(3*sample));sub_time<(3*sample);sub_time=sub_time+(sample/20))
                                  {
                                  output=control_arr[counter]*(sub_time-(step-
(3*sample)))/(3*sample);

        fprintf(graph4,"\n%e\t%e\t%e",sub_time,output,control_arr[counter]);
                                  }


                  }
            else
                  {
                  step=time;


                  /* Rise of signal - not necessary to seperate the functions but
useful for tests*/

                  for(sub_time=(step-
(3*sample));sub_time<(step);sub_time=sub_time+(sample/20))
                                  {
                                  output=pulse_arr[bits]*(sub_time-(step-
(3*sample)))/(3*sample);
                                  if(output>pulse1_arr[bits])
                                        {
        fprintf(graph4,"\n%e\t%e\t%e",sub_time,output,pulse_arr[bits]);
                                        }
                                  }


                  }

            /* number of samples per bit slot 1 bit slot gets 200 samples
            if it overlaps 100channels it get 2000*/




                  /* drop of signal */

        if(diagram==1)
                  {


        for(sub_time=(step);sub_time<(step+(bit_slot*overlap));sub_time=sub_time+(sam
ple/10))
                                  {
                                  output=control_arr[counter]*(exp(-4*(sub_time-
step)/(bit_slot*overlap)));

        fprintf(graph4,"\n%e\t%e\t%e",sub_time,output,control_arr[counter]);
                                  }

                  }
                  else
                  {

        for(sub_time=(step);sub_time<(step+(bit_slot*overlap));sub_time=sub_time+(sam
ple/10))
```

```c
                               {
                               output=pulse_arr[bits]*(exp(-4*(sub_time-
step)/(bit_slot*overlap)));
                               if(output>pulse1_arr[bits-1])
                                       {
        fprintf(graph4,"\n%e\t%e\t%e",sub_time,output,pulse_arr[bits]);
                                       }
                               }
                       }

                bits--;
                counter--;
                }
printf("\n Complete !! check file signal_v_time.dat for report\a");
}




void riempi(int *a)
{


a[0]=1;a[1]=1;a[2]=0;a[3]=1;a[4]=0;a[5]=0;a[6]=1;a[7]=1;a[8]=0;a[9]=1;a[10]=0;
        a[11]=1;a[12]=1;a[13]=0;a[14]=1;a[15]=1;
}




void riempi1(int *a)
{
        a[0]=1;a[1]=1;a[2]=0;a[3]=1;a[4]=0;a[5]=1;a[6]=0;a[7]=1;a[8]=1;
        a[9]=1;a[10]=1;a[11]=0;a[12]=0;a[13]=0;a[14]=1;a[15]=1;
}




void copia(int k,int *s,int *s0)
{
        int i;
        for(i=0;i<k;i++)
                s0[i]=s[i];
}




void putint(double k)
{
        printf("%f",k);
        printf("\n");
}




void shift(int k,int *s)
{
        int i;
        for(i=0;i<k-1;i++)
                s[k-1-i]=s[k-2-i];
}
```

```
int reazione(int k int *c int *s)
{
        int i
        int x=0,

        for(i=0,i<k i++)
                x=x^(c[i]&s[i])
        return(x),
}




int getint()
{
        int k,
        printf("introduci intero "),
        scanf("%d" &k)

        return(k)
}




int compare(int k int *s int *s0)
{
        int i,
        for(i=0 i<k,i++)
        {
        if (s0[i]!=s[i]) return(1),
        }
        return(0),
}




double modula(int bit double intensity)
{
        if (bit==1) return(intensity),
        else return(0 0)
}




    /* da qui iniziano le funzioni di canale*/
long genera_unif(long v)
{
   long r t,v0 q s,v1
   int a,
   a=16808, v0=10000,
   q=m/a,
   r=m%a,
   if(cont==0)
      {
        cont++
        return(v0),
      }
   else
      {            •
```

```c
            s=v/q;
            t=v%q;
            v1=a*t-s*r;
            if(v1<0)  v1=v1+m;
            cont++;
            return(v1);
        }
}




void genera_gauss(double u1,double u2,double sigma)
{
    double f1,f2;
    float pi;
    pi=3.14;
    f1=sqrt(-2*log(u1));
    f2=2*pi*u2;
    g1=f1*cos(f2)*sigma;
    g2=f1*sin(f2)*sigma;
}




double rumore(long cont2, double N0, double pulse_power)
{
    double u1,u2,sigma,vx,N;

    N=pulse_power/N0;  /* N0 = pulse to noise ratio */
    sigma=sqrt(N/2);
    if(cont2%2==0)
      {
        v=genera_unif(v);vx=v; u1=vx/m;
        v=genera_unif(v);vx=v; u2=vx/m;
        genera_gauss(u1,u2,sigma);
         return(g1);
      }
    else return(g2);
}




int decidi(double uscita,double soglia)
{
        if(uscita<soglia) return(0);
        else return(1);
}




int confronta(int bit,int decisione)
{
        if(bit==decisione) return(0);
        else return(1);
}




double TPA(double sum)
{
        double output,c,L,e,I_spa,I_tpa,konst;/*B*/
```

```c
        B=3*pow(10,-10);/* USING NEW BETA VALUE FROM T31 typically 2x10E-12*/
        L=pow(10,-4); /* L=pow(10,-4)*/
         konst=1.3522;

         e=exp((-1)*Alpha*L);
         c=1+(B*sum/Alpha)*(1-e);
         I_spa=sum*(1-e/c)*Alpha*L/(Alpha*L+log(c));
         I_tpa=sum*(1-e/c)*log(c)/(Alpha*L+log(c));
         output=konst*(I_spa+I_tpa/2);
        /* double output;
         output=sum;*/
         return(output);
}



void shift_arr(double *pulse_arr)
{
        int i;
        for(i=(chan_number*3)+2;i>0;i--)
            pulse_arr[i]=pulse_arr[i-1];
}



double fill_in(double avg,double std,double *pulse)
{
double r1,r2;
double ranf();
double sum=0;

        r1 = -log(1-ranf());
        r2 =  2*pi*ranf();
        r1 =  sqrt(2*r1);

        ran1  = (r1*cos(r2)*std*0.25)+(avg);
        ran2  = r1*sin(r2);/*not used*/
/*adds the channel accumulative noise to the data signal*/
        sum=pulse[0]+(ran1);
/*fprintf(out,"%f\t%f\n",sum,soglia);*/


        return(sum);
}


double ranf()
{
        /* Uniform random number generator x(n+1)= a*x(n)  mod c
           with a = pow(7,5) and c = pow(2,31)-1. */

const int ia=16807,ic=2147483647,iq=127773,ir=2836;
int il,ih,it;
double rc;

ih = iseed/iq;
il = iseed%iq;
it = ia*il-ir*ih;
if (it > 0)
   {
   iseed = it;
   }
else
   {
iseed = ic+it;
   }
```

```
rc = 1c,
/*printf("random = %f\t",1seed/rc),*/
return 1seed/rc



}


double thr_optim()
{
int 1 q,
double sum,temp
sum = 0,

q=rint(chan_number*(percentage/100))
temp=-4/q      /* assuming channel bit rate is constant and does not interfer with
next - bit
                        hence no need to take into account last bit in that
channel*/

        for(1=1 1<q+1 1++)
                {
                sum = sum + exp(temp),
                temp=temp-(4/q),
                }
/* divide sum by 2 as this was how the previous program worked, this is not
necessary
it was however kept to keep results within same tolerences*/
return (sum/2)
}


double STD(double chan_no_avg)
{
/*Calculates the standard deviation (std) for a specific average value based on the
number of channels etc*/

double std=0,

/*Get a percentage deviation from the average*/

std=0 248*exp(- 0000000000005*chan_no_avg),
std=std*chan_no_avg*10/(pow(10,(NO_det/10))),

/* 1 and 0 noise- 10/pow(10 no_det/10) - no_det is the
S/N ration hence if its large thenoise is small if its small the noise is large*/

return (std)
}


double time_delay()
{
/*calculates the time delay asan exponential of the total time between 10% and
100%*/

double eqn sum,
eqn=(1-(percentage-10)*0 01111)
sum=exp(-1*eqn)                                                      ʿ


return (sum)
}
```

Index